40208

National Library of Canada
Bibliothèque nationale du Canada

CANADIAN THESES ON MICROFICHE

THÈSES CANADIENNES SUR MICROFICHE

NAME OF AUTHOR/*NOM DE L'AUTEUR* TERRENCE WILLIAM KRAUSS

TITLE OF THESIS/*TITRE DE LA THÈSE* TIME VARIATIONS OF VOLUME-AVERAGED RADAR REFLECTIVITY IN ALBERTA HAILSTORMS

UNIVERSITY/*UNIVERSITÉ* ALBERTA

DEGREE FOR WHICH THESIS WAS PRESENTED/ *GRADE POUR LEQUEL CETTE THÈSE FUT PRÉSENTÉE* MASTER OF SCIENCE

YEAR THIS DEGREE CONFERRED/*ANNÉE D'OBTENTION DE CE GRADE* 1978

NAME OF SUPERVISOR/*NOM DU DIRECTEUR DE THÈSE* K. D. HAGE

Permission is hereby granted to the NATIONAL LIBRARY OF CANADA to microfilm this thesis and to lend or sell copies of the film.

The author reserves other publication rights, and neither the thesis nor extensive extracts from it may be printed or otherwise reproduced without the author's written permission.

L'autorisation est, par la présente, accordée à la BIBLIOTHÈQUE NATIONALE DU CANADA de microfilmer cette thèse et de prêter ou de vendre des exemplaires du film.

L'auteur se réserve les autres droits de publication; ni la thèse ni de longs extraits de celle-ci ne doivent être imprimés ou autrement reproduits sans l'autorisation écrite de l'auteur.

DATED/*DATÉ* July 24/78 SIGNED/*SIGNÉ* T. W. Krauss

PERMANENT ADDRESS/*RÉSIDENCE FIXE*
1417 - 26 ST. S.E.
MEDICINE HAT, ALBERTA
T1A 2G1

NL-91 (3-74)

National Library of Canada

Cataloguing Branch
Canadian Theses Division

Ottawa, Canada
K1A 0N4

Bibliothèque nationale du Canada

Direction du catalogage
Division des thèses canadiennes

NOTICE

The quality of this microfiche is heavily dependent upon the quality of the original thesis submitted for microfilming. Every effort has been made to ensure the highest quality of reproduction possible.

If pages are missing, contact the university which granted the degree.

Some pages may have indistinct print especially if the original pages were typed with a poor typewriter ribbon or if the university sent us a poor photocopy.

Previously copyrighted materials (journal articles, published tests, etc.) are not filmed.

Reproduction in full or in part of this film is governed by the Canadian Copyright Act, R.S.C. 1970, c. C-30. Please read the authorization forms which accompany this thesis.

THIS DISSERTATION
HAS BEEN MICROFILMED
EXACTLY AS RECEIVED

AVIS

La qualité de cette microfiche dépend grandement de la qualité de la thèse soumise au microfilmage. Nous avons tout fait pour assurer une qualité supérieure de reproduction.

S'il manque des pages, veuillez communiquer avec l'université qui a conféré le grade.

La qualité d'impression de certaines pages peut laisser à désirer, surtout si les pages originales ont été dactylographiées à l'aide d'un ruban usé ou si l'université nous a fait parvenir une photocopie de mauvaise qualité.

Les documents qui font déjà l'objet d'un droit d'auteur (articles de revue, examens publiés, etc.) ne sont pas microfilmés.

La reproduction, même partielle, de ce microfilm est soumise à la Loi canadienne sur le droit d'auteur, SRC 1970, c. C-30. Veuillez prendre connaissance des formules d'autorisation qui accompagnent cette thèse.

LA THÈSE A ÉTÉ
MICROFILMÉE TELLE QUE
NOUS L'AVONS REÇUE

NL-339 (3/77)

THE UNIVERSITY OF ALBERTA

TIME VARIATIONS OF VOLUME-AVERAGED RADAR REFLECTIVITY IN ALBERTA HAILSTORMS

by

© TERRENCE WILLIAM KRAUSS

A THESIS

SUBMITTED TO THE FACULTY OF GRADUATE STUDIES AND RESEARCH
IN PARTIAL FULFILMENT OF THE REQUIREMENTS FOR THE DEGREE
OF MASTER OF SCIENCE

IN

METEOROLOGY

DEPARTMENT OF GEOGRAPHY

EDMONTON, ALBERTA

FALL, 1978

THE UNIVERSITY OF ALBERTA

FACULTY OF GRADUATE STUDIES AND RESEARCH

The undersigned certify that they have read, and recommend to the Faculty of Graduate Studies and Research, for acceptance, a thesis entitled "Time Variations of Volume-Averaged Radar Reflectivity in Alberta Hailstorms", submitted by Terrence William Krauss in partial fulfilment of the requirements for the degree of Master of Science in Meteorology.

Keith D. Hage
Supervisor

T.A. Peterson

Date July 14, 1978

DEDICATED TO

my patient and loving wife, Lorie,

who has supported my efforts in every way,

my parents,

whose understanding and encouragement over

the years have made this work possible.

ABSTRACT

An attempt is made at developing a radar parameter sufficiently correlated with hailfall at the surface that it may be used for cloud-seeding evaluation purposes.

The parameter is volume-averaged radar reflectivity $\bar{\eta}$, applied to low-level PPI scans. The parameter $\bar{\eta}$ is tested on 9 Alberta hailstorm case studies from 1975 and 1976, using Alberta Hail Project 10.4 cm wavelength radar data. Cumulative distribution curves for $\bar{\eta}$ according to maximum hailsize reported at the surface are obtained. The problems associated with $\bar{\eta}$ are comparable with those of equivalent radar reflectivity for hailstorms, although, $\bar{\eta}$ appears to be sensitive to, and a good indicator of, overall storm intensity. The quality of the 1975 and 1976 radar data is discussed.

A spectral analysis of the $\bar{\eta}$ time series for the storms reveals possibilities of preferred cycles. Fluctuations in $\bar{\eta}$ imply a storm concept consisting of a large circulation cell with periodicity of approximately 30 minutes, upon which is superimposed small-scale perturbations with possible periodicities of approximately 10 and 15 minutes.

The analysis of changes in $\bar{\eta}$ with respect to cloud-seeding events, suggests a positive cloud-seeding effect in some storms, however, unequivocal seeding effects were not detected.

ACKNOWLEDGEMENTS

I am indebted to various people and organizations whose cooperation and support have enabled me to complete this thesis.

My sincerest thanks go to the staff of the Atmospheric Sciences Division of the Research Council of Alberta for their cooperation. In particular, I would like to thank Dr. G.G. Goyer for suggesting the thesis topic and for his advice, supervision, and support throughout the period during which this research was carried out. I am grateful to Drs. B.L. Barge and R.G. Humphries for their guidance during numerous valuable discussions and for their unlimited enthusiasm in radar meteorology. I also wish to express my appreciation to Dr. J. Ramsden for writing the computer program and for his instrumental assistance with the computer-radar data.

On the university staff, I thank Dr. K.D. Hage, my departmental supervisor, for his helpful suggestions and reviews of this dissertation. Special thanks to Dr. E.P. Lozowski who helped me formulate my own ideas during the early stages of this study. I also thank Dr. T.A. Petersen, Chairman of the Department of Rural Economy who served on my examining committee.

I am grateful to Mr. J. Renick and the staff of the Alberta Hail Project for their efforts during the field project.

Last, but certainly not least, I wish to thank several people who gave freely of their time: Ms. M. Tatchyn for typing the manuscript; Ms. S. Allen for providing help with the drafting; Mr. J. Gertz for providing help with the diagrams.

This thesis was accomplished with financial support from the Research Council of Alberta.

TABLE OF CONTENTS

Page

DEDICATION.. iv

ABSTRACT.. v

ACKNOWLEDGEMENTS.. vi

TABLE OF CONTENTS... vii

LIST OF TABLES.. x

LIST OF FIGURES... xi

TABLE OF ABBREVATIONS... xviii

CHAPTER

1 INTRODUCTION.. 1

1.1 Background on Hail Suppression........................... 1

1.2 1975-76 Alberta Hail Project Seeding Techniques.......... 2

1.3 Alberta Hail Project Evaluation.......................... 7

1.4 Radar and Evaluation..................................... 7

2 THEORY... 9

2.1 Introduction... 9

2.2 The Meteorological Radar Equation........................ 9

2.3 The Evaluation Parameter................................. 12

3 THE RADAR FACILITIES....................................... 17

3.1 The Alberta Hail Project Radar System.................... 17

3.2 The Alberta Hail Project Radar - Computer System......... 19

3.3 Error Analysis... 22

4 DATA ANALYSIS.. 25

4.1 Analysis of Digital Radar Data........................... 25

4.2 Storm Selection.. 28

4.3 Data Sample.. 29

4.4 The Relation Between $\overline{n}$ and Hailfall at the Surface... 30

CHAPTER Page

4.5 Time Series Analysis.................................. 38

5 THE 17 JULY, 1976 CASE STUDIES.......................... 40

5.1 Introduction.. 40

5.2 17 July, 1976: Storm A................................ 40

5.3 Storm A: Power Spectrum............................... 44

5.4 Storm A: Spectrum Analysis............................ 53

5.5 17 July, 1976: Storm B................................ 57

5.6 Storm B: Power Spectrum Analysis...................... 65

5.7 Spectra Comparison.................................... 65

6 THE AUGUST, 1976 CASE STUDIES............................ 69

6.1 Introduction.. 69

6.2 The 6 August, 1976 Storm.............................. 69

6.3 The 12 August, 1976 Storm............................. 78

6.4 The 15 August, 1976 Storm............................. 91

6.5 The 20 August, 1976 Storm............................. 101

6.6 The 24 August, 1976 Storm............................. 112

7 THE 20 JULY, 1975 CASE STUDIES........................... 126

7.1 Introduction.. 126

7.2 20 July, 1975: Storm A................................ 128

7.3 20 July, 1975: Storm B................................ 134

7.4 20 July, 1975: Storm C................................ 145

7.5 Summary of 1975 Data.................................. 151

8 SUMMARY.. 154

8.1 Data Summary.. 154

8.2 $\overline{\eta}$ as a Hail Suppression Evaluation Parameter....... 156

9 CONCLUSIONS AND RECOMMENDATIONS........................... 163

9.1 Concluding Remarks.................................... 163

CHAPTER Page

BIBLIOGRAPHY.. 166

APPENDICES

A THE TUKEY LOW-PASS FILTER........................... 170

B THE POWER SPECTRUM OF RED-NOISE AND WHITE-NOISE 173

C COMPUTER PROGRAM.................................... 175

LIST OF TABLES

TABLE Page

2.1 Radar beam height versus range.......................... 15

4.1 Storm sample used in analysis.......................... 29

4.2 Hailsize name and the assumed hail diameter range......... 34

5.1 Lag 1.5 to 15 minute autocorrelation coefficients of $\bar{\eta}$ for storm A on 17 July, 1976.......................... 56

5.2 Lag 1.5 to 15 minute autocorrelation coefficients of $\bar{\eta}$ for storm B on 17 July, 1976.......................... 68

6.1 Lag 1.5 to 15 minute autocorrelation coefficients of $\bar{\eta}$ for the storm on 6 August, 1976.......................... 77

6.2 Lag 1.5 to 15 minute autocorrelation coefficients of $\bar{\eta}$ for the storm on 12 August, 1976.......................... 88

6.3 Lag 1.5 to 15 minute autocorrelation coefficients of $\bar{\eta}$ for the storm on 15 August, 1976.......................... 101

6.4 Lag 1.5 to 15 minute autocorrelation coefficients of $\bar{\eta}$ for the storm on 20 August, 1976.......................... 110

6.5 Lag 1.5 to 15 minute autocorrelation coefficients of $\bar{\eta}$ for the storm on 24 August, 1976.......................... 122

7.1 Lag 1.5 to 15 minute autocorrelation coefficients of $\bar{\eta}$ for Storm A on 20 July, 1975.......................... 132

7.2 Lag 1.5 to 15 minute autocorrelation coefficients of $\bar{\eta}$ for Storm B on 20 July, 1975.......................... 143

7.3 Lag 1.5 to 15 minute autocorrelation coefficients of $\bar{\eta}$ for Storm C on 20 July, 1975.......................... 151

LIST OF FIGURES

FIGURE		Page
1.1	Map showing the area of the Alberta Hail Project........	3
1.2	Cloud seeding techniques for 1975......................	4
1.3	Cloud seeding techniques for 1976......................	4
3.1	Diagram of the radar receiver and display system........	18
3.2	Radar beam "bin" volume representation.................	20
3.3	PPI echo in digitized form.............................	21
3.4	Relative error(percent) in $\overline{\eta}$ calculation as a function of the number of bins in a given PPI echo..............	24
4.1	The basic radar display using the interactive computer display facility..................................	26
4.2	The display shown in Fig. 4.1 after a portion of the PPI has been outlined for further detailed study........	26
4.3	The new display limited to that portion of the PPI outlined in Fig. 4.2.................................	27
4.4	The same data shown in Fig. 4.3 displayed by means of reflectivity contours................................	27
4.5	The cumulative distribution of all hail reports according to $\overline{\eta}$....................................	32
4.6	The cumulative distribution for the individual maximum-hailsize categories versus $\overline{\eta}$..................	33
4.7	The mean $\overline{\eta}$ values obtained for the five categories of maximum hailsize, and the 90% confidence interval.......	35
4.8	Radar reflectivity as a function of the diameter of uniform, wet-ice spheres.............................	37
4.9	Diameter versus radar reflectivity from a hail spectrum for 10.0 cm wavelength radar..........................	37
5.1	Map showing the synoptic situation, and a brief synoptic summary for storms on 17 July, 1976....................	41
5.2	Rawinsonde sounding from Calgary at 18:00 MDT 17 July, 1976..	42

FIGURE Page

5.3 Map showing hailswath resulting from storm A on 17 July, 1976. 43

5.4 PPI echoes for storm A on 17 July, 1976. Time = 19:30 - 20:15 MDT. 45

5.5 PPI echoes for storm A on 17 July, 1976. Time = 20:30 - 21:00 MDT. 46

5.6 PPI echoes for storm A on 17 July, 1976. Time = 21:15 - 21:29 MDT. 47

5.7 PPI echoes for storm A on 17 July, 1976. Time = 21:45 - 22:00 MDT. 48

5.8 PPI echoes for storm A on 17 July, 1976. Time = 22:15 - 22:45 MDT. 49

5.9 $\overline{\eta}$ versus time for storm A on 17 July, 1976. 50

5.10 Unsmoothed power spectrum of $\overline{\eta}$ for storm A on 17 July, 1976. 51

5.11 Three-point Daniell-filtered power spectrum of $\overline{\eta}$ for storm A on 17 July, 1976. 51

5.12 Three-point Daniell-filtered power spectrum of Tukey-filtered $\overline{\eta}$ highpass data for storm A on 17 July, 1976. 54

5.13 Map showing the hailswath resulting from storm B on 17 July, 1976. 58

5.14 PPI echoes for storm B on 17 July, 1976. Time = 21:15 - 21:29 MDT. 59

5.15 PPI echoes for storm B on 17 July, 1976. Time = 21:45 - 22:30 MDT. 60

5.16 PPI echoes for storm B on 17 July, 1976. Time = 22:45 - 23:30 MDT. 61

5.17 PPI echoes for storm B on 17 July, 1976. Time = 23:45 - 00:29 (18 July) MDT. 62

5.18 PPI echoes for storm B on 17 July, 1976. Time = 00:44 - 01:29 (18 July) MDT. 63

5.19 $\overline{\eta}$ versus time for storm B on 17 July, 1976. 64

FIGURE Page

5.20 Unsmoothed power spectrum of $\overline{\eta}$ for storm B on 17 July, 1976.......... 66

5.21 Three-point Daniell-filtered power spectrum of $\overline{\eta}$ for storm B on 17 July, 1976.......... 66

5.22 Three-point Daniell-filtered power spectrum of Tukey-filtered $\overline{\eta}$ highpass data for storm B on 17 July, 1976.......... 67

6.1 Map showing the synoptic situation and a brief synoptic summary for the storm on 6 August, 1976.......... 70

6.2 Rawinsonde sounding from Rocky Mountain House at 18:00 MDT, 6 August, 1976.......... 71

6.3 Map showing the hailswath resulting from the storm on 6 August, 1976.......... 73

6.4 PPI echoes for the storm on 6 August, 1976. Time = 16:31 - 17:59 MDT.......... 74

6.5 $\overline{\eta}$ versus time for the storm on 6 August, 1976.......... 75

6.6 Unsmoothed power spectrum of $\overline{\eta}$ for the storm on 6 August, 1976.......... 76

6.7 Three-point Daniell-filtered power spectrum of $\overline{\eta}$ for the storm on 6 August, 1976.......... 76

6.8 Map showing the synoptic situation, and a brief synoptic summary for the storm on 12 August, 1976.......... 79

6.9 Rawinsonde sounding from Red Deer at 15:00 MDT, 12 August, 1976.......... 80

6.10 Map showing the hailswath resulting from the storm on 12 August, 1976.......... 81

6.11 PPI echoes for the storm on 12 August, 1976. Time = 17:00 - 18:14 MDT.......... 82

6.12 PPI echoes for the storm on 12 August, 1976. Time = 18:29 - 19:45 MDT.......... 83

6.13 PPI echoes for the storm on 12 August, 1976. Time = 20:00 - 20:45 MDT.......... 84

6.14 PPI echoes for the storm on 12 August, 1976. Time = 21:00 - 22:00 MDT.......... 85

FIGURE Page

6.15 $\overline{\eta}$ versus time for the storm on 12 August, 1976.......... 87

6.16 Unsmoothed power spectrum of $\overline{\eta}$ for the storm on 12 August, 1976.................................... 89

6.17 Three-point Daniell-filtered power spectrum of $\overline{\eta}$ for the storm on 12 August, 1976....................... 89

6.18 Three-point Daniell-filtered power spectrum of Tukey-filtered $\overline{\eta}$ highpass data for the storm on 12 August, 1976.................................... 90

6.19 Map showing the synoptic situation and a brief synoptic summary for the storm on 15 August, 1976....... 92

6.20 Rawinsonde sounding from Rocky Mountain House at 18:00 MDT, 15 August, 1976.......................... 93

6.21 Map showing the hailswath resulting from the storm on 15 August, 1976................................ 94

6.22 PPI echoes for the storm on 15 August, 1976. Time = 17:45 - 18:45 MDT.............................. 96

6.23 PPI echoes for the storm on 15 August, 1976. Time = 19:00 - 19:47 MDT.............................. 97

6.24 $\overline{\eta}$ versus time for the storm on 15 August, 1976.......... 98

6.25 Unsmoothed power spectrum of $\overline{\eta}$ for the storm on 15 August, 1976.................................... 99

6.26 Three-point Daniell-filtered power spectrum of $\overline{\eta}$ for the storm on 15 August, 1976....................... 99

6.27 Three-point Daniell-filtered power spectrum of Tukey-filtered $\overline{\eta}$ highpass data for the storm on 15 August, 1976.................................... 100

6.28 Map showing the synoptic situation and a brief synoptic summary for the storm on 20 August, 1976....... 103

6.29 Rawinsonde sounding from Rocky Mountain House at 18:00 MDT, 20 August, 1976.......................... 104

6.30 Map showing the hailswath resulting from the storm on 20 August, 1976................................ 105

6.31 PPI echoes for the storm on 20 August, 1976. Time = 19:00 - 20:15 MDT.............................. 106

Page

FIGURE

6.32 PPI echoes for the storm on 20 August, 1976. Time = 20:30 - 21:15 MDT.................................... 107

6.33 $\overline{\eta}$ versus time for the storm on 20 August, 1976.......... 108

6.34 Unsmoothed power spectrum of $\overline{\eta}$ for the storm on 20 August, 1976.................................... 109

6.35 Three-point Daniell-filtered power spectrum of $\overline{\eta}$ for the storm on 20 August, 1976......................... 109

6.36 Three-point Daniell-filtered power spectrum of Tukey-filtered $\overline{\eta}$ highpass data for the storm on 20 August, 1976.................................... 111

6.37 Map showing the synoptic situation and a brief synoptic summary for the storm on 24 August, 1976....... 113

6.38 Rawinsonde sounding from Rocky Mountain House at 18:00 MDT, 24 August, 1976.......................... 114

6.39 Map showing the hailswath resulting from the storm on 24 August, 1976................................ 115

6.40 PPI echoes for the storm on 24 August, 1976. Time = 16:29 - 17:44 MDT................................ 116

6.41 PPI echoes for the storm on 24 August, 1976. Time = 17:59 - 18:44 MDT................................ 117

6.42 PPI echoes for the storm on 24 August, 1976. Time = 18:59 - 19:45 MDT................................ 118

6.43 PPI echoes for the storm on 24 August, 1976. Time = 20:00 - 20:45 MDT................................ 119

6.44 PPI echoes for the storm on 24 August, 1976. Time = 21:00 - 21:29 MDT................................ 120

6.45 $\overline{\eta}$ versus time for the storm on 24 August, 1976.......... 121

6.46 Unsmoothed power spectrum of $\overline{\eta}$ for the storm on 24 August, 1976.................................... 123

6.47 Three-point Daniell-filtered power spectrum of $\overline{\eta}$ for the storm on 24 August, 1976......................... 123

6.48 Three-point Daniell-filtered power spectrum of Tukey-filtered $\overline{\eta}$ highpass data for the storm on 24 August, 1976.................................... 124

FIGURE Page

7.1 An example of a radar echo from the 1975 data which displays "missing rays" 127

7.2 PPI echoes for storm A on 20 July, 1975. Time = 15:30 - 16:30 MDT 129

7.3 PPI echoes for storm A on 20 July, 1975. Time = 16:45 - 17:15 MDT 130

7.4 $\overline{\eta}$ versus time for storm A on 20 July, 1975 131

7.5 Unsmoothed power spectrum of $\overline{\eta}$ for storm A on 20 July, 1975 133

7.6 Three-point Daniell-filtered power spectrum of $\overline{\eta}$ for storm A on 20 July, 1975 133

7.7 Map showing the hailswaths which resulted from storm B and storm C on 20 July, 1975 135

7.8 PPI echoes for storm B on 20 July, 1975. Time = 15:30 - 16:45 MDT 137

7.9 PPI echoes for storm B on 20 July, 1975. Time = 17:00 - 18:14 MDT 138

7.10 PPI echoes for storm B on 20 July, 1975. Time = 18:29 - 19:01 MDT 139

7.11 PPI echoes for storm B on 20 July, 1975. Time = 19:14 - 19:59 MDT 140

7.12 $\overline{\eta}$ versus time for storm B on 20 July, 1975 141

7.13 Unsmoothed power spectrum of $\overline{\eta}$ for storm B on 20 July, 1975 142

7.14 Three-point Daniell-filtered power spectrum of $\overline{\eta}$ for storm B on 20 July, 1975 142

7.15 Three-point Daniell-filtered power spectrum of Tukey-filtered $\overline{\eta}$ highpass data for storm B on 20 July, 1975 144

7.16 PPI echoes for storm C on 20 July, 1975. Time = 17:45 - 18:59 MDT 146

7.17 PPI echoes for storm C on 20 July, 1975. Time = 19:16 - 20:00 MDT 147

FIGURE Page

7.18 PPI echoes for storm C on 20 July, 1975. Time = 20:15 - 21:00 MDT.................................. 148

7.19 $\overline{\eta}$ versus time for storm C on 20 July, 1975.............. 149

7.20 Unsmoothed power spectrum of $\overline{\eta}$ for storm C on 20 July, 1975.. 150

7.21 Three-point Daniell-filtered power spectrum of $\overline{\eta}$ for storm C on 20 July, 1975............................ 150

7.22 Three-point Daniell-filtered power spectrum of Tukey-filtered $\overline{\eta}$ highpass data for storm C on 20 July, 1975.. 152

8.1 Three-point Daniell-filtered average power spectrum for the seven storms of 1976........................... 155

8.2 Three-point Daniell-filtered average power spectrum for the four non-seeded storm of 1976.................. 160

8.3 Three-point Daniell-filtered average power spectrum for the three seeded storms of 1976..................... 162

A.1 The Tukey filter weight function......................... 171

A.2 The Tukey filter response function....................... 171

TABLE OF ABBREVIATIONS

AgI	Silver Iodide
AGL	Above Ground Level
AHP	Alberta Hail Project
ALHAS	Alberta Hail Studies
ARC	Alberta Research Council
AWMB	Alberta Weather Modification Board
C-band	5 cm wavelength band
CRT	cathode-ray-tube
CYQF	Red Deer station identifier
CYRM	Rocky Mountain House station identifier
CYYC	Calgary station identifier
dBm	power in decibels above 1 milliwatt
dBZ	equivalent radar reflectivity in decibels above 1 $mm^6 m^{-3}$
DFT	discrete Fourier transform
E, ERN	east, eastern
FFT	fast Fourier transform
L/W	long-wave (planetary scale)
mb	millibar
MDT	Mountain Daylight Time
MSL	mean sea level
N, NE, NW	north, northeast, northwest
PPI	Plan-Position Indicator radar display
PVA	positive vorticity advection
R	ridge
S-band	10 cm wavelength band
S/W	short-wave (synoptic scale)
S, SE, SW	south, southeast, southwest
T	trough
W, WRN	west, western
X-band	3 cm wavelength band
Z	Greenwich Mean Time

CHAPTER 1

INTRODUCTION

1.1 Background on Hail Suppression

The hailstorm poses a serious problem for agriculture in the Province of Alberta with annual crop losses averaging $40 to $50 million (Renick, 1975). Agricultural claims for hail damage are received on an average of 50 days each season (1 June to 10 September) in Alberta (Summers and Wojtiw, 1971), with 50 percent of the years' damage occurring on 4 days, and 80 percent of the damage on the worst 12 days (Wojtiw, 1975a).

There are hypotheses which suggest that hail may be suppressed by injecting (seeding) ice nucleating agents such as silver iodide (AgI) into growing convective clouds. The claim is made that the growth of large damaging hail is inhibited through the introduction of high concentrations of ice nuclei, all competing for a finite supply of supercooled water. Considering the agricultural losses, even partially successful hail suppression programs would be economically beneficial; thus numerous hail suppression experiments have been carried out in North America and abroad. Claims of decreases in hail damage have been made in a few cases, but due to the lack of significant evidence in support of such claims, no general agreement exists among the scientific community about their validity (Hitschfeld, 1974; Neyman, 1977).

The Alberta Hail Project (AHP), under the auspices of the Alberta Weather Modification Board (AWMB) with participation by the Alberta Research Council (ARC), is among the most significant hail suppression programs currently in progress. The AWMB established under Alberta Agriculture in 1974, was formed in response to the recommendations of the Special Legislative Committee on Crop Insurance and Weather Modification to the Legislative Assembly of Alberta (March 1973). It was granted a five year mandate to administer hail suppression and hail research programs with continuing evaluation to determine the scientific and economic feasibility of hail suppression using current technology. An area of 47360 km^2 (18,500 mi^2) centered on the radar site at the Red Deer Industrial Airport was designated for the project (Figure 1.1). Although the AHP cloud seeding experiment began in 1974, its organization and many of its researches are extensions of the former Alberta Hail Studies (ALHAS) project which originated in 1956. The ALHAS project was devoted entirely to basic hailstorm research and began experimental seeding of storms with AgI for hail damage reduction in 1970.

1.2 1975 - 76 Alberta Hail Project Seeding Techniques

The AHP cloud seeding program runs from the middle of June to the middle of September each year. The cloud seeding is conducted by seven turbo-charged twin-engined aircraft either from cloud top, utilizing dropable pyrotechnic flares, or from cloud base with pyrotechnic flares mounted on the aircraft wings.

The cloud-top seeding method was first developed by Simpson et al. (1970) in Florida, and adapted to Alberta hailstorms by Summers et al. (1972). It is closely related to the Alberta multi-cell storm concept as described by Douglas and Hitschfeld (1959), Chisholm and Renick (1972), and Marwitz (1972).

In 1974 and 1975, seeding was confined to growing cloud towers and the main storm-inflow area at cloud base (Figure 1.2). Seeding rates varied but,

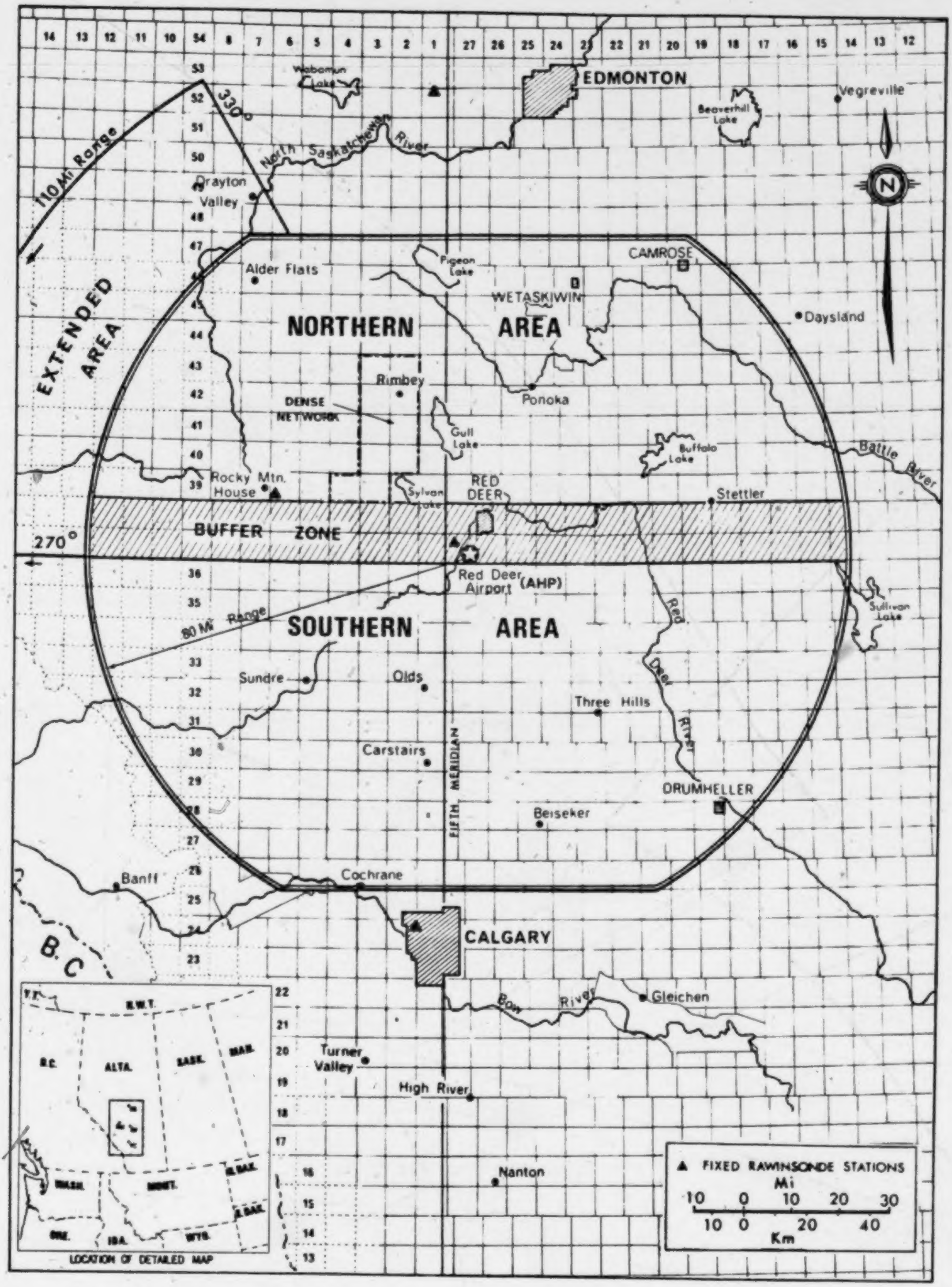
EDMONTON
Wabamun Lake
Beaverhill Lake
Vegreville
North Saskatchewan River
110 Mi Range
330°
Drayton Valley
EXTENDED AREA
Alder Flats
Pigeon Lake
CAMROSE
WETASKIWIN
Daysland
NORTHERN AREA
Rimbey
DENSE NETWORK
Ponoka
Gull Lake
Buffalo Lake
Battle River
Rocky Mtn. House
Sylvan Lake
RED DEER
Stettler
BUFFER ZONE
270°
Red Deer Airport (AHP)
Sullivan Lake
80 Mi Range
SOUTHERN AREA
Red Deer River
Sundre
Olds
Three Hills
Carstairs
FIFTH MERIDIAN
DRUMHELLER
Beiseker
Banff
Cochrane
CALGARY
B.C
Bow River
Gleichen
Turner Valley
High River
Nanton
N
Y.T.
N.W.T.
B.C.
ALTA.
SASK.
MAN.
WASH.
MONT.
N. DAK.
S. DAK.
ORE.
IDA.
WYO.
LOCATION OF DETAILED MAP
▲ FIXED RAWINSONDE STATIONS
Mi
10 0 10 20 30
10 0 20 40
Km

Fig. 1.1: Map showing the area of the Alberta Hail Project. (From Deibert (ed.), 1977)

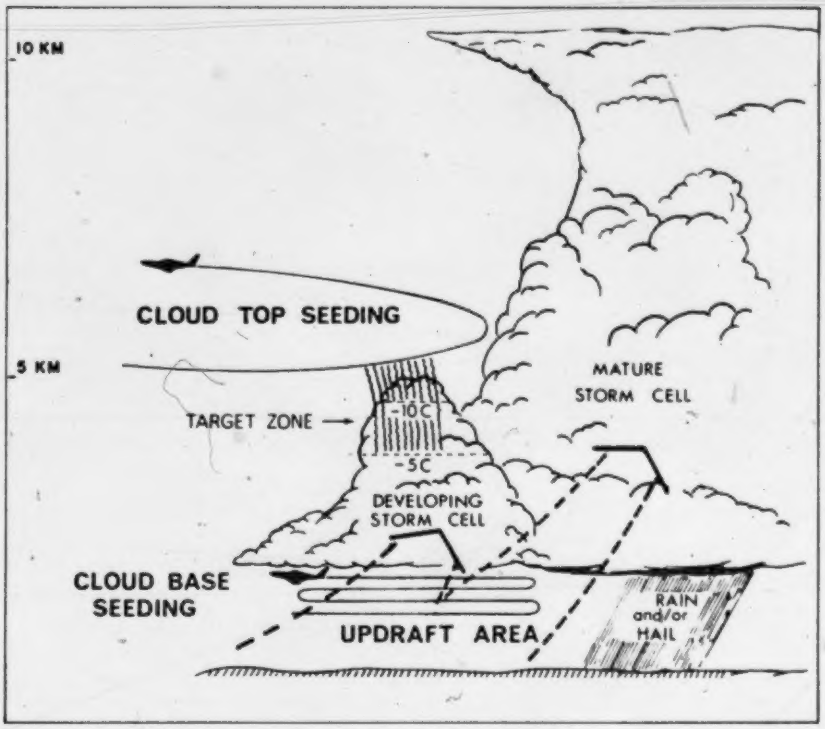
10 KM
5 KM
CLOUD TOP SEEDING
TARGET ZONE
-10C
-5C
DEVELOPING STORM CELL
MATURE STORM CELL
CLOUD BASE SEEDING
UPDRAFT AREA
RAIN and/or HAIL

Fig. 1.2: Cloud seeding techniques for 1975. (From Deibert (ed.), 1976).

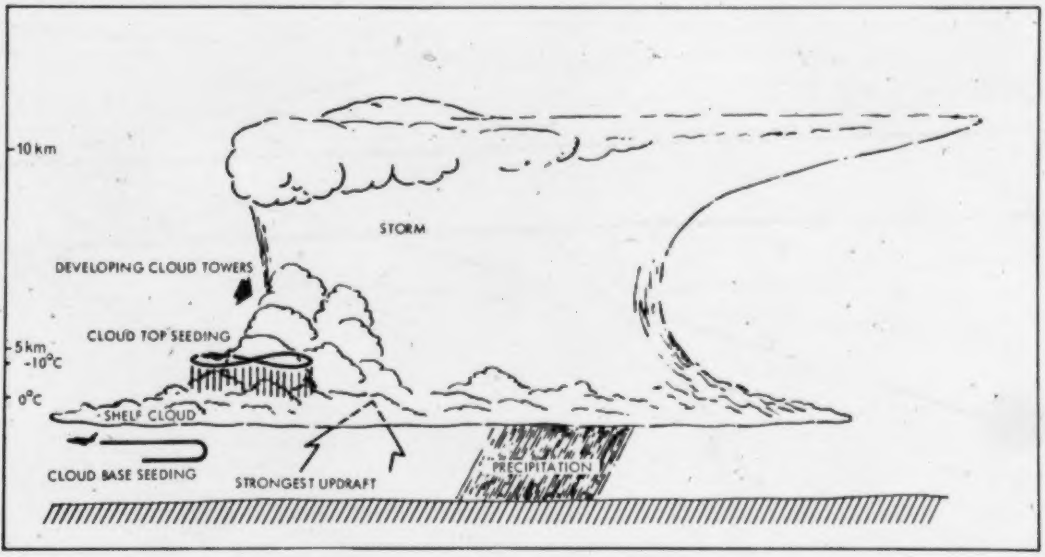
10 km
STORM
DEVELOPING CLOUD TOWERS
CLOUD TOP SEEDING
5 km
-10°C
0°C
SHELF CLOUD
CLOUD BASE SEEDING
STRONGEST UPDRAFT
PRECIPITATION

Fig. 1.3: Cloud seeding techniques for 1976. (From Barge et al., 1976).

in general, cloud-top flares were dropped from approximately the -12°C level at 5 second intervals (approximately 300 m). Base flares were ignited once every 7 minutes unless the updraft at cloud base exceeded 5 ms^{-1}, when 5 base flares were burned simultaneously. Both methods were used when possible with a higher priority given to cloud-top seeding; however, storm type and amount of cloud cover often determined which seeding technique was used.

Seeding procedures were changed slightly in 1976 (Figure 1.3), as a result of radar studies performed at Alberta Research Council (Barge et al., 1976). It is now felt that seeding the smaller growing cloud towers at the edge of the storm more heavily at an earlier stage will give better results. Seeding was performed by aircraft flying a "figure 8" flight pattern above the new growth region at approximately the -10°C level and dropping AgI pyrotechnic flares approximately 2 km apart. If the shelf cloud was obscured by mid-level cloud, seeding was confined to the weaker updrafts around the edge of the storm at cloud base.

In 1975 the cloud-top seeding flares were 50 gm AgI, WM-105 formulation from Olin corporation. These flares fall approximately 1800 m during their one-minute burn time. The cloud-base seeding flares were 70 gm AgI, SR-14 fusees (Nuclei Engineering Incorporated) which burn for 7 minutes.

In 1976 the cloud-seeding flare types included those from 1975 plus 70 gm AgI, TB1 cloud-top flares (Nuclei Engineering Inc.) which have a burn time of 35 seconds after an 11 second delay, and TB1 cloud base fusees (Nuclei Engineering Inc.) which contain 150 gm of AgI with a burntime of 4 minutes.

Cloud-seeding operations both years were carried out according to the following criteria (Deibert ed., 1976). The procedure was to declare a day "experimental" at the first appearance of a 35 dBZ radar echo inside the northern area. Then the next member in a random series of envelopes was opened and the "seed" or "no-seed" instruction contained therein was carried out. If the instruction was "seed", all storms with radar reflectivities greater than 35 dBZ occurring within the project area were seeded for the remainder of the day. If the instruction was "no-seed", storms in the northern area were not seeded unless they were moving southward and expected to enter the southern area, in which case the no-seed decision was overruled and the storms seeded.

A buffer zone was established between the northern and southern areas to facilitate earlier seeding of southward-moving storms close to the southern area border. Storms that formed in this zone and were forecast or observed to move south or east were seeded as though they were in the southern area. If the storm was forecast to track northward, the zone was considered as part of the northern area and randomization procedures were used.

On 23 July, 1976 the AWMB authorized the project management to extend the limits of the northern project area to 176 km (110 mi) towards the northwest in order to include what is called a storm "breeding" area, and enable earlier seeding of storms moving into the area from that direction.

In the southern area, the 35 dBZ radar reflectivity criterion for initiating seeding of all storms was used. However, when the forecast called for large hail, seeding often commenced prior to the first appearance of a 35 dBZ echo.

1.3 Alberta Hail Project Evaluation

Evaluation of the AHP to date has been based primarily on statistical tests on hailfall measurements from "seed" and "no-seed" hailstorms from the randomized experiment (Wong, 1975, Wong, 1976). However, due to the high degree of variability in space and time of the output of hail from a storm, large numbers of seeded and unseeded cases must be observed in order to detect any differences between the two with adequate statistical confidence. It appears that unless the seeding is very effective, conventional statistical analyses require periods of time which may be unacceptable in many places (Schickendanz and Changnon, 1970; Goyer, 1975). The probability of evaluating statistically the efficacy of cloud-seeding by the AHP using present techniques was reduced after the decision was made by the AWMB to seed all potential hailstorms in both the northern and southern sectors in 1977, thus ending the randomized portion of the experiment after only 3 years of operation.

The field of hail suppression is in need of some fresh evaluation methods which are able to abridge the excessive time requirement imposed by a conventional statistical evaluation of hailfall measurements.

1.4 Radar and Evaluation

Weather radar has long been considered essential in weather-modification experiments because of its value as a short-term forecasting tool and as a basis for directing the field operations; but only recently has it been considered as a source of data to evaluate the seeding effects. The major uses of calibrated radar data, either in real time, or in subsequent analysis, as given by Changnon and

Morgan (1976), include:

1. Delineating developing hailstorms for directing seeding activities.
2. Counting hailstorms in seeded and nonseeded areas as part of an evaluation.
3. Monitoring various physical changes in storms before and after seeding for evaluation.
4. Determining the surface area covered by hail for evaluation and directing post-storm surveys.
5. Ascertaining the echo volumes containing hail for direction of seeding activities.

The usefulness of radar as an evaluation tool is that it is able to scan a large volume in space in a relatively short period of time, and is able to provide quantitative information concerning echo structures and meteorological processes. An objective evaluation must be based on a method which is able to monitor the hail-producing capacity of a hail storm prior to, during, and after cloud seeding not just the hailstorm results such as total hail mass, or the effects such as total crop damage, which are merely functions of this hail-producing capacity (Goyer, private communication). Radar may be able to accomplish this.

CHAPTER 2

THEORY

2.1 Introduction

The central problem described here is to find a radar parameter, sufficiently correlated with hailfall at the surface, to warrant its use as an evaluation parameter.

It is particularly difficult to find clear relations between radar parameters and precipitation type and rate for thunderstorms since they contain unknown and variable combinations of rain with wet, dry, or slushy hail of various sizes and concentrations. In spite of these difficulties, useful relations between radar parameters and hail have been noted by Geotis (1963), Barge (1972), Changnon and Morgan (1976), and Eccles (1976).

2.2 The Meteorological Radar Equation

The meteorological radar equation relates the precipitation particles which comprise the illuminated "target" to the echo power received. Probert-Jones (1962), showed that the meteorological radar equation is obtained by substituting the "radar reflectivity" η, of small spherical drops, as given by (2.2.1):

$$\eta = \int_{\sigma} n(\sigma)\, \sigma \, d\sigma = \frac{\Sigma \sigma_i}{\text{unit volume}} = \frac{64\,\pi^5}{\lambda^4} \left| \frac{\epsilon - 1}{\epsilon + 2} \right|^2 \Sigma r^6 \qquad (2.2.1)$$

where σ_i are the radar cross-sections of all the individual scatterers, $\pi = 3.14159$, ϵ is the dielectric constant, r is the particle radius and λ is the wavelength of the radar being used; into an appropriate form of the radar equation for a distributed target given by (2.2.2):

$$\overline{P}_r \simeq \frac{\pi^3 c}{16 \ln 2} \frac{P_t \tau}{\lambda^2} G^2 \theta \Phi \frac{1}{R^2} \left| \frac{\varepsilon - 1}{\varepsilon + 2} \right|^2 \Sigma r^6 \qquad (2.2.2)$$

where c is the speed of light (3×10^8 ms^{-1}), $\overline{P}_r$ is the average returned power, P_t is the peak transmitted power, τ is the pulse duration, G is the antenna gain, θ and Φ are the azimuth and elevation beamwidths respectively, and R is the distance from the radar to the target. The result is the meteorological radar equation (2.2.3):

$$\overline{P}_r \simeq \frac{c}{1024 \ln 2\, \pi^2} \underbrace{\left[P_t\, \tau\, \lambda^2\, G^2\, \theta \Phi \right]}_{\text{radar parameters}} \underbrace{\frac{\eta}{R^2}}_{\text{target parameters}} \qquad (2.2.3)$$

The equation is often written in terms of the radar reflectivity factor Z. By definition:

$$Z \equiv \underset{\text{unit volume}}{\Sigma N_i D_i^6} = \frac{\lambda^4 \eta}{\pi^5} \left| \frac{\varepsilon + 2}{\varepsilon - 1} \right|^2 \qquad (2.2.4)$$

where D_i are the diameters of all the individual scatterers comprising the target, and N_i the number concentration. The meteorological radar equation in terms of the radar reflectivity factor is:

$$\overline{P}_r \simeq \frac{\pi^3 c}{1024 \ln 2} \left[\frac{P_t\, \tau\, G^2\, \theta \Phi}{\lambda^2} \right] \left[\frac{Z}{R^2} \left| \frac{\varepsilon - 1}{\varepsilon + 2} \right|^2 \right] \qquad (2.2.5)$$

According to Smith (1970), the most important assumptions underlying the meteorological radar equation are:

1. The scatterers are homogeneous dielectric spheres, with diameters small compared to the wavelength, allowing Rayleigh scattering theory to be used. This applies to water spheres with $D_i < 0.07\ \lambda$ (Gunn and East, 1954), and to ice spheres with $D_i < 0.16\ \lambda$ (Ryde, 1946).
2. The illuminated volume is filled with scatterers.
3. The radar reflectivity factor Z is uniform throughout the illuminated volume.
4. The scatterers all have the same dielectric constant, that is, they are all water drops or all ice spheres.
5. Multiple scattering is negligible.
6. The main lobe of the antenna beam pattern can be described adequately by the Gaussian function.
7. Microwave attenuation along the propagation path between the radar and the target is negligible.
8. The incident and back-scattered waves are linearly polarized.

Where one or more of the assumptions break down (2.2.4) can be used to define an "equivalent radar reflectivity factor" Z_e. Z_e is sometimes referred to as a measure of "what the radar sees", and can be considered to be a parameter which is calculated from the radar measurements. For hailstorms (2.2.5) should more appropriately be written as:

$$\overline{P}_r \simeq \frac{\pi^3 c}{1024 \ln 2} \left[\frac{P_t \tau G^2 \theta \Phi}{\lambda^2} \right] \left[\frac{Z_e}{R^2} \left| \frac{\epsilon - 1}{\epsilon + 2} \right|^2 \right] \qquad (2.2.6)$$

2.3 The Evaluation Parameter

According to the hypothesis being tested by the AHP, the size distribution of hailstones will be shifted towards smaller sizes and their number concentration will be increased as a result of effective seeding. This stems from the hypothesis that the large, damaging hailstones occur because of a natural deficiency of ice nuclei, and that the injection of suitable numbers of ice nuclei (AgI) into the storm promotes the formation of a larger number of smaller, less damaging hailstones, many of which could melt during their fall to the surface.

If the hypothesis is correct, what changes in the radar reflectivity are expected? From its definition in (2.2.4), the radar reflectivity factor varies as the sixth power of the target diameter and only as the first power of the number concentration of the scatterers. Eccles (1976), found that for hail below the 0°C level the relation is:

$$Z = \Sigma D_1^{5.26}$$

and above the 0°C level:

$$Z = \Sigma D_i^{5.5}$$

These are very close to the Rayleigh relation.

As an example, assume that a volume in space contains a hailstone concentration of .01 m^{-3}, with each hailstone having a diameter of 20 mm. The radar reflectivity factor is:

$$Z_1 = \Sigma N_1 D_1^6 = (.01\ m^{-3})(20\ mm)^6$$

$$= 6.40 \times 10^{5}\ \mathrm{mm}^{6}\ \mathrm{m}^{-3}$$

$$= 58.06\ \mathrm{dBZ}$$

According to English (1973) the natural concentration would have to be increased by at least a factor of 100 in order for depletion to become significant. Assuming that the supply of supercooled water is fixed, the new diameter of the hailstones will be D_2 where:

$$D_2 = 2\left(\frac{N_1 r_1^{3}}{N_2}\right)^{1/3} = \left(\frac{(.01)\ (10^{3})}{1.0}\right)^{1/3} = 4.31\ \mathrm{mm}$$

The new radar reflectivity factor will be:

$$Z_2 = \Sigma N_2 D_2^{6} = (1.0\ \mathrm{m}^{-3})\ (4.31\ \mathrm{mm})^{6}$$

$$= 6.40 \times 10^{3}\ \mathrm{mm}^{6}\ \mathrm{m}^{-3}$$

$$= 38.06\ \mathrm{dBZ}$$

The radar reflectivity factor has been reduced by a factor of 100 (20 dBZ). Therefore, effective seeding should lead to a decrease in the reflectivity of the volume which contains the hailstones within a storm.

Nonetheless, reflectivity alone has been shown to be a rather inconsistent indicator of hail (Barge, 1972; Changnon, 1972; Martner and Dye, 1978). However, it has been found by Chisholm (1968) and Changnon and Morgan (1976), that there is a good correlation between high surface reflectivity areas on a given day and the area of hail at the surface, and that hail shafts near the ground generally exist in steep reflectivity gradients.

With this in mind, the parameter chosen for study was radar reflectivity η, averaged over the volume of the storm echo near the surface. The modifier "near the surface" in this case means echoes returned from the 1° to 2° elevation angles of the radar antenna, but not including ground clutter. Table 2.1 gives the height above ground of the radar beam for a given range at low elevation angles. The reflectivity values received from the low levels can be assumed to come from precipitation scatterers which actually reach the ground. In this way the parameter utilizes the good correlation between high surface reflectivity areas and hailfall areas at the ground. Volume averaging is used in order to take into account the fact that the radar beam diverges with increasing range and that the reflectivity values are determined over larger volumes as the target - antenna distance increases.

A useful expression involving η can be found in (2.2.3). This equation expresses the average received power $\overline{P}_r$ in terms of the average radar cross section or reflectivity η of the array of scatterers distributed throughout the volume illuminated by the radar beam. This form is preferred because all terms are either known or easily measured, and all uncertainties are associated with the radar cross section only.

According to Smith (1970), the radar cross section depends on the following characteristics:

1. Shape
2. Size
3. Dielectric constant
4. Viewing aspect

Table 2.1: Radar Beam Height (meters above ground)

Range		Elevation Angle (degrees)			Beam Width (meters)
mi.	km	1°	2°	3°	
20	32	619	1177	1735	642
30	48	973	1811	2647	964
40	64	1358	2474	3590	1285
50	80	1773	3168	4562	1606
60	96	2218	3892	5565	1927
70	112	2693	4646	6597	2248
80	128	3198	5430	7660	2569
90	144	3733	6244	8752	2891
100	160	4298	7088	9875	3212

From equation $h = \dfrac{R(R + 2\, r_e \sin \theta)}{r_e + \sqrt{r_e^2 + R(R + 2\, r_e \sin \theta)}}$

θ = elevation in degrees

R = range in kilometers

$r_e = \frac{4}{3}$ earth's radius (mean radius of earth is 6371 km).

It should be noted that the radar cross section bears no universal relationship to the actual geometrical area of the target even though its dimensions are ($mm^2\ m^{-3}$).

The proposed evaluation parameter therefore is based on η the radar reflectivity, where:

$$\eta \equiv \sum_{\substack{\text{unit}\\ \text{volume}}} \sigma_i = \left(\frac{1024\, \ln 2\, \pi^2}{c\ [P_t\ \tau\ \lambda^2\ G^2\ \theta\ \Phi\ ]} \right) \overline{P}_r\, R^2$$

Applied to a storm situation the evaluation parameter is volume-averaged radar reflectivity η, defined as:

$$\eta = \frac{\int_0^V \eta\, d\, V}{\int_0^V dV}$$

where volume averaging is carried out over the region in space covered by the 1° to 2° elevation scans. It is proposed that η is sensitive to reflectivity changes and is able to indicate the presence of steep reflectivity gradients, which as mentioned, have also been associated with hail. This method presents a frequent measurement of the hail producing capacity of the storm. Changes in η with time are analyzed in an effort to detect cloud seeding effects.

CHAPTER 3

THE RADAR FACILITIES

3.1 The Alberta Hail Project Radar System

Figure 3.1 depicts the general aspects of the AHP radar system. All of the radar data for this thesis were obtained with the AHP S-band (10.4 cm wavelength) radar. The characteristics of the S-band radar are as follows (Barge, 1974; Leung, 1977):

frequency	2.880 GHZ
pulse repetition frequency	480 s^{-1}
pulse duration	1.75 μs
peak power (nominal)	200 kw
beam dimensions	1.15° (all planes)
antenna gain	43.2 dB (at pedestal)
antenna rotation rate	8 rpm
elevation program	Spiral scan: 1° per revolution to 8° in 1.5 min, or 20° in 3.0 min.

The S-band radar is equipped with a variable polarization antenna and a dual channel receiver, and is capable of transmitting elliptically polarized radiation at any chosen axial ratio and orientation. The received radiation is resolved by the antenna microwave circuits into its main and orthogonal components which then enter separate receiving channels. Only the main component was used in this study.

In addition, a C-band (5.4 cm wavelength) radar is used in a surveillance

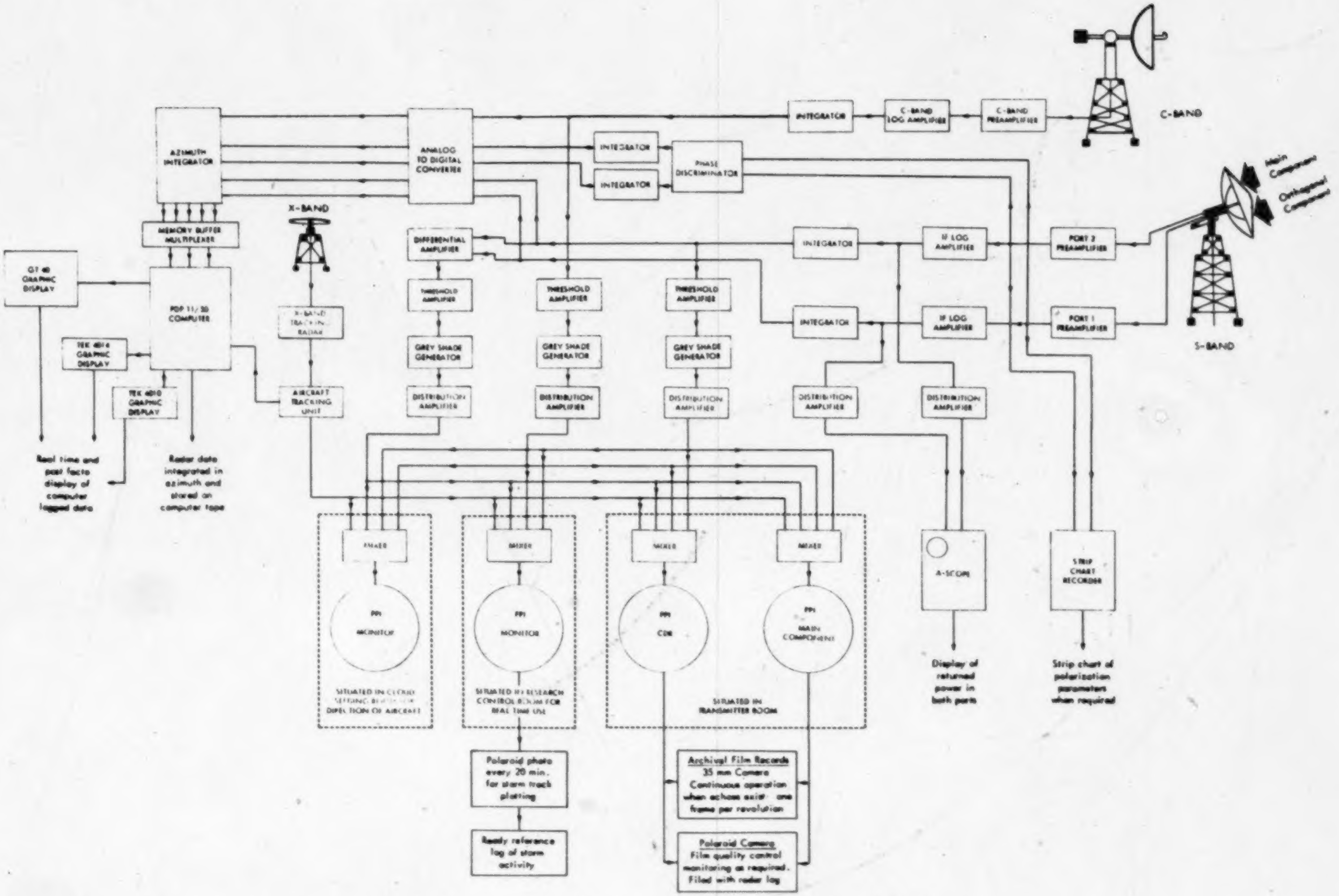
C-BAND
S-BAND
X-BAND
Main Component
Orthogonal Component
AZIMUTH INTEGRATOR
ANALOG TO DIGITAL CONVERTER
INTEGRATOR
PHASE DISCRIMINATOR
INTEGRATOR
C-BAND LOG AMPLIFIER
C-BAND PREAMPLIFIER
MEMORY BUFFER MULTIPLEXER
GT 40 GRAPHIC DISPLAY
PDP 11/20 COMPUTER
TEK 4014 GRAPHIC DISPLAY
TEK 4010 GRAPHIC DISPLAY
X-BAND TRACKING RADAR
AIRCRAFT TRACKING UNIT
DIFFERENTIAL AMPLIFIER
THRESHOLD AMPLIFIER
GREY SHADE GENERATOR
DISTRIBUTION AMPLIFIER
IF LOG AMPLIFIER
PORT 2 PREAMPLIFIER
PORT 1 PREAMPLIFIER
MIXER
PPI MONITOR
PPI CDR
PPI MAIN COMPONENT
A-SCOPE
STRIP CHART RECORDER
Real time and post facto display of computer logged data
Radar data integrated in azimuth and stored on computer tape
SITUATED IN CLOUD SEEDING AIRCRAFT FOR DIRECTION OF AIRCRAFT
SITUATED IN RESEARCH CONTROL ROOM FOR REAL TIME USE
SITUATED IN TRANSMITTER ROOM
Display of returned power in both ports
Strip chart of polarization parameters when required
Polaroid photo every 20 min. for storm track plotting
Ready reference log of storm activity
Archival Film Records 35 mm Camera Continuous operation when echoes exist - one frame per revolution
Polaroid Camera Film quality control monitoring as required. Filed with radar log

Fig. 3.1: Diagram of the radar receiver and display system. (From Leung, 1977).

mode, or when the S-band is turned off for servicing or because of strong winds. Finally an X-band (3.2 cm wavelength) radar is used for tracking aircraft.

3.2 The Alberta Hail Project Radar - Computer System

A PDP 11/50 computer system is used to record radar data on magnetic tape. Using calibration information, the numbers stored on tape are converted into received power (Barge, Humphries, and Johnson; 1976). The parameter tested here was applied to computer-recorded radar data, therefore it is important to know the characteristics of the data.

For each radar pulse the return signal is detected and logarithmically amplified. It is then averaged in 7 μs intervals or "bins" which correspond to a length of 1.05 km. The height and width of the bins are determined by the radar beam dimensions at a given range. A bin volume thus represents a volume in space for which a certain radar reflectivity has been measured. Figure 3.2 depicts the bin volume and Figure 3.3 shows a storm echo as it is recorded on magnetic tape.

The equation for calculating $\overline{\eta}$ from the stored data is:

$$\overline{\eta} = \frac{\sum\limits_{\text{bins}} k\, \overline{P}_{r_i}\, r_i^2\, V_i}{\sum\limits_{\text{bins}} V_i}$$

where: $$k = \frac{1024\, \ln 2\, \pi^2}{c\, P_t\, \tau\, \lambda^2\, G^2\, \theta\, \Phi}$$

and the bin volume is given as

$$V_i \simeq R_i^2\, \theta\, \Phi\, \Delta R \qquad \Delta R = 1.05 \text{ km}$$

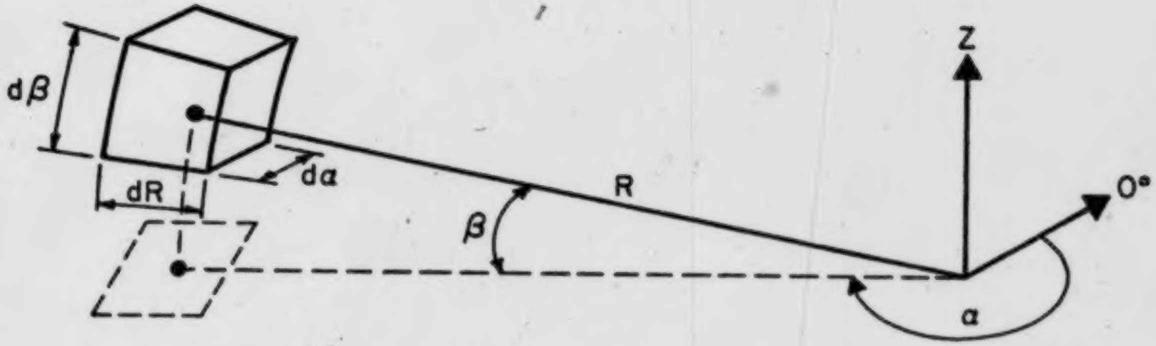
Z
0°
dβ
dR
dα
R
β
α

Fig. 3.2: Radar beam "bin" volume representation.

```
******************************************************************************
******************************************************************************
******************************************************************************
******************************************************************************
******************************************************************************
******************************************************************************
******************************************************************************
******************************************************************************
********************************************21********************************
******************************************2422********************************
**************************************2128322620******************************
**************************************2638372922******************************
**************************************2133373320******************************
****************************************232624********************************
****************************************28282721******************************
****************************************212424********************************
******************************************************************************
******************************************************************************
**************************************202222**********************************
************************************222931272722******************************
************************************223134333225******************************
**********************************2128323837342621****************************
****************************313136424145424039343131**************************
******************2625293737535150504643414244433433**************************
****************234645405351575452474239424442353221**************************
****************274754555353595754494336424137292121**************************
****************21315158585858575247443639363534292624************************
********************353942445051464644333135424034353936**********************
******************2034251820304137393626314550403434374437********************
******************1925********222223323349515043403022263721******************
******************18****************213142343846383121************************
********************************************29362824**************************
******************************************************************************
******************************************************************************
******************************************************************************
******************************************************************************
******************************************************************************
******************************************************************************
******************************************************************************
******************************************************************************
******************************************************************************
******************************************************************************
******************************************************************************
******************************************************************************
```

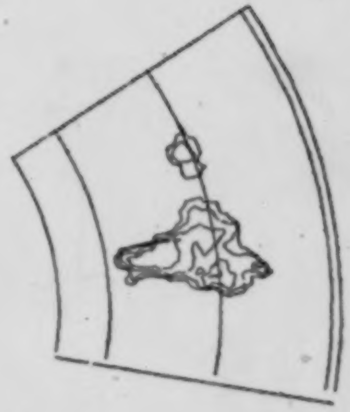

Fig. 3.3: PPI echo in digitized form.

The summation is over the total number of bins which comprise the echo.

3.3 Error Analysis

The AHP radar is considered to be a stable system and its specifications fluctuate very little (Humphries, Barge and Johnson, 1977). Since the analysis deals mostly with changes in η, the primary concern is with "relative errors". Although the value of η calculated for the AHP radar system (or most meteorological radars, for that matter) may have an absolute error of ± 3 dB (± 50%), the relative error is considerably less. The absolute error would appropriately be adopted when comparing $\bar{\eta}$ values with those obtained by a radar system elsewhere.

The main source of relative error is "signal fluctuation "due to a fluctuating echo with other errors assumed to be constant. From theoretical considerations Marshall (1971) showed that if, on a plan-position indicator (PPI) display, every independent datum was displayed separately with signal level reported accurately, the resolution in position would be as good as theoretically possible and the target intensity level would be known everywhere with a standard deviation σ = 5.57 dB. If the data are combined and averaged in groups of j independent data, the standard deviation is related to the number of independent data by:

$$\sigma = \frac{5.57}{\sqrt{j}} \quad \text{dB}$$

The AHP S-band radar has 4 independent samples per range bin and

10 pulses per degree azimuth (Barge, Humphries, and Johnson, 1976). The computer averages 10 pulses for each range bin; consequently 40 samples of the returned power are averaged. Not all of the samples are independent, however, since decorrelation in azimuth occurs over one beam-width. Moreover pulse-to-pulse frequency shifts of the magnetron and "shuffling" of precipitation also lead to further decorrelation (Atlas, 1964). The number of independent samples contributing to each average is assumed to be 16 and therefore, the target intensity level would have a standard deviation of:

$$\sigma = \frac{5.57}{\sqrt{16}} = 1.39 \text{ dB}$$

Since this analysis involves averaging over a number of bins, for a given echo the appropriate standard deviation for $\overline{\eta}$ may in addition be decreased by the factor $1/\sqrt{m}$ where m is the total number of bins. Figure 3.4 shows the relation between the relative error involved in $\overline{\eta}$ and the number of bins in the echo. Since only well-developed storms were seeded, the number of bins usually exceeded 100. Therefore during the times of interest a relative error of less than $\pm$ 0.139 dB (3%) may be assumed. Adding the relative error due to transmitter fluctuations, which may be assumed to be no more than $\pm$ .5 dB (12%), the relative error involved with $\overline{\eta}$ is not more than $\pm$ 0.639 dB (15%).

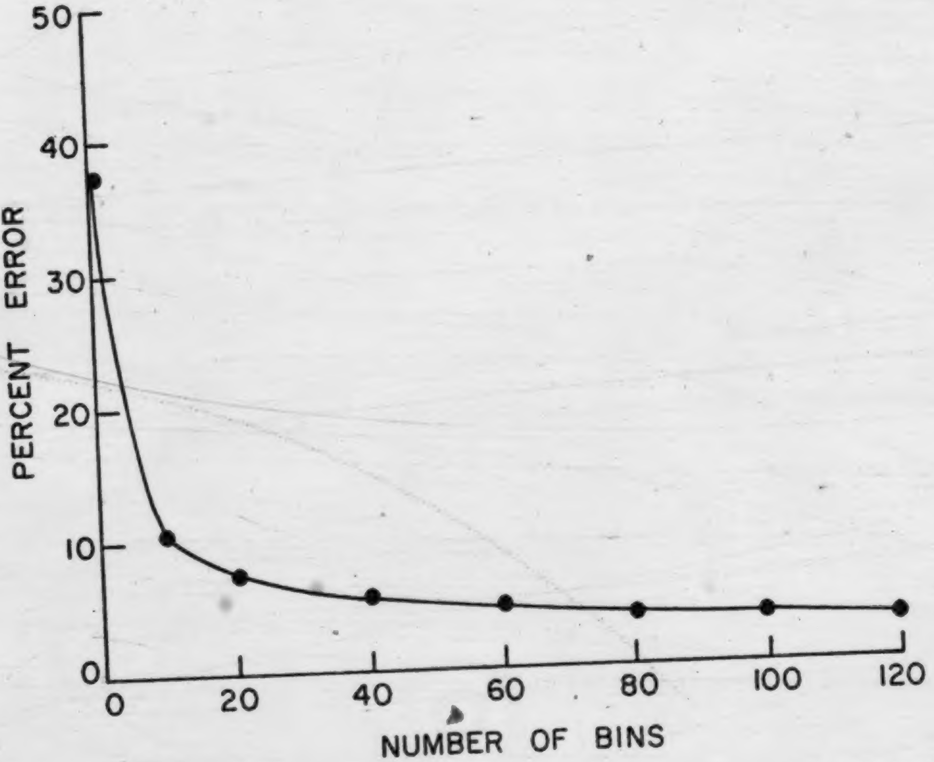

Fig. 3.4: Relative error (percent) in $\overline{n}$ calculation as a function of the number of bins in a given PPI echo.

CHAPTER 4

DATA ANALYSIS

4.1 Analysis of Digital Radar Data

The computer was programmed to perform the calculation of $\overline{\eta}$ (see Appendix C for program). However, before numerical operations were carried out the digitized data had to be properly prepared. This operation was accomplished with the AHP interactive computer display facility. Briefly, the interactive display facility provides the following capabilities (Ramsden et al., 1976):

1. The data are displayed in the conventional PPI format.
2. The data analyst is provided with a means to define a portion of the PPI, both for display purposes and for extraction of data for subsequent numerical processing.
3. Any portion of the data may be displayed at any chosen scale in any desired degree of detail up to the maximum resolution provided by the data.
4. Permanent copies of any display are available immediately.

The interactive display facility is operated from a cathode-ray-tube (CRT) graphical display terminal, and uses a CRT screen both for input of instructions and for output of graphical displays. Figure 4.1 shows the basic display which consists of the PPI display, the antenna elevation display, and the command list. The command list is displayed at all times and input of a command is accomplished simply by positioning a cross-hair cursor over a desired command in the list and pressing any key on the keyboard.

Initially the display consists of a complete PPI. However, the analyst

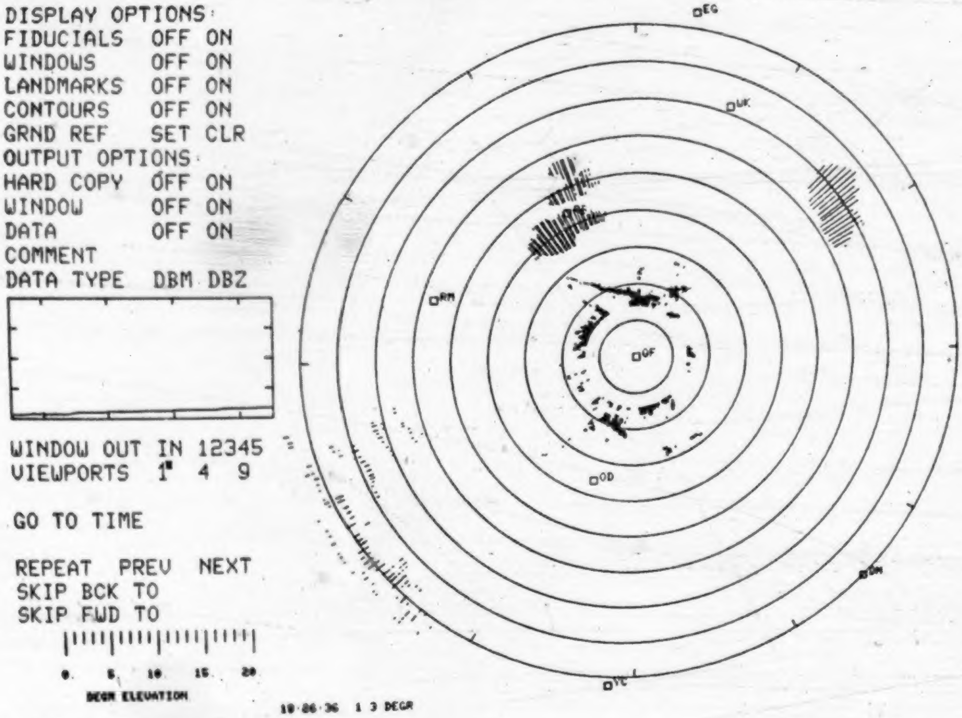
DISPLAY OPTIONS
FIDUCIALS OFF ON
WINDOWS OFF ON
LANDMARKS OFF ON
CONTOURS OFF ON
GRND REF SET CLR
OUTPUT OPTIONS
HARD COPY OFF ON
WINDOW OFF ON
DATA OFF ON
COMMENT
DATA TYPE DBM DBZ
WINDOW OUT IN 12345
VIEWPORTS 1 4 9
GO TO TIME
REPEAT PREV NEXT
SKIP BCK TO
SKIP FWD TO
0. 5. 10. 15. 20
DEGR ELEVATION
10·26·36 1.3 DEGR
EG
UK
RM
GF
OD
DM
YC

Fig. 4.1: The basic radar display using the interactive computer display facility. (From Ramsden et al., 1976).

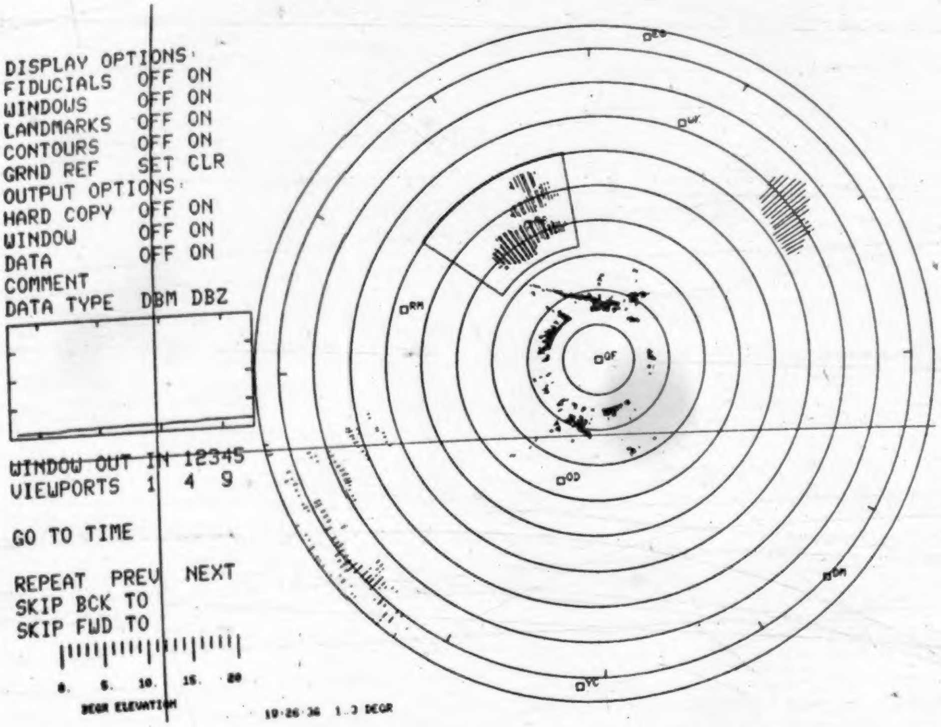
DISPLAY OPTIONS
FIDUCIALS OFF ON
WINDOWS OFF ON
LANDMARKS OFF ON
CONTOURS OFF ON
GRND REF SET CLR
OUTPUT OPTIONS
HARD COPY OFF ON
WINDOW OFF ON
DATA OFF ON
COMMENT
DATA TYPE DBM DBZ
WINDOW OUT IN 12345
VIEWPORTS 1 4 9
GO TO TIME
REPEAT PREV NEXT
SKIP BCK TO
SKIP FWD TO
0. 5. 10. 15. 20
DEGR ELEVATION
10·26·36 1.3 DEGR
EG
UK
RM
GF
OD
DM
YC

Fig. 4.2: The display shown in Fig. 4.1 after a portion of the PPI has been outlined for further detailed study. Note the cross-hair cursor positioned over the "window in" command. (From Ramsden et al., 1976).

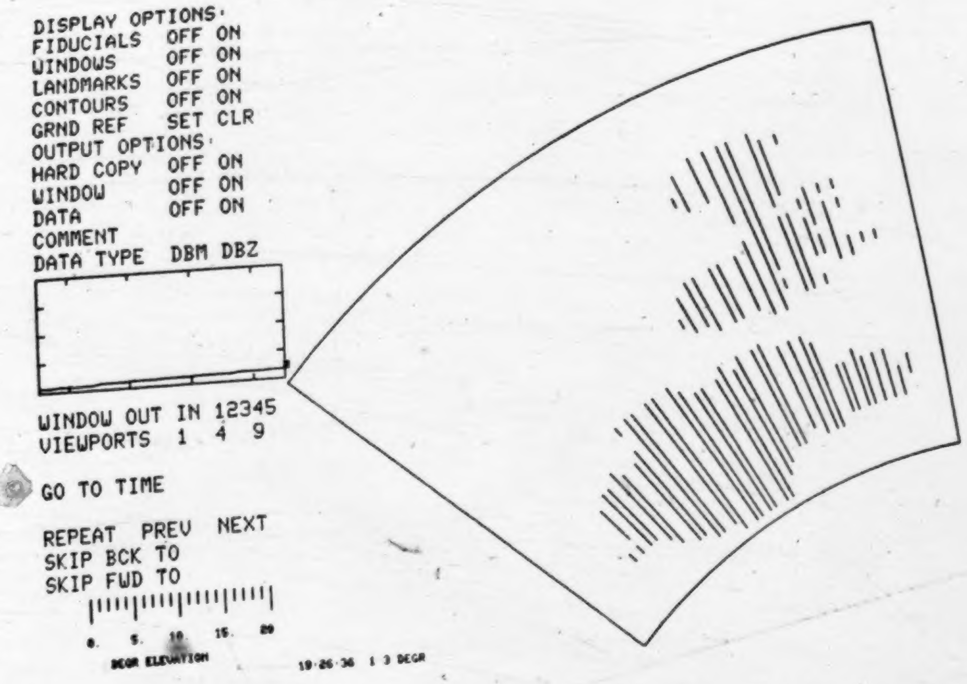
DISPLAY OPTIONS:
FIDUCIALS OFF ON
WINDOWS OFF ON
LANDMARKS OFF ON
CONTOURS OFF ON
GRND REF SET CLR
OUTPUT OPTIONS:
HARD COPY OFF ON
WINDOW OFF ON
DATA OFF ON
COMMENT
DATA TYPE DBM DBZ
WINDOW OUT IN 12345
VIEWPORTS 1 4 9
GO TO TIME
REPEAT PREV NEXT
SKIP BCK TO
SKIP FWD TO
0. 5. 10. 15. 20
DEGR ELEVATION
19·26·36 1 3 DEGR

Fig. 4.3: The new display limited to that portion of the PPI outlined in Fig. 4.2. (From Ramsden et al., 1976).

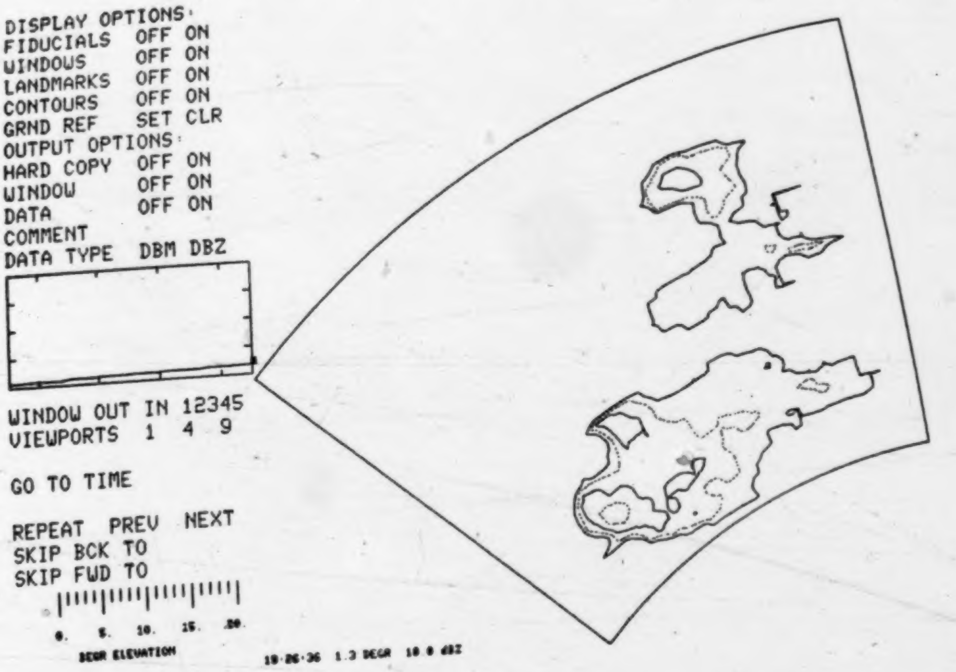
DISPLAY OPTIONS:
FIDUCIALS OFF ON
WINDOWS OFF ON
LANDMARKS OFF ON
CONTOURS OFF ON
GRND REF SET CLR
OUTPUT OPTIONS:
HARD COPY OFF ON
WINDOW OFF ON
DATA OFF ON
COMMENT
DATA TYPE DBM DBZ
WINDOW OUT IN 12345
VIEWPORTS 1 4 9
GO TO TIME
REPEAT PREV NEXT
SKIP BCK TO
SKIP FWD TO
0. 5. 10. 15. 20.
DEGR ELEVATION
19·26·36 1.3 DEGR 10.0 dBZ

Fig. 4.4: The same data shown in Fig. 4.3 displayed by means of reflectivity contours. (From Ramsden et al., 1976).

is able to select a portion of the PPI (a "window") to extract data for numerical processing. Figures 4.2 and 4.3 depict the "window" feature. Subsequent displays will consist only of those data lying within the indicated portion of the PPI.

The radar echoes can be represented by radial lines or by contours of equivalent radar reflectivity using the "contours on" display option (Figure 4.4). The lowest contour value is always 20 dBZ; the contour interval may be chosen by the analyst to be any value from 0.5 dBZ to 20 dBZ.

Using this technique, individual storms were tracked and the data extracted from which the values for $\bar{\eta}$ were calculated.

4.2 Storm Selection

The analysis was aimed at determining what effects cloud seeding may have on the parameter $\bar{\eta}$ and if indeed the parameter $\bar{\eta}$ is correlated with hailfall at the surface to a degree sufficient to warrant its use as an evaluation parameter. Therefore it was necessary to choose storms where the time of seeding and the extent of hailfall were accurately known.

Only storms with well-defined boundaries during most of their lifetime were chosen. In general, a storm was chosen if a window could be drawn around the storm echo, and tracked in this way throughout its' lifetime within the project area, with no other storms intruding or merging with it. This eliminated storms which were parts of "squall lines" or of agglomerations of many embedded storms. All storms selected were from the northern "randomized" area of the project. Only those which tracked sufficiently distant (more than 36 km) from the radar antenna thus permitting near constant viewing aspect were used. Both seeded and non-seeded storms were chosen in this manner.

4.3 Data Sample

For the purposes here, 10 storms were chosen for analysis. Of these, 5 storms were seeded and 5 storms were not seeded. Hail was reported to have fallen from 9 of the storms, with only rain reported from the remaining storm. The storms will be referred to by date, with letters A, B, etc. added to distinguish several storms occurring on the same day. Table 4.1 lists the entire storm sample for the analysis.

Table 4.1 Storm Sample

No.		
1.	20 JULY 1975: A	Rain: non-seeded
2.	20 JULY 1975: B	Hail: seeded
3.	20 JULY 1975: C	Hail: seeded
4.	17 JULY 1976: A	Hail: seeded
5.	17 JULY 1976: B	Hail: non-seeded*
6.	6 AUGUST 1976	Hail: seeded
7.	12 AUGUST 1976	Hail: non-seeded
8.	15 AUGUST 1976	Hail: non-seeded
9.	20 AUGUST 1976	Hail: seeded
10.	24 AUGUST 1976	Hail: non-seeded

---

* 1 cloud top flare was dropped into the storm early in its lifetime but for this analysis it has been considered to be non-seeded.

The 7 storms from the 1976 hail season were the only storms in 1976 which met the requirements for selection, therefore any subjective bias in sample selection in these cases is minimal.

The 3 storms of 20 July 1975 were chosen mostly for comparison purposes. As will be discussed later, the 1975 digitized radar data was often of questionable quality with certain portions of it missing. 20 July, 1975 was a rare occasion in that 3 storms met the requirements for selection thus, the storm data could be compared with other data on the same day as well as the 1976 data, to see if the quality was consistent and acceptable for this type of analysis.

The data were extracted and the values of $\bar{\eta}$ were calculated. In most cases a PPI was obtained every 1.5 minutes. However, certain portions of the storms on 12 August 1976, 15 August 1976, and 24 August 1976, occurred while the radar was on a full 20° elevation program and, therefore, a PPI at the desired level occurred at 3.0 min intervals.

4.4 The Relation Between $\bar{\eta}$ and Hailfall at the Surface

In order to use the parameter $\bar{\eta}$ to test for cloud seeding effects, it was first necessary to verify its' assumed relation with hailfall at the surface. Responses from farmers using hail reporting cards, and information solicited through telephone surveys following storms, were the major sources of hailfall data.

Since radar reflectivity (and consequently the evaluation parameter) vary as the sixth power of the target diameter and only as the first power of the number concentration, it was decided to relate the reported maximum size of the hail which fell at the surface to the value of $\bar{\eta}$ which existed at that time. Although the time of the echo for which $\bar{\eta}$ is calculated is known to within an accuracy of several seconds, the time of a hail report by a farmer is unlikely to have a precision better than 5 minutes (Williams and Douglas, 1963). Moreover, because certain regions within the project area, particularly the western portion, are sparsely populated, hail reports may not have been received from regions where hail fell. Furthermore, even if a hail report is correct, the comparison with $\bar{\eta}$ is accurate only if the point surface observation is representative of the precipitation which fell from the volume sampled by the radar beam.

The method used to test the relation of $\bar{\eta}$ with hailfall at the surface was to combine the maximum hailsize reports with the values of $\bar{\eta}$ recorded closest in time for all 9 hailstorms. The time involved for the hail to fall from the echo volume to the surface was not accounted for in view of the accuracy of the reports. Although some reports are in error and contribute to the variance, by combining all of the reports and assuming more good reports than bad reports, the averages are likely to indicate the true relation.

The farmers are asked to report the maximum hailsize in one of 6 categories associated with the sizes of familiar objects (Table 4.2). A total of 358 hail reports were received from the 9 hailstorms that were analysed. Figure 4.5 shows the cumulative distribution of all the hail reports according to their $\bar{\eta}$ values. The range of $\bar{\eta}$ values for which hail was reported was from $0.62 \times 10^{-11} \mathrm{cm}^{-1}$ to $2.57 \times 10^{-9} \mathrm{cm}^{-1}$, with a median value of $4.20 \times 10^{-10} \mathrm{cm}^{-1}$.

Figure 4.6 shows the cumulative frequency curve for the individual maximum-size categories. The categories for golfball and larger-size hail were

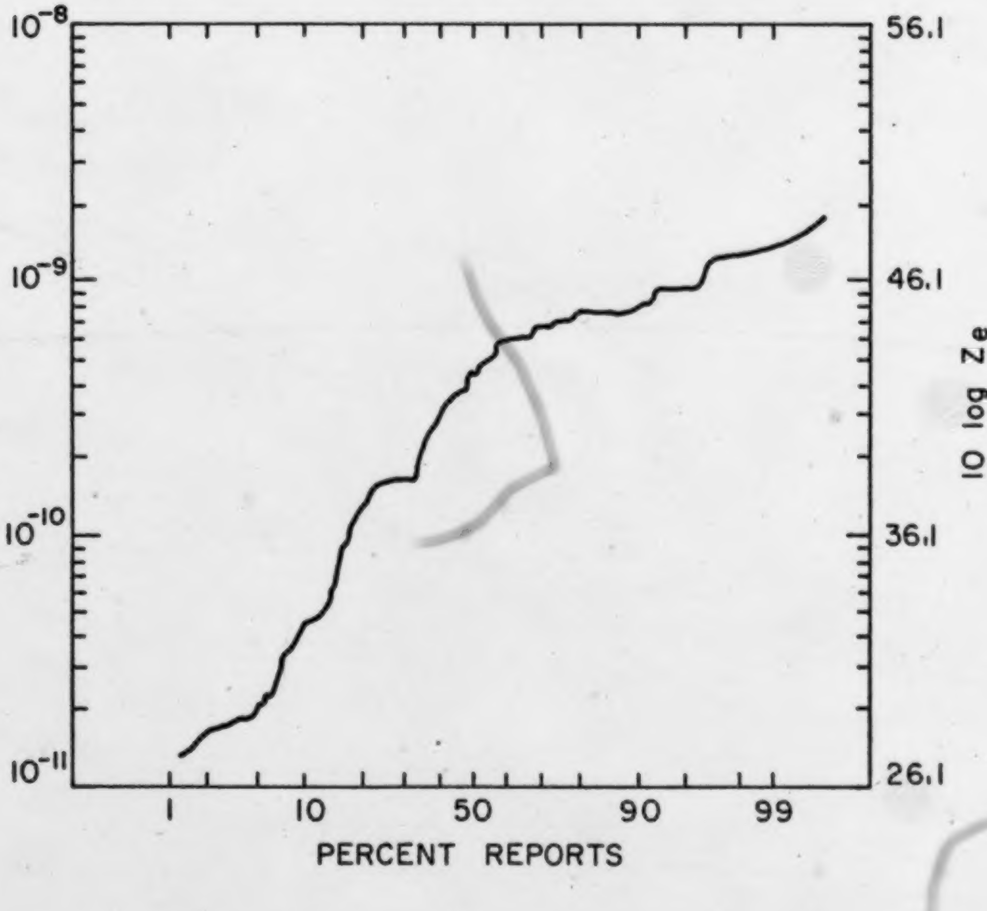

Fig. 4.5: The cumulative distribution of all hail reports according to $\bar{\eta}$.

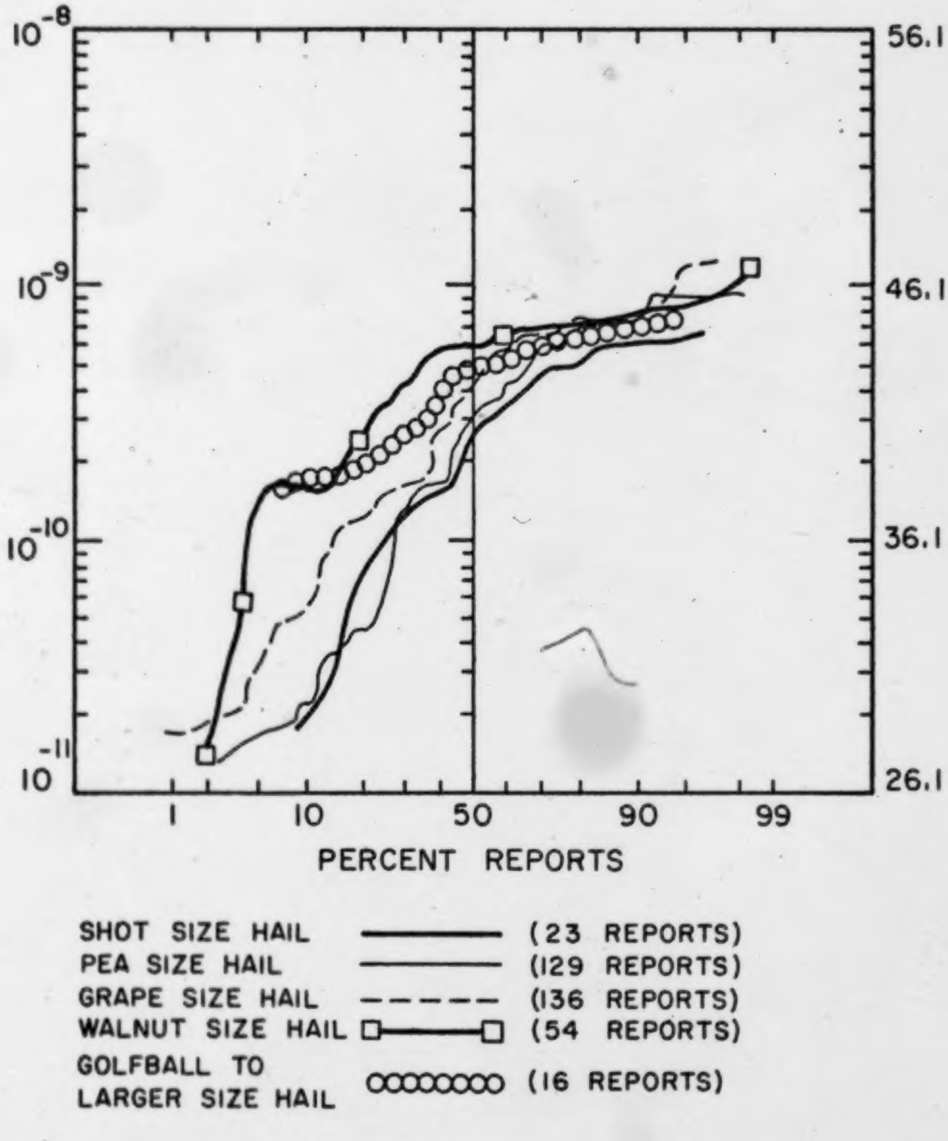

Fig. 4.6: The cumulative distribution for the individual maximum-hailsize categories versus $\bar{\eta}$.

Table 4.2: Hailsize name and the assumed hail diameter range.

Hailsize Name	Assumed Diameter Range (cm)
Shot	.1 - .3
Pea	.4 - 1.2
Grape	1.3 - 2.0
Walnut	2.1 - 3.2
Golfball	3.3 - 5.2
Larger	>5.2

Source: Wojtiw, 1975b

---

combined since only 1 report of hail larger than golfball size was reported. One can see that, within each size category, a large spread in $\bar{\eta}$ values occurred. The larger $\bar{\eta}$ values within the smaller hailsize categories may be due to the fact that the farmer may be located at the edge of the hailswath and receiving small hail even though the storm may be producing large hail which is falling elsewhere. However, if $\bar{\eta}$ is correlated well with hailfall, large hail should not be associated with small values of $\bar{\eta}$. Walnut size hail was reported at quite low values of $\bar{\eta}$, but these reports are few and may well be ones where the time is in considerable error, or the maximum hailsize was overestimated.

A plot of the mean $\bar{\eta}$ values for the 5 categories of maximum hailsize, along with the 90% confidence intervals for the individual means calculated using the statistic t-test, is given in Figure 4.7. The median and mean $\bar{\eta}$ values for the individual size categories indicate that larger hail tends to occur with increasing

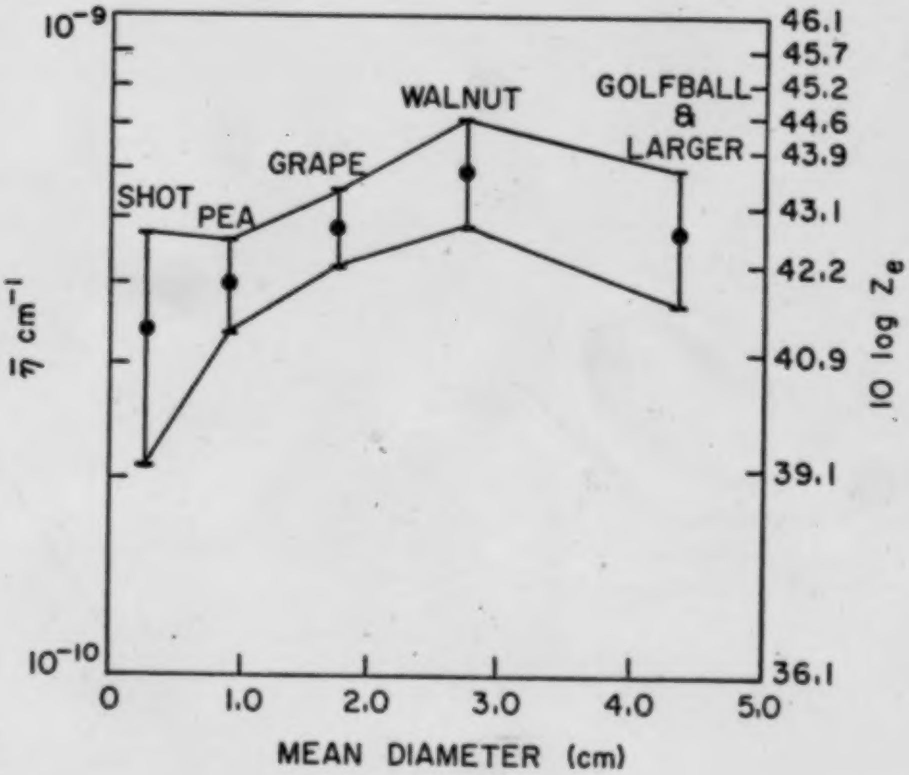

Fig. 4.7: The mean $\bar{\eta}$ values obtained for the five categories of maximum hailsize, and the 90% confidence interval.

$\bar{\eta}$ values for the maximum size categories shot through walnut. A deviation in the trend occurs for the hailsize category of golfball and larger. There is a sampling problem relating to the largest hail sizes since only 16 reports of golfball and larger size hail were received; however, this trend of increasing, then decreasing reflectivity with size has been found by others. Theoretical calculations for monodisperse hail by Atlas and Ludlam (1961) showed that radar reflectivity has an oscillatory behavior once the size of the scattering particles extends beyond the Rayleigh region (Figure 4.8). The maxima and minima in reflectivity for scatterers which are no longer small with respect to the radar wavelength are characteristic of Mie's scattering functions. Sulakvelidze et al. (1965) obtained smooth curves for the diameter versus radar reflectivity relationship for a series of calculated hailstone spectra (Figure 4.9). The $\bar{\eta}$ versus maximum hailsize relation summarized in Figure 4.7 resembles the curves of the theoretical work cited. Therefore, the decreasing values of $\bar{\eta}$ associated with hail larger then 3 cm diameter are not likely due to a sampling problem, but rather, due to the inherent limitations of radar to adequately differentiate between large scatterers.

It is worthy to note the merit of the 10 cm wavelength radar when viewing hail. Shorter wavelength radars yield oscillating radar reflectivities at smaller target diameters and also attenuate severely, thus making hail detection more difficult.

The comparison of maximum hailsize to $\bar{\eta}$ values in this case using a 10.4 cm wavelength radar, indicates that $\bar{\eta}$ is related to hailfall at the surface

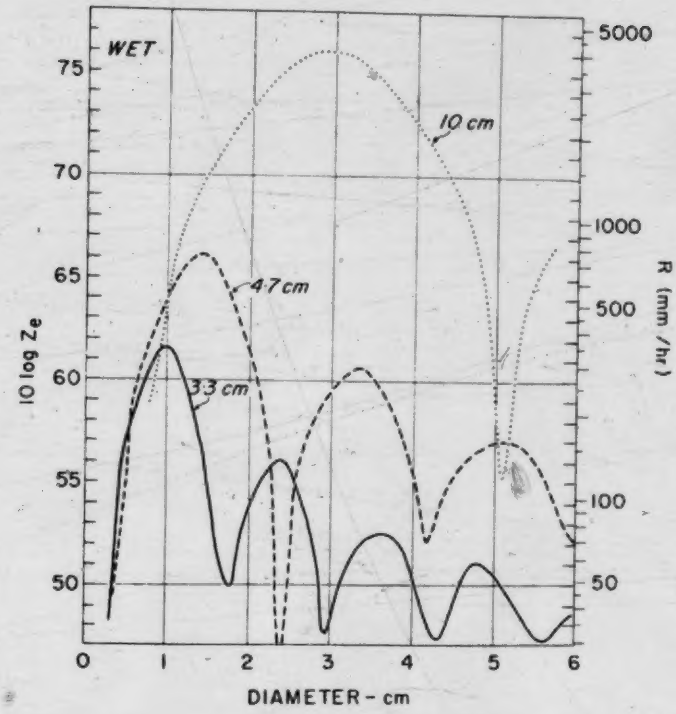

Fig. 4.8: Radar reflectivity as a function of the diameter of uniform, wet-ice spheres. The units of Z_e are (mm^6m^{-3}). (From Atlas and Ludlam, 1961).

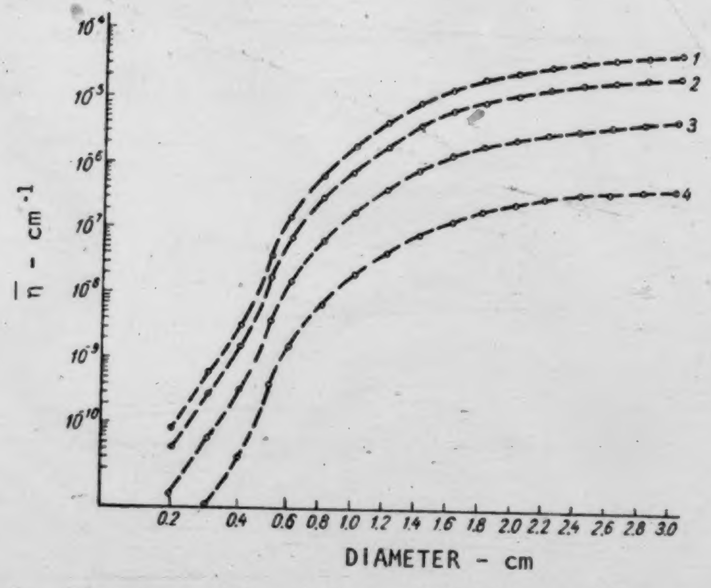

Fig. 4.9: Diameter versus radar reflectivity from a hail spectrum for 10.0 cm wavelength radar. Hail concentrations: (1) $10m^{-3}$; (2) $5m^{-3}$; (3) $1m^{-3}$; (4) $0.01m^{-3}$. (From Sulakvelidze et al.,1965).

such that the probability of larger size hail falling at the surface increases with increasing values of $\bar{\eta}$ for hailstone diameters less than 3 cm.

4.5 Time Series Analysis

For each storm the $\bar{\eta}$ values were plotted as a function of time. For seeded storms, the type, amount and time of seeding were also noted. Although the detailed fluctuations of a time series may be quite irregular, certain statistical properties may remain fixed from one period to another. A statistical analysis was performed on each time series, to better understand the basic properties of the time series, their variability, and the characteristics of their periodic and irregular oscillations. Since the time series variate $\bar{\eta}$ is related to the type, size and amount of precipitation, such an analysis helps in the physical understanding of storms.

The time series analysis consisted of computing the power spectrum by the fast Fourier transform (FFT) method. The computer program used was one developed and tested by Lachapelle (1977). The FFT is a highly efficient procedure for computing the discrete Fourier transform (DFT) of a time series consisting of discrete data samples. Its advantage lies in the fact that the coefficients for the DFT are calculated iteratively, which results in a considerable saving of computation time. Given a record of N observations taken at a set time interval Δt, a total of N/2 harmonics can be calculated, the last one having a period of $2\Delta t$. The contribution of each harmonic to the total variance of the time series is referred to as the power of each harmonic, and the power spectrum of a time series shows the contributions of oscillations of different frequencies to the variance of the time series.

Prior to the FFT analysis, the program required that the data be modified accordingly:

1. The mean M, variance S^2, and standard deviation S, were calculated.
2. The mean was removed.
3. Zeroes were added to the data set until a desired size of 2^n was achieved.
4. The data were standardized using the relationship

   $Y_i = (x_i - M)/S$

   where $i = 1, 2, \ldots, 2^n$.

Several reasons for statistical spectroscopy on meteorological variates are given by Panofsky and Brier (1963):

1. The spectrum may be necessary to understand the physics underlying the variation of a time series.
2. Significant maxima and minima are important for forecasting, even if they are not sharp peaks or troughs, for they indicate the likelihood or unlikelihood of variations with certain average periods.
3. Cloud seeders and other personnel engaged in weather control claim they can change the spectrum significantly.
4. The extent of the spectrum shows the variability of the quantity and how quickly instruments have to respond in order to measure it.

The results of this analysis follow.

CHAPTER 5

THE 17 JULY,1976 CASE STUDIES

5.1 Introduction

Two severe hailstorms occurred on 17 July, 1976. Figure 5.1 depicts the synoptic situation which prevailed and includes a brief synoptic summary. Figure 5.2 shows the rawinsonde sounding from Calgary at 18:00 MDT which describes the environmental conditions. The two storms formed in approximately the same region and tracked approximately across the same area. What is of particular interest is that one storm was heavily seeded while the other was essentially unseeded (only one cloud-top flare released into it), because of the late hour at which it entered the project area. These two storms resulted in 242 reports of hail at the surface acceptable for this study. This represents 67.6 per cent of the total number of hail reports used in determining the relation of $\overline{n}$ with hailfall at the surface. Therefore, the relationships deduced in Chapter 4 were greatly influenced by what occurred on this day.

The radar constant used for the day was 73.2 dBm with a peak transmitted power of 286 kw.

5.2 17 July, 1976: Storm A

Storm A entered the northwest portion of the project area shortly after 19:00 MDT and tracked eastward. Figure 5.3 shows the resulting hailswath of storm A. Hail as large as golfballs was reported at the surface. The dashed line attempts to isolate the region of hail from the region where rain only was reported to have fallen. The approximate times of storm progression are also indicated. Radar-estimated storm tops exceeded 10 km AGL, with radar reflectivities greater

SYNOPTIC SUMMARY

17 JULY 1976

SYNOPSIS: AFTER 14 JULY, L/W PATTERNS SHIFTED W TEMPORARILY. WITH THE L/W RIDGE OVER ALBERTA FOR A FEW DAYS, S/W'S WERE DRIVEN NORTH OF ALBERTA AND A PRONOUNCED SURFACE HIGH PRESSURE CELL BUILT OVER WRN CANADA. THIS L/W RIDGE THEN MOVED E ONCE AGAIN ALLOWING THE FIRST OF THE NEW SERIES OF S/W TROUGHS TO REACH THE AHP AREA LATE ON THE 17TH. ALTHOUGH NOT A WELL MARKED TROUGH (NEGLIBLE PVA FLOWS), 500 MB HEIGHTS FELL RAPIDLY. MEANWHILE THE SURFACE HIGH DROPPED SE AND A WAVE FORMED ON THE FRONT IN SE B.C. THE COMBINED EFFECTS TRIGGERED THE WAITING INSTABILITY AND ONE OF THE LARGEST STORMS OF THE YEAR ENSUED.

AHP AREA: LIGHT NE SURFACE WINDS VEERING TO STRONG SW AT 500 MB. TWO LARGE STORMS FORMED RAPIDLY IN THE NORTH DURING EARLY EVENING, PROPAGATING ESE WITH TOPS EXCEEDING 12 KM.

TROUGH (T) OR RIDGE (R) PASSAGE TIME	12 HOUR 500 MB CHANGE IN				HAIL SIZE CATEGORY	NO. HAIL REPORTS N / S
	VORTICITY ($10^{-5}s^{-1}$)	HEIGHTS * (M)	THICKNESS* (M)	TEMPS. (°C)		
R-17/0100Z T-18/0600Z	0	- 30	- 60	- 2	6	286/3

* DIURNAL EFFECTS REMOVED

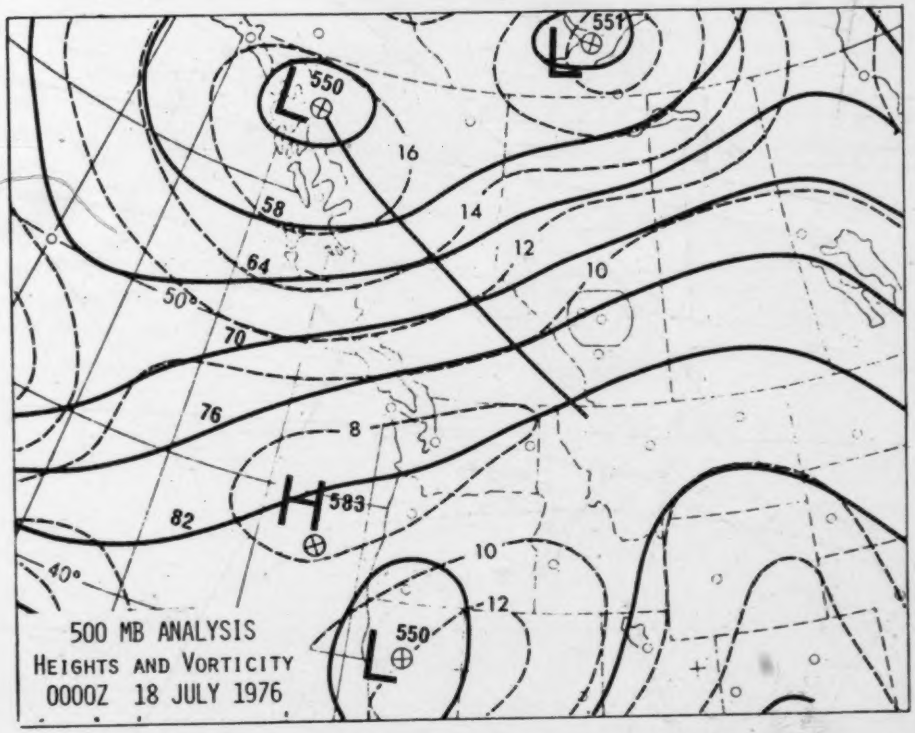

Fig. 5.1: Map showing the synoptic situation, and a brief synoptic summary for storms on 17 July, 1976. (From Deibert (ed.), 1977).

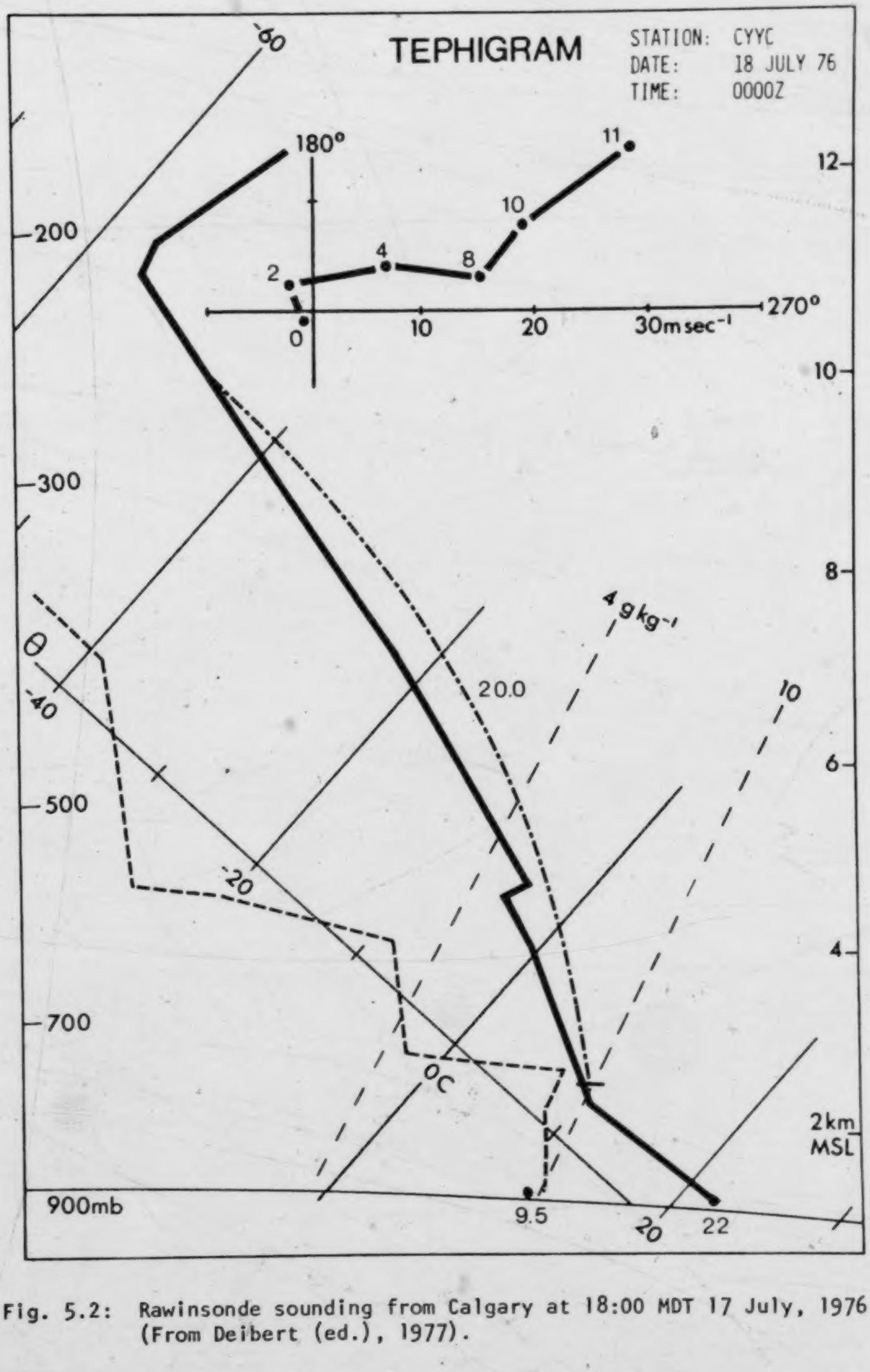

Fig. 5.2: Rawinsonde sounding from Calgary at 18:00 MDT 17 July, 1976. (From Deibert (ed.), 1977).

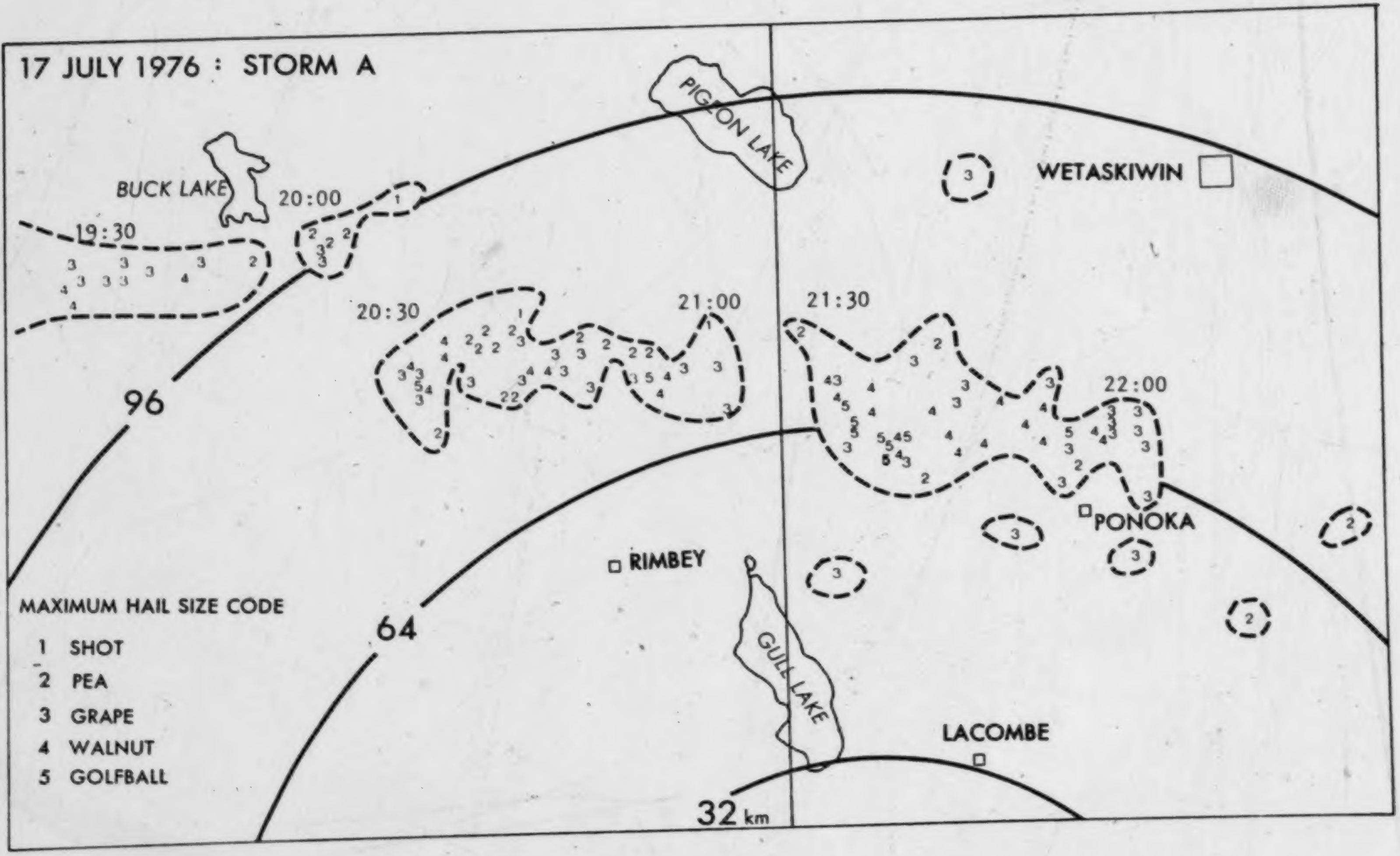
17 JULY 1976 : STORM A
BUCK LAKE
PIGEON LAKE
WETASKIWIN
19:30
20:00
20:30
21:00
21:30
22:00
96
64
32 km
RIMBEY
PONOKA
GULL LAKE
LACOMBE
MAXIMUM HAIL SIZE CODE
1 SHOT
2 PEA
3 GRAPE
4 WALNUT
5 GOLFBALL

Fig. 5.3: Map showing hailswath resulting from storm A on 17 July, 1976.

than 60 dBZ. Figures 5.4 through 5.8 show low-elevation PPI scans at approximately 15 minute intervals throughout the storm lifetime.

Figure 5.9 shows the $\bar{\eta}$ time series as computed from the digitized radar data. The right-hand vertical axis gives the equivalent radar reflectivity values computed from $\bar{\eta}$ using (2.2.4). In calculating Z_e, the quantity $[\varepsilon + 2/\varepsilon - 1]^2$ conventionally is taken to be the value for water 0.93 (Battan, 1973). The histogram at the top of the graph indicates the number of cloud-seeding flares released during each 15 minute interval as reported in the flight operations summary for the day. The dashed line superimposed on the time series is the trend in the data determined by using a low-pass Tukey filter described in Appendix A.

It is of particular interest to note that the $\bar{\eta}$ value at 21:00 MDT is approximately 1.6×10^{-10} cm^{-1}, a relatively low value, whereas the PPI scan at 21:00:41 MDT indicates that reflectivity exceeded 60 dBZ. Although one would not expect as low an $\bar{\eta}$ value with such high reflectivity, it is apparent from the PPI that the reason is that high reflectivity volumes have decreased while the overall storm extent, bounded by the 20 dBZ contour, has increased slightly. The time 21:00 MDT corresponded with the break in the hailswath at the surface which indicates that the storm intensity decreased significantly at this time. This would not be deduced readily from the PPI alone. In fact, one may be inclined to suspect the storm to have intensified since the areal extent of the echo had increased. In this instance the parameter $\bar{\eta}$ appears to be quite sensitive to storm intensity.

5.3 Storm A: Power Spectrum

The power spectrum of the raw data is presented in Figure 5.10. Although

Fig. 5.4: PPI echoes for storm A on 17 July, 1976. Elevation - 2.0°
Reflectivity = from 20dBZ by 10dBZ. Time = 19:30 - 20:15 MDT.

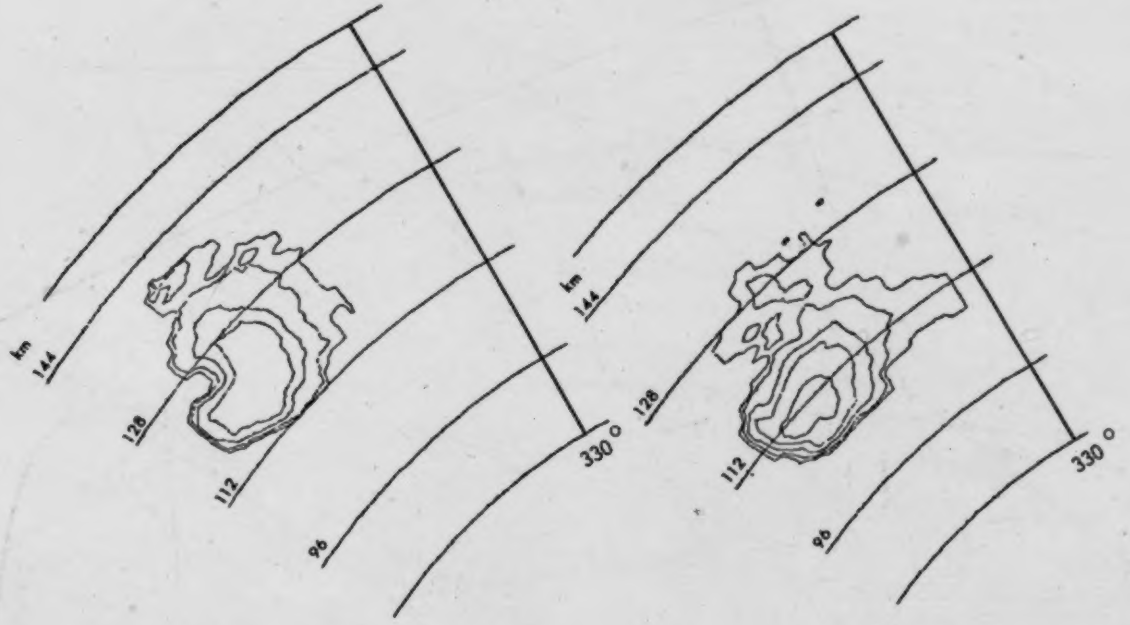

19:30:17 $\overline{\eta} = 6.73\times10^{-10}\text{cm}^{-1}$ 19:45:13 $\overline{\eta} = 2.57\times10^{-9}\text{cm}^{-1}$

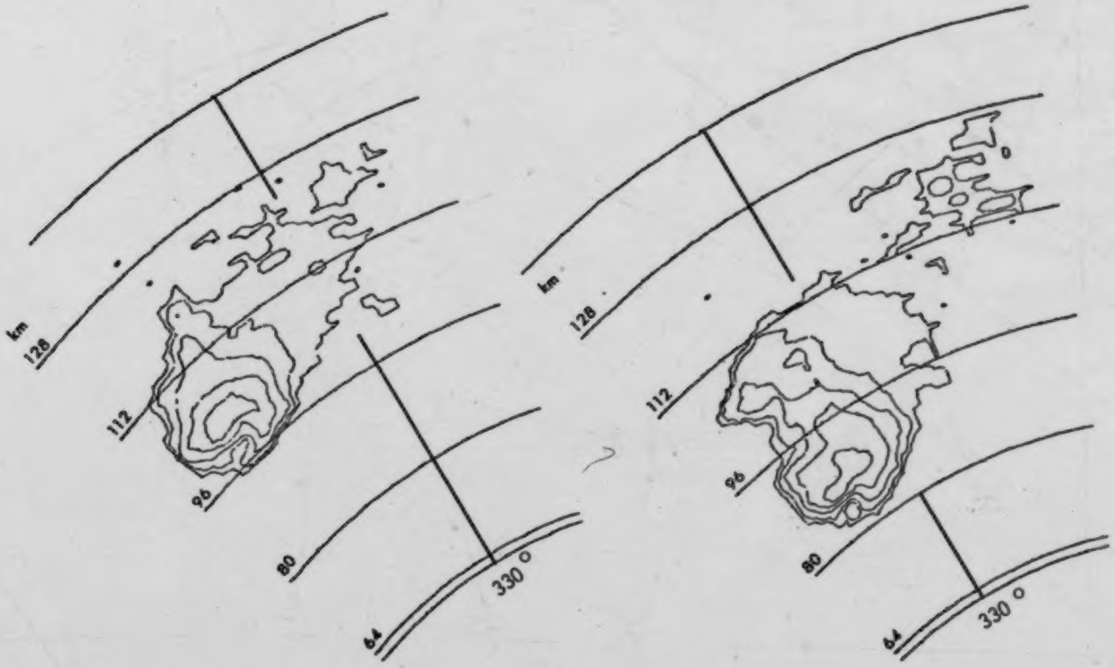

20:01:03 $\overline{\eta} = 1.52\times10^{-9}\text{cm}^{-1}$ 20:15:58 $\overline{\eta} = 1.30\times10^{-9}\text{cm}^{-1}$

Fig. 5.5: PPI echoes for storm A on 17 July, 1976. Elevation - 2.1° Reflectivity = from 20dBZ by 10dBZ. Time = 20:30 - 21:00 MDT.

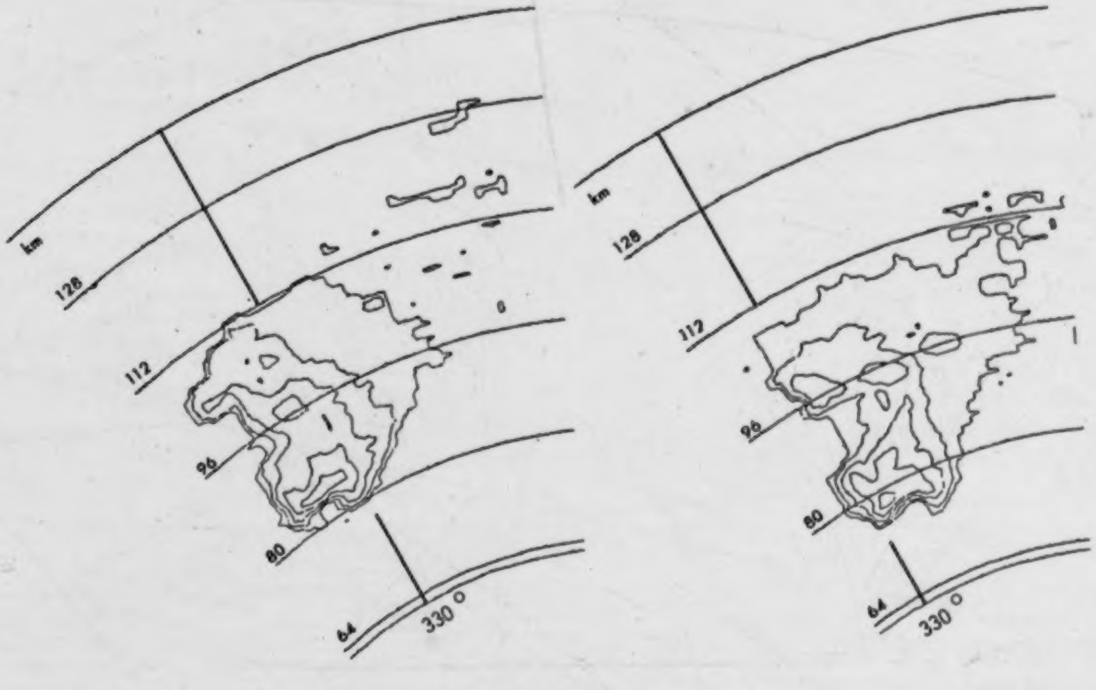
km
128
112
96
80
64
330°
km
128
112
96
80
64
330°

20:30:54 $\overline{\eta} = 6.58 \times 10^{-10}\,\mathrm{cm}^{-1}$ 20:45:50 $\overline{\eta} = 3.52 \times 10^{-10}\,\mathrm{cm}^{-1}$

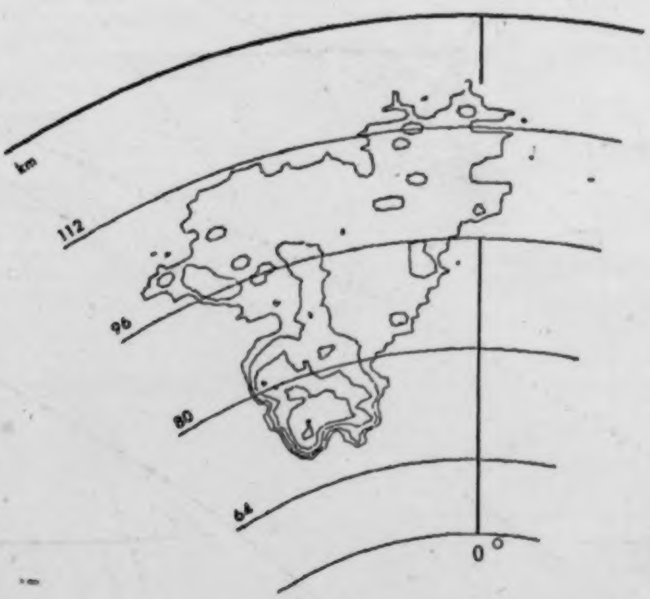
km
112
96
80
64
0°

21:00:46 $\overline{\eta} = 1.60 \times 10^{-10}\,\mathrm{cm}^{-1}$

Fig. 5.6: PPI echoes for storm A on 17 July, 1976. Elevation ~ 2.1°
Reflectivity = from 20dBZ by 10 dBZ. Time = 21:15 - 21:29 MDT.

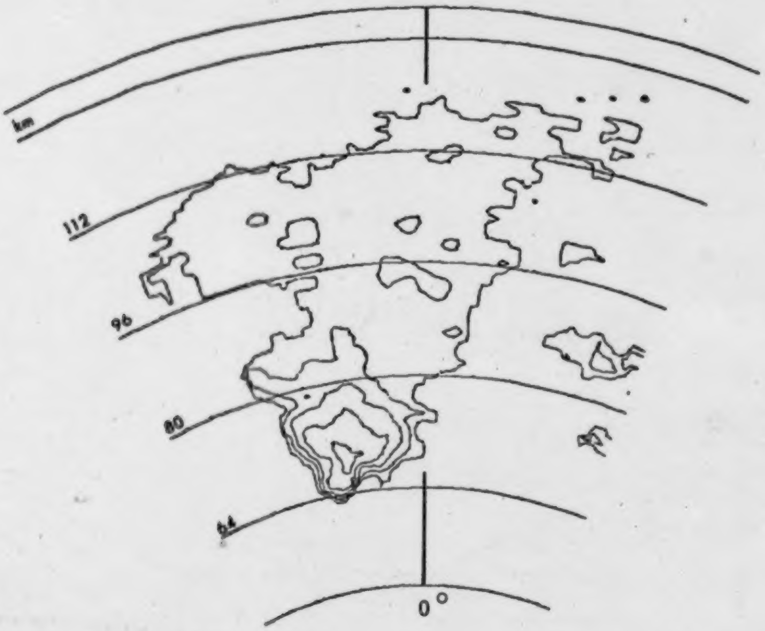

21:15:42 $\bar{n} = 2.33\times10^{-10}\text{cm}^{-1}$

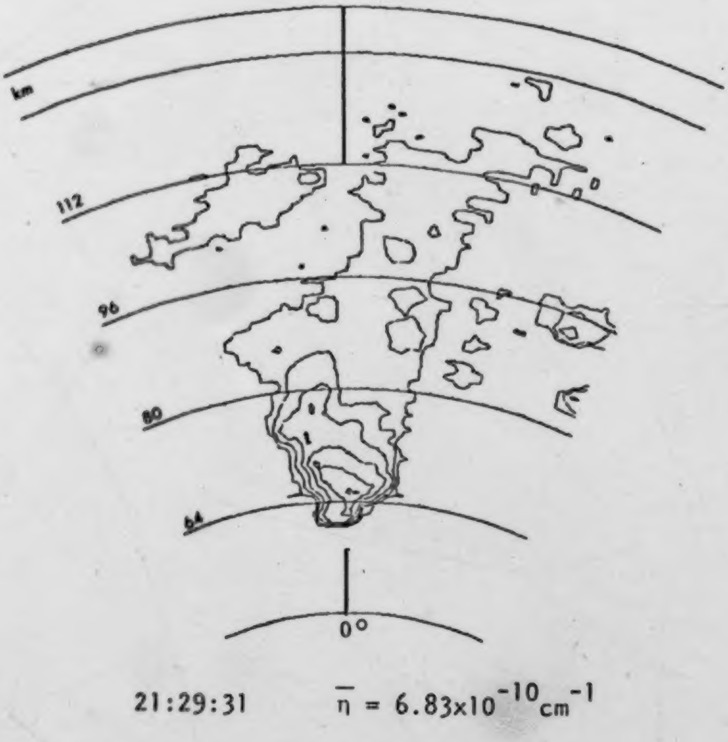

21:29:31 $\bar{n} = 6.83\times10^{-10}\text{cm}^{-1}$

Fig. 5.7: PPI echoes for storm A on 17 July, 1976. Elevation - 2.2°
Reflectivity = from 20dBZ by 10dBZ. Time = 21:45 - 22:00 MDT.

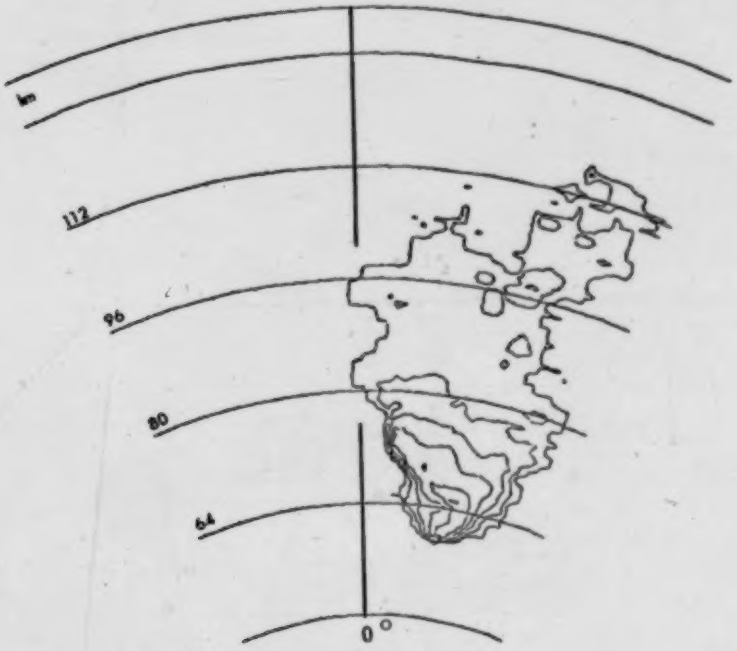

21:45:33 $\overline{n} = 8.94\times10^{-10}\text{cm}^{-1}$

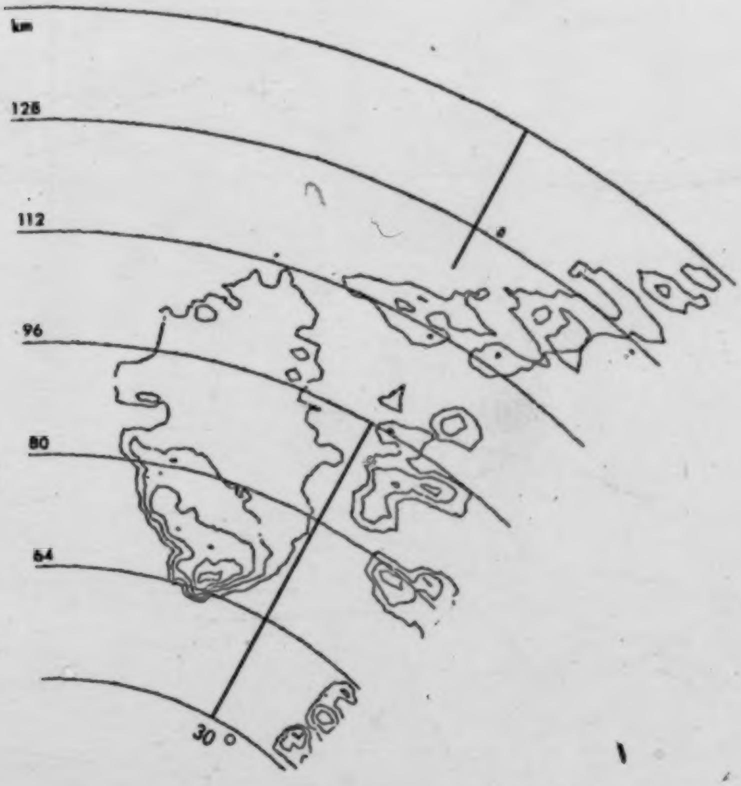

22:00:30 $\overline{n} = 1.22\times10^{-10}\text{cm}^{-1}$

Fig. 5.8: PPI echoes for storm A on 17 July, 1976. Elevation - 2.2°
Reflectivity = from 20 dBZ by 10 dBZ. Time 22:15 - 22:45 MDT.

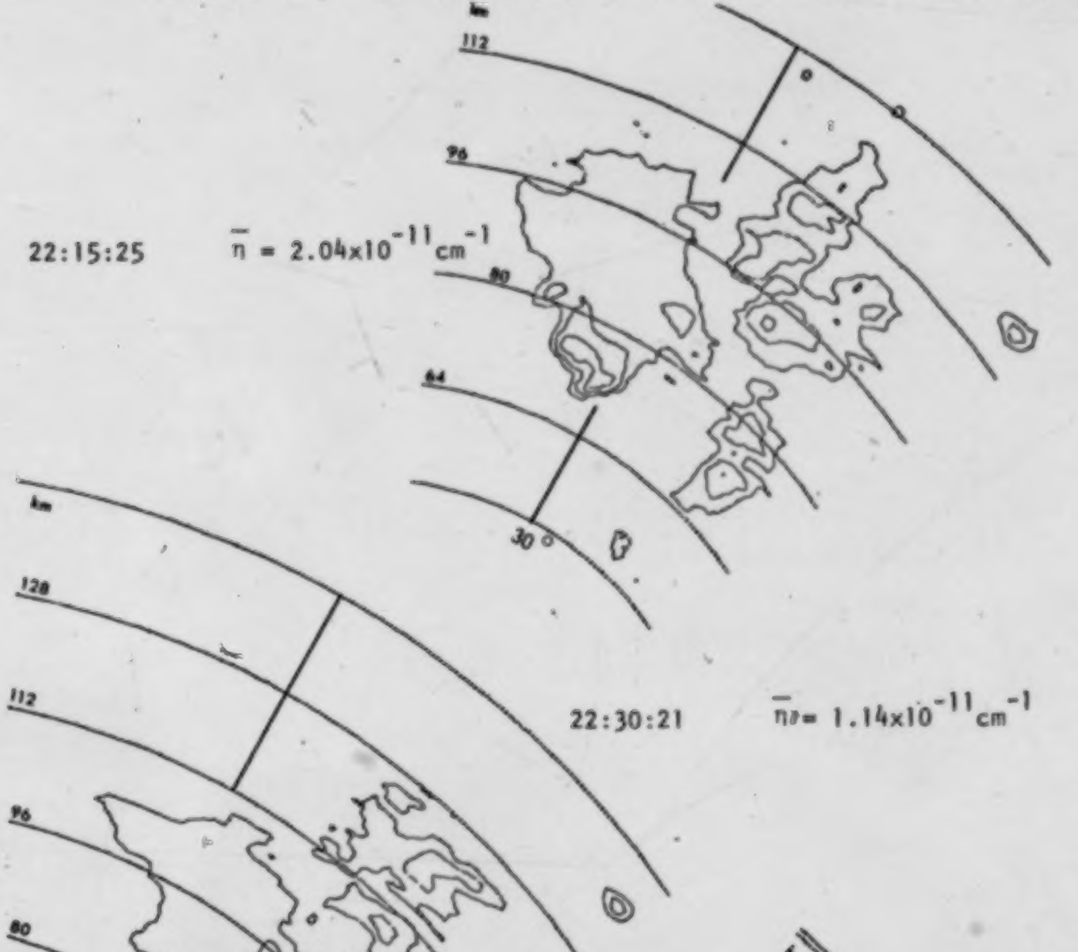

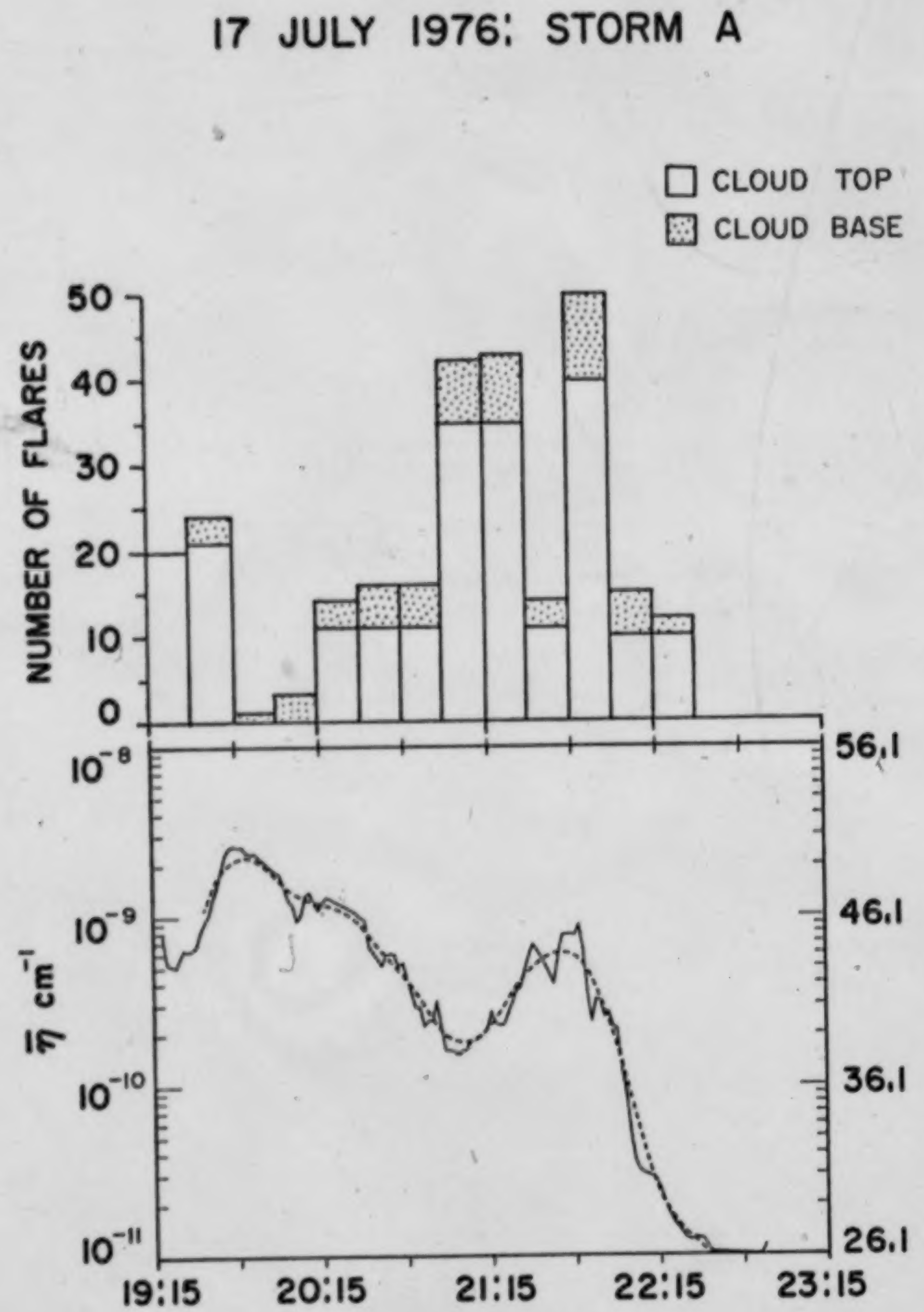

Fig. 5.9: $\bar{\eta}$ versus time for storm A on 17 July, 1976. Dashed line indicates trend. Type and number of cloud-seeding flares released during 15 minute intervals is shown.

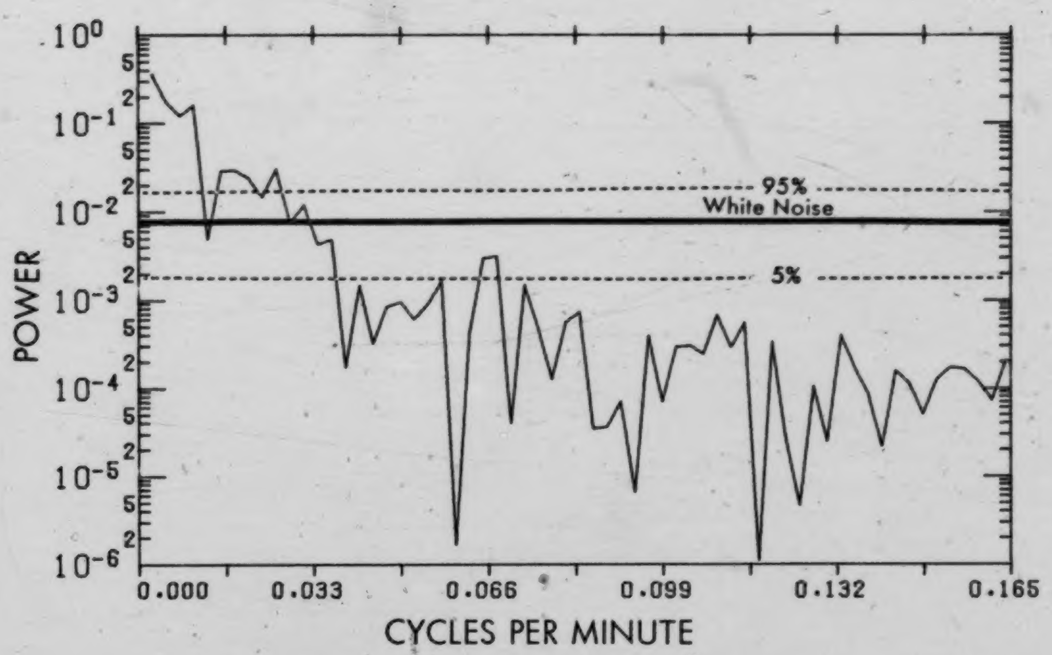

Fig. 5.10: Unsmoothed power spectrum of $\overline{\eta}$ for storm A on 17 July, 1976, showing the white-noise spectrum and 90% confidence interval.

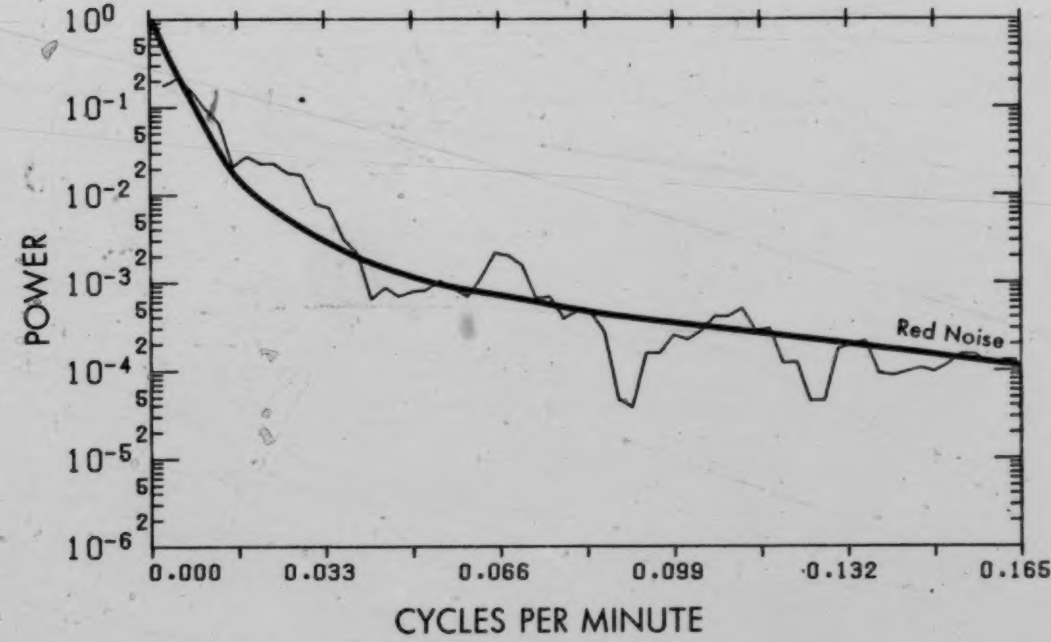

Fig. 5.11: Three-point Daniell-filtered power spectrum of $\overline{\eta}$ for storm A on 17 July, 1976, showing the red-noise spectrum.

all possible harmonics were computed, (up to 0.333 cycles per minute), the spectrum is only plotted for frequencies up to 0.165 cycles per minute or periods of approximately 6 minutes (4 Δt). Figure 5.11 shows the power spectrum which has been smoothed using a three-point running average applied to the periodogram. The reason for smoothing is that, if the spectra of two different portion of the same stationary time series are derived, the individual points of the spectrum will most likely look quite different. Spectrum analysis does not attempt to determine the individual amplitudes of each harmonic, but is aimed at obtaining the smooth underlying spectrum which is the same for different portions of the same stationary time series. It was once thought that particular outstanding powers represented exact periodicities, however, it has been found that individual peaks in the spectra of irregular oscillating time series can be accidental at a certain frequency.

The three-point running average also called the Daniell power spectral estimate (Kanasewich, 1975), produces an estimate of the continuous spectrum viewed through a rectangular window of bandwidth equal to 3 f_N/m, where f_N is the folding or Nyguist frequency ($f_N = 1/2\ \Delta t$), and m is the number of spectral lines. The end points were ignored with the filter applied only as needed. Many authors (Blackman and Tukey, 1958; Jenkins, 1961) express the need for bringing the resultant spectrum close to that of "white noise"; also called "prewhitening" or the removal of the trend in the data. For a full explanation of white noise see Appendix B. The reason for prewhitening is that the average value of the power at any particular frequency may be distorted during computation since the effect of a spectral window is to spread the power from the large peaks into adjacent frequencies. Thus spectral estimates are considered to be more precise when the power is spread over all frequencies.

The power spectrum was computed using the Tukey filtered high-pass data and is shown in Figure 5.12. It was found that the FFT program was able to discern the high frequency powers capably in the presence of substantial low frequency power, nevertheless, a smoothed FFT spectral analysis of the high pass data did bring out more clearly any preferred small scales.

5.4 Storm A: Spectrum Analysis

The value of the white-noise power is applied to the unsmoothed power spectrum in Figure 5.10 assuming a Chi-square distribution. The number of degrees of freedom ν for the periodogram analysis was determined by using:

$$\nu = \left(\frac{N^1 - 2}{2^{n-1}} \right) D \tag{5.4.1}$$

where N^1 is the number of independent data values, 2^{n-1} is the number of spectral lines obtained from N data values supplemented by $2^n - N$ zeroes, and D is the width of the Daniell filter used on the periodogram. The number of independent data values in the original N pieces of data depends on the amount of autocorrelation ρ, and has been shown by Eddy et al., (1968) to equal to:

$$N^1 = N \left(\frac{1 - \rho^2}{1 + \rho^2} \right)$$

The number of independent data values is then reduced by 2 degrees of freedom since the mean and variance were calculated from the data.

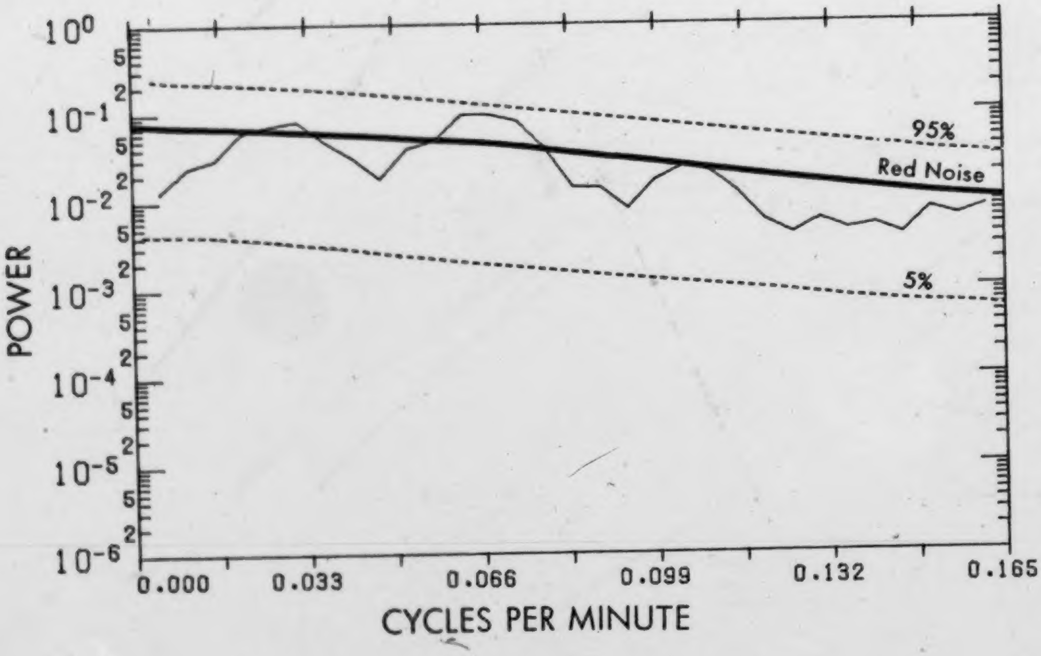

Fig. 5.12: Three-point Daniell-filtered power spectrum of Tukey-filtered $\overline{n}$ highpass data for storm A on 17 July, 1976. The red-noise spectrum and 90% confidence interval are shown.

The 95% confidence limits were obtained by multiplying the white-noise value by $\chi^2 .95/\nu$ and $\chi^2 .05/\nu$ for the upper and lower limits, respectively. The $\overline{\eta}$ series does not display random fluctuations characteristic of white noise.

The spectrum displays a general suppression of relative variance at higher frequencies and consequent inflation at lower frequencies as compared to the even distribution of white noise. This phenomenon, a characteristic of spectra derived from data with an appreciable autocorrelation between successive measurements, has been called "red noise" (Gilman et al., 1963). For a full explanation of red noise see Appendix B.

The lag one (1.5 min) to lag ten (15 min) autocorrelation coefficients were computed as follows:

$$R(\tau) = \frac{1}{(N-2)\, S_x^2} \sum_{t=1}^{N-\tau} (X_t - X)\,(\overline{X}_{t+\tau} - \overline{X}) \qquad (5.4.2)$$

where N is the number of data points (reduced by 2 in denominator since the mean $\overline{X}$, and the variance S_x^2 were computed from the data), and τ is the lag number. Table 5.1 gives the results.

The autocorrelation coefficients confirm that the time series depends on its immediate past and that a red-noise spectrum which allows for persistence should be applied.

The values of the red-noise power are applied to the smoothed power spectrum in Figure 5.11 using an autocorrelation value $\rho = .992$ for the red-noise curve determined from the relation $\rho = [R(1)^2 + R(2)]^{1/2}$. From the definition

Table 5.1: Lag 1.5 to 15 minute autocorrelation coefficients of $\overline{\eta}$ for storm A on 17 July, 1976.

LAG NUMBER	LAG TIME (min)	AUTOCORRELATION COEFFICIENT
1	1.5	.999
2	3.0	.970
3	4.5	.936
4	6.0	.898
5	7.5	.855
6	9.0	.810
7	10.5	.765
8	12.0	.719
9	13.5	.672
10	15.0	.625

of pure red-noise

$$R(1)^2 = R(2)$$

Since this is not the case with experimental data, the value of ρ should be modified to approximate pure red-noise. It was this value for ρ which was also used in the calculation of N^1.

The values of the red-noise power are applied to the smoothed high-pass power spectrum in Figure 5.12 using an autocorrelation value $\rho = .684$. We may assume a Chi-square distribution with the number of degrees of freedom ν calculated using (5.4.1). In this case D=3, since a three-point running average is used.

The red-noise adequately describes the nature of the smoothed power spectrum. The computed spectral estimate does not display any significant peaks with respect to the 95 per cent upper confidence limit, nevertheless, preferred cycles were displayed having periods of 32.0, 16.0 and 9.6 minutes.

The possible relationships between the variation of the time series and cloud-seeding events will be discussed in a separate section after all the individual storm cases have been presented.

5.5 17 July, 1976: Storm B

Storm B entered the project area shortly after 21:00 MDT and tracked eastward just south of storm A. It also had echo-top heights similar to those of storm A. Figure 5.13 shows the resulting hailswath from storm B with approximate times of the storm progression indicated. Golfball size hail and one report of larger-than-golfball size hail was reported at the surface. Figure 5.14 through 5.18 show low-elevation PPI scans at approximately 15 minute intervals throughout the lifetime of storm B. Once again, reflectivities in excess of 60 dBZ were measured.

Figure 5.19 gives the $\bar{\eta}$ time series. Only one cloud-top seeding flare was released into the storm at 22:05 MDT, as shown in the diagram. The dashed line indicates the trend in the data computed using the Tukey filter in Appendix A. A notable feature of the time series is that it displays a relatively uniform nature as compared with storm A which peaked, decreased significantly in magnitude and then surged to a peak once again before dissipating. Storm B reached a high plateau which gradually peaked at approximately 23:30 MDT and then dissipated. This difference is also displayed in the form of the hailswath. The hailswath for storm A

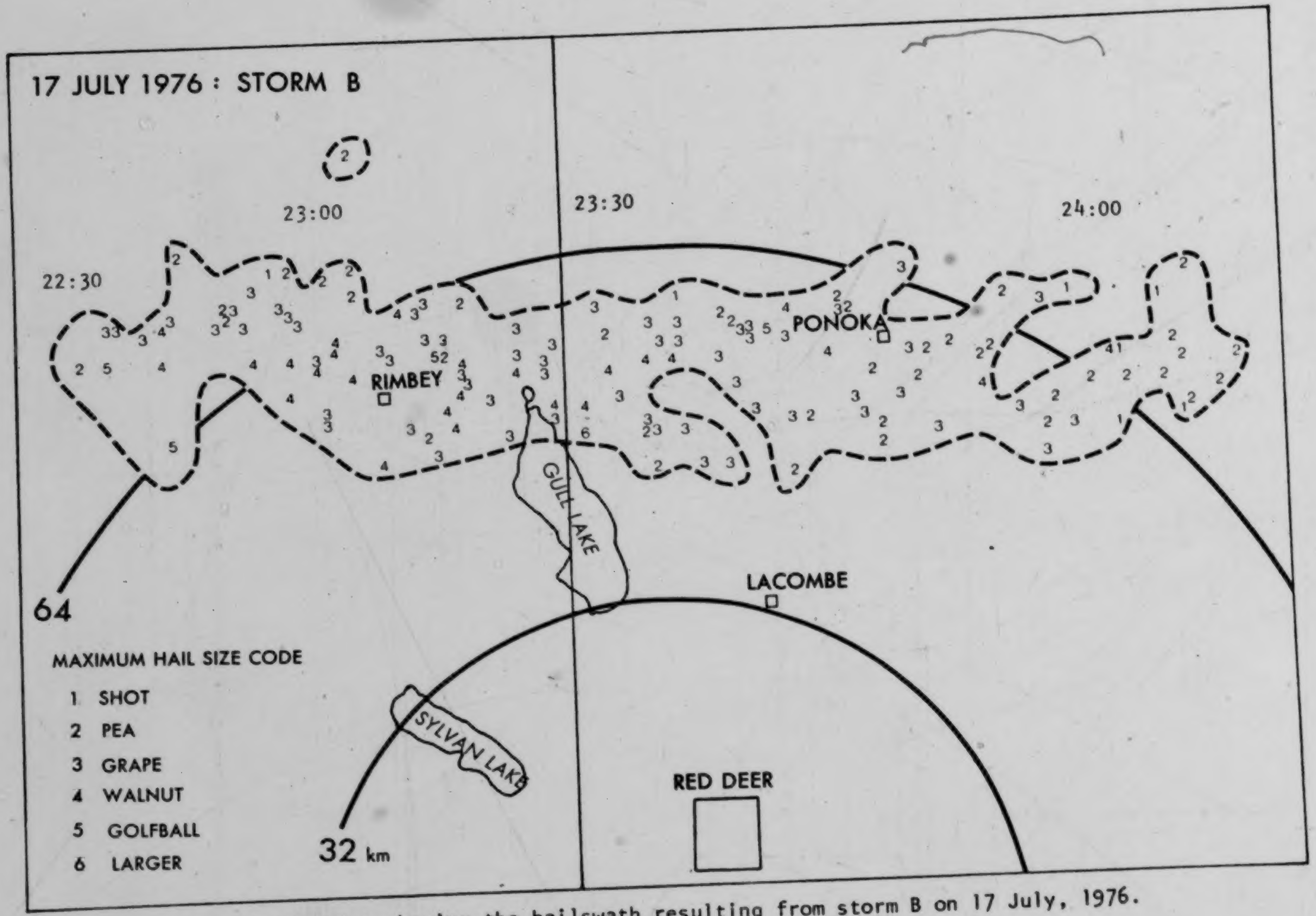
17 JULY 1976 : STORM B
22:30
23:00
23:30
24:00
RIMBEY
PONOKA
LACOMBE
RED DEER
GULL LAKE
SYLVAN LAKE
64
32 km
MAXIMUM HAIL SIZE CODE
1 SHOT
2 PEA
3 GRAPE
4 WALNUT
5 GOLFBALL
6 LARGER

Fig. 5.13: Map showing the hailswath resulting from storm B on 17 July, 1976.

Fig. 5.14: PPI echoes for storm B on 17 July, 1976. Elevation - 2.0°
Reflectivity = from 20dBZ by 10dBZ. Time = 21:15 - 21:29 MDT.

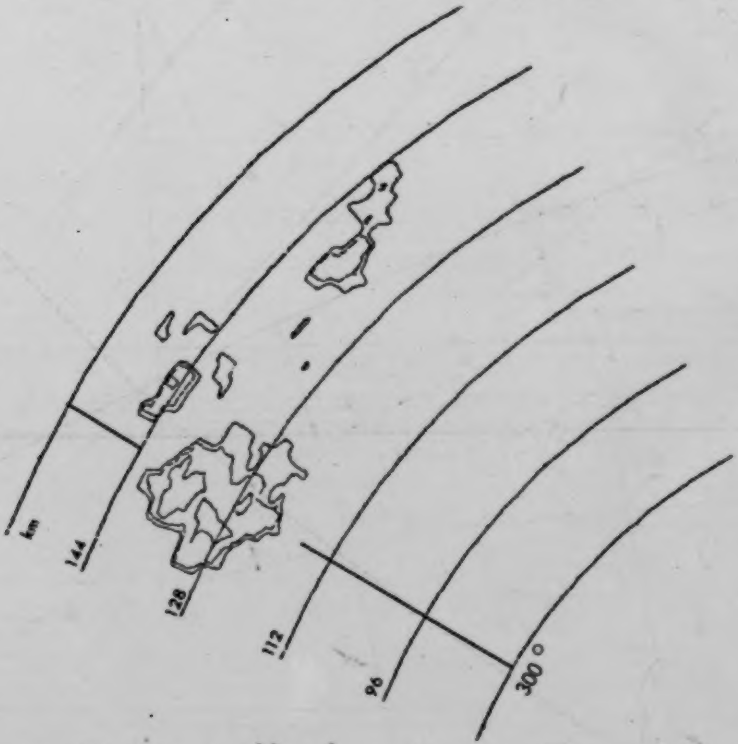

21:15:41 $\overline{\eta} = 5.05\times10^{-11}\,\text{cm}^{-1}$

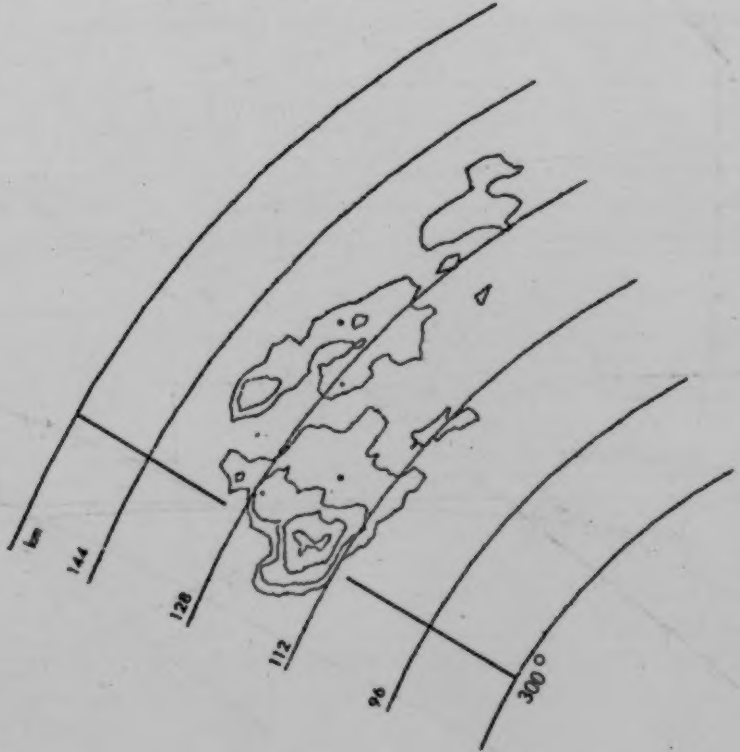

21:29:30 $\overline{\eta} = 1.04\times10^{-10}\,\text{cm}^{-1}$

Fig. 5.15: PPI echoes for storm B on 17 July, 1976. Elevation - 2.0°
Reflectivity = from 20dBZ by 10dBZ. Time = 21:45 - 22:30 MDT.

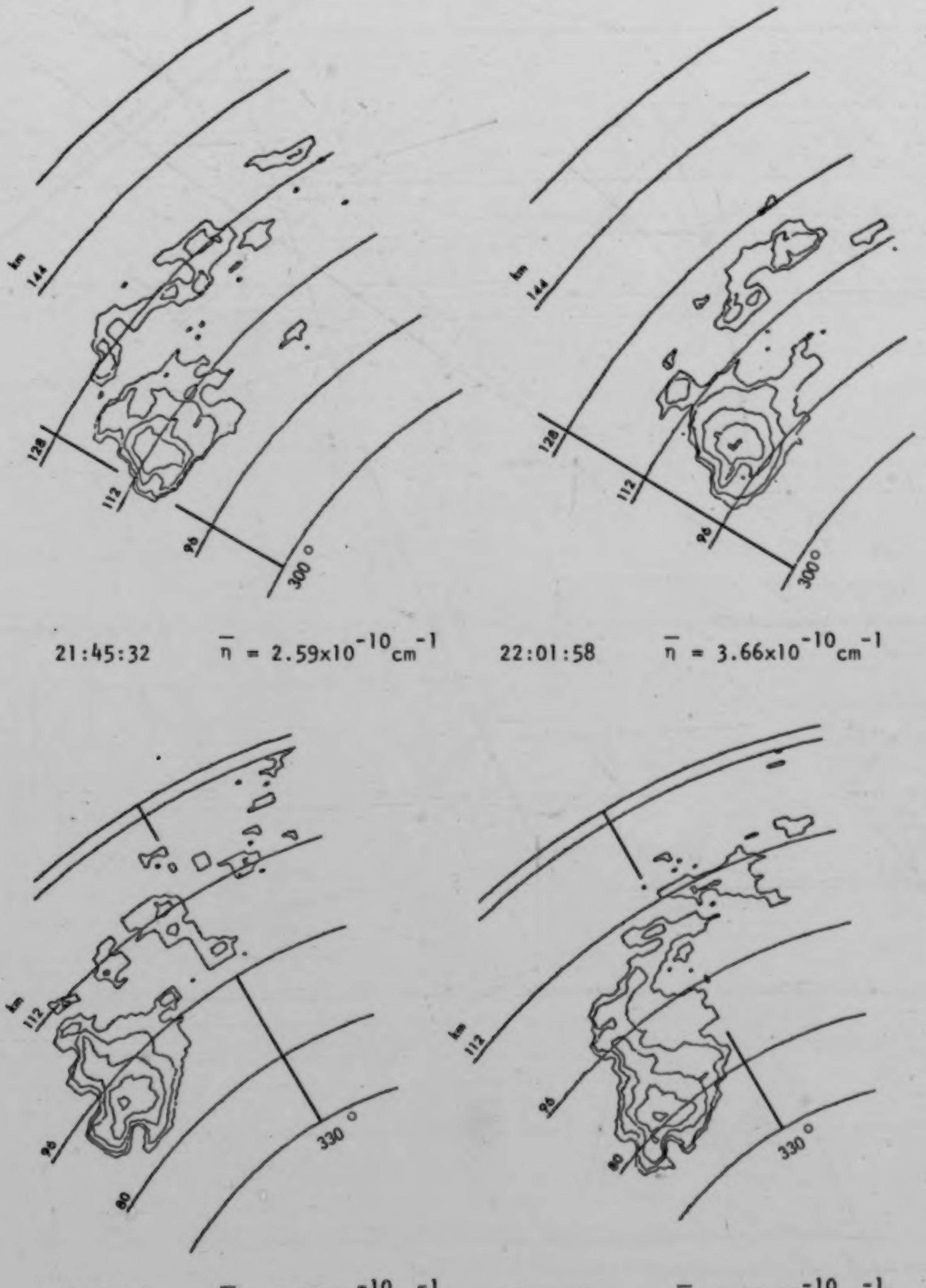

21:45:32 $\bar{\eta} = 2.59\times10^{-10}\mathrm{cm}^{-1}$ 22:01:58 $\bar{\eta} = 3.66\times10^{-10}\mathrm{cm}^{-1}$

22:15:24 $\bar{\eta} = 3.40\times10^{-10}\mathrm{cm}^{-1}$ 22:30:20 $\bar{\eta} = 3.42\times10^{-10}\mathrm{cm}^{-1}$

Fig. 5.16: PPI echoes for stormB on 17 July, 1976. Elevation ~ 2.1°
Reflectivity = from 20dBZ by 10dBZ. Time 22:45 - 23:30 MDT.

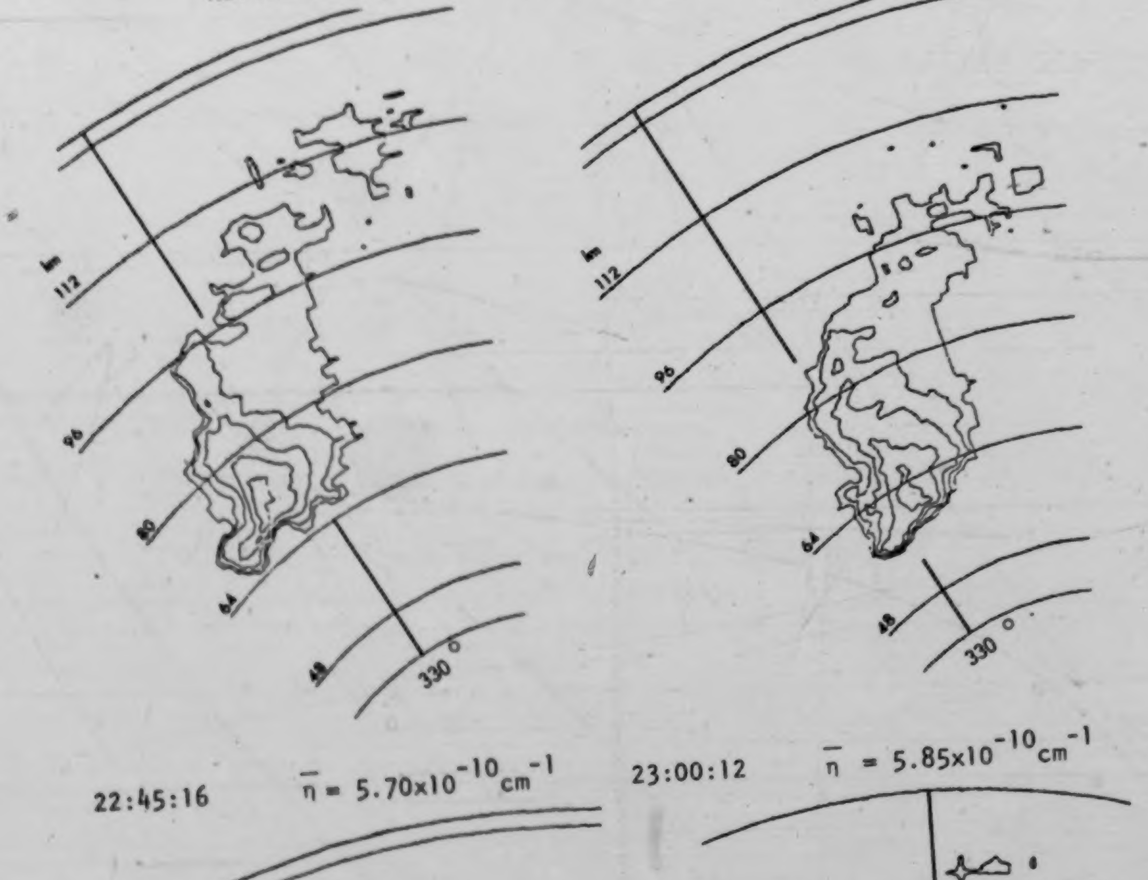

22:45:16 $\overline{n} = 5.70\times10^{-10}\,\mathrm{cm}^{-1}$

23:00:12 $\overline{n} = 5.85\times10^{-10}\,\mathrm{cm}^{-1}$

23:15:07 $\overline{n} = 6.46\times10^{-10}\,\mathrm{cm}^{-1}$

23:30:04 $\overline{n} = 7.36\times10^{-10}\,\mathrm{cm}^{-1}$

Fig. 5.17: PPI echoes for storm B on 17 July, 1976. Elevation - 2.2°
Reflectivity = from 20dBZ by 10dBZ. Time = 23:45 - 00:29 MDT.

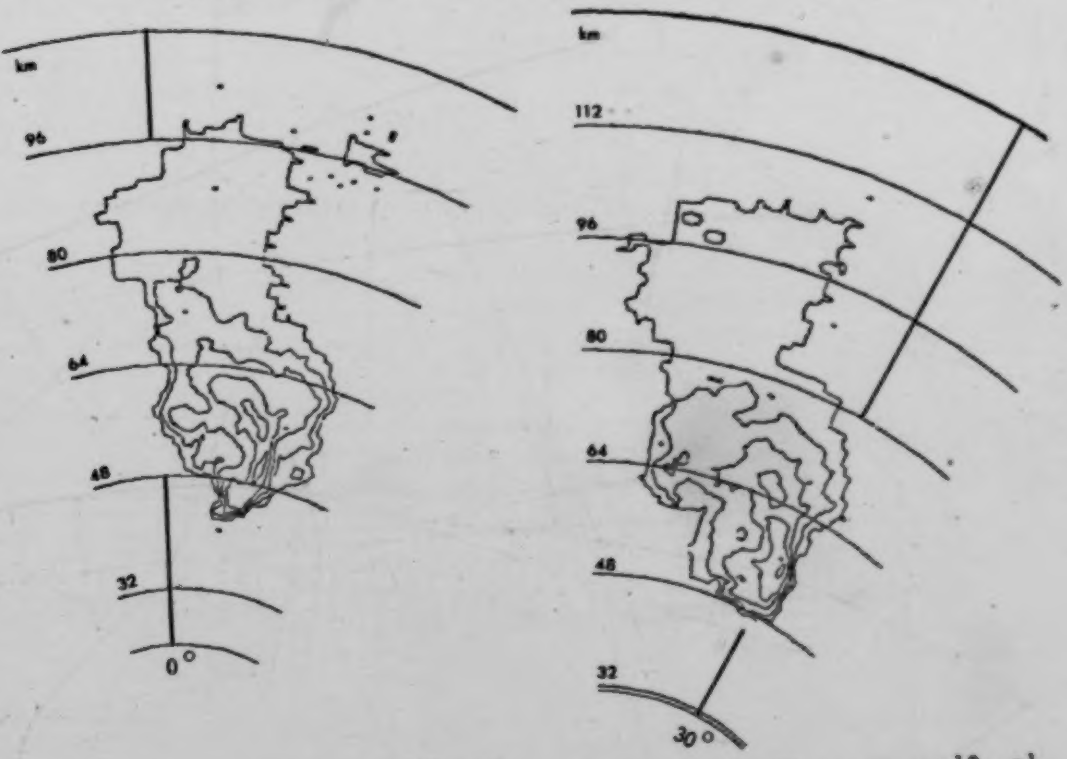
km
96
80
64
48
32
0°
km
112
96
80
64
48
32
30°

23:45:00 $\overline{n} = 4.70\times10^{-10}\mathrm{cm}^{-1}$

23:59:56 $\overline{n} = 1.50\times10^{-10}\mathrm{cm}^{-1}$

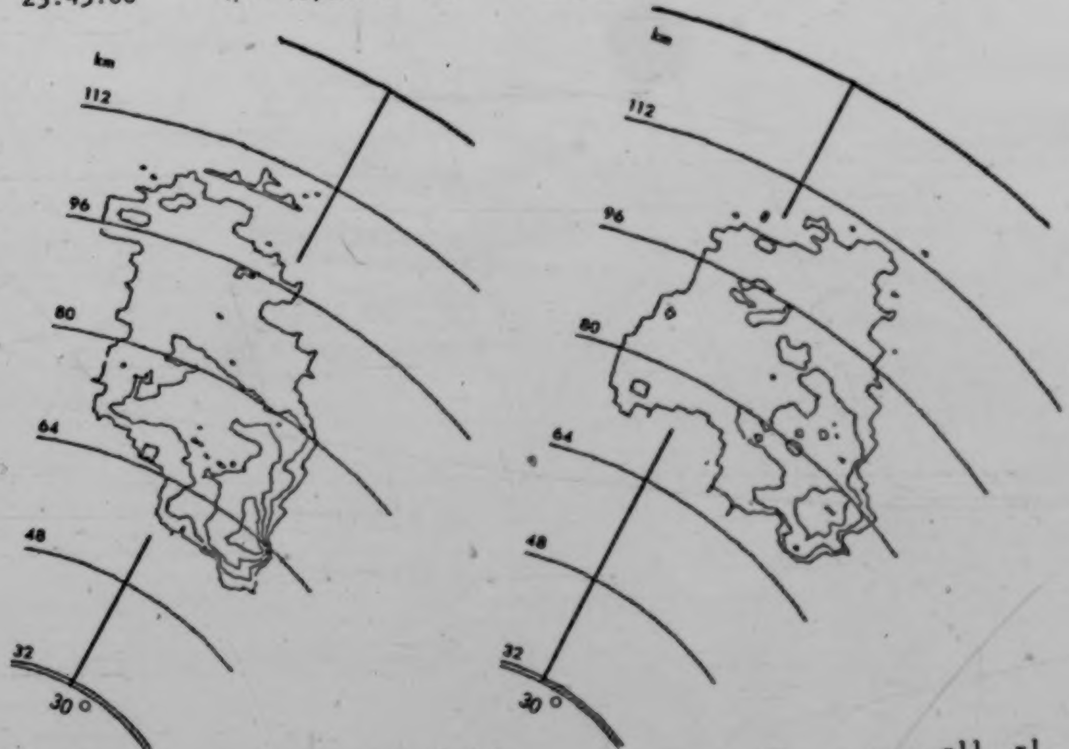
km
112
96
80
64
48
32
30°
km
112
96
80
64
48
32
30°

00:14:52 $\overline{n} = 8.10\times10^{-11}\mathrm{cm}^{-1}$

00:29:47 $\overline{n} = 2.24\times10^{-11}\mathrm{cm}^{-1}$

Fig. 5.18: PPI echoes for storm B on 17 July, 1976 Elevation ~ 2.2°
Reflectivity = from 20dBZ by 10dBZ. Time = 00:44 - 01:29 MDT.
(18 July, 1976)

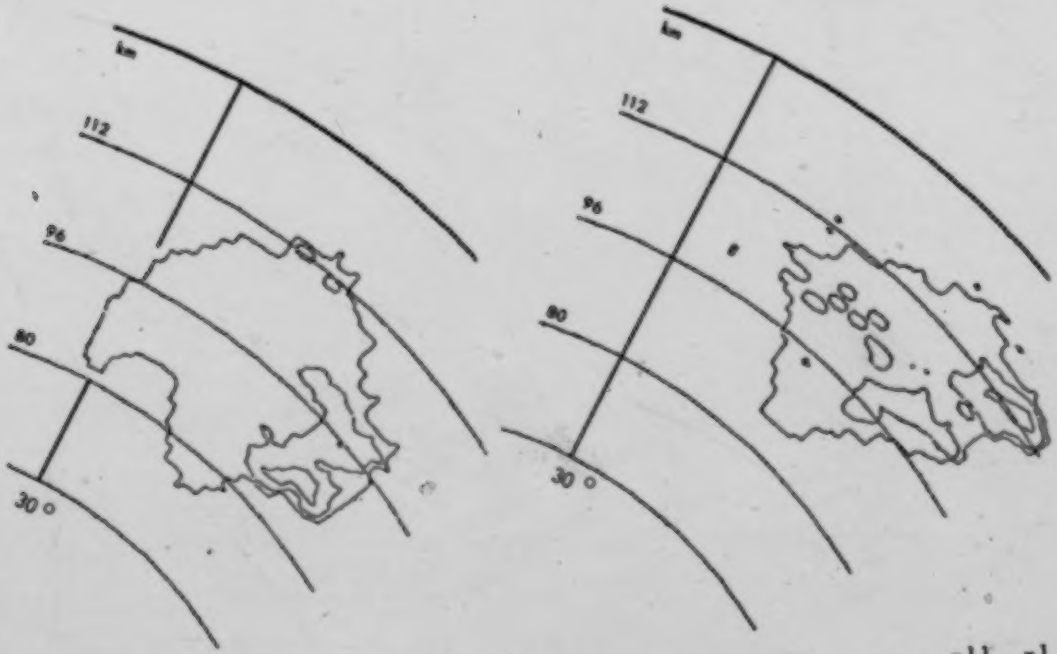

00:44:43 $\overline{n} = 1.31\times10^{-11}\,cm^{-1}$ 00:59:39 $\overline{n} = 1.65\times10^{-11}\,cm^{-1}$

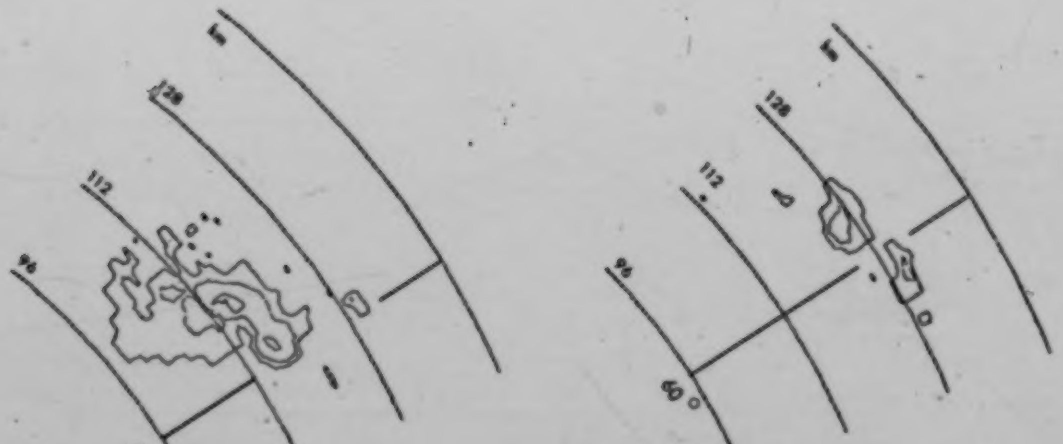

01:16:04 $\overline{n} = 1.50\times10^{-11}\,cm^{-1}$ 01:29:30 $\overline{n} = 9.60\times10^{-12}\,cm^{-1}$

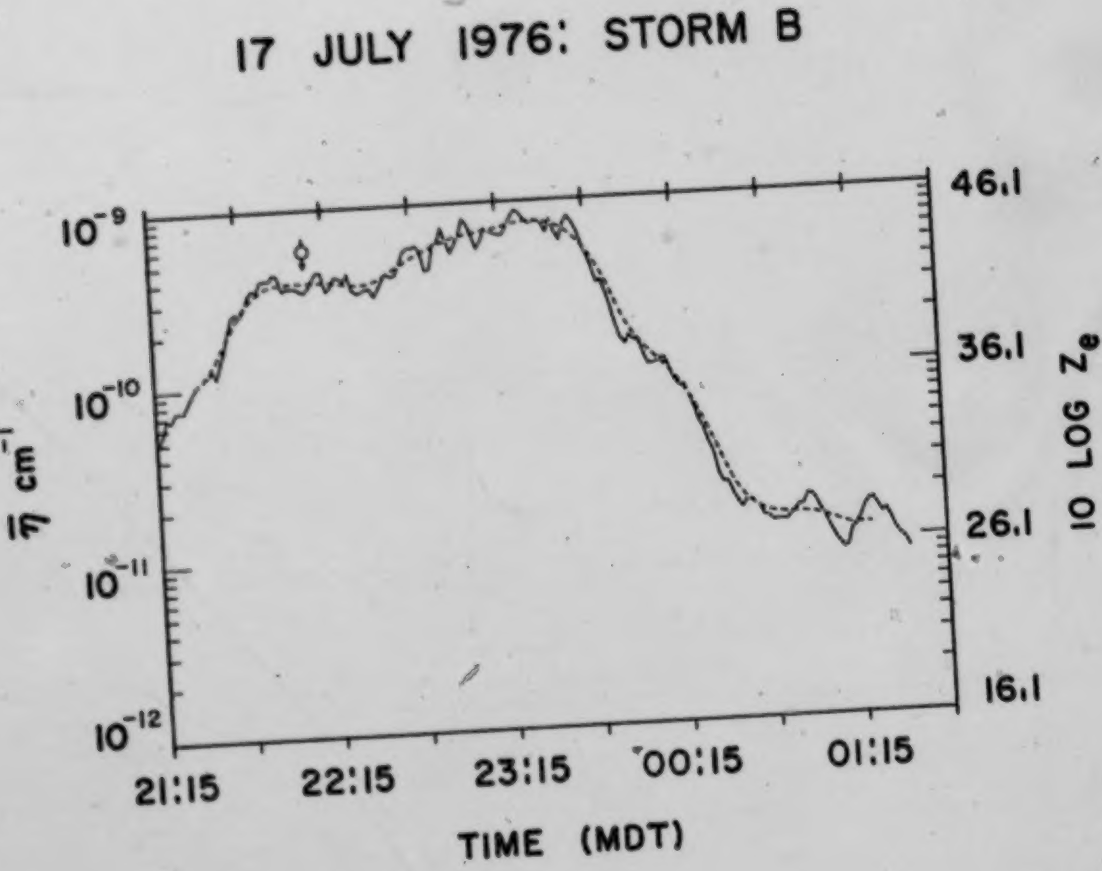

Fig. 5.19: $\bar{n}$ versus time for storm B on 17 July, 1976. Dashed line indicates trend. The time when one cloud-top flare was released in the storm is noted.

displays an intermittency while the hailswath for storm B is continuous. The $\bar{\eta}$ values obtained for storm A at its onset were considerably higher than any values obtained for storm B. Although this difference is not evident in the size of hail reported at the surface early in storm A, this is due possibly to inadequate sampling in a sparsely-populated area. Comparable precipitation did occur otherwise for similar $\bar{\eta}$ values. Storm B continued on into the early morning hours of the following day.

5.6 Storm B: Power Spectrum Analysis

Figure 5.20 gives the unsmoothed power spectrum for storm B. The smoothed power spectrum using a three-point running average is presented in Figure 5.21.

As was the case with storm A, the power spectrum displays the red-noise phenomenon. Table 5.2 gives the autocorrelation coefficients of the time series for lag one (1.5 min) to lag ten (15 min), computed using (5.4.2).

The values of the red-noise power are applied to the smoothed power spectrum in Figure 5.21 using an autocorrelation value $\rho = .986$, and to the highpass data smoothed power spectrum in Figure 5.22 using an autocorrelation value $\rho = .299$. The 95 per cent confidence limits were constructed assuming a Chi-square distribution as in storm A.

Significant peaks exist at 0.049 and 0.109 cycles per minute corresponding to cycle periods of 20.4 and 9.2 minutes respectively.

5.7 Spectra Comparison

Storm B displayed a noticeable lack of power at 0.066 cycles per minute

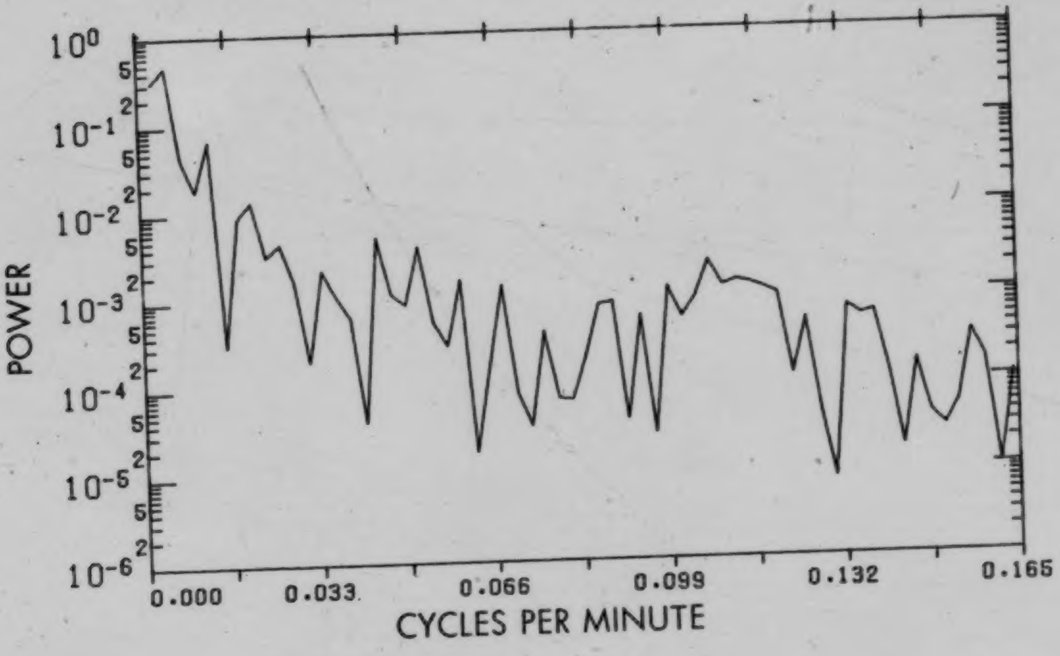

Fig. 5.20: Unsmoothed power spectrum of $\overline{n}$ for storm B on 17 July, 1976.

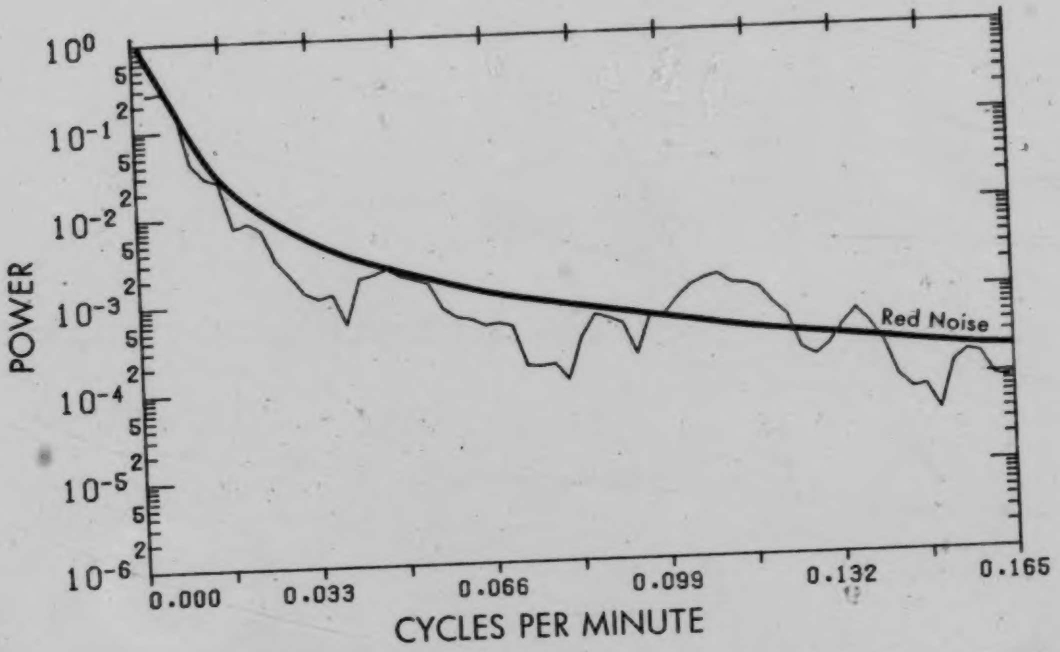

Fig. 5.21: Three-point Daniell-filtered power spectrum of $\overline{n}$ for storm B on 17 July, 1976, showing the red-noise spectrum

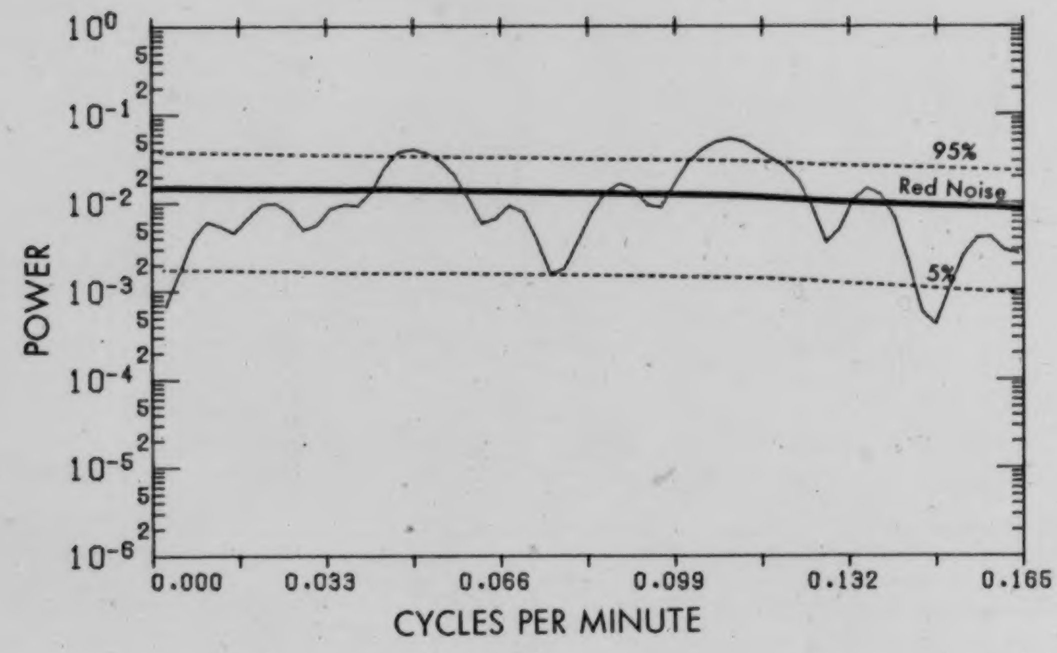

Fig. 5.22: Three-point Daniell-filtered power spectrum of Tukey-filtered $\overline{n}$ highpass data for storm B on 17 July, 1976. The red-noise spectrum and 90% confidence interval are shown.

Table 5.2: Lag 1.5 to 15 minute autocorrelation coefficients of $\bar{\bar{n}}$ for storm B on 17 July, 1976.

LAG NUMBER	TIME LAG (min)	AUTOCORRELATION COEFFICIENT
1	1.5	.990
2	3.0	.963
3	4.5	.941
4.	6.0	.926
5	7.5	.913
6	9.0	.893
7	10.5	.866
8	12.0	.834
9	13.5	.805
10	15.0	.783

whereas storm A displayed a preferred frequency. Storm A does, however, show a broad peak coinciding with the significant peak for storm B at approximately 0.11 cycles per minute, although well within the confidence interval.

The Chi-square test for goodness-of-fit was applied to the two raw spectra to see if the observed power distribution for storm A differed significantly from that of storm B. The results indicated that even at very low confidence limits the two spectra could constitute a sample from a population with the same power distribution function.

A physical interpretation of the preferred cycles exhibited is discussed in a later section after all the storm data has been presented.

CHAPTER 6

THE AUGUST, 1976 CASE STUDIES

6.1 Introduction

Five storms which occurred during the month of August, 1976 were analyzed. The storms chosen on August 6, 12, 15, 20 and 24, combined to yield 67 reports of hail at the surface and are included in this study in order to compare the variations of $\overline{\eta}$ in storms with lower energy than the energy associated with the two storms discussed in Chapter 5.

The storms on August 6 and 20 were seeded while those on August 12, 15 and 24 were not. Since smaller storms are generally thought to be among the most likely to be affected by cloud seeding, seeding effects may be more easily detected.

6.2 The 6 August, 1976 Storm

The storm on 6 August, 1976 differs from most of the other storms in this study because it did not form in the foothill regions and track eastward across the project area, but rather formed on the plains in the vicinity of Buffalo Lake and went through its life cycle within a region of less than 300 km^2 over a time period of 1.5 hours. The synoptic summary is given in Figure 6.1 and the environmental conditions are shown by the tephigram in Figure 6.2. Although the presence of the lake would offer an opportunity to study the thermodynamic influence of a lake on a convective storm for comparison with the lake effect proposed by Warner (1976), this analysis was not undertaken. Before any changes in $\overline{\eta}$ can be associated with cloud seeding, however, the presence of the lake would have to be taken into consideration.

SYNOPTIC SUMMARY

06 AUGUST 1976

SYNOPSIS: THE SECOND S/W TROUGH IN THE CURRENT SERIES ARRIVED OVER THE AHP AREA AROUND NOON. THE SURFACE PRESSURE PATTERN DID NOT REFLECT THE S/W TOO WELL, WITH ONLY A WEAK FRONTAL TROUGH ACROSS CENTRAL ALBERTA.

AHP AREA: LIGHT AND VARIABLE WINDS AT ALL LEVELS. MOST CONVECTIVE DEVELOPMENT OVER THE AHP AREA TOOK PLACE IN THE NE QUADRANT, WHERE THE TIMING OF THE SYNOPTIC S/W SUPPORT WAS MOST FAVORABLE. CELLS FORMED RAPIDLY AROUND NOON, WITH SOME TOPS EXCEEDING 13 KM BY MAXIMUM TEMPERATURE TIME WHILE MOVING NORTHWARD.

TROUGH (T) OR RIDGE (R) PASSAGE TIME	12 HOUR 500 MB CHANGE IN				HAIL SIZE CATEGORY	NO. HAIL REPORTS N / S
	VORTICITY ($10^{-5}s^{-1}$)	HEIGHTS * (M)	THICKNESS* (M)	TEMPS. (°C)		
T-06/1900Z	0	- 40	- 50	- 1	3	11/0

* DIURNAL EFFECTS REMOVED

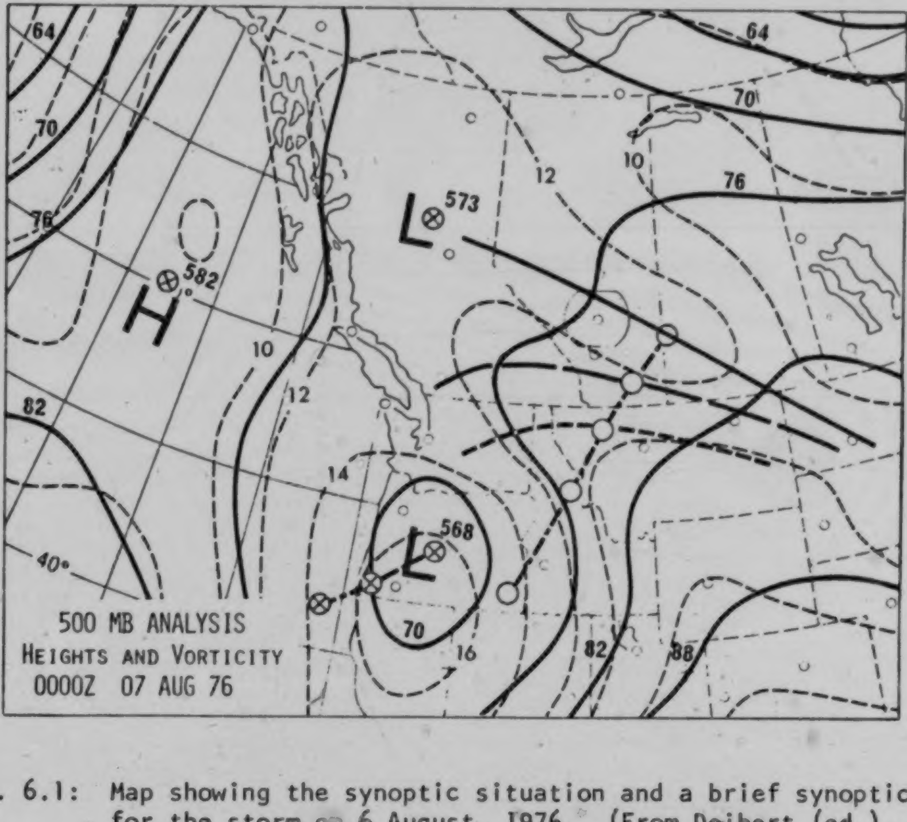
64
64
70
70
76
76
82
82
88
10
10
12
12
14
16
70
5
40°
L 573
H 582
L 568
500 MB ANALYSIS
HEIGHTS AND VORTICITY
0000Z 07 AUG 76

Fig. 6.1: Map showing the synoptic situation and a brief synoptic summary for the storm on 6 August, 1976. (From Deibert (ed.), 1976)

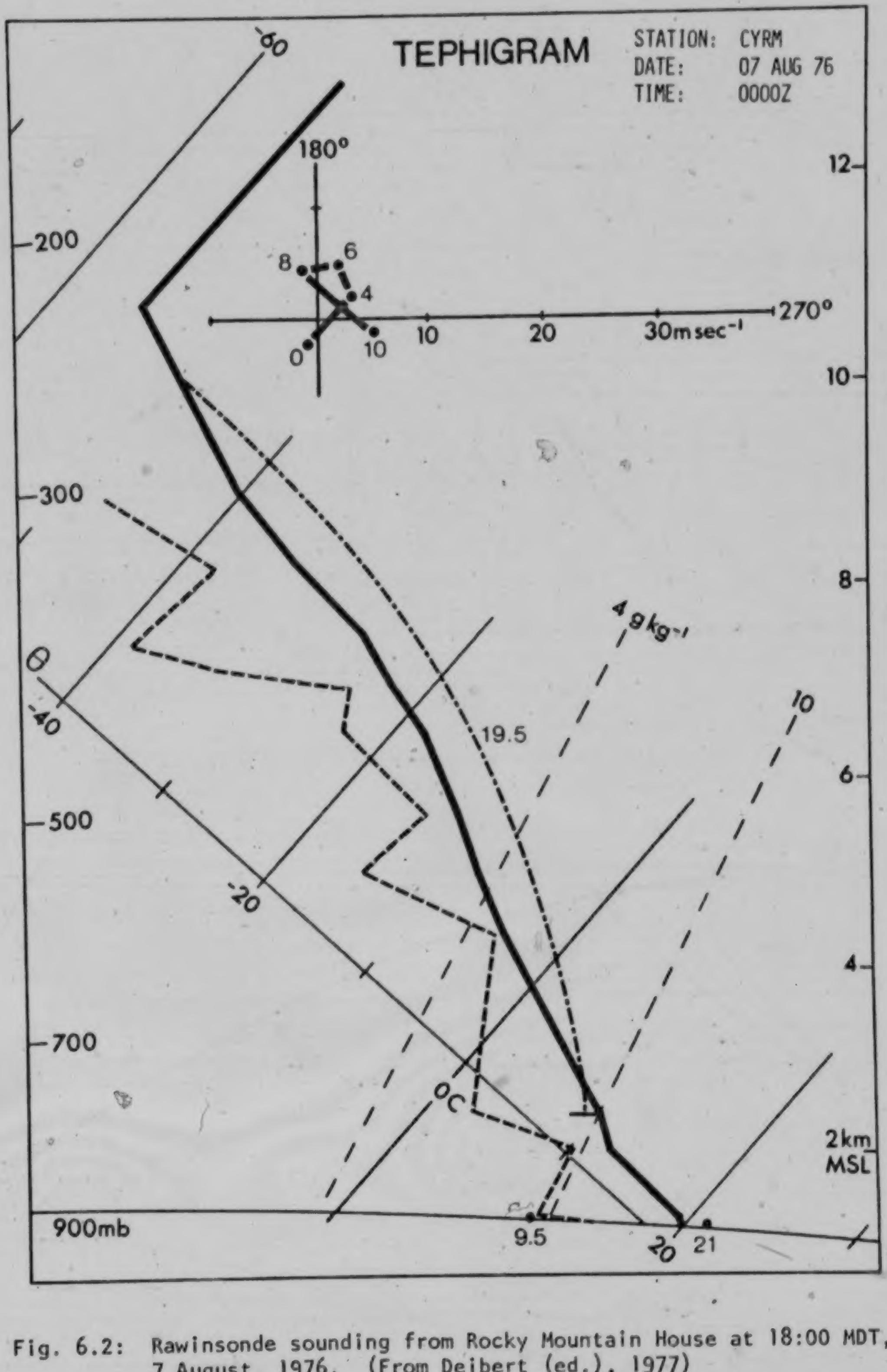

Fig. 6.2: Rawinsonde sounding from Rocky Mountain House at 18:00 MDT, 7 August, 1976. (From Deibert (ed.), 1977)

The hailswath from the storm is shown in Figure 6.3. Only 5 reports of hail at the surface were received and the maximum hailsize reported was grape size.

PPI scans of the storm at approximately 15 minute intervals are given in Figure 6.4. The storm developed from the minimum detectable signal to reflectivities greater than 50 dBZ in less than half an hour.

The $\bar{\eta}$ time series is given in Figure 6.5, which also indicates the time and amount of seeding which was done. The dashed line represents the trend in the data computed using the Tukey filter described in Appendix A.

The radar constant used for the day was 75.5 dBm with a peak transmitted power of 168 kw.

The unsmoothed power spectrum of the data is given in Figure 6.6 and the smoothed power spectrum, using a three-point running average, is given in Figure 6.7. The frequency resolution of the spectrum is not as good in this case as in the previous cases. The storm lasted just over 1.5 hours and the number of data points available was 63. The FFT algorithm requires that the number of data points be a power of two. If the number of values is not a power of two, zeroes are added until the total number meets this requirement. The number of spectral lines between frequencies 0.0 and (1/2 Δt) cycles per minute depends on the relation $m = 2^{n-1}$ where m is the number of spectral lines and n is an integer. In this case the value for n is 6 and therefore, $2^6 = 64$, which means that one zero was added to complete the data set. The number of spectral lines in this case is 32. The number of spectral lines for each storm on 17 July 1976, was 128 resulting in

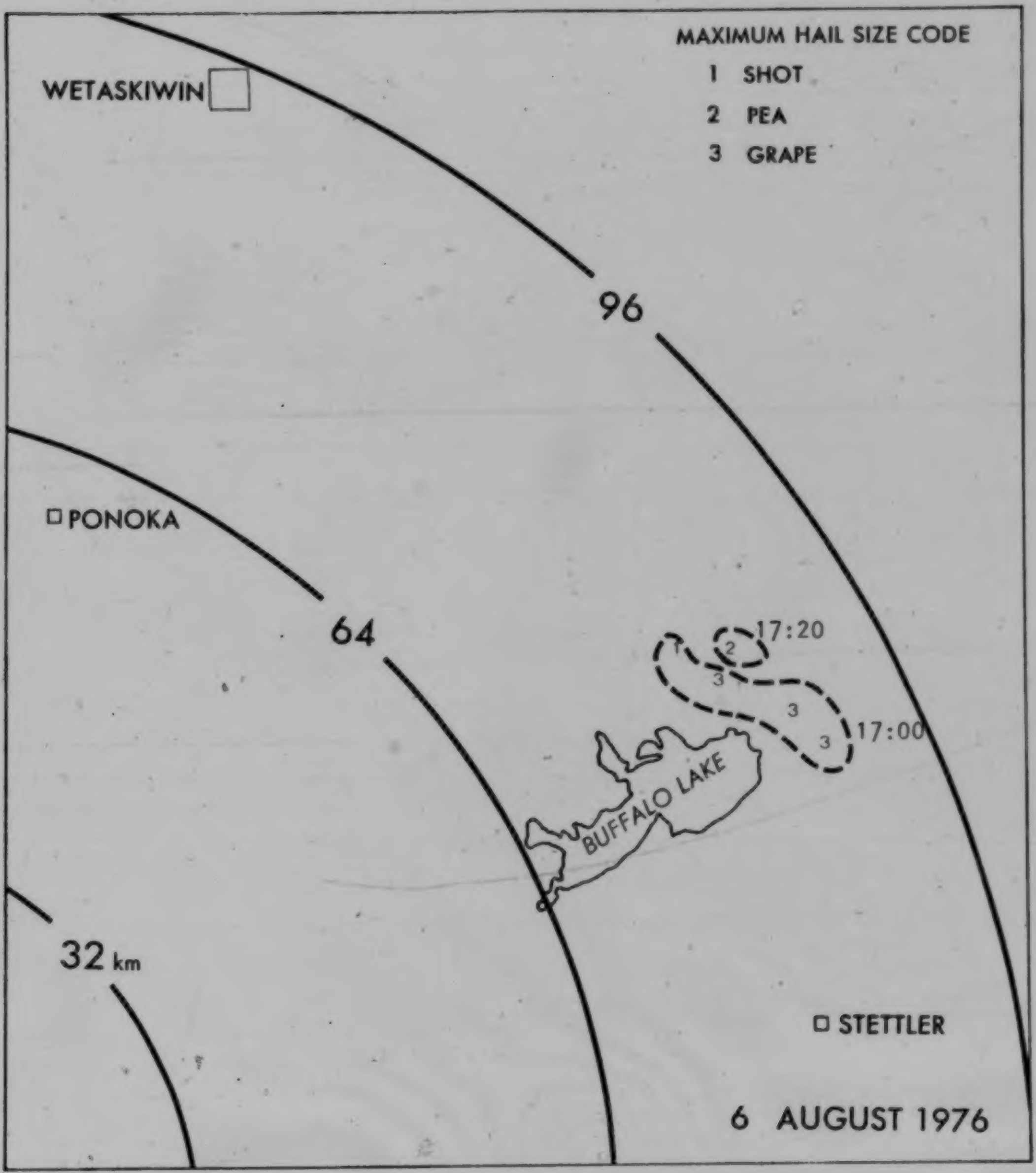
MAXIMUM HAIL SIZE CODE
1 SHOT
2 PEA
3 GRAPE
WETASKIWIN
96
PONOKA
64
32 km
17:20
17:00
2
3
3
3
BUFFALO LAKE
STETTLER
6 AUGUST 1976

Fig. 6.3: Map showing the hailswath resulting from the storm on 6 August, 1976.

Fig. 6.4: PPI echoes for the storm on 6 August, 1976. Elevation - 2.2°
Reflectivity = from 20 dBZ by 10 dBZ. Time = 16:31- 17:59 MDT.

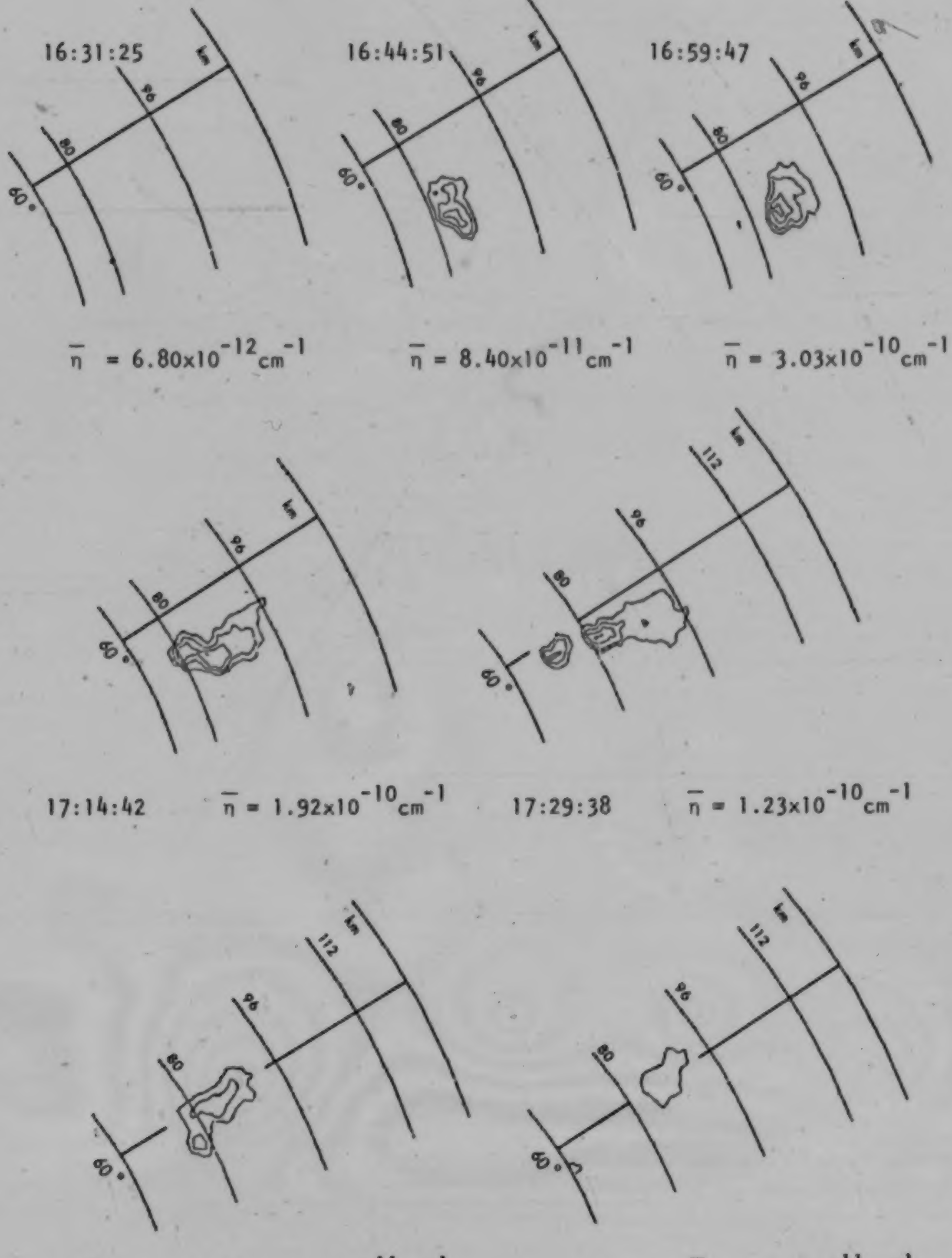

16:31:25 $\overline{\eta} = 6.80\times10^{-12}\,\mathrm{cm}^{-1}$

16:44:51 $\overline{\eta} = 8.40\times10^{-11}\,\mathrm{cm}^{-1}$

16:59:47 $\overline{\eta} = 3.03\times10^{-10}\,\mathrm{cm}^{-1}$

17:14:42 $\overline{\eta} = 1.92\times10^{-10}\,\mathrm{cm}^{-1}$

17:29:38 $\overline{\eta} = 1.23\times10^{-10}\,\mathrm{cm}^{-1}$

17:46:03 $\overline{\eta} = 2.54\times10^{-11}\,\mathrm{cm}^{-1}$

17:59:29 $\overline{\eta} = 1.73\times10^{-11}\,\mathrm{cm}^{-1}$

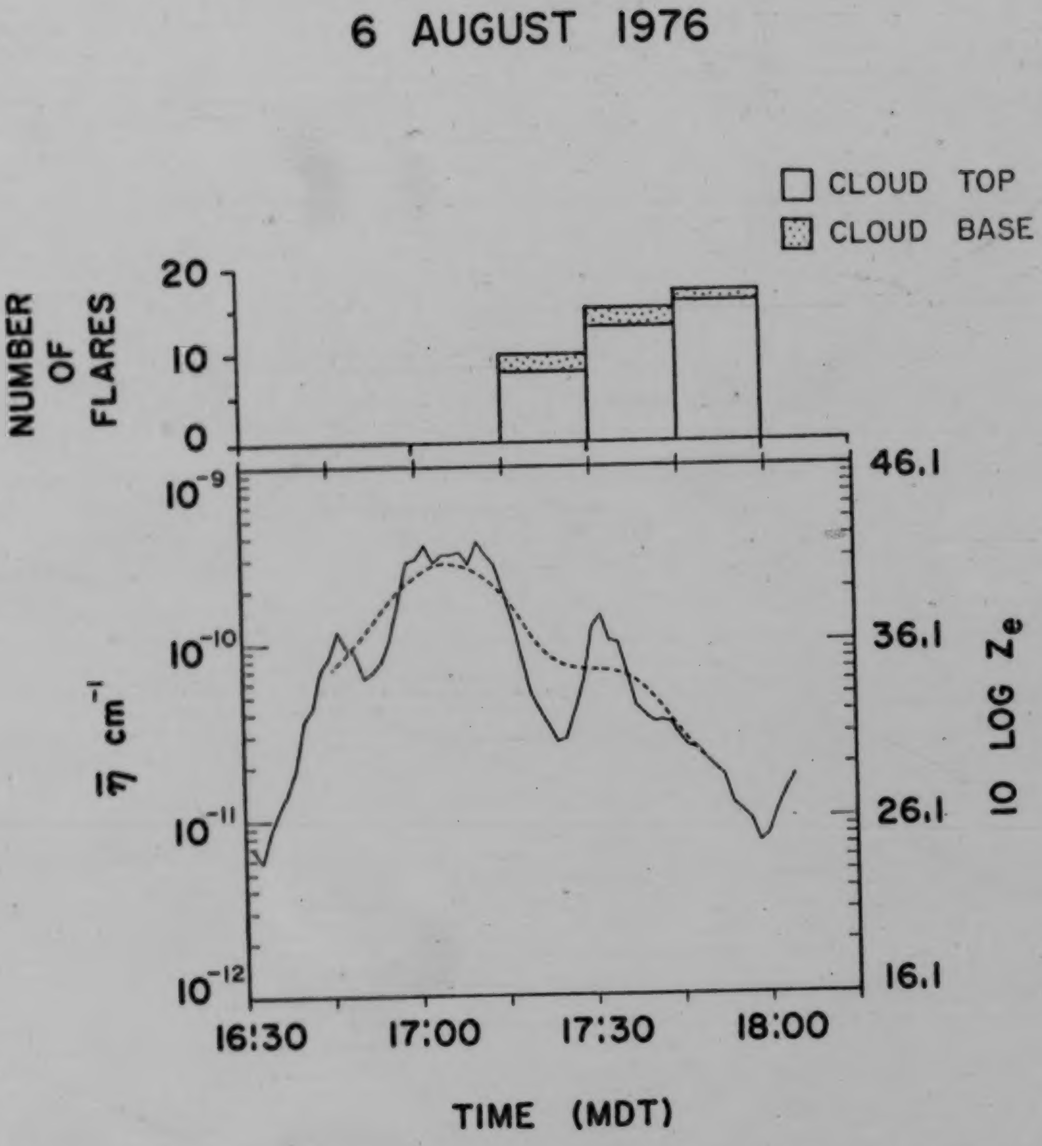

Fig. 6.5: $\bar{\eta}$ versus time for the storm on 6 August, 1976. Dashed line indicates trend. Type and number of cloud-seeding flares released during 15 minute intervals is shown.

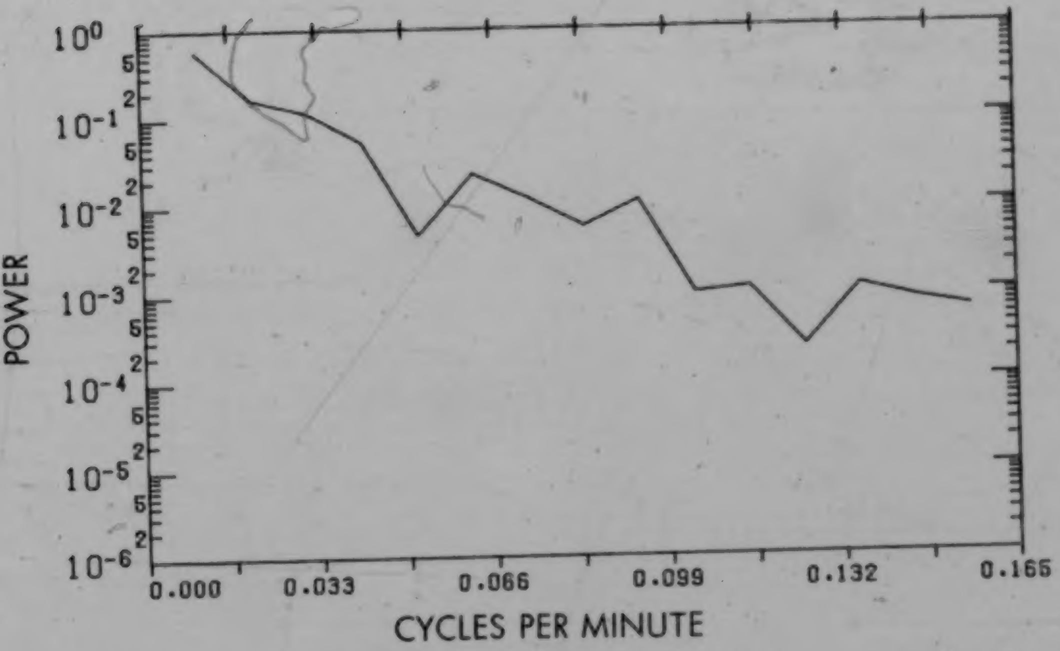

Fig. 6.6: Unsmoothed power spectrum of $\overline{n}$ for the storm on 6 August, 1976.

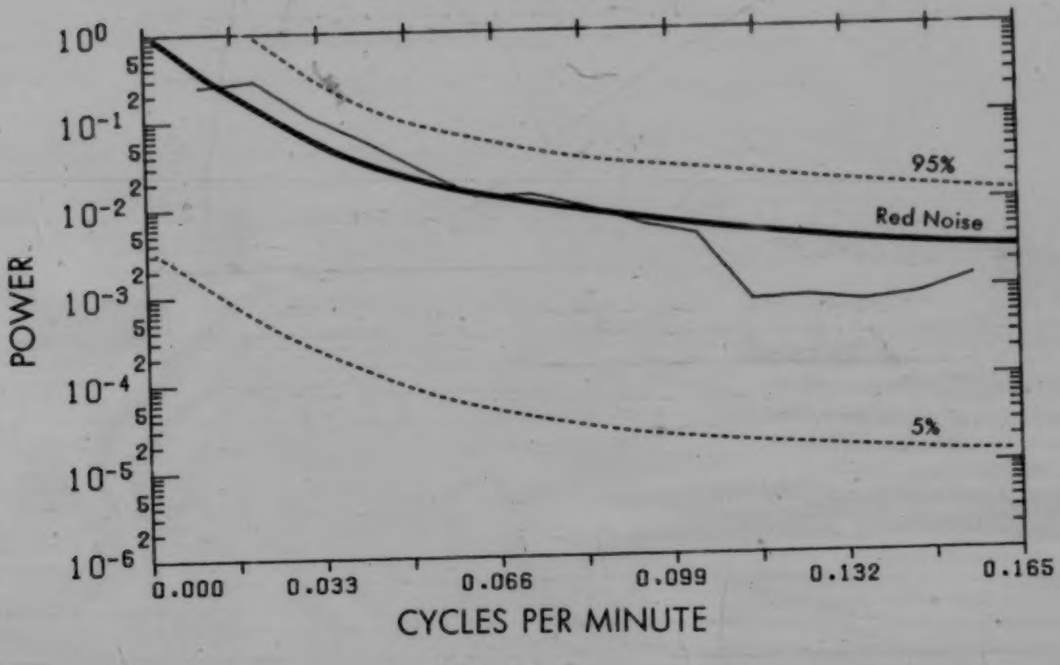

Fig. 6.7: Three-point Daniell-filtered power spectrum of $\overline{n}$ for the storm on 6 August, 1976, showing the red-noise spectrum and 90% confidence interval.

considerably more detail. This is the reason for the very smooth looking spectrum of 6 August, 1976 as compared with those from 17 July, 1976.

Table 6.1 gives the autocorrelation coefficients of the time series for lag one (1.5 min) to lag ten (15 min), computed using (5.4.2).

Table 6.1: Lag 1.5 to 15 minute autocorrelation coefficients of $\bar{\eta}$ for the storm on 6 August, 1976.

LAG NUMBER	TIME LAG (min)	AUTOCORRELATION COEFFICIENT
1	1.5	.972
2	3.0	.891
3	4.5	.769
4	6.0	.654
5	7.5	.529
6	9.0	.430
7	10.5	.325
8	12.0	.238
9	13.5	.140
10	15.0	.054

The values of the red-noise power assuming a Chi-square distribution are applied to the smoothed power spectrum in Figure 6.7 using an autocorrelation value $\rho = .958$.

There are no small-scale preferred frequencies consistent throughout the data. The application of the Tukey highpass filter used in this study results in 10 data points being lost at each end of the data set. This loss is unacceptable in this case due to the small sample size originally, therefore the power spectrum of the highpass filtered data revealed no useful information.

It should be noted that the two cloud-base flares were burned at 17:22 MDT and 17:27 MDT, respectively, and that 8 cloud-top flares were released at 17:29 MDT according to the flight summary. The decline in $\overline{\eta}$ preceded the cloud seeding. This is not obvious from Figure 6.5 which does not show the exact time of seeding.

The storm on 6 August, 1976 exemplifies the sampling problem involved in using only surface hailfall measurements in evaluating the output of a given storm since the presence of the lake for this case severly limited the number of observations obtainable.

6.3 The 12 August, 1976 Storm

The storm on 12 August, 1976 entered the project area from the northwest and spent over five hours in the northwest quadrant of the project area before dissipating. The storm was not seeded.

The synoptic summary is given in Figure 6.8 and the environmental conditions are shown by the tephigram in Figure 6.9. The hailswath is shown in Figure 6.10 which indicates that 6 hail reports were received, including one report of golfball size hail. It is difficult to say if this report was accurate since so few hail reports were received from this sparsely-populated area.

PPI scans of the storm at approximately 15 minute intervals are given in Figures 6.11 through 6.14. Radar reflectivities exceeded 40 dBZ at the time the storm entered the project area. The storm was very slow moving. Two centers

SYNOPTIC SUMMARY

12 AUGUST 1976

SYNOPSIS: THE L/W RIDGE NOW SHIFTED E OVER SASKATCHEWAN. A N-S SURFACE TROUGH OF LOW PRESSURE FORMED OVER ALBERTA IN RESPONSE TO A S/W TROUGH PASSING JUST NW OF THE AREA; THIS LED TO AN INCREASE IN LOW-LEVEL MOISTURE OVER THE PROJECT AREA.

AHP AREA: LIGHT EASTERLY SURFACE WINDS BECOMING SW AT 500 MB. THE MOST SIGNIFICANT STORM CELL DEVELOPMENTS WERE ALONG THE FOOTHILLS WHERE MAXIMUM TOPS EXCEEDED 13 KM BY LATE EVENING WHILE MOVING N.

TROUGH (T) OR RIDGE (R) PASSAGE TIME	12 HOUR 500 MB CHANGE IN				HAIL SIZE CATEGORY	NO. HAIL REPORTS N / S
	VORTICITY ($10^{-5}s^{-1}$)	HEIGHTS * (M)	THICKNESS* (M)	TEMPS. (°C)		
T-13/0100Z	0	- 20	+ 10	0	5	33/14

* DIURNAL EFFECTS REMOVED

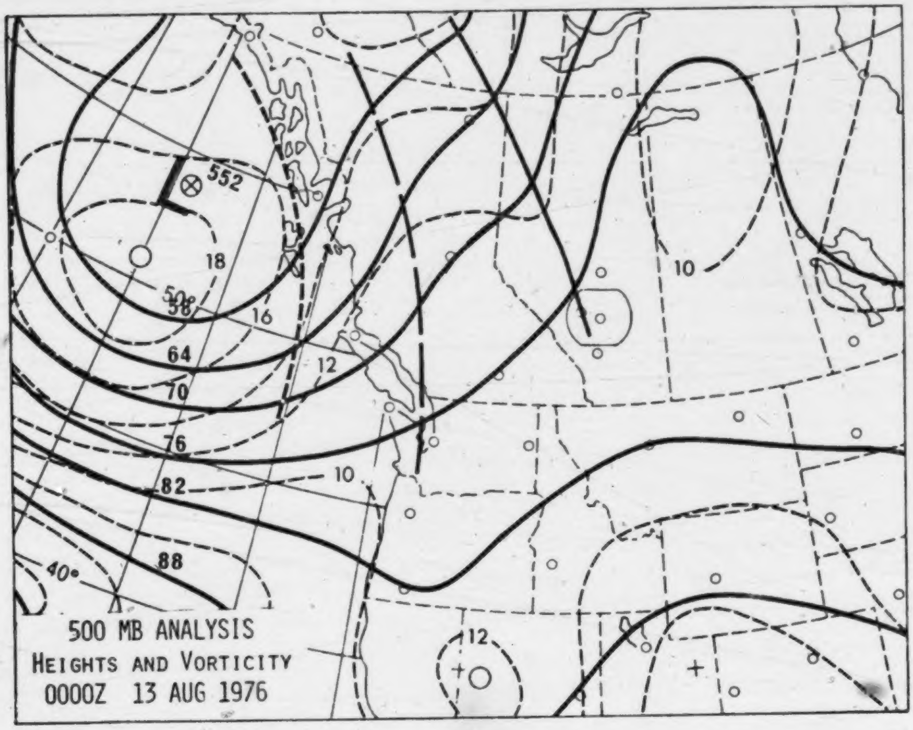
L
552
18
508
58
16
64
70
12
76
82
10
88
40°
10
12
500 MB ANALYSIS
HEIGHTS AND VORTICITY
0000Z 13 AUG 1976

Fig. 6.8: Map showing the synoptic situation, and a brief synoptic summary for the storm on 12 August, 1976. (From Deibert (ed.), 1977)

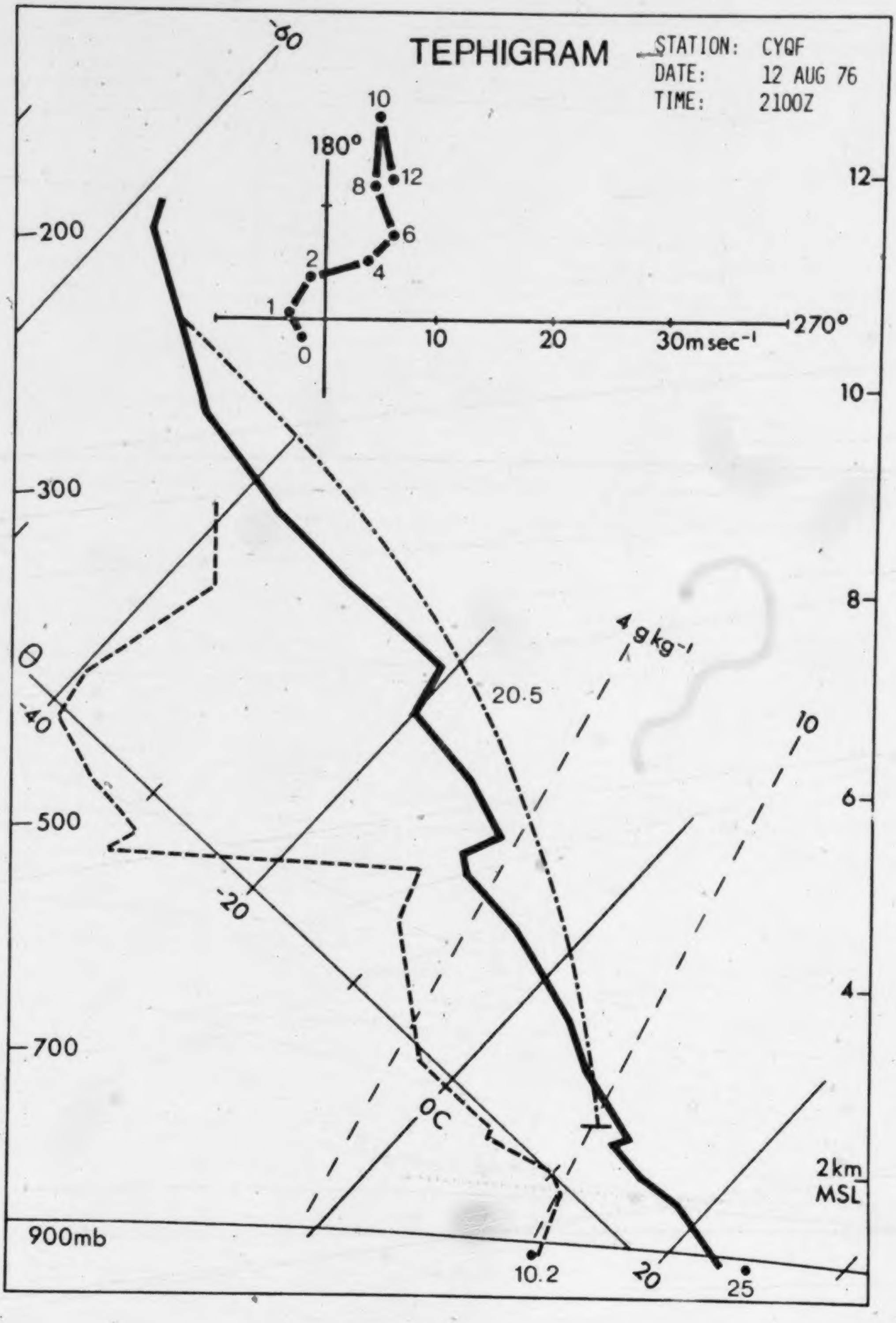

Fig. 6.9: Rawinsonde sounding from Red Deer at 15:00 MDT, 12 August, 1976. (From Deibert (ed.), 1977)

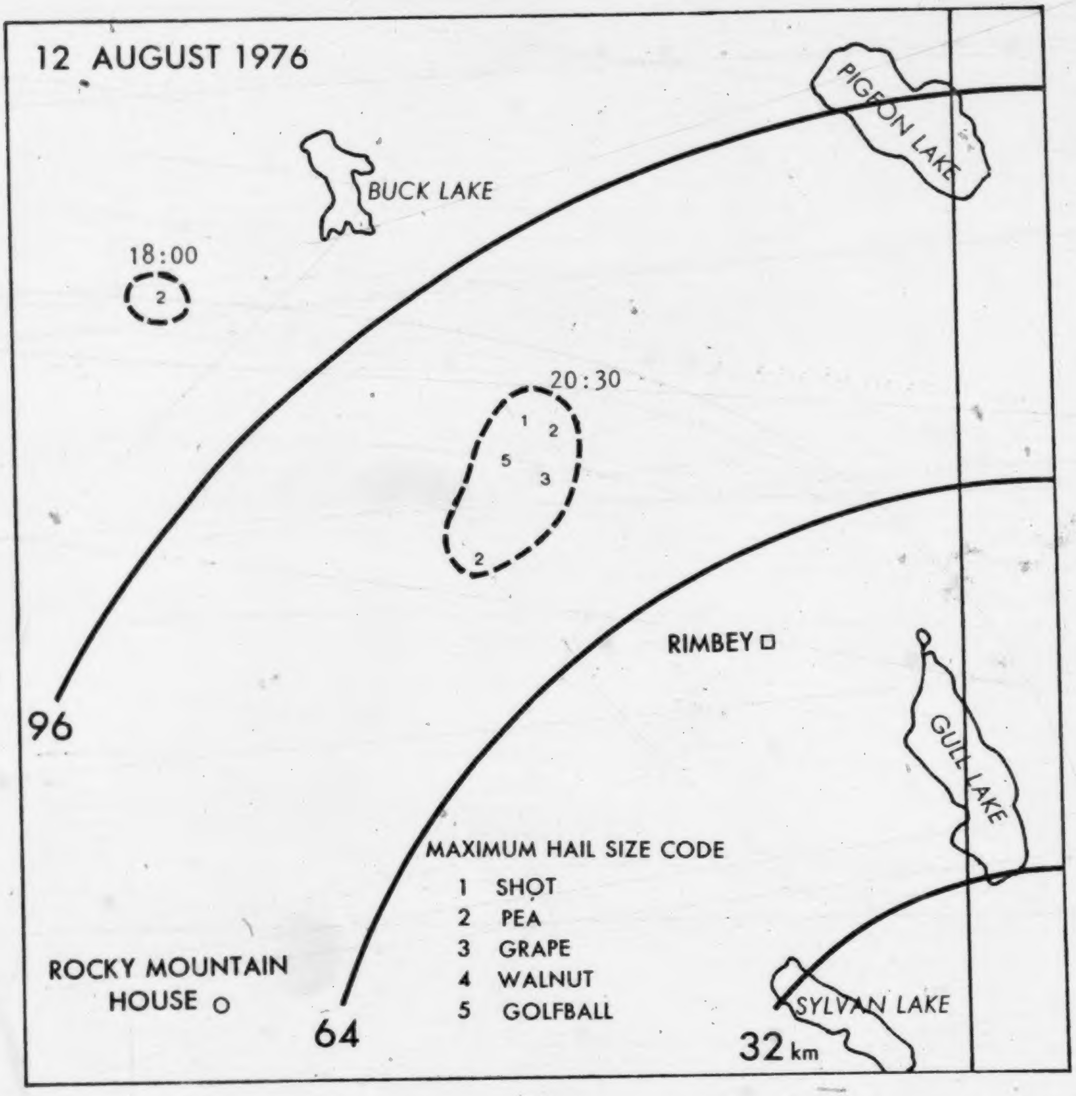
12 AUGUST 1976
PIGEON LAKE
BUCK LAKE
18:00
2
20:30
1
2
5
3
2
RIMBEY
96
GULL LAKE
MAXIMUM HAIL SIZE CODE
1 SHOT
2 PEA
3 GRAPE
4 WALNUT
5 GOLFBALL
ROCKY MOUNTAIN HOUSE
64
SYLVAN LAKE
32 km

Fig. 6.10: Map showing the hailswath resulting from the storm on 12 August, 1976.

Fig. 6.11: PPI echoes for the storm on 12 August, 1976. Elevation ~ 1.9°
Reflectivity = from 20 dBZ by 10 dBZ. Time = 17:00 - 18:14 MDT.

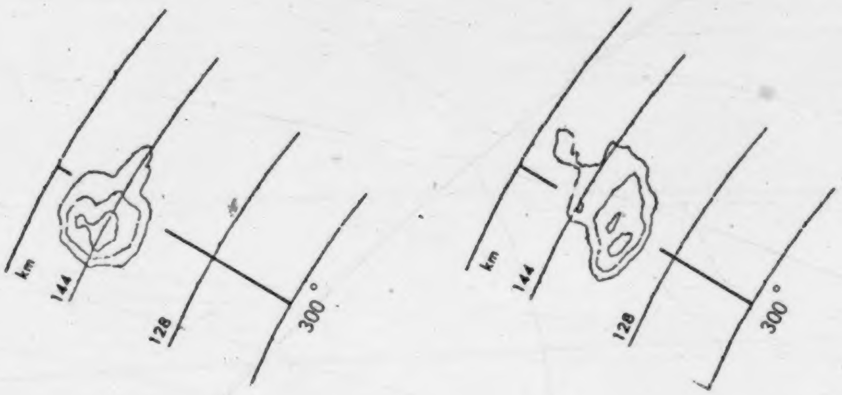

17:00:13 $\overline{\eta} = 2.09 \times 10^{-10} cm^{-1}$ 17:15:09 $\overline{\eta} = 1.07 \times 10^{-10} cm^{-1}$

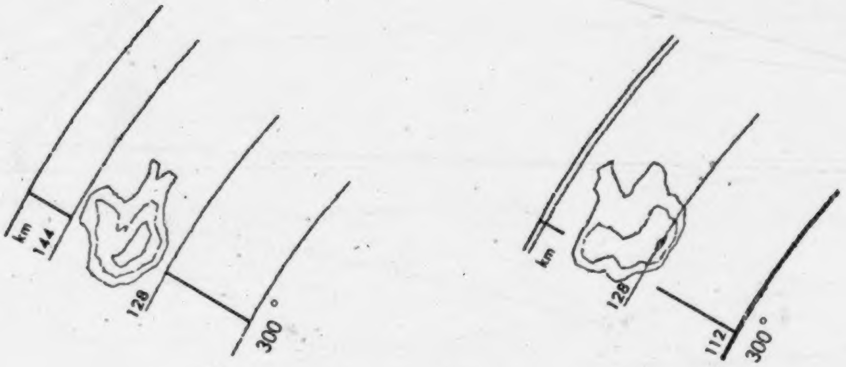

17:30:04 $\overline{\eta} = 1.90 \times 10^{-10} cm^{-1}$ 17:45:00 $\overline{\eta} = 7.28 \times 10^{-11} cm^{-1}$

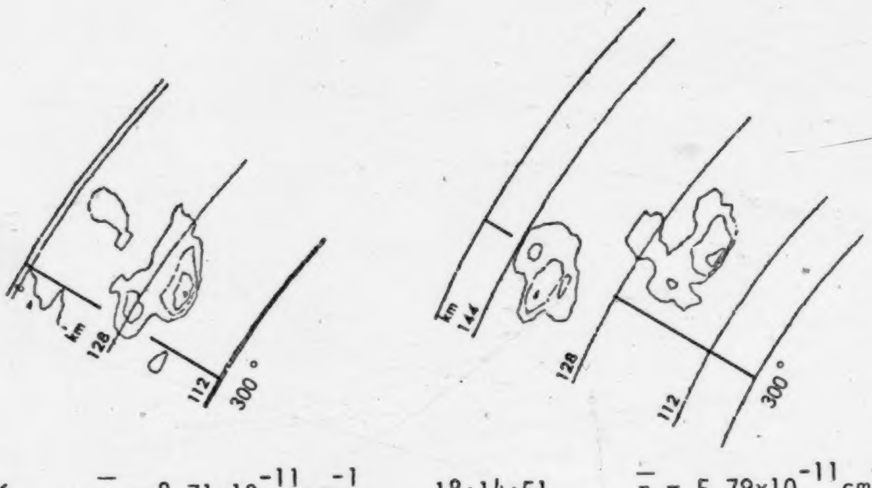

17:59:56 $\overline{\eta} = 8.71 \times 10^{-11} cm^{-1}$ 18:14:51 $\overline{\eta} = 5.79 \times 10^{-11} cm^{-1}$

Fig. 6.12: PPI echoes for the storm on 12 August, 1976. Elevation ~ 2.0°
Reflectivity = from 20 dBZ by 10 dBZ. Time = 18:29 - 19:45 MDT.

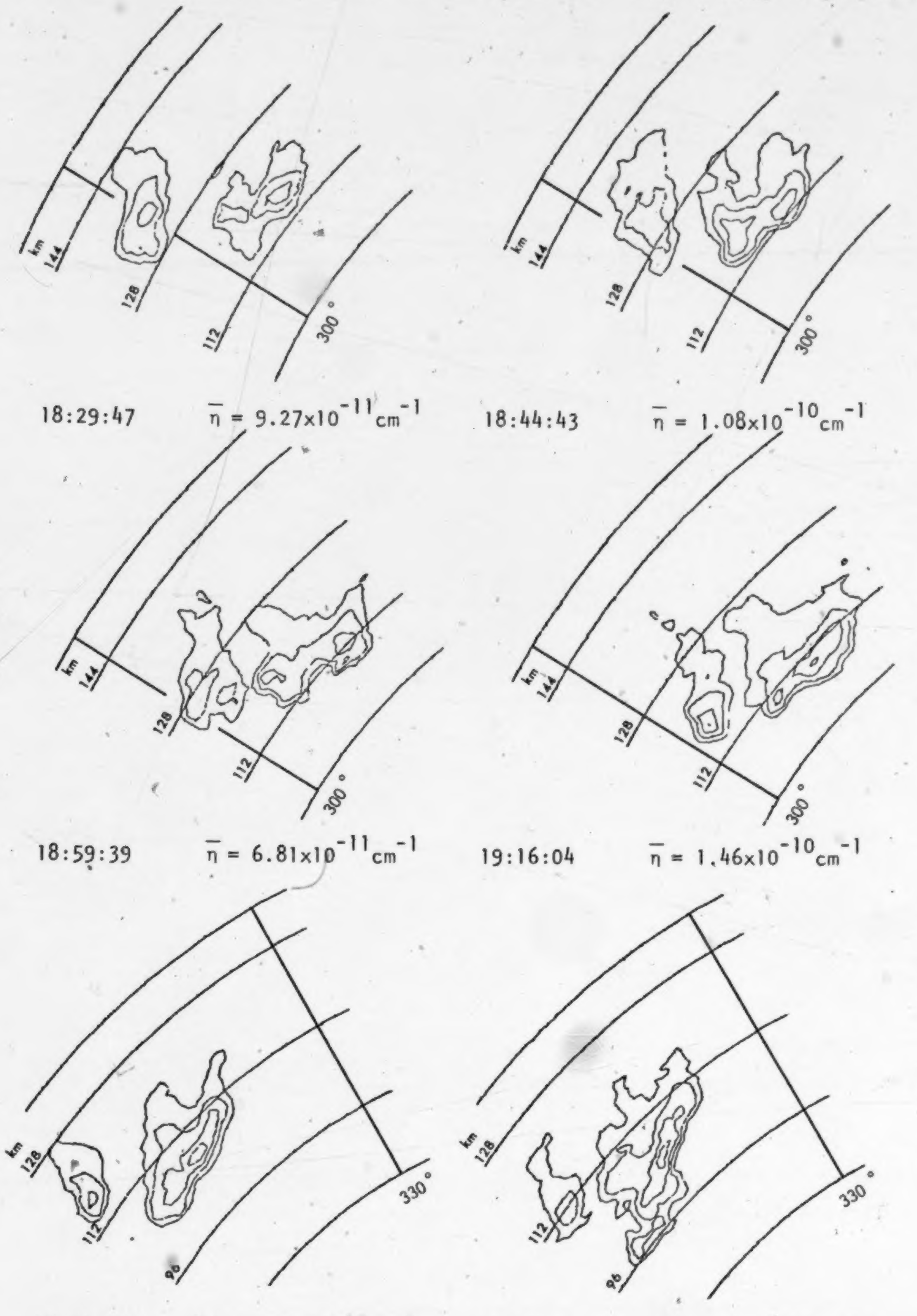

18:29:47 $\overline{\eta} = 9.27\times10^{-11}\,\mathrm{cm}^{-1}$ 18:44:43 $\overline{\eta} = 1.08\times10^{-10}\,\mathrm{cm}^{-1}$

18:59:39 $\overline{\eta} = 6.81\times10^{-11}\,\mathrm{cm}^{-1}$ 19:16:04 $\overline{\eta} = 1.46\times10^{-10}\,\mathrm{cm}^{-1}$

19:31:00 $\overline{\eta} = 2.39\times10^{-10}\,\mathrm{cm}^{-1}$ 19:45:55 $\overline{\eta} = 1.84\times10^{-10}\,\mathrm{cm}^{-1}$

Fig. 6.13: PPI echoes for the storm on 12 August, 1976. Elevation ~ 2.0° Reflectivity = from 20 dBZ by 10 dBZ. Time = 20:00 - 20:45 MDT.

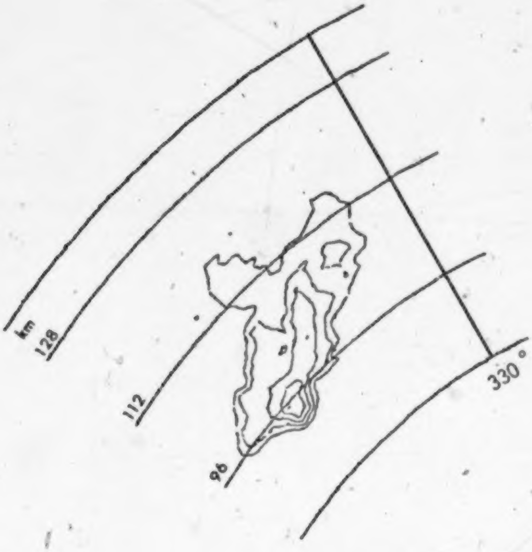

20:00:51 $\overline{n} = 3.62\times10^{-10}\text{cm}^{-1}$ 20:15:47 $\overline{n} = 3.64\times10^{-10}\text{cm}^{-1}$

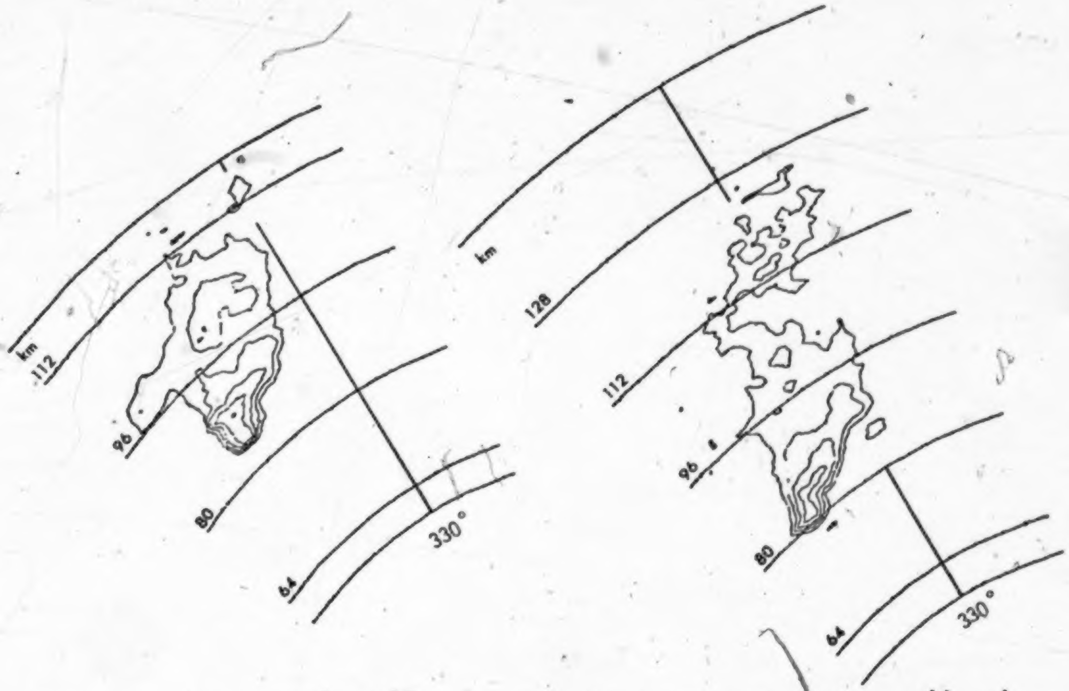

20:29:13 $\overline{n} = 3.06\times10^{-10}\text{cm}^{-1}$ 20:45:38 $\overline{n} = 8.75\times10^{-11}\text{cm}^{-1}$

Fig. 6.14: PPI echoes for the storm on 12 August, 1976. Elevation - 2.0°
Reflectivity = from 20 dBZ by 10 dBZ. Time = 21:00 - 22:00 MDT.

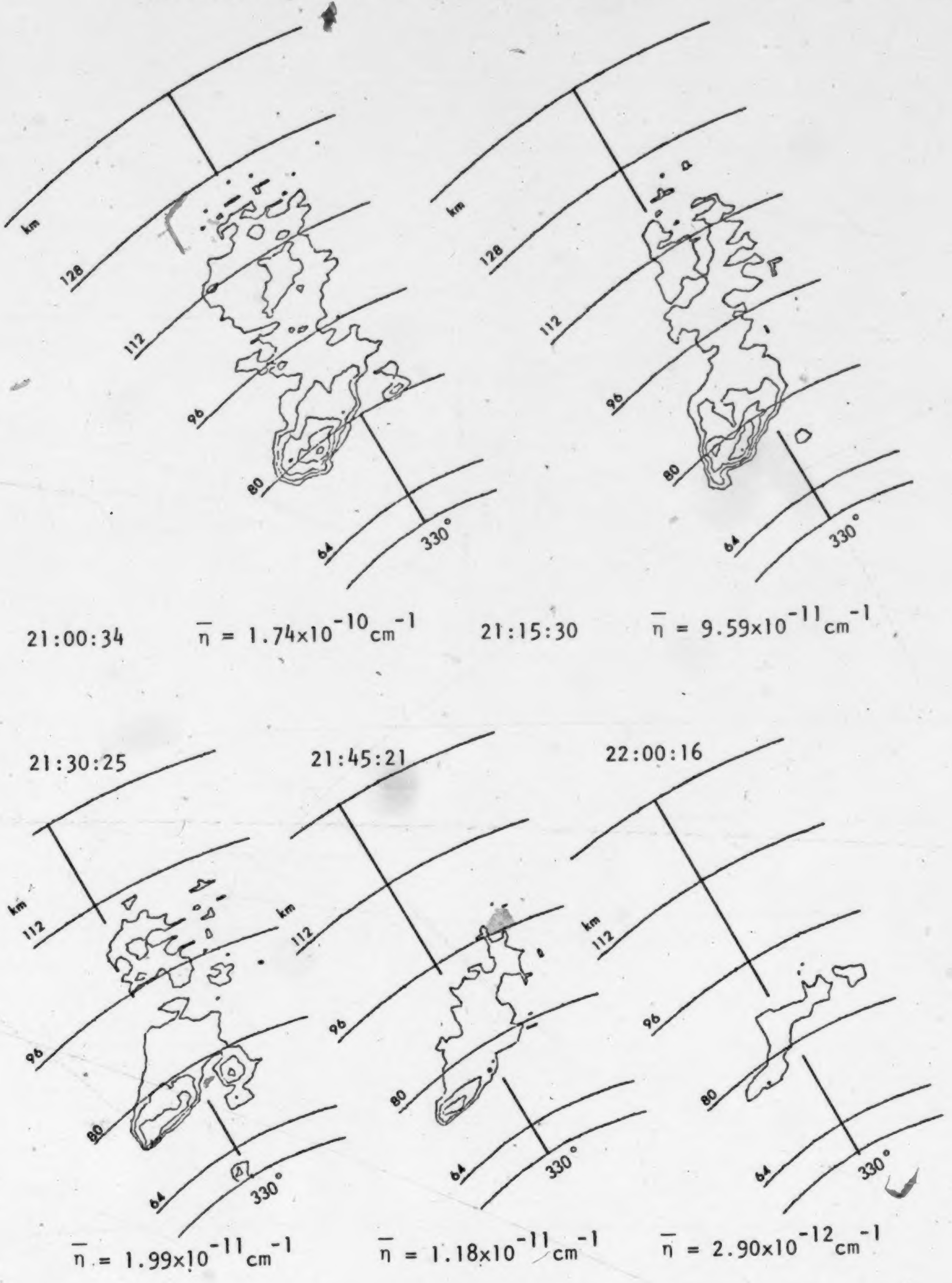

21:00:34 $\overline{\eta} = 1.74\times10^{-10}\,\mathrm{cm}^{-1}$

21:15:30 $\overline{\eta} = 9.59\times10^{-11}\,\mathrm{cm}^{-1}$

21:30:25 $\overline{\eta} = 1.99\times10^{-11}\,\mathrm{cm}^{-1}$

21:45:21 $\overline{\eta} = 1.18\times10^{-11}\,\mathrm{cm}^{-1}$

22:00:16 $\overline{\eta} = 2.90\times10^{-12}\,\mathrm{cm}^{-1}$

of precipitation are evident from the PPI scans over the period from around 18:00 MDT to shortly before 20:00 MDT. After uniting, maximum radar reflectivity exceeded 60 dBZ, and reflectivities exceeding 50 dBZ persisted until approximately 21:30 MDT after which the storm dissipated rapidly. The $\overline{\eta}$ time series for 12 August, 1976 is given in Figure 6.15. The dashed line represents the trend in the data computed using the Tukey filter described in Appendix A.

The radar constant for the day was 74.2 dBm with a peak transmitted power of 227 kw.

There existed during this day a period of time during which the radar was on a full 20 degree elevation scan. This meant that a PPI at one-degree elevation was obtained every 3 minutes instead of every 1.5 minutes as in the previous cases. The calculation of the power spectrum demands that the time interval remain constant between data points. Therefore, the data had to be modified in order to meet the requirement. Two alternatives existed. Firstly, every other data point during the 1.5-minute scans could be removed resulting in a data interval of 3 minutes. Secondly, data could be interpolated between known data points during the time the radar was on the full 3-minute scan. The radar was put on the 3-minute scan at 21:00 MDT during this day. Since the storm ended at 22:03 MDT, only 21 data points were missing. Therefore, it was decided that linear interpolation would be used. The error involved should be minimal since the storms already discussed had autocorrelation coefficients greater than .95 for a 1.5-minute time lag. Linear interpolation should represent a respectable approximation.

The autocorrelation coefficients of the time series for lag one (1.5 min)

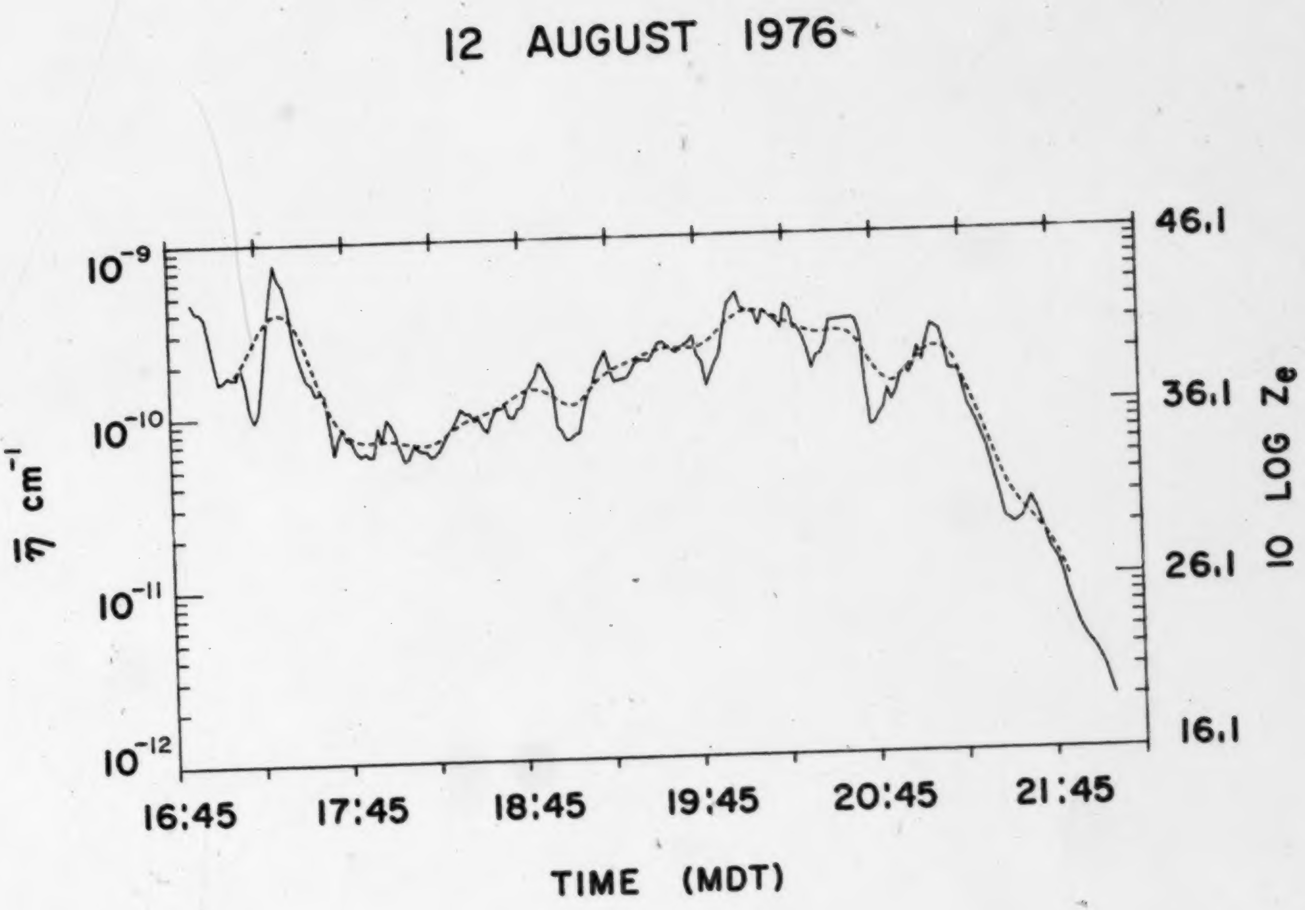

Fig. 6.15: $\overline{\eta}$ versus time for the storm on 12 August, 1976. Dashed line indicates trend.

to lag ten (15 min) computed using (5.4.2) and including the 21 interpolated data points, are given in Table 6.2.

Table 6.2: Lag 1.5 to 15 minute autocorrelation coefficients of $\bar{n}$ for the storm on 12 August, 1976.

LAG NUMBER	TIME LAG (min)	AUTOCORRELATION COEFFICIENT
1	1.5	.936
2	3.0	.821
3	4.5	.687
4	6.0	.554
5	7.5	.457
6	9.0	.396
7	10.5	.365
8	12.0	.349
9	13.5	.329
10	15.0	.311

The unsmoothed power spectrum of the data is given in Figure 6.16 and the smoothed power spectrum, using a three-point running average, is given in Figure 6.17. The highpass data smoothed power spectrum is given in Figure 6.18. The values of the red-noise power are applied to the smoothed raw data power spectrum using an autocorrelation value $\rho = .921$, and to the highpass data smoothed power spectrum using an autocorrelation value $\rho = .690$. A broad peak at 0.057 cycles per minute corresponding to a cycle period of 17.5 minutes appears significant at the 95 per cent confidence level, assuming a Chi-square distribution in

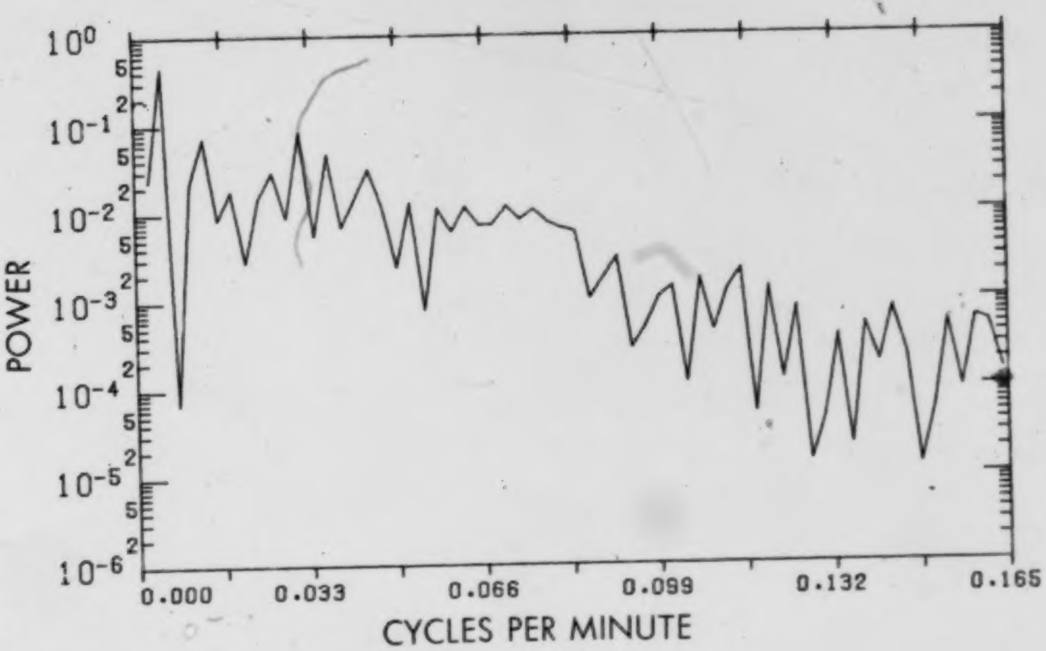

Fig. 6.16: Unsmoothed power spectrum of $\overline{\eta}$ for the storm on 12 August, 1976.

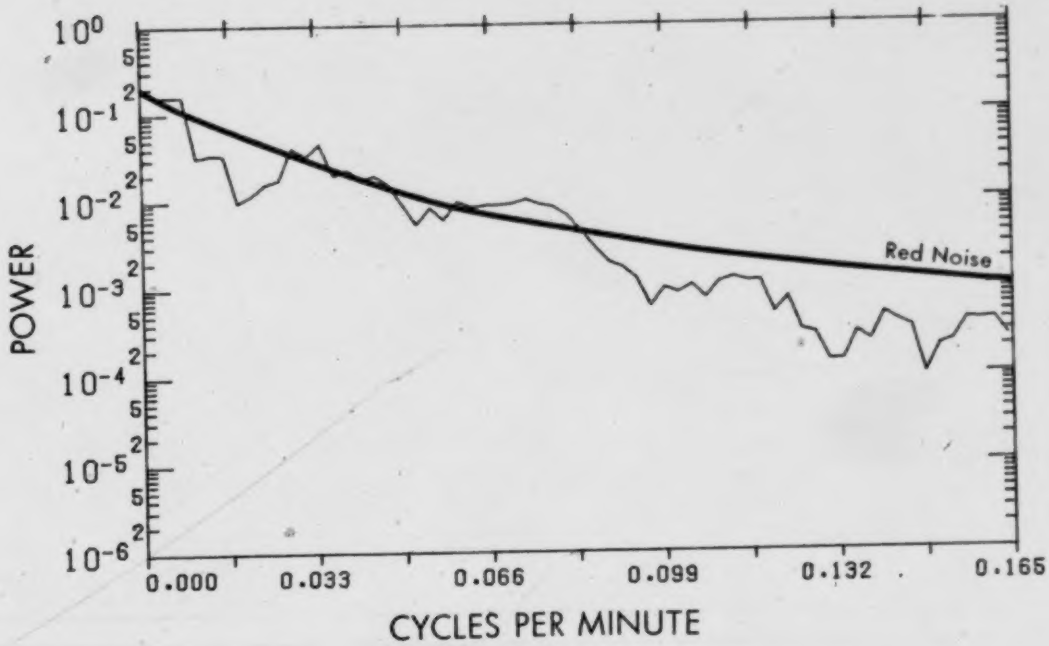

Fig. 6.17: Three-point Daniell-filtered power spectrum of $\overline{\eta}$ for the storm on 12 August, 1976. The red-noise spectrum is shown.

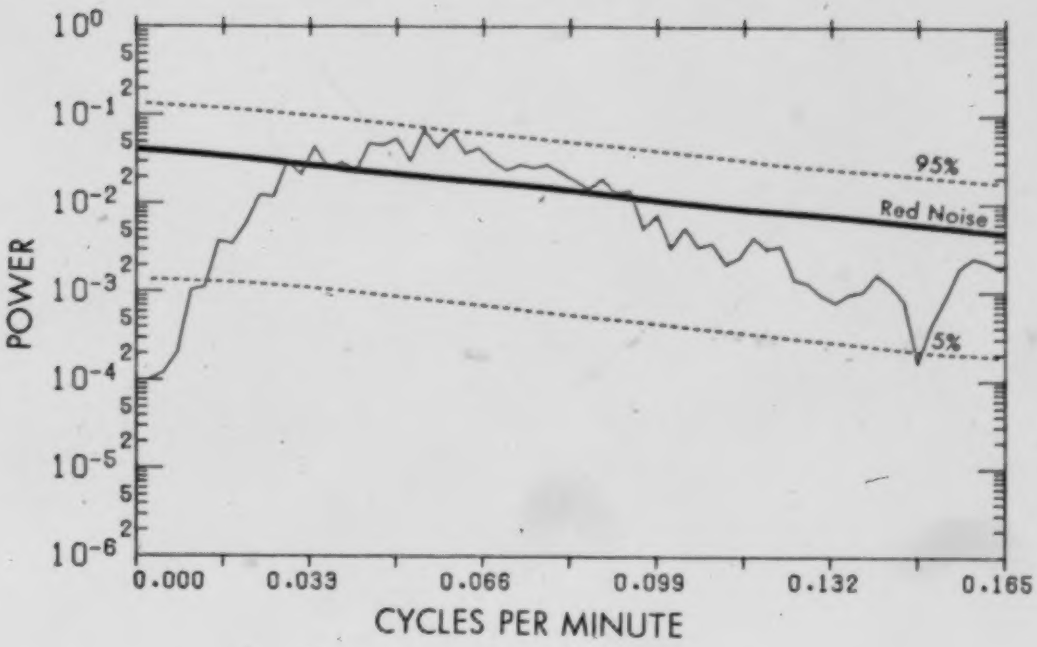

Fig. 6.18: Three-point Daniell-filtered power spectrum of Tukey-filtered η highpass data for the storm on 12 August, 1976. The red-noise spectrum and 90% confidence interval are shown.

Figure 6.18. It should be noted that at the 95 per cent confidence level, at least 3 of the spectral lines in the 64 lines displayed in Figure 6.18 could reach statistical significance by chance due to statistical fluctuations. Therefore, the broad peak in the power spectrum at 0.057 cycles per minute should more appropriately be interpreted as a preferred cycle.

The time series displays greater small-scale variation and less autocorrelation than the series previously discussed. This is most likely due to the fact that the storm was not a well-organized system but consisted of at least two precipitation centers, each with its own associated scales of variability, for a major portion of its lifetime. For example, fluctuations in the precipitation in one core would not coincide necessarily with the fluctuations in the other core. For this reason, this storm may not be a good example of a non-seeded storm for comparison with seeded storms.

6.4 The 15 August, 1976 Storm

The storm on 15 August, 1976 was one which formed in the central portion of the northern project area and tracked towards the northwest. The synoptic summary is given in Figure 6.19 and the environmental conditions are shown by the tephigram in Figure 6.20. The storm was associated with a rapidly moving trough which came out of the southeast. Many storms occurred on this day which was declared a no-seed day in the North. The hailswath associated with this particular storm is shown in Figure 6.21. Six reports of hail were received from this storm with grape size hail reported as the maximum size.

PPI scans of the storm at approximately 15-minute intervals are given

SYNOPTIC SUMMARY

15 AUGUST 1976

SYNOPSIS: THE MOST SIGNIFICANT SYNOPTIC CHANGES OCCURRING DURING THE CURRENT SERIES OF S/W WERE ASSOCIATED WITH THIS THIRD RAPIDLY-MOVING TROUGH. RELATIVELY STRONG PVA AND LARGE HEIGHT AND THICKNESS FALLS PRECEEDED IT, WITH THE TROUGH MOTION BEING 165 AT 60 KPH. A MAJOR SURFACE LOW AND FRONTAL WAVE FORMED OVER MONTANA, THUS ADVECTING ADDITIONAL MOISTURE INTO THE ERN PORTION OF THE AHP AREA.

AHP AREA:. SURFACE WINDS LIGHT, NW IN THE MORNING BECOMING E IN THE EVENING, WITH SE WINDS ALOFT. THE MAIN STORM DEVELOPMENT WAS WELL AFTER MAXIMUM TEMPERATURE TIME, MAINLY OVER THE ERN HALF, WITH TOPS EXCEEDING 14 KM WHILE MOVING TO THE NW. THIS HIGHLY-ORGANIZED STORM CONTINUED OVER NIGHT, PRODUCING THE MOST SERIOUS HAILFALL OF THE SUMMER.

TROUGH (T) OR RIDGE (R) PASSAGE TIME	12 HOUR 500 MB CHANGE IN				HAIL SIZE CATEGORY	NO. HAIL REPORTS N / S
	VORTICITY ($10^{-5}s^{-1}$)	HEIGHTS * (M)	THICKNESS* (M)	TEMPS. (°C)		
T-16/1000Z	+ 5	- 100	- 40	+ 1	6	190/153

* DIURNAL EFFECTS REMOVED

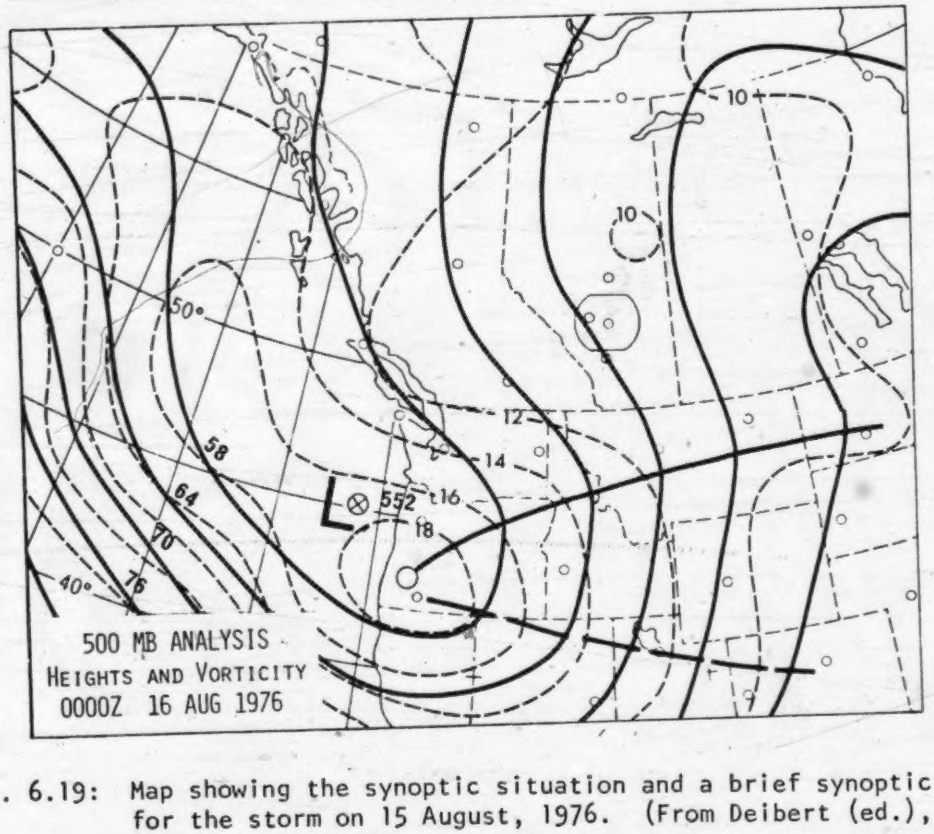

Fig. 6.19: Map showing the synoptic situation and a brief synoptic summary for the storm on 15 August, 1976. (From Deibert (ed.), 1977).

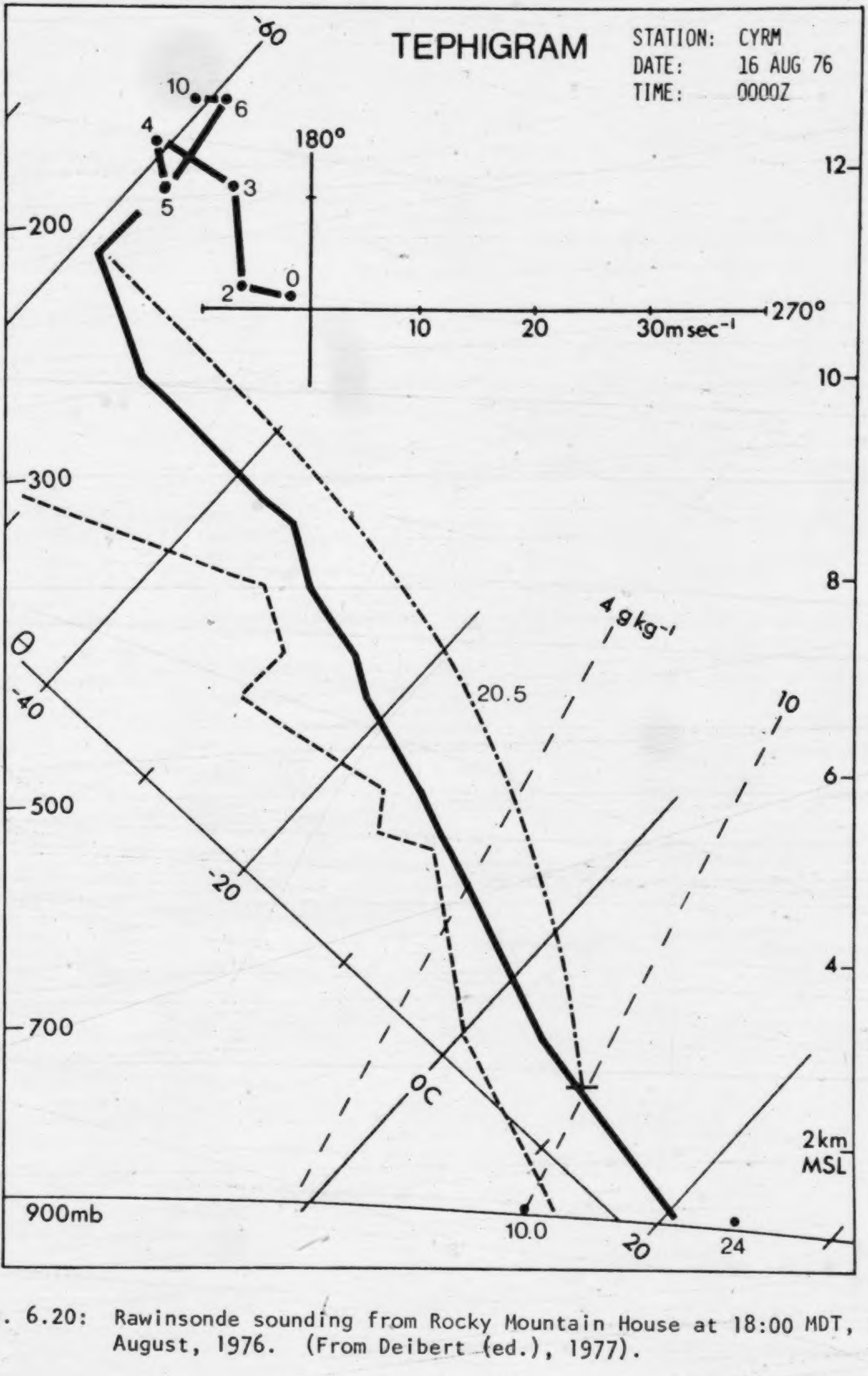

Fig. 6.20: Rawinsonde sounding from Rocky Mountain House at 18:00 MDT, 15 August, 1976. (From Deibert (ed.), 1977).

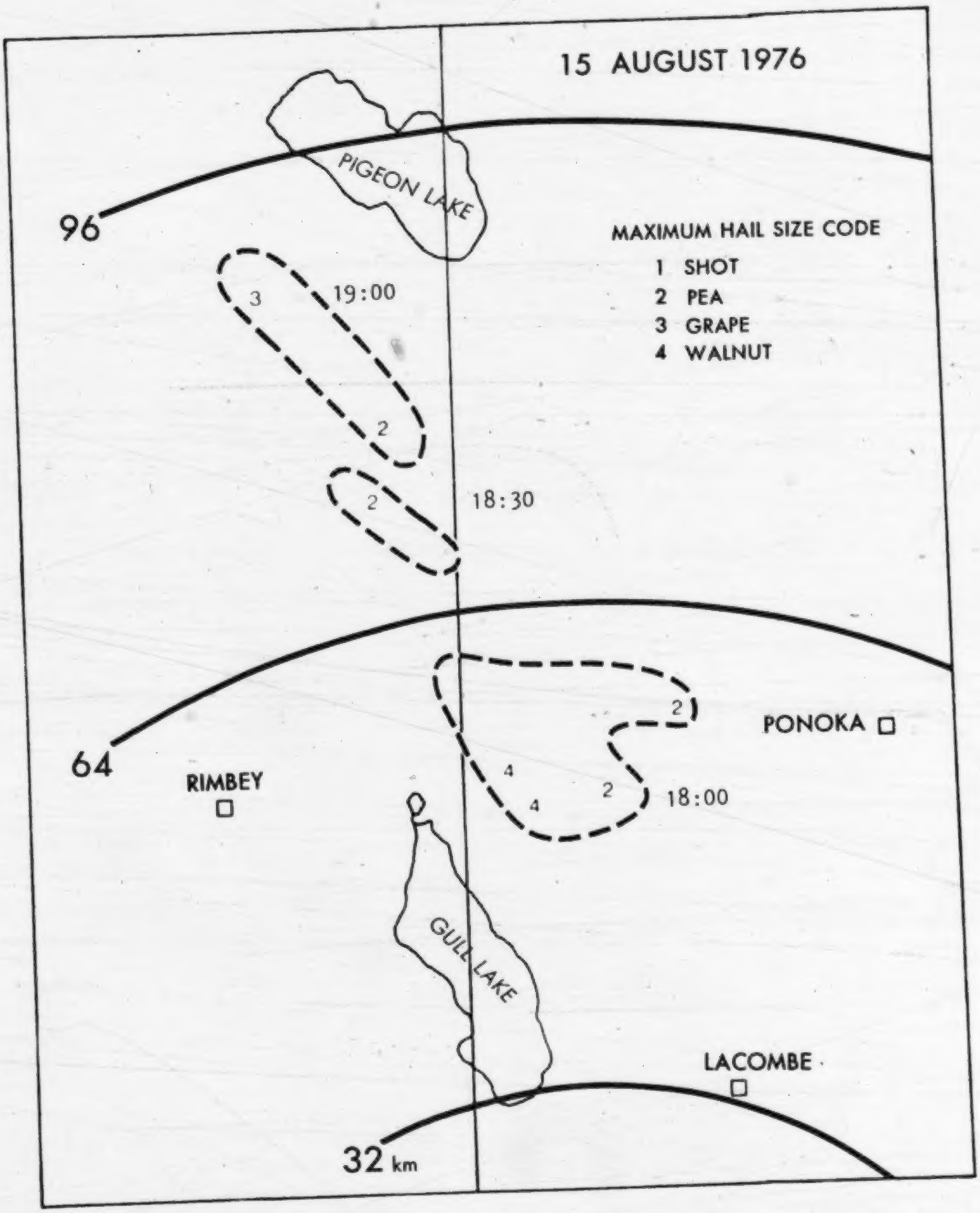
15 AUGUST 1976
PIGEON LAKE
96
MAXIMUM HAIL SIZE CODE
1 SHOT
2 PEA
3 GRAPE
4 WALNUT
3
19:00
2
2
18:30
64
2
PONOKA
4
4
2
18:00
RIMBEY
GULL LAKE
LACOMBE
32 km

Fig. 6.21: Map showing the hailswath resulting from the storm on 15 August, 1976.

in Figures 6.22 and 6.23. Reflectivities in excess of 50 dBZ were recorded.

The radar constant used for the day was 74.2 dBm with a peak transmitted power of 227 kw.

The $\bar{\eta}$ time series for the storm is given in Figure 6.24. The dashed line represents the trend in the data computed using the Tukey filter described in Appendix A.

As was the case with the 12 August, 1976 storm there was a period of time during this day in which the radar was on a full three-minute scan. The period was from 18:07 MDT to 19:47 MDT. Thirty two points of a total 86 data points for this day were interpolated. This is not a desirable situation. However, as mentioned earlier, previous time series possess autocorrelation coefficients greater than .90 for 1.5 minute time lags and, therefore, linear interpolation was felt to be preferable to determining the power spectrum from data spaced three minutes apart.

The autocorrelation coefficients of the data for lag one (1.5 min) to lag ten (15 min), computed using (5.4.2) are given in Table 6.3.

The unsmoothed power spectrum of the raw data is given in Figure 6.25 and the smoothed power spectrum, using a three-point running average, is given in Figure 6.26. The smoothed power spectrum of the filtered highpass data is given in Figure 6.27. The values of the red-noise power are applied to the raw data smoothed power spectrum using an autocorrelation value ρ = .937, and to the highpass data smoothed power spectrum using ρ = .695. There were no statistically significant cycles evident at the 95 per cent confidence level assuming a Chi-square

Fig. 6.22: PPI echoes for the storm on 15 August, 1976. Elevation ~ 2.0° Reflectivity = from 20 dBZ by 10 dBZ. Time = 17:45 - 18:45 MDT.

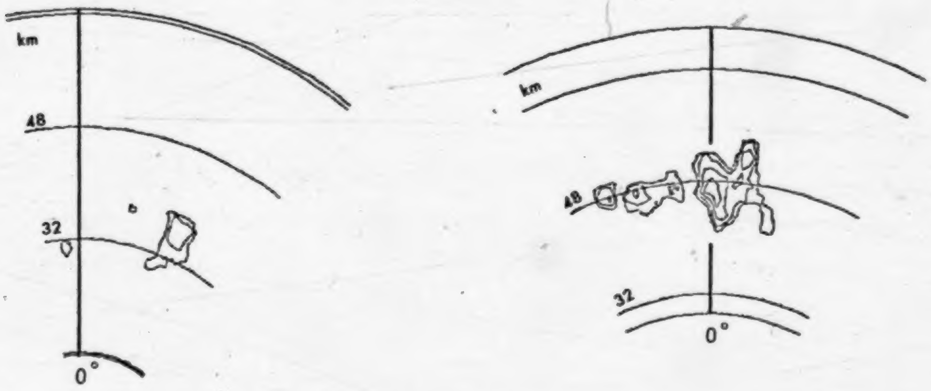

17:45:23 $\bar{n} = 1.00 \times 10^{-11} \mathrm{cm}^{-1}$ 18:00:18 $\bar{n} = 1.61 \times 10^{-10} \mathrm{cm}^{-1}$

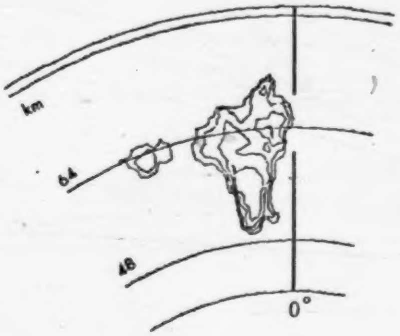

18:15:13 $\bar{n} = 4.93 \times 10^{-10} \mathrm{cm}^{-1}$

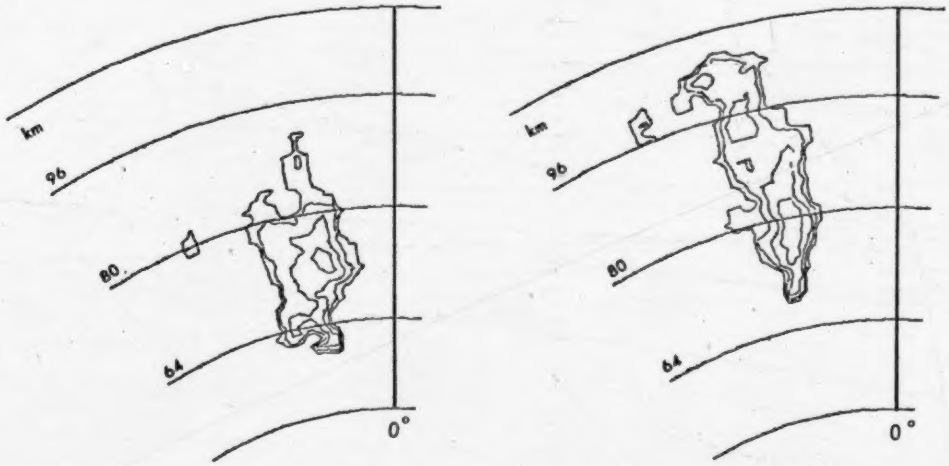

18:30:09 $\bar{n} = 1.57 \times 10^{-10} \mathrm{cm}^{-1}$ 18:45:05 $\bar{n} = 2.97 \times 10^{-10} \mathrm{cm}^{-1}$

Fig. 6.23: PPI echoes for the storm on 15 August, 1976. Elevation ~ 2.0°
Reflectivity = from 20 dBZ by 10 dBZ. Time = 19:00 - 19:47 MDT.

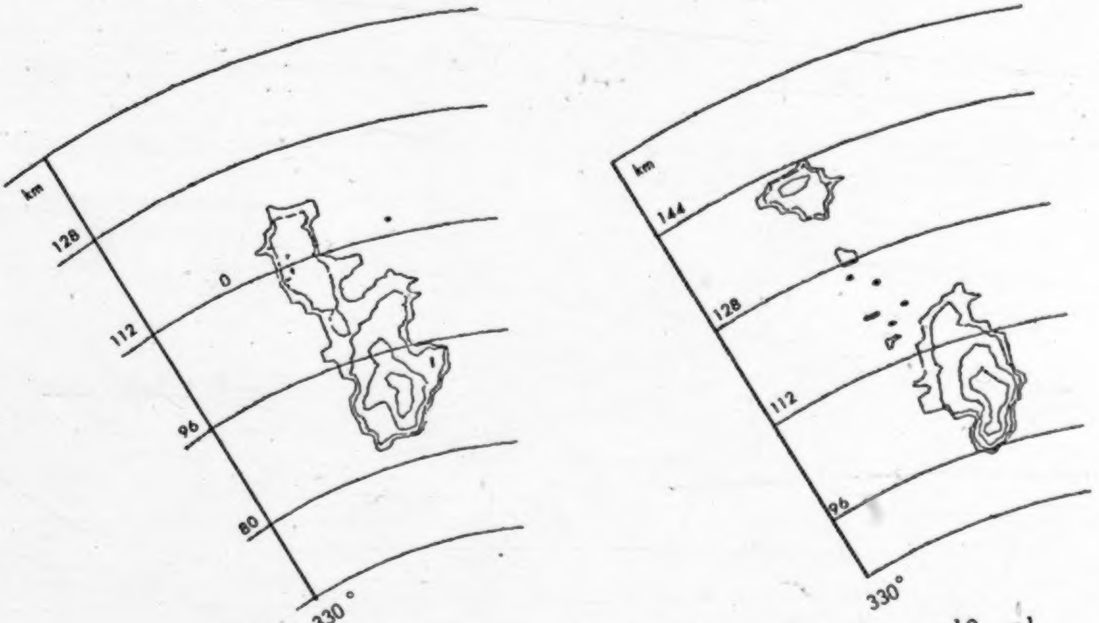

19:00:00 $\overline{\eta} = 1.39\times10^{-10}\,\mathrm{cm}^{-1}$ 19:17:55 $\overline{\eta} = 3.17\times10^{-10}\,\mathrm{cm}^{-1}$

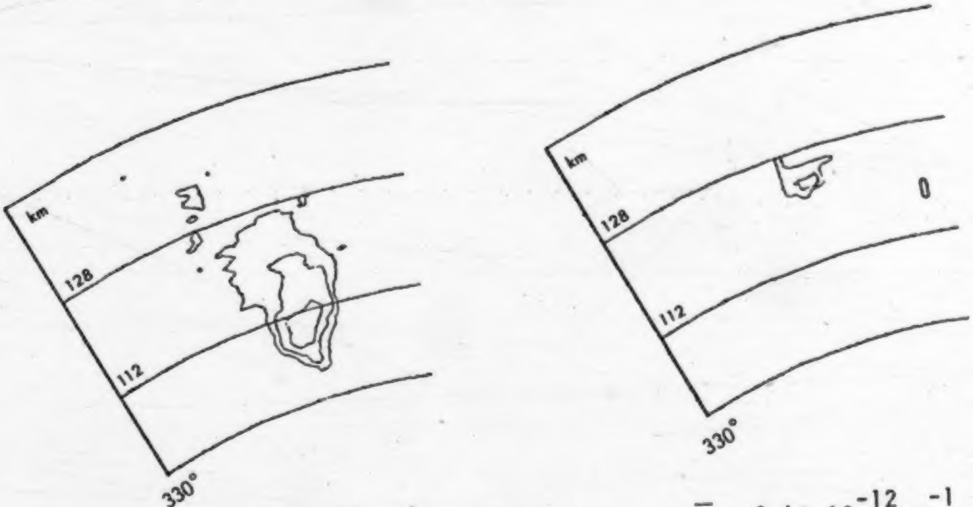

19:29:59 $\overline{\eta} = 6.59\times10^{-11}\,\mathrm{cm}^{-1}$ 19:47:53 $\overline{\eta} = 8.40\times10^{-12}\,\mathrm{cm}^{-1}$

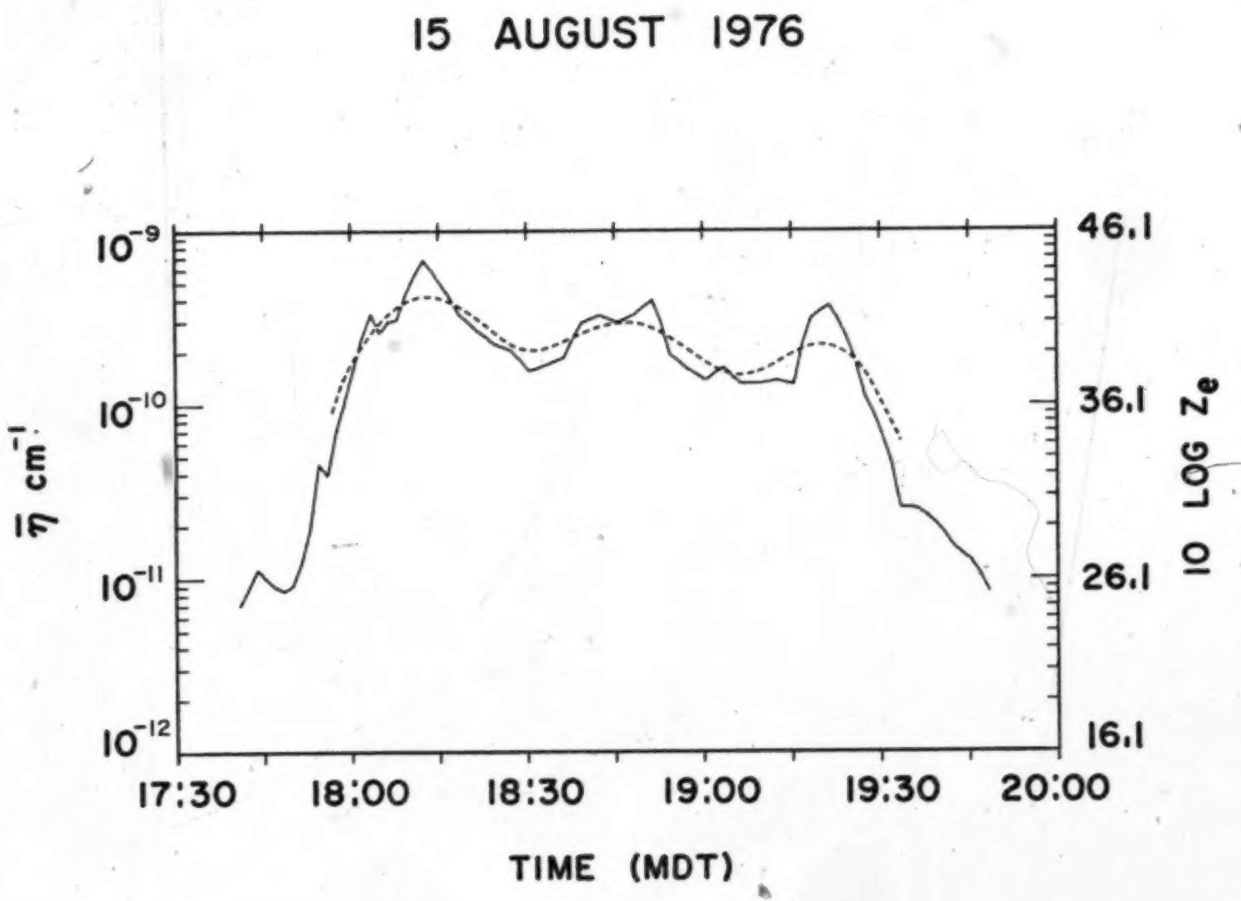

Fig. 6.24: $\bar{\eta}$ versus time for the storm on 15 August, 1976. Dashed line indicates trend.

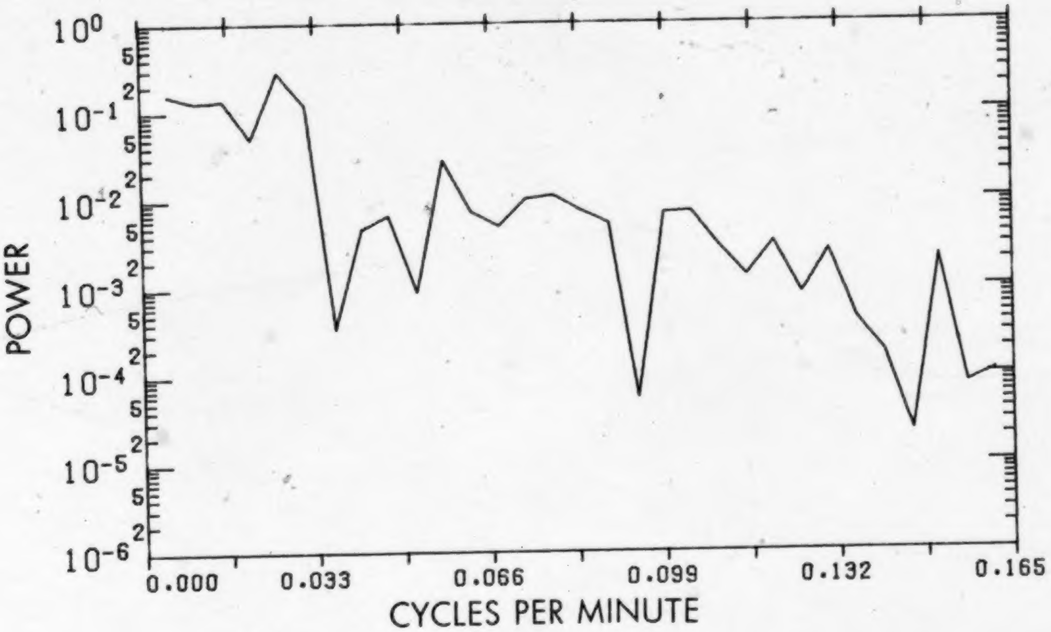

Fig. 6.25: Unsmoothed power spectrum of $\overline{\eta}$ for the storm on 15 August, 1976.

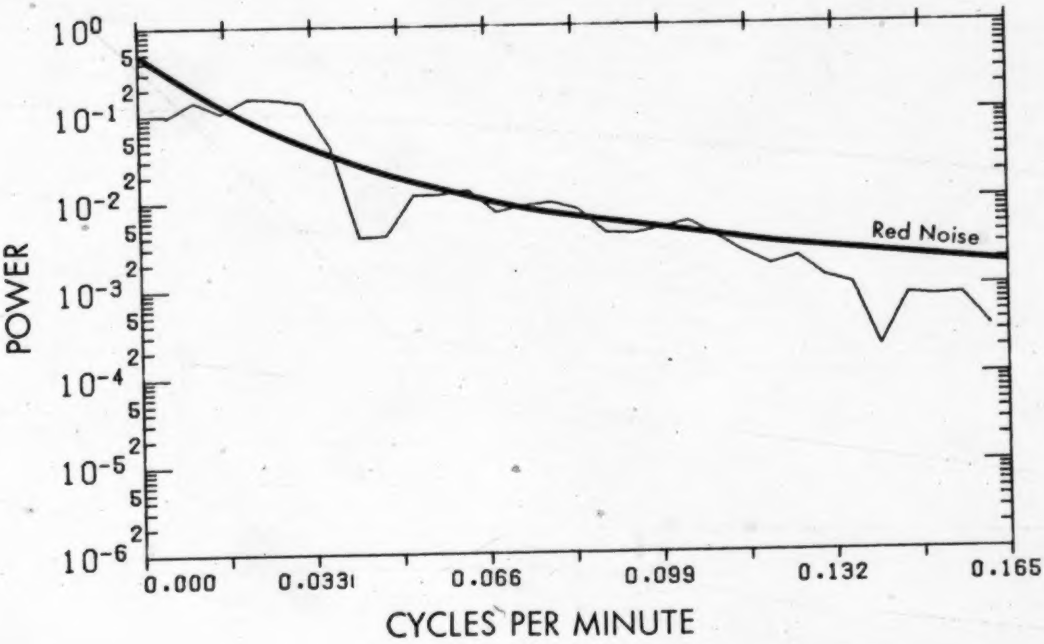

Fig. 6.26: Three-point Daniell-filtered power spectrum of $\overline{\eta}$ for the storm on 15 August, 1976. The red-noise spectrum is shown.

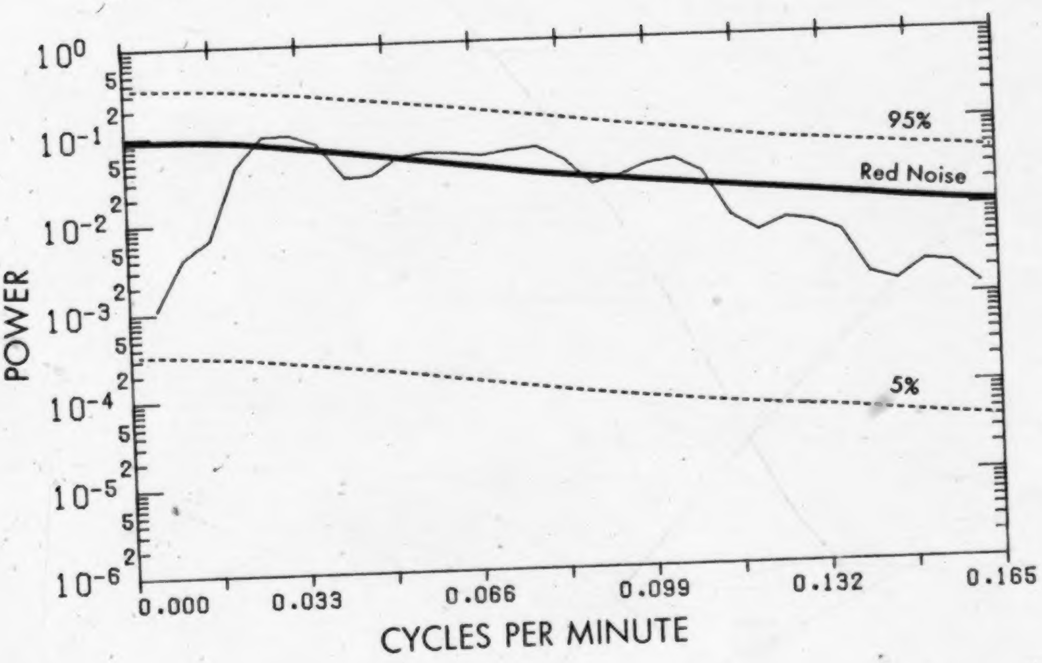

Fig. 6.27: Three-point Daniell-filtered power spectrum of Tukey-filtered $\bar{\eta}$ highpass data for the storm on 15 August, 1976. The red-noise spectrum and 90% confidence interval are shown.

Table 6.3: Lag 1.5 to 15 minute autocorrelation coefficients of $\overline{\eta}$ for the storm on 15 August, 1976.

LAG NUMBER	TIME LAG (min)	AUTOCORRELATION COEFFICIENT
1	1.5	.958
2	3.0	.840
3	4.5	.701
4	6.0	.570
5	7.5	.451
6	9.0	.341
7	10.5	.223
8	12.0	.105
9	13.5	-.009
10	15.0	-.108

distribution, although a preferred frequency appears to exist in Figures 6.26 and 6.27 near 0.025 cycles per minute. This corresponds to a cycle period of 40.0 minutes.

Red-noise cannot represent the data completely in this case since the autocorrelation coefficients were negative at long time lags. By definition $R(\tau + 1) = R(\tau)^2$ which approaches zero for large lag times τ, but never acquires negative values. The red-noise representation is still superior to that of white noise.

6.5 The 20 August, 1976 Storm

The storm on 20 August, 1976 formed just inside the northwestern project boundary and tracked eastward, dissipating in the northeast quadrant approximately 2.5 hours later. The storm was seeded.

The synoptic summary is given in Figure 6.28 and the environmental conditions are shown by the tephigram in Figure 6.29. The resulting hailswath is shown in Figure 6.30 which indicates that 8 hail reports were received, all reporting pea-size hail as the maximum size.

PPI scans of the storm at approximately 15 minute intervals are given in Figures 6.31 and 6.32. The storm started as three tiny centers and grew into two significant precipitation cores which later joined to form one major storm center. Maximum reflectivities were slightly in excess of 40 dBZ.

The $\bar{\eta}$ time series for 20 August, 1976 is given in Figure 6.33 which also indicates the time and amount of cloud seeding. The dashed line represents the trend in the data computed using the Tukey filter described in Appendix A. The radar constant used for the day was 72.3 dBm with a peak transmitted power of 351 kw.

The radar operated at a 1.5-minute scan period the entire day and therefore, no interpolation of data points was necessary.

The autocorrelation coefficients of the data for lag one (1.5 min) to lag ten (15 min) computed using (5.4.2) are given in Table 6.4. The time series displayed very high autocorrelation despite the storms rather complex nature.

The unsmoothed power spectrum of the raw data is given in Figure 6.34 and the smoothed power spectrum using a three-point running average is given in Figure 6.35. The values of the red-noise power are applied to the smoothed power spectrum using an autocorrelation value ρ = .985.

The highpass data smoothed power spectrum with the red-noise power

SYNOPTIC SUMMARY

20 AUGUST 1976

SYNOPSIS: THE MOST IMPORTANT SYNOPTIC FEATURE HERE WAS A RAPIDLY-MOVING TROUGH PASSING THROUGH AHP BEFORE NOON. (NOTE: 12-HR CHANGES SHOWN ARE FOR 20/00-12Z.) THE APPARENT WEAK RIDGING BEHIND THE TROUGH WAS QUASI-STATIONARY, HENCE NOT A S/W FEATURE. THIS RESULTED FROM THE START OF RETROGRESSION FROM E TO W OF THE L/W RIDGE.

SURFACE PRESSURE FEATURES WERE LITTLE-CHANGED FROM THE 19TH, WITH SOUNDINGS FOR BOTH DAYS SHOWING THAT THE INCREASE IN INSTABILITY WAS A RESULT OF UPPER-LEVEL CHANGES.

AHP AREA: W WINDS AT ALL LEVELS. SEVERAL ORGANIZED CELLS FORMED ALONG THE FOOTHILLS NEAR NOON. THESE DEVELOPED TOPS TO 9 KM WHILE MOVING RAPIDLY E THROUGH THE AREA AND DECAYED AFTER MAXIMUM TEMPERATURE TIME.

TROUGH (T) OR RIDGE (R) PASSAGE TIME	12 HOUR 500 MB CHANGE IN				HAIL SIZE CATEGORY	NO. HAIL REPORTS N / S
	VORTICITY ($10^{-5}s^{-1}$)	HEIGHTS * (M)	THICKNESS* (M)	TEMPS. (°C)		
T-20/1600Z	+ 4	- 10	0	- 2	3	19/1

* DIURNAL EFFECTS REMOVED

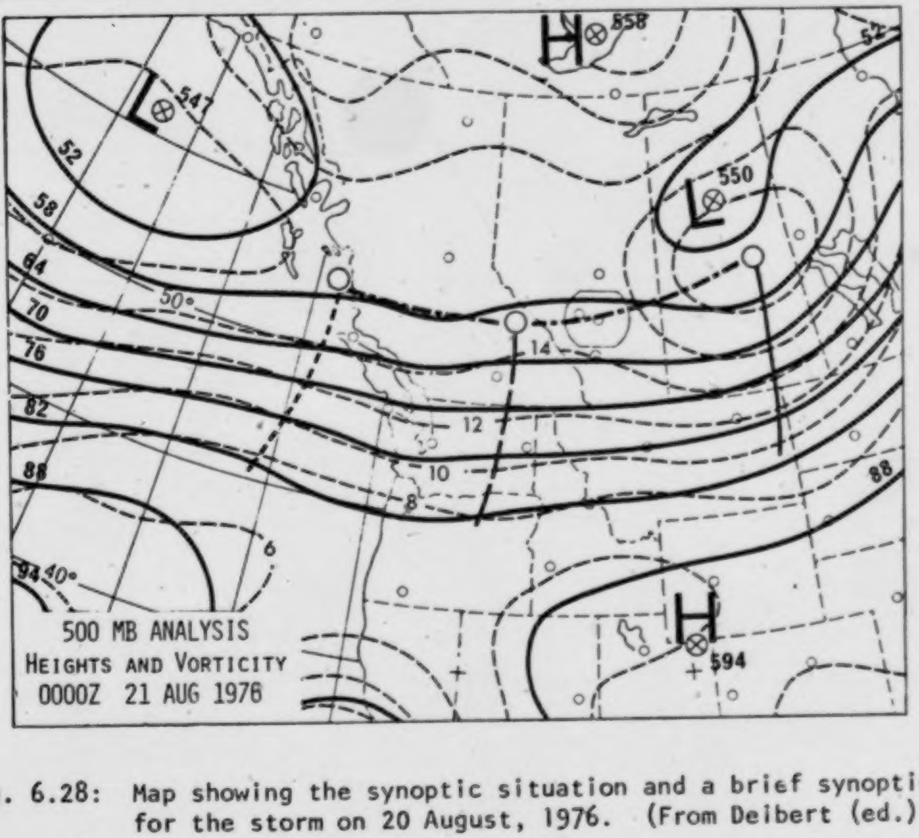
H
558
52
L
547
52
58
64
70
76
82
88
94
50°
40°
14
12
10
8
6
L
550
52
88
H
594
500 MB ANALYSIS
HEIGHTS AND VORTICITY
0000Z 21 AUG 1976

Fig. 6.28: Map showing the synoptic situation and a brief synoptic summary for the storm on 20 August, 1976. (From Deibert (ed.), 1977)

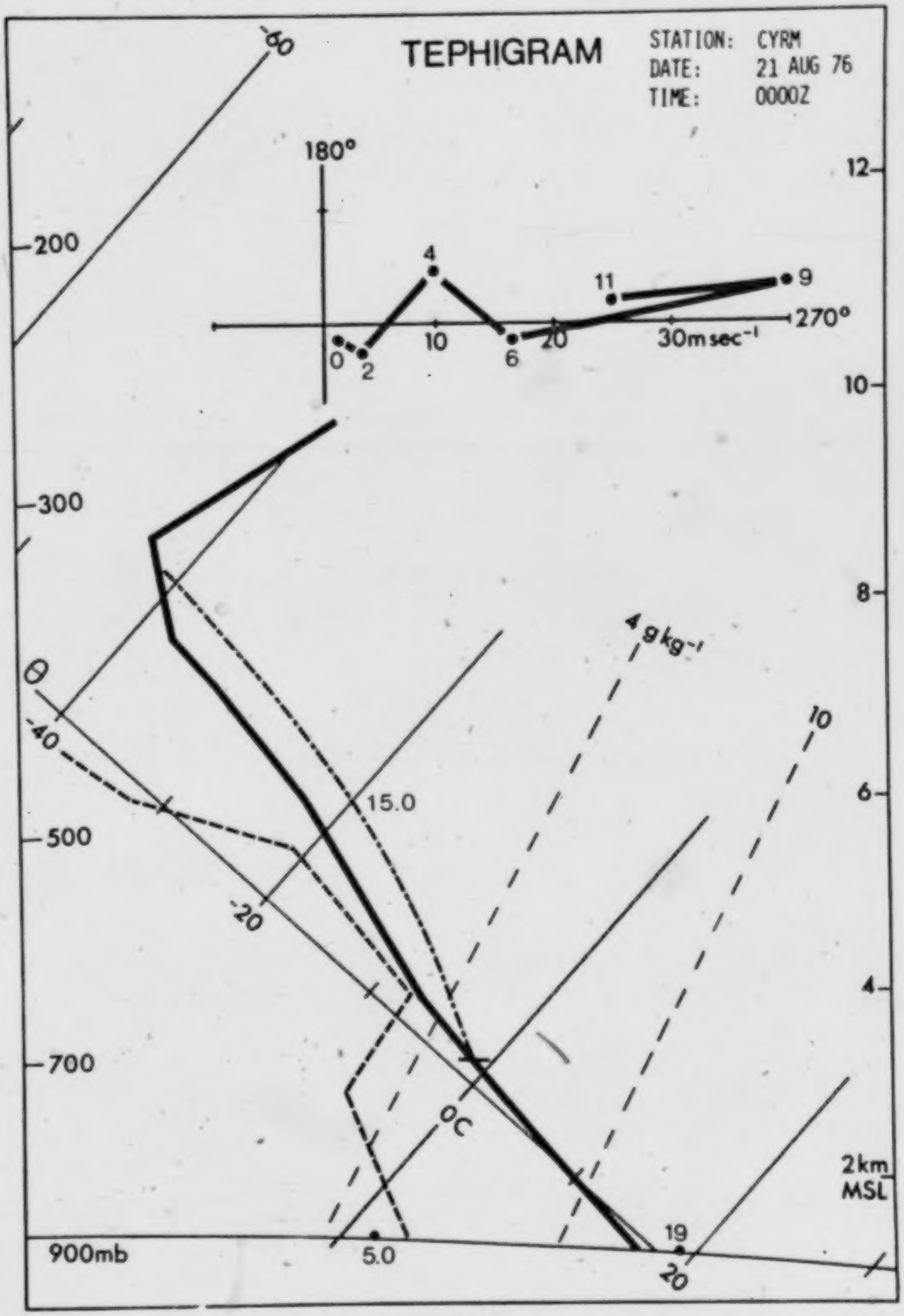

Fig. 6.29: Rawinsonde sounding from Rocky Mountain House at 18:00 MDT, 20 August, 1976. (From Deibert (ed.), 1977)

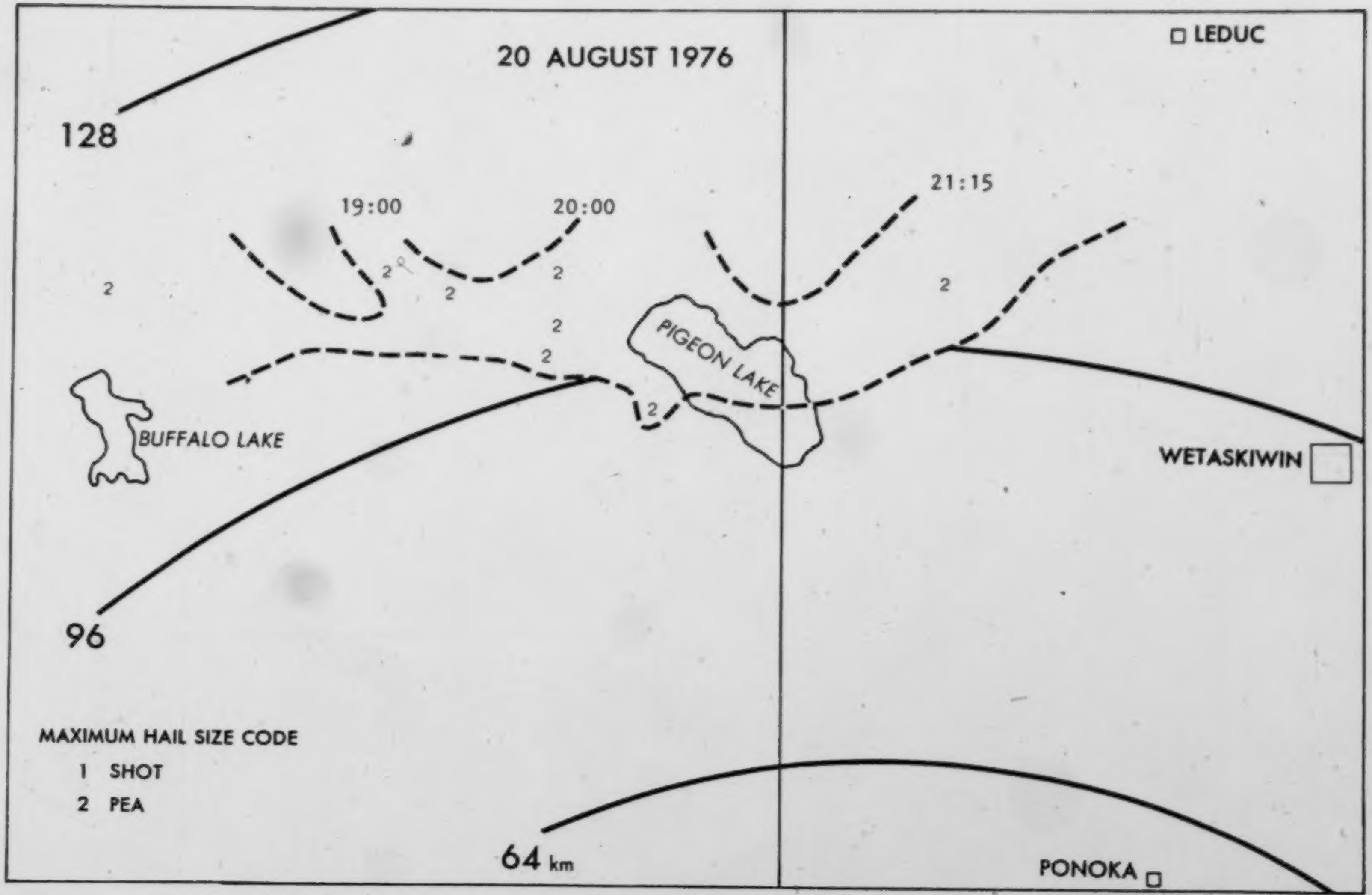
20 AUGUST 1976
LEDUC
128
19:00
20:00
21:15
2
2
2
2
2
2
2
2
PIGEON LAKE
BUFFALO LAKE
WETASKIWIN
96
MAXIMUM HAIL SIZE CODE
1 SHOT
2 PEA
64 km
PONOKA

Fig 6.30: Map showing the hailswath resulting from the storm on 20 August, 1976.

Fig. 6.31: PPI echoes for the storm on 20 August, 1976. Elevation - 2.0°
Reflectivity = from 20 dBZ by 10 dBZ. Time = 19:00 - 20:15 MDT.

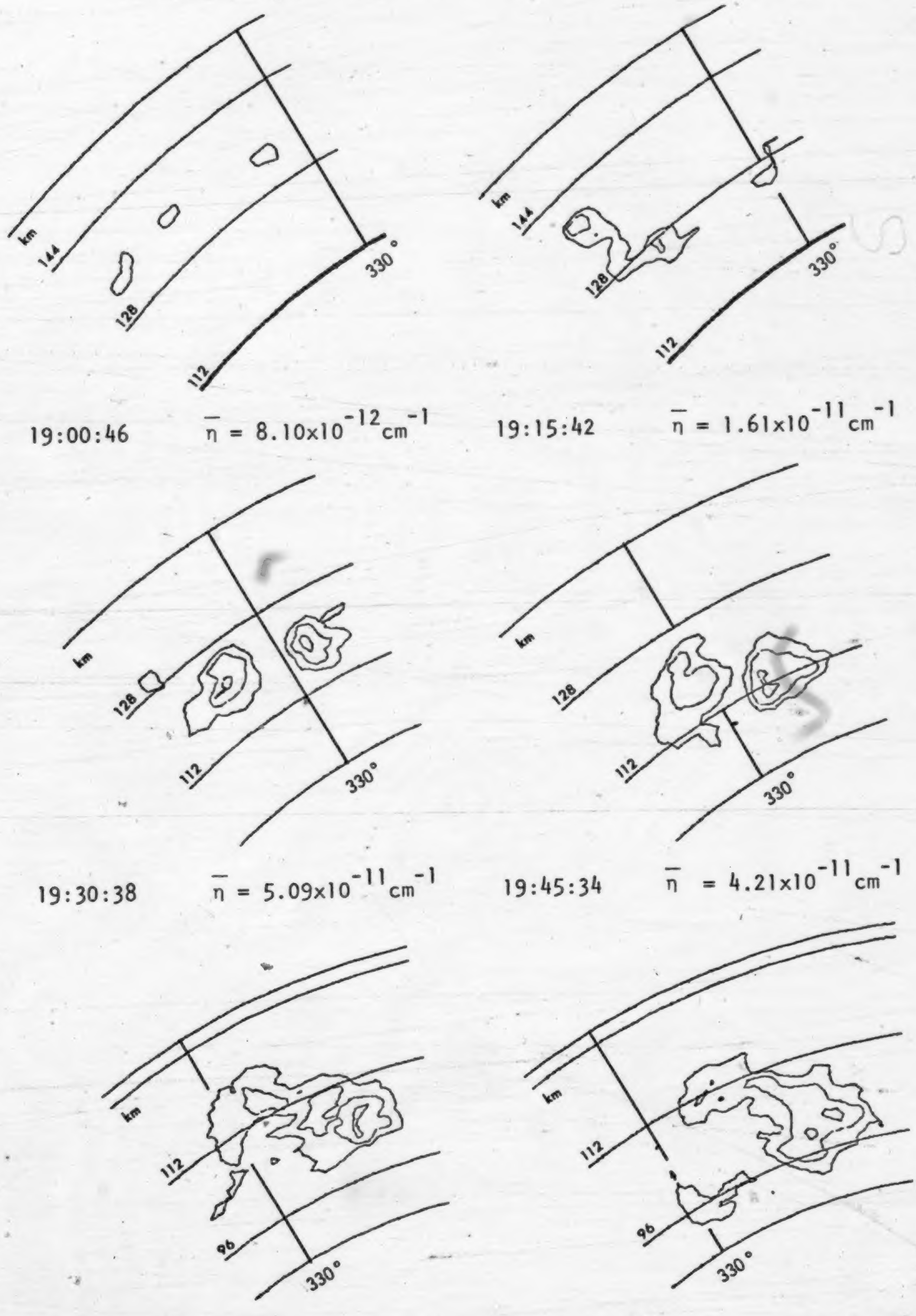

19:00:46 $\bar{\eta} = 8.10\times10^{-12}\,cm^{-1}$

19:15:42 $\bar{\eta} = 1.61\times10^{-11}\,cm^{-1}$

19:30:38 $\bar{\eta} = 5.09\times10^{-11}\,cm^{-1}$

19:45:34 $\bar{\eta} = 4.21\times10^{-11}\,cm^{-1}$

20:00:30 $\bar{\eta} = 2.24\times10^{-11}\,cm^{-1}$

20:15:25 $\bar{\eta} = 2.08\times10^{-11}\,cm^{-1}$

Fig. 6.32: PPI echoes for the storm on 20 August, 1976. Elevation ~ 2.1° Reflectivity = from 20 dBZ by 10 dBZ. Time = 20:30 - 21:15 MDT.

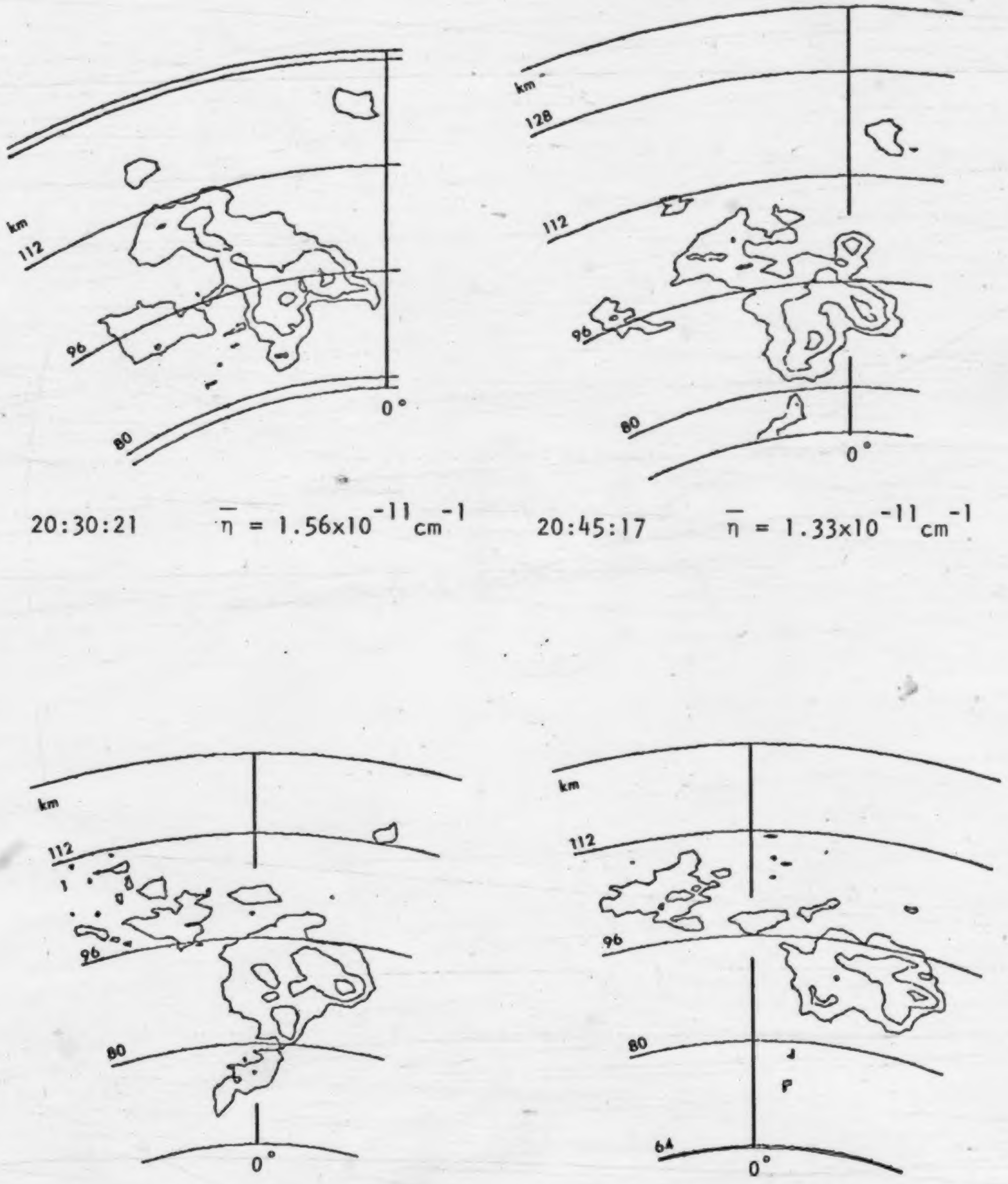
km
112
96
80
0°
km
128
112
96
80
0°
km
112
96
80
0°
km
112
96
80
64
0°

20:30:21 $\overline{\eta} = 1.56\times10^{-11}\,\mathrm{cm}^{-1}$

20:45:17 $\overline{\eta} = 1.33\times10^{-11}\,\mathrm{cm}^{-1}$

21:00:13 $\overline{\eta} = 8.70\times10^{-12}\,\mathrm{cm}^{-1}$

21:15:09 $\overline{\eta} = 6.80\times10^{-12}\,\mathrm{cm}^{-1}$

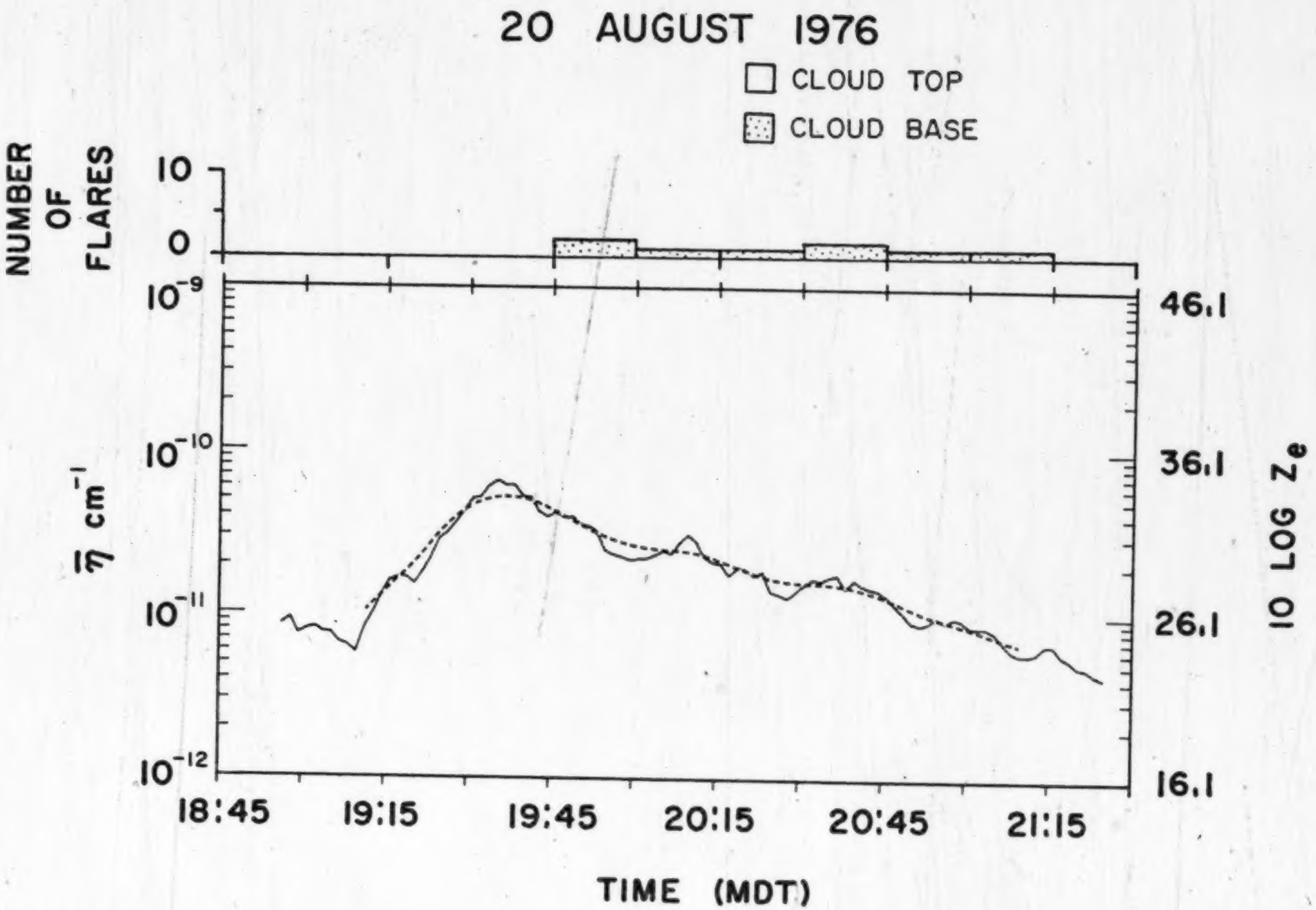

Fig. 6.33: $\overline{\eta}$ versus time for the storm on 20 August, 1976. Dashed line indicates trend. Type and number of cloud-seeding flares released during 15 minute intervals is shown.

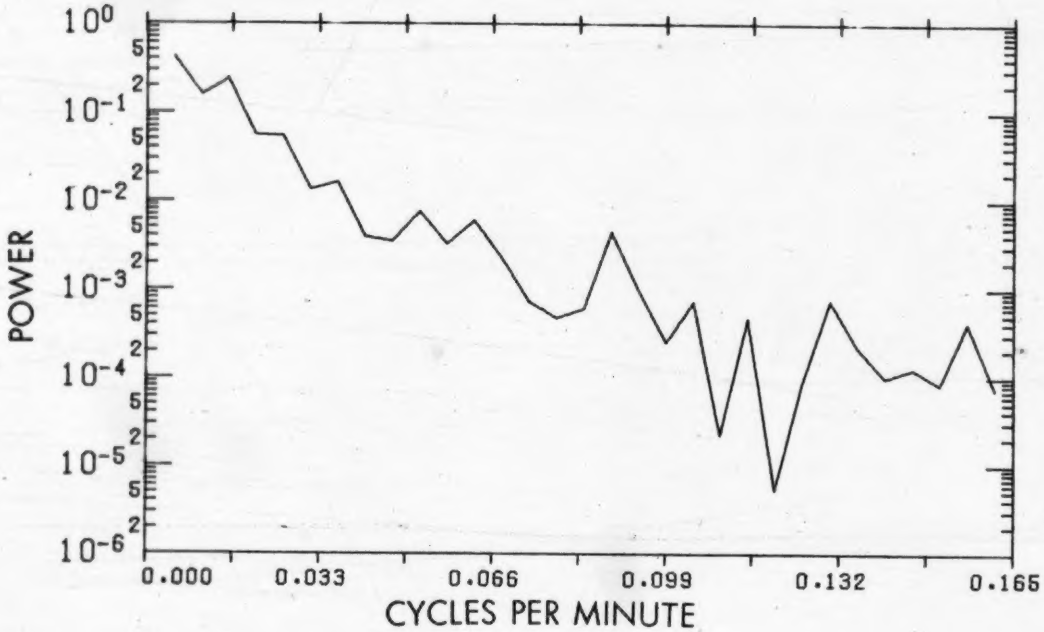

Fig. 6.34: Unsmoothed power spectrum of $\overline{\eta}$ for the storm on 20 August, 1976.

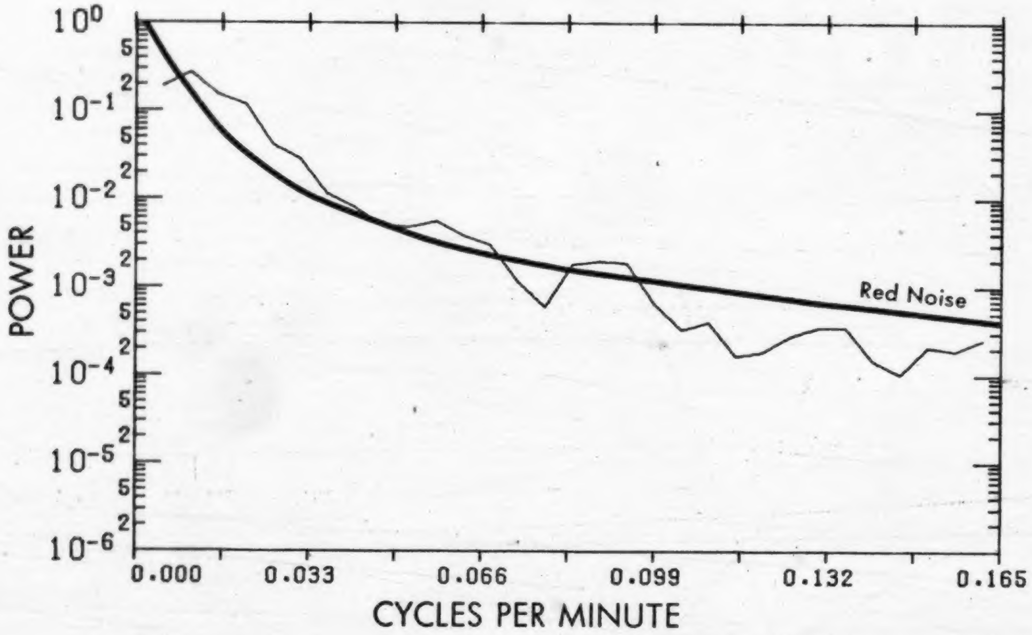

Fig. 6.35: Three-point Daniell-filtered power spectrum of $\overline{\eta}$ for the storm on 20 August, 1976. The red-noise spectrum is shown.

Table 6.4: Lag 1:5 to 15 minute autocorrelation coefficients of $\overline{n}$ for the storm on 20 August, 1976.

LAG NUMBER	TIME LAG (min)	AUTOCORRELATION COEFFICIENT
1	1.5	.993
2	3.0	.953
3	4.5	.898
4	6.0	.832
5	7.5	.764
6	9.0	.690
7	10.5	.622
8	12.0	.548
9	13.5	.473
10	15.0	.399

applied to it using an autocorrelation value of $\rho = .740$ is given in Figure 6.36.

There were no statistically significant peaks at the 95 per cent confidence level assuming a Chi-square distribution. However, preferred cycles were displayed at 0.031, 0.057, and 0.089 cycles per minute. These frequencies correspond to cycles with periods of 32.3, 17.5, and 11.2 minutes.

This storm was seeded with 8 cloud-base flares burned over a period of approximately 1.25 hours.

A feature of this storm which contrasted with the other hailstorms in this study was the very slow rate at which it dissipated. No other storm displayed such a long drawn out decline in the trend. The storm passed over Pigeon Lake during

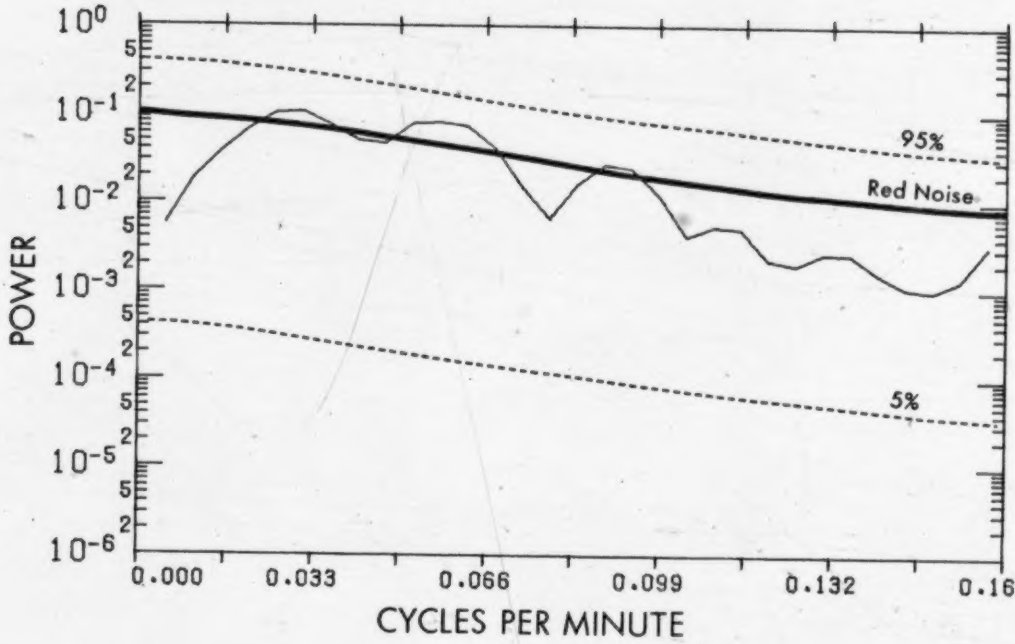

Fig. 6.36: Three-point Daniell-filtered power spectrum of Tukey-filtered $\overline{\eta}$ highpass data for the storm on 20 August, 1976. The red-noise spectrum and 90% confidence interval are shown.

the period 20:30 MDT to 21:00 MDT but the $\bar{\eta}$ time series did not display any change during this period which could be credited to a lake effect.

6.6 The 24 August, 1976 Storm

A severe storm occurred in the northern area on 24 August, 1976. The storm formed in the foothills region near the western boundary of the project area and tracked northeastward. The synoptic summary is given in Figure 6.37 and the environmental conditions are shown by the tephigram in Figure 6.38. This storm was not seeded.

The hailswath for this storm is shown in Figure 6.39. The storm produced sporadic patches of hail, indicating that it experienced several cycles in intensity. Walnut size hail was reported in two instances, however, the majority of the hailswath indicates pea-and grape-size as the maximum sizes.

PPI scans of the storm at approximately 15-minute intervals are given in Figures 6.40 to 6.44. Reflectivities in excess of 50 dBZ were recorded.

The $\bar{\eta}$ time series for 24 August, 1976 is given in Figure 6.45. The dashed line represents the trend in the data computed using the Tukey filter described in Appendix A. The trend indicates at least three major intensifications in $\bar{\eta}$ during the storm lifetime. The radar constant for the day was 74.0 dBm with a peak transmitted power of 238 kw.

The radar operated on a three-minute scan for the period 17:20 MDT to 19:08 MDT and consequently 37 data points had to be interpolated.

The autocorrelation coefficients of the data for lag one (1.5 min) to lag ten (15 min), computed using (5.4.2) are given in Table 6.5.

SYNOPTIC SUMMARY

24 AUGUST 1976

SYNOPSIS: L/W FEATURES, VIZ THE RIDGE OVER MID-CONTINENT AND THE E PACIFIC TROUGH, GAINED AMPLITUDE FROM AUGUST 21-23, FORCING S/W FEATURES N OF ALBERTA. THE RIDGE STARTED TO COLLAPSE ON THE 24TH, THEN MOVED E, ALLOWING THE MAIN 500 MB STREAM TO DROP S OVER CENTRAL ALBERTA WITH AN EMBEDDED S/W TROUGH. A SURFACE TROUGH OF LOW PRESSURE FORMED ALONG THE FOOTHILLS IN RESPONSE TO THIS S/W, GRADUALLY EVOLVING INTO A LOW CENTER BY THE NEXT MORNING.

AHP AREA: SURFACE WINDS LIGHT S OVER MOST OF THE AREA VEERING TO SW AT 500 MB. A SINGLE-CELL STORM DEVELOPED SW OF CYRM DURING LATE AFTERNOON TRACKING NE 35 KPH, WITH MAXIMUM TOPS 12 KM, THEN DYING LATE IN THE EVENING.

TROUGH (T) OR RIDGE (R) PASSAGE TIME	12 HOUR 500 MB CHANGE IN				HAIL SIZE CATEGORY	NO. HAIL REPORTS N / S
	VORTICITY ($10^{-5}s^{-1}$)	HEIGHTS * (M)	THICKNESS* (M)	TEMPS. (°C)		
R-24/1900Z T-25/1000Z	0	- 20	- 20	+ 1	4	46/0

* DIURNAL EFFECTS REMOVED

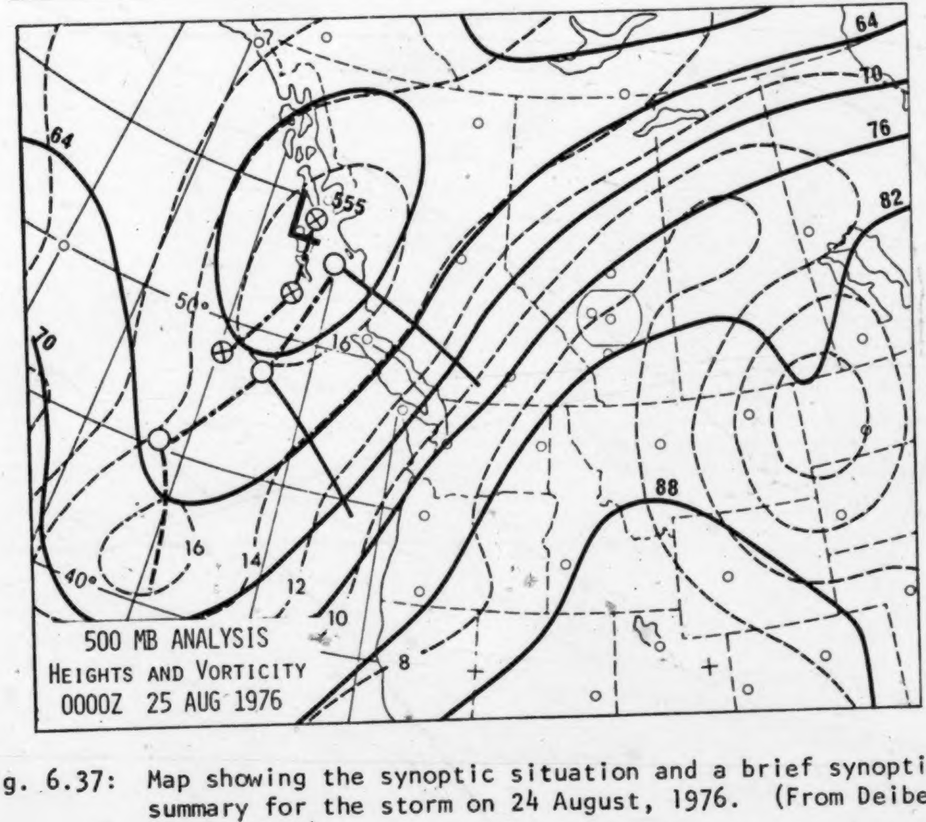

Fig. 6.37: Map showing the synoptic situation and a brief synoptic summary for the storm on 24 August, 1976. (From Deibert (ed.), 1977)

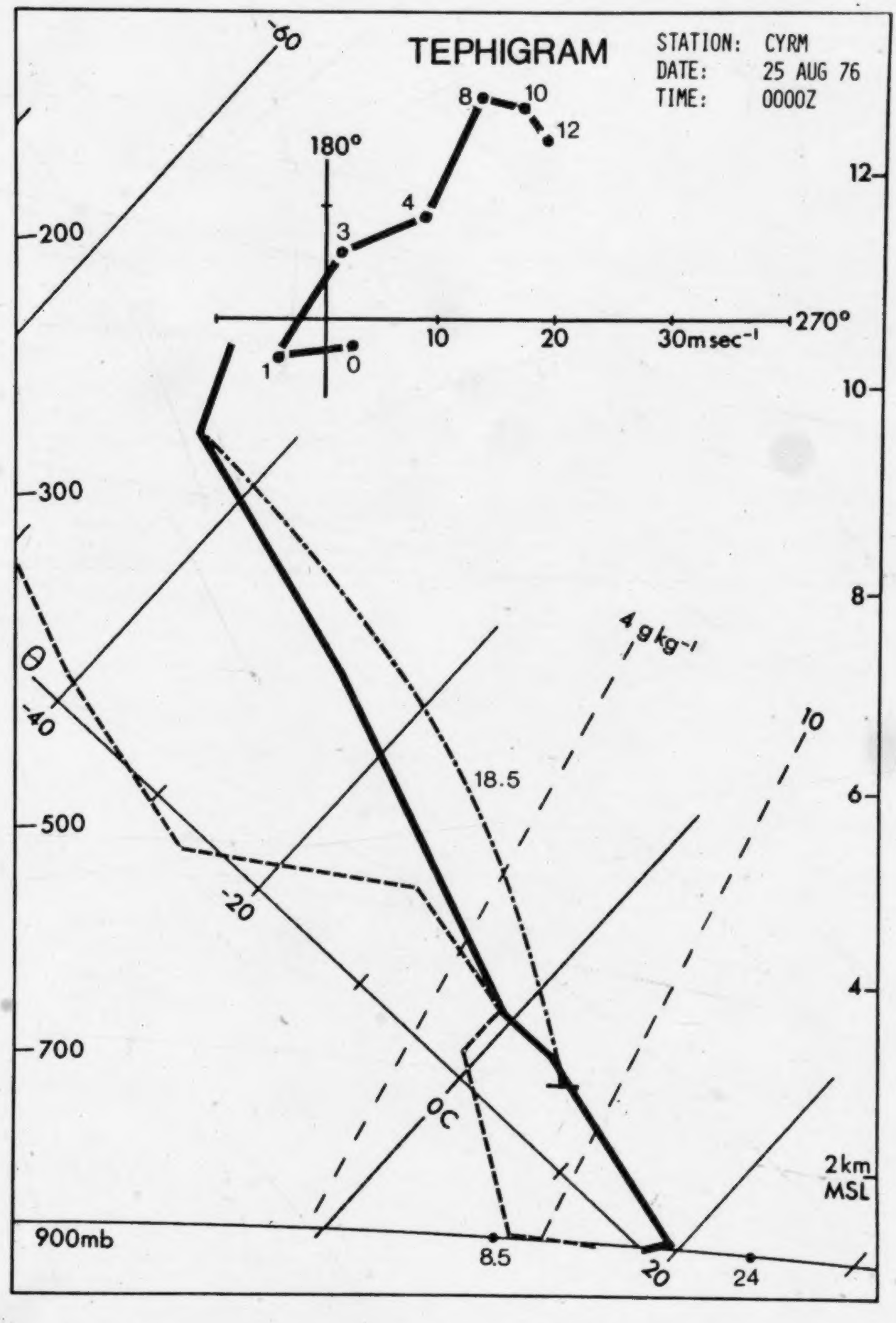

Fig. 6.38: Rawinsonde sounding from Rocky Mountian House at 18:00 MDT, 24 August, 1976. (From Deibert (ed.), 1977)

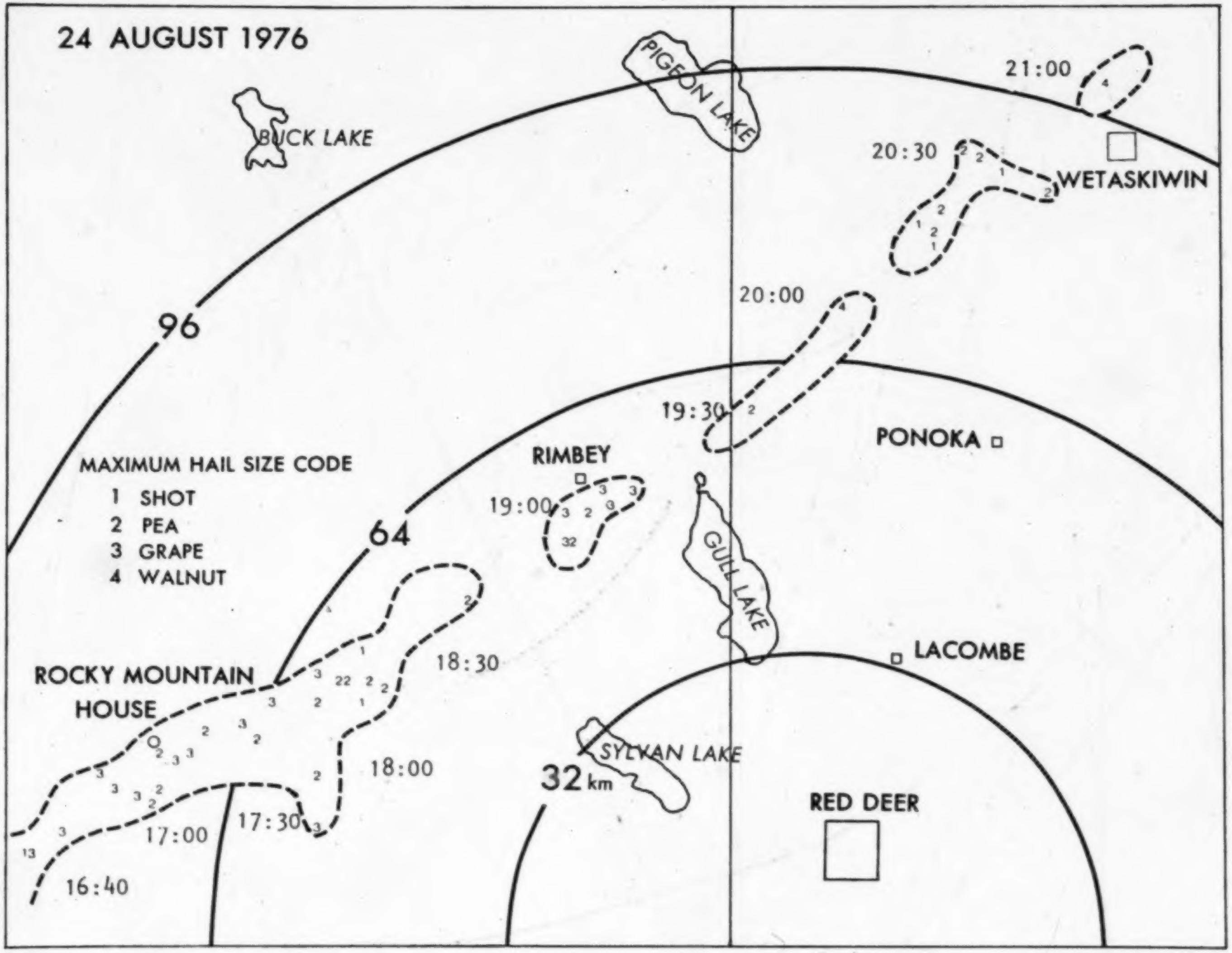
24 AUGUST 1976
BUCK LAKE
PIGEON LAKE
WETASKIWIN
PONOKA
RIMBEY
GULL LAKE
LACOMBE
SYLVAN LAKE
RED DEER
ROCKY MOUNTAIN HOUSE
96
64
32 km
MAXIMUM HAIL SIZE CODE
1 SHOT
2 PEA
3 GRAPE
4 WALNUT
16:40
17:00
17:30
18:00
18:30
19:00
19:30
20:00
20:30
21:00

Fig. 6.39: Map showing the hailswath resulting from the storm on 24 August, 1976.

Fig. 6.40: PPI echoes for the storm on 24 August, 1976. Elevation - 1.9°
Reflectivity = from 20 dBZ by 10 dBZ. Time = 16:29 - 17:44 MDT.

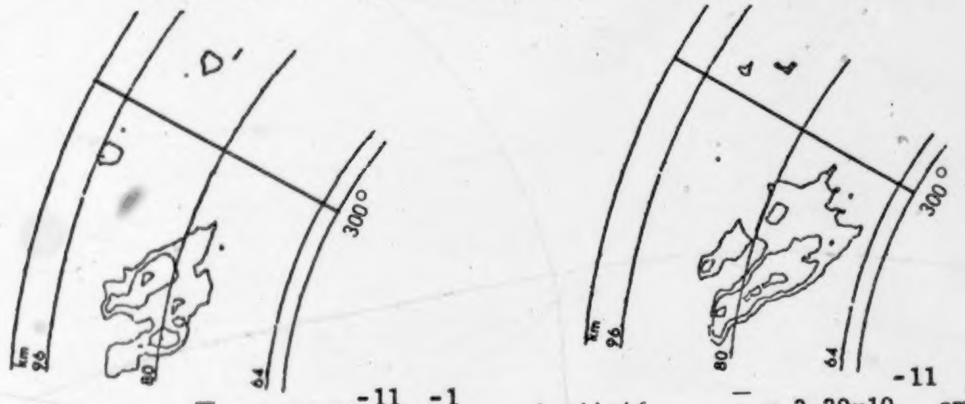

16:29:51 $\overline{\eta} = 2.23\times10^{-11}\ \mathrm{cm}^{-1}$ 1 :44:46 $\overline{\eta} = 3.20\times10^{-11}\ \mathrm{cm}^{-1}$

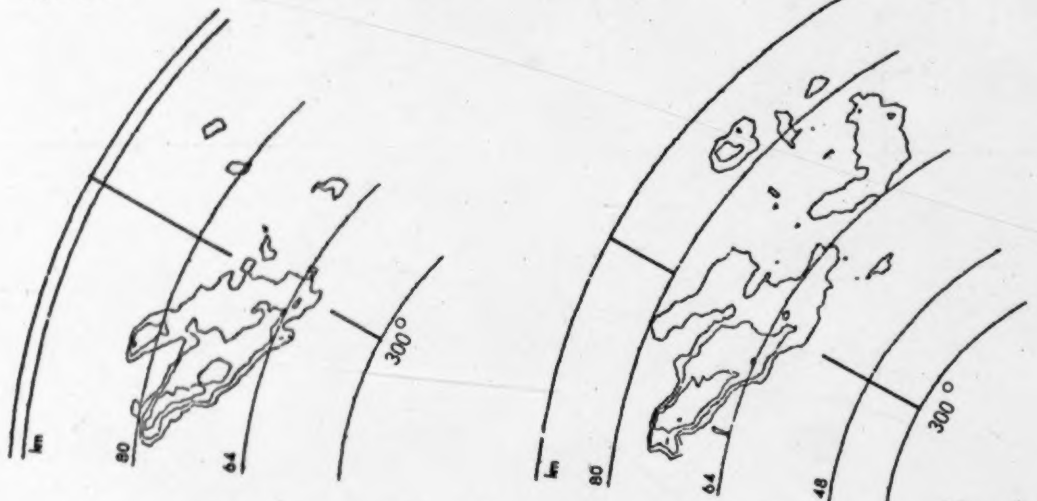

16:59:43 $\overline{\eta} = 4.91\times10^{-11}\ \mathrm{cm}^{-1}$ 17:16:08 $\overline{\eta} = 3.75\times10^{-11}\ \mathrm{cm}^{-1}$

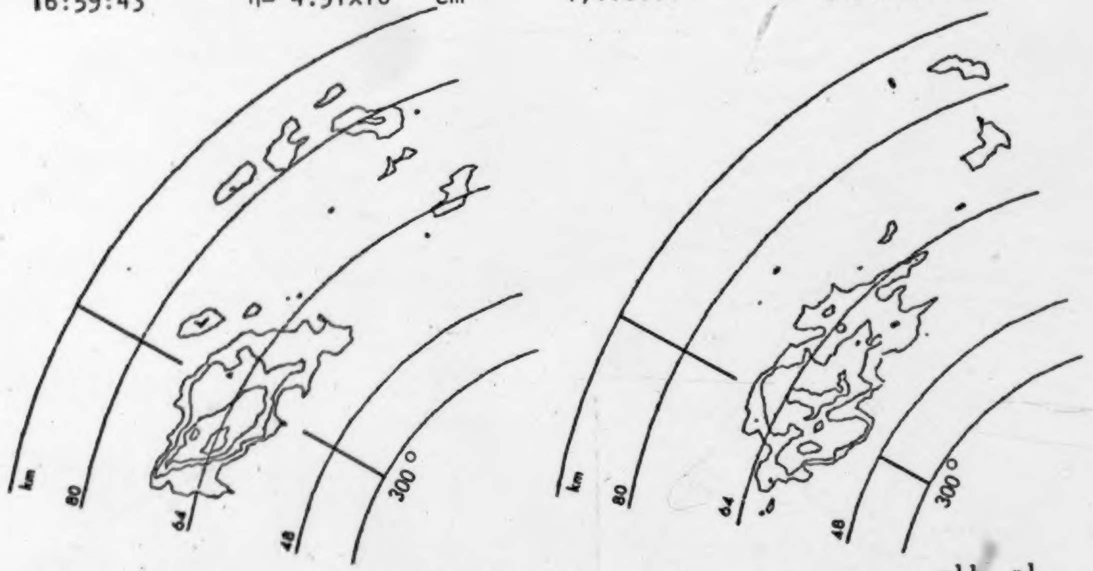

17:29:34 $\overline{\eta} = 1.28\times10^{-10}\ \mathrm{cm}^{-1}$ 17:44:30 $\overline{\eta} = 2.52\times10^{-11}\ \mathrm{cm}^{-1}$

Fig. 6.41: PPI echoes for the storm on 24 August, 1976. Elevation ~ 2.0° Reflectivity = from 20 dBZ by 10 dBZ. Time = 17:59 - 18: 44 MDT.

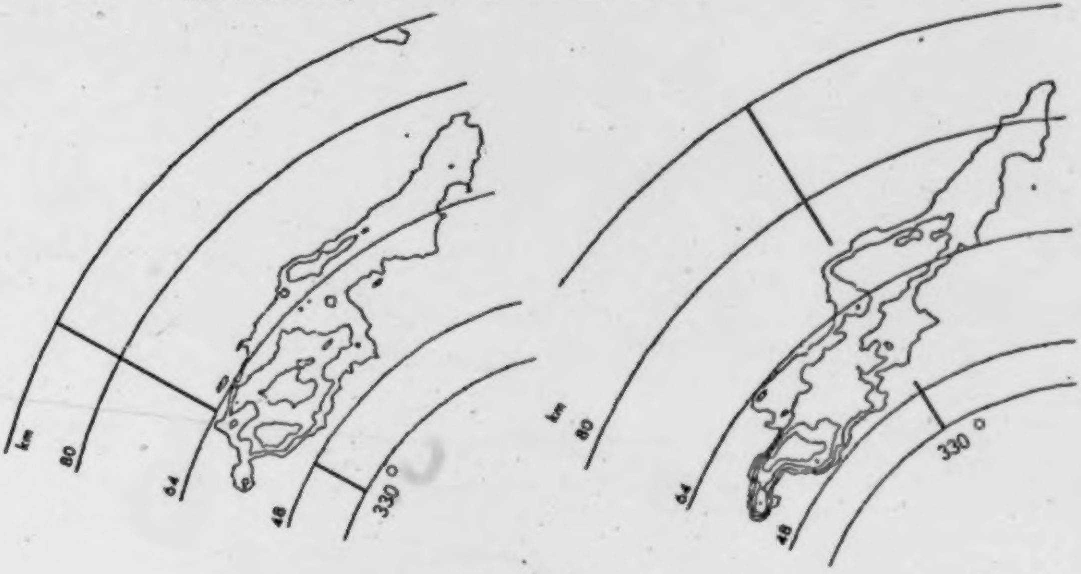

17:59:26 $\bar{\eta} = 1.85\times10^{-11}\,\mathrm{cm}^{-1}$ 18:14:22 $\bar{\eta} = 6.34\times10^{-11}\,\mathrm{cm}^{-1}$

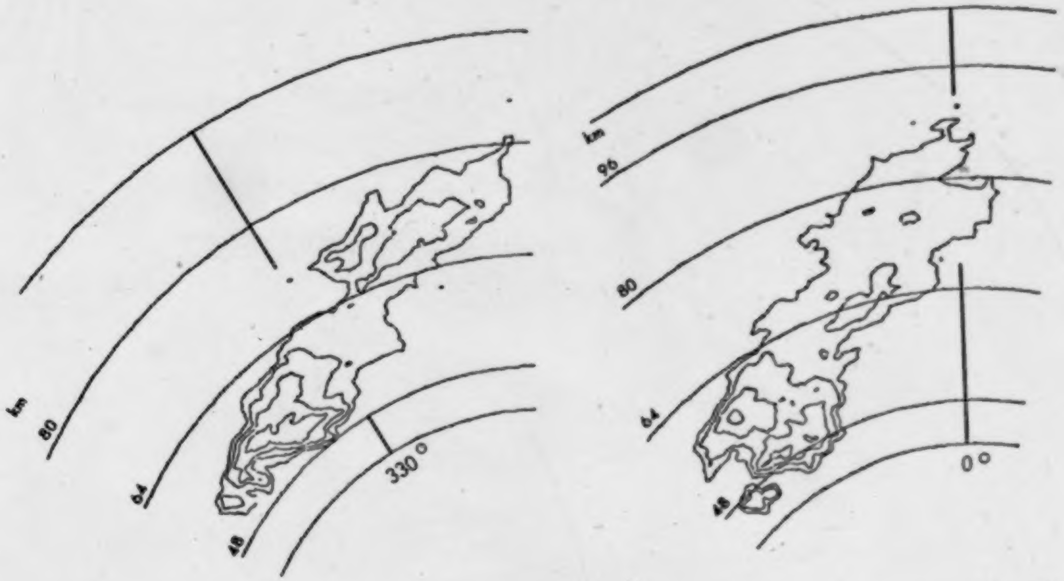

18:29:18 $\bar{\eta} = 1.02\times10^{-10}\,\mathrm{cm}^{-1}$ 18:44:13 $\bar{\eta} = 4.00\times10^{-11}\,\mathrm{cm}^{-1}$

Fig. 6.42: PPI echoes for the storm on 24 August, 1976. Elevation ~ 2.1°
Reflectivity = from 20 dBZ by 10 dBZ. Time = 18:59 - 19:45 MDT.

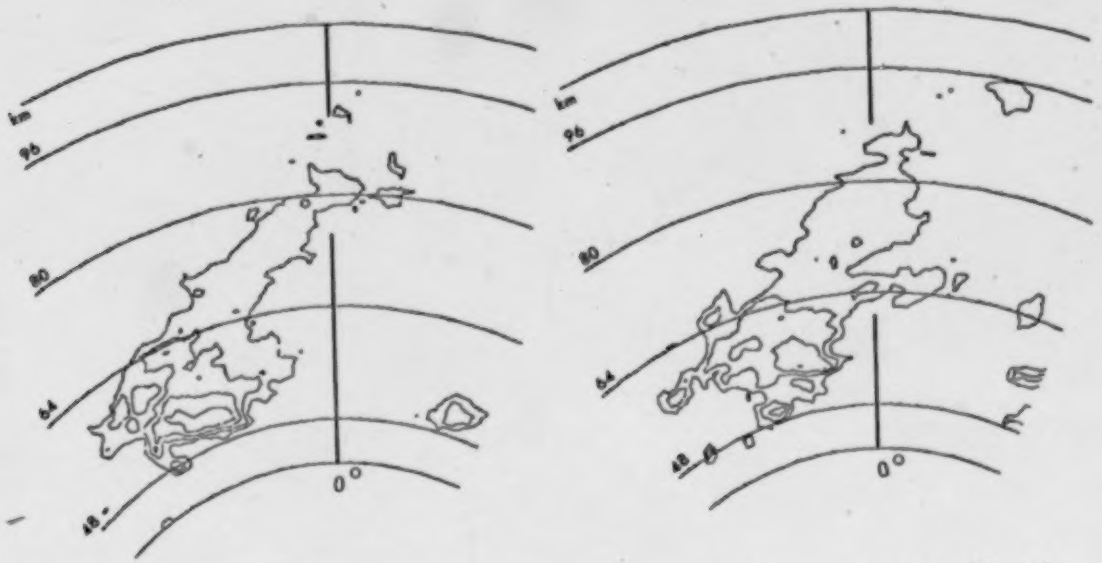
km
96
80
64
48
0°
km
96
80
64
48
0°

18:59:09 $\bar{\eta} = 4.37 \times 10^{-11} \mathrm{cm}^{-1}$

19:15:35 $\bar{\eta} = 2.40 \times 10^{-11} \mathrm{cm}^{-1}$

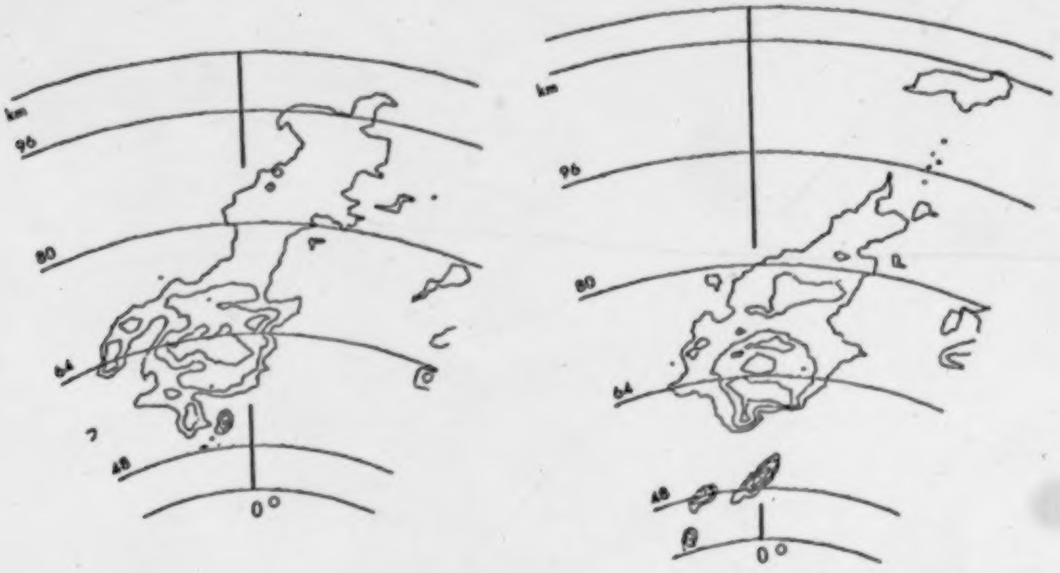
km
96
80
64
48
0°
km
96
80
64
48
0°

19:30:30 $\bar{\eta} = 1.74 \times 10^{-11} \mathrm{cm}^{-1}$

19:45:26 $\bar{\eta} = 2.03 \times 10^{-11} \mathrm{cm}^{-1}$

Fig. 6.43: PPI echoes for the storm on 24 August, 1976. Elevation ~2.1° Reflectivity = from 20 dBZ by 10 dBZ. Time = 20:00 - 20:45 MDT.

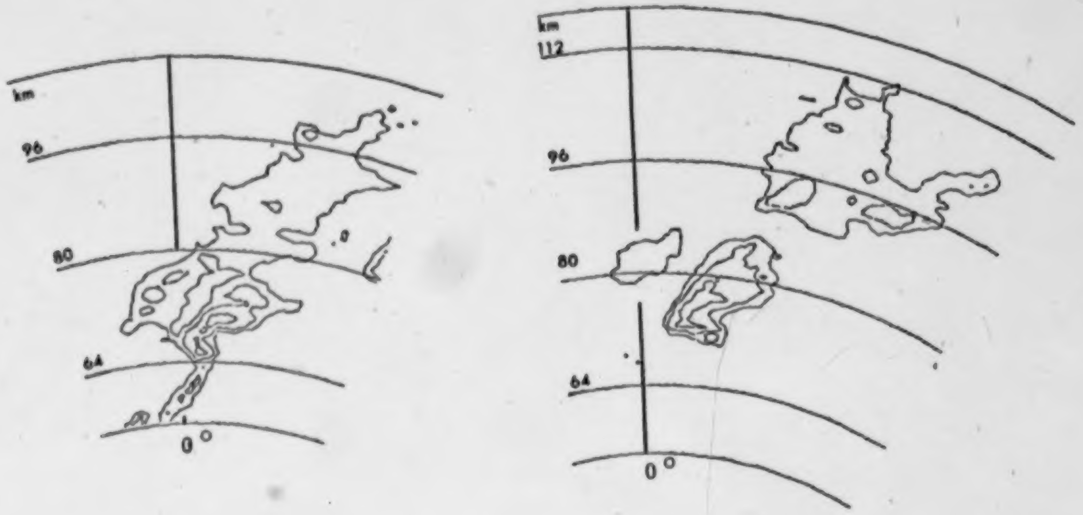

20:00:22 $\bar{\eta} = 1.32\times10^{-11}\,\mathrm{cm}^{-1}$ 20:15:18 $\bar{\eta} = 1.96\times10^{-11}\,\mathrm{cm}^{-1}$

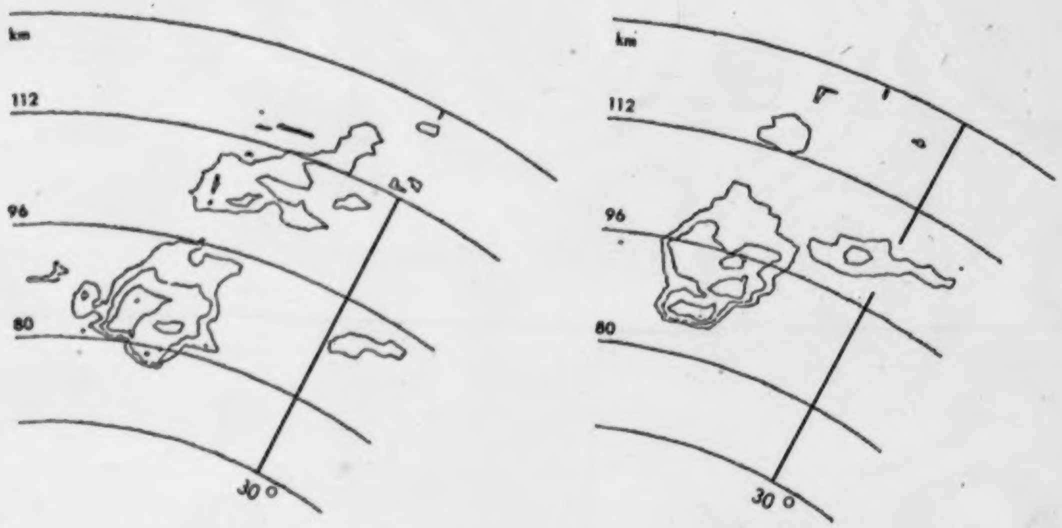

20:30:13 $\bar{\eta} = 5.53\times10^{-11}\,\mathrm{cm}^{-1}$ 20:45:09 $\bar{\eta} = 4.43\times10^{-11}\,\mathrm{cm}^{-1}$

Fig. 6.44: PPI echoes for the storm on 24 August, 1976. Elevation ~ 2.1°
Reflectivity = from 20 dBZ by 10 dBZ. Time = 21:00 - 21:29 MDT.

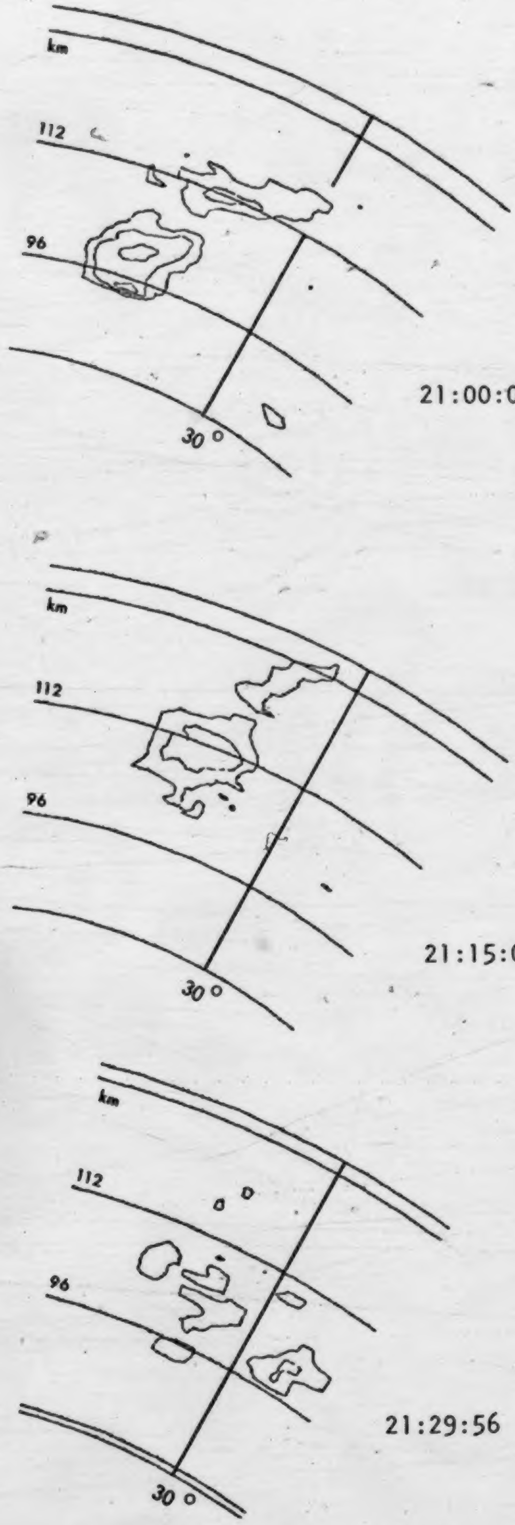
km
112
96
30°
km
112
96
30°
km
112
96
30°

21:00:05 $\bar{\eta} = 5.35\times10^{-11}\,\mathrm{cm}^{-1}$

21:15:01 $\bar{\eta} = 2.75\times10^{-11}\,\mathrm{cm}^{-1}$

21:29:56 $\bar{\eta} = 8.80\times10^{-12}\,\mathrm{cm}^{-1}$

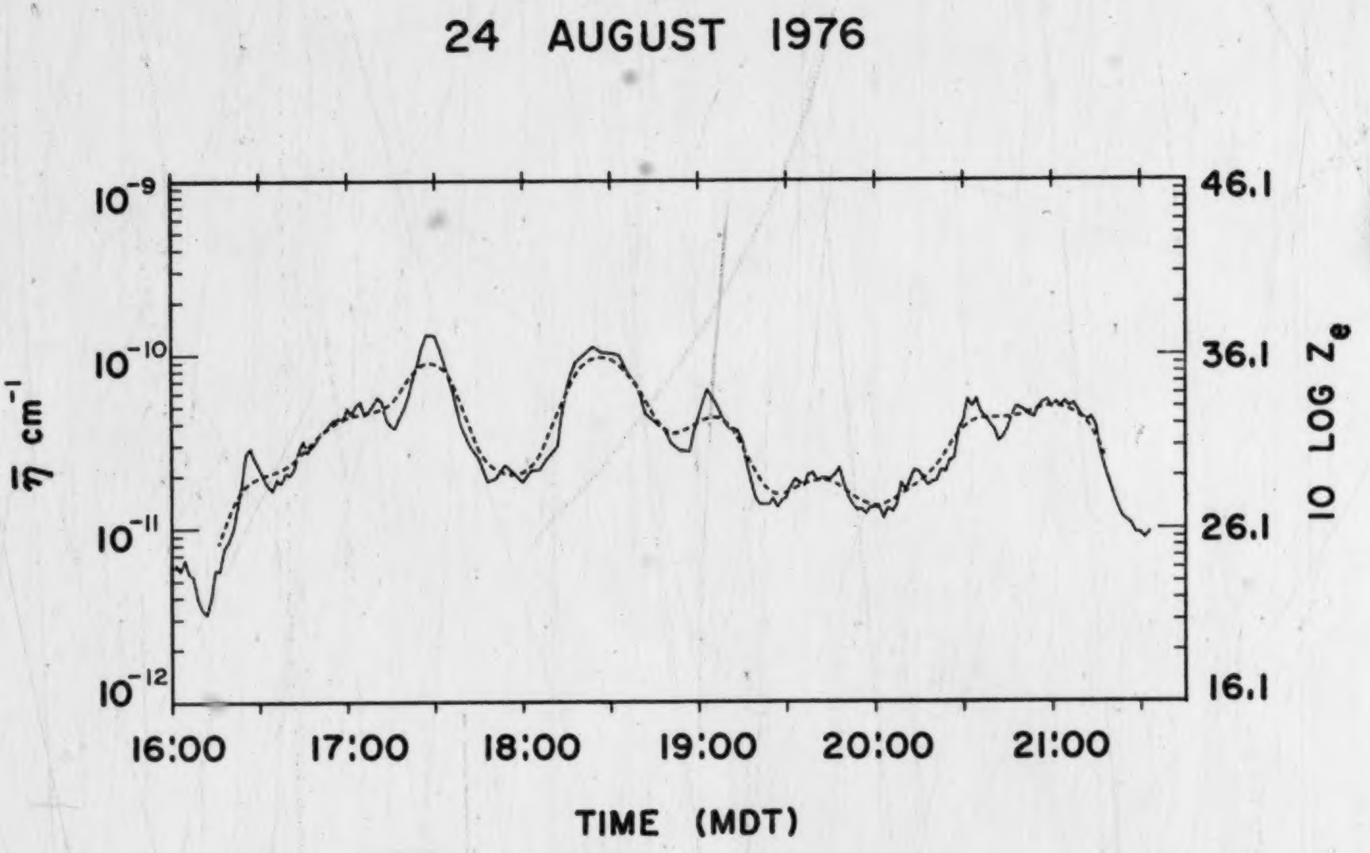

Fig. 6.45: $\overline{\eta}$ versus time for the storm on 24 August, 1976. Dashed line indicates trend.

Table 6.5: Lag 1.5 to 15 minute autocorrelation coefficients of $\overline{n}$ for the storm on 24 August, 1976.

LAG NUMBER	TIME LAG (min)	AUTOCORRELATION COEFFICIENT
1	1.5	.936
2	3.0	.821
3	4.5	.687
4	6.0	.554
5	7.5	.457
6	9.0	.396
7	10.5	.365
8	12.0	.349
9	13.5	.329
10	15.0	.311

The unsmoothed power spectrum of the raw data is given in Figure 6.46, and the smoothed power spectrum, using a three-point running average, is given in Figure 6.47. The values of the red-noise power are applied to the smoothed power spectrum using an autocorrelation value $\rho = .921$. The highpass data smoothed power spectrum with the red-noise power applied to it using an autocorrelation value of $\rho = .806$ is given in Figure 6.48.

Once again, no statistically significant peaks in the power spectrum were found assuming a Chi-square distribution. However, preferred cycles are suggested by the broad peaks in Figure 6.48 near the frequencies 0.034 and 0.117 cycles per minute. The corresponding cycle periods are 29.4 and 8.5 minutes respectively. These appear to be the major and minor fluctuations in the overall

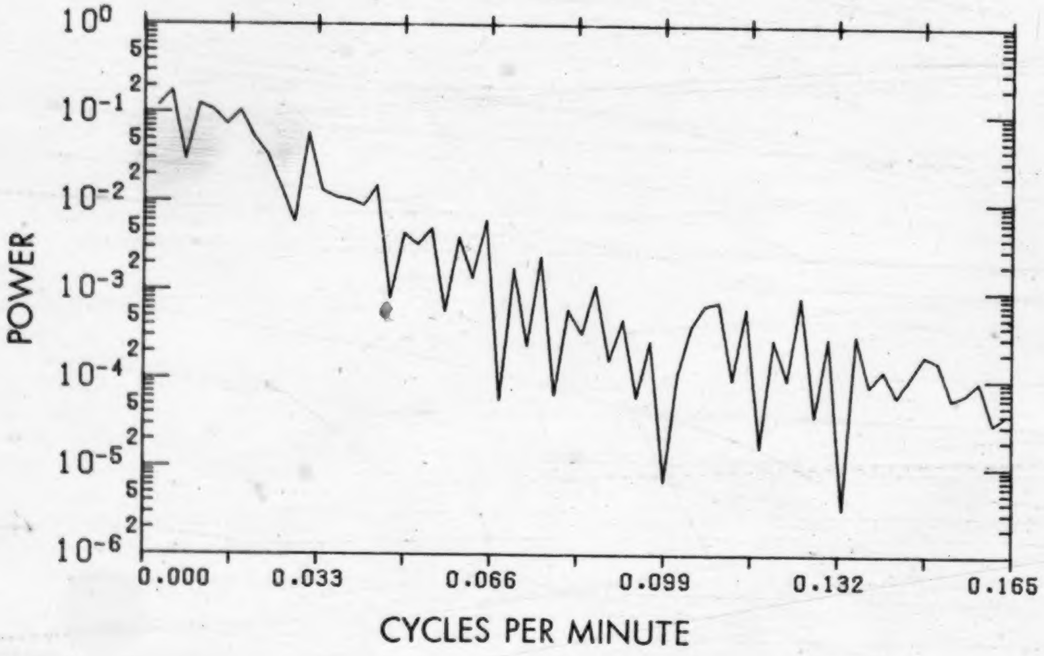

Fig. 6.46: Unsmoothed power spectrum of $\overline{\eta}$ for the storm on 24 August, 1976.

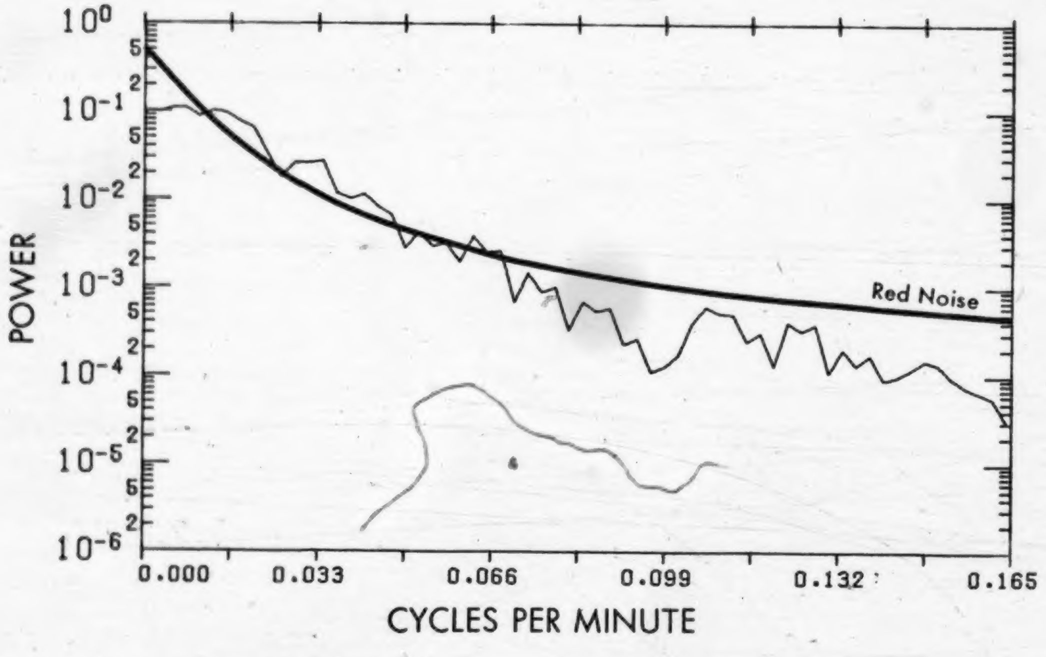

Fig. 6.47: Three-point Daniell-filtered power spectrum of $\overline{\eta}$ for the storm on 24 August, 1976. The red-noise spectrum is shown.

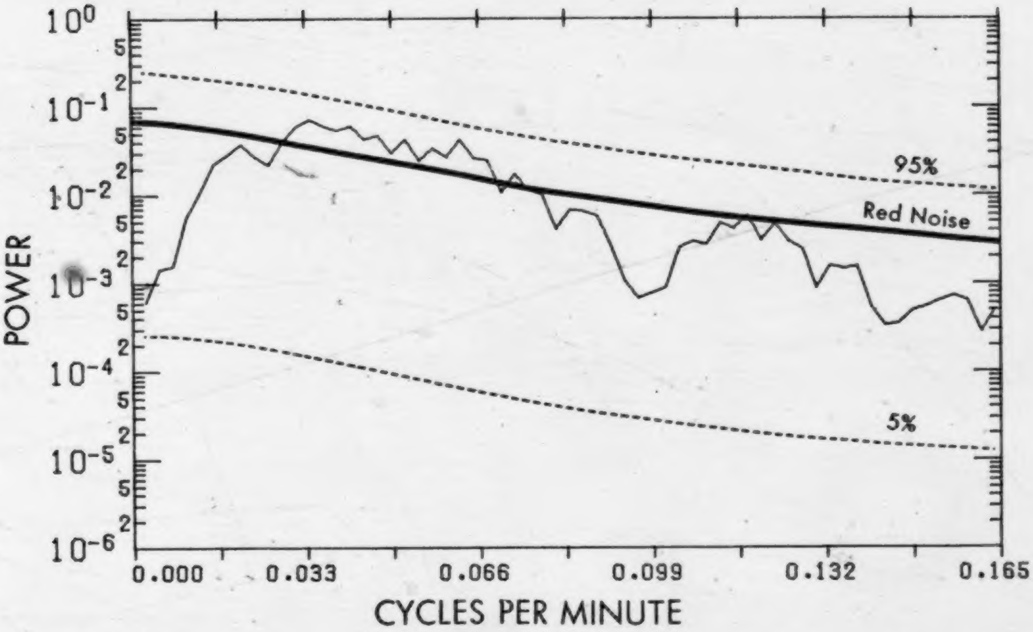

Fig. 6.48: Three-point Daniell-filtered power spectrum of Tukey-filtered $\overline{\eta}$ highpass data for the storm of 24 August, 1976. The red-noise spectrum and 90% confidence interval are shown.

storm intensity which caused the rather sporadic hailfall.

This concludes the presentation of the August, 1976 storm data. Further interpretation and discussion of the data is given in a following chapter after all of the storm data have been presented.

CHAPTER 7

THE 20 JULY, 1975 CASE STUDIES

7.1 Introduction

Three storms which occurred on 20 July, 1975 were analyzed. All three storms formed in the foothills region and tracked eastward across the northern area. The first storm, designated as storm A, is included in this study for comparison purposes since only rain was reported to have fallen from it. The second storm (storm B) and the third storm (storm C) are analyzed in order to investigate the usefulness of the AHP 1975 digitized data. At times during 1975 portions of returned echoes are missing due to a computer recording malfunction. The result was that individual rays or groups of rays were often lost. An example of an echo showing the missing rays is given in Figure 7.1. The gaps did not always occur nor did they occur at the same spot in the echoes. As a result it was impossible to predetermine the error associated with the $\bar{\eta}$ calculation when missing rays were encountered.

The program used to calculate $\bar{\eta}$ was modified to take into account missing rays. When missing rays were encountered, the bin volumes for the rays on adjacent sides, were interpolated across the gap to account for the missing volume. The known power values in adjacent rays were assumed to represent the increased volume, rather than interpolating the returned power values for the missing rays.

The error in $\bar{\eta}$ would be minimal if the rays on each side of a gap are representative of what was actually there. However, the error is large if the missing rays occurred in a region with a high reflectivity gradient.

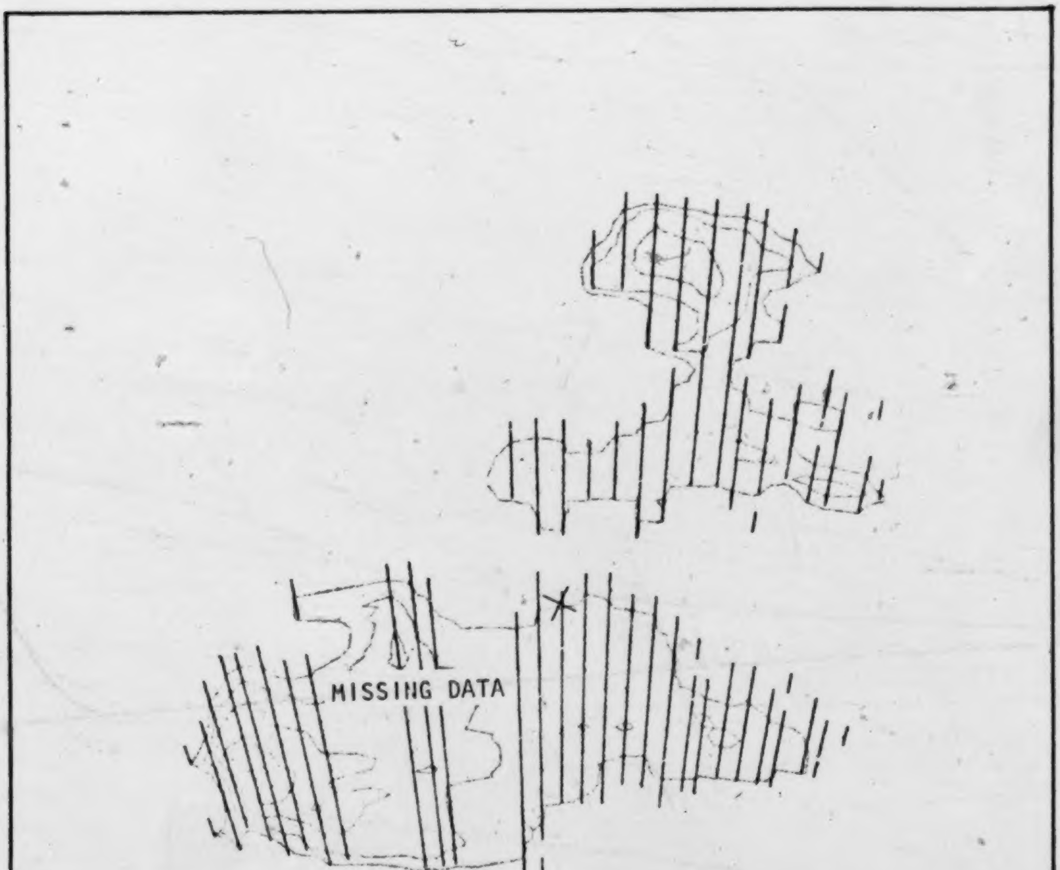
MISSING DATA

Fig. 7.1 An example of a radar echo from the 1975 data which displays "missing rays".

The storms from 1976 displayed $\bar{\eta}$ time series with lag one autocorrelation coefficients greater than 0.90 and no dramatic changes in $\bar{\eta}$ occurring over short periods of time. This characteristic would also be expected of 1975 storms and, therefore, erratic changes in $\bar{\eta}$ values would probably indicate the misrepresentation of missing data by interpolation.

7.2 20 July, 1975: Storm A

Storm A is included in this study as a test case. No hail was reported to have fallen from it, however, radar reflectivities greater than 40 dBZ were recorded during its lifetime. The test was to see if the $\bar{\eta}$ values were sufficiently small to characterize a rainstorm as opposed to the $\bar{\eta}$ values for hailstorms already discussed.

PPI scans of the storm at approximately 15-minute intervals are given in Figures 7.2 and 7.3. The $\bar{\eta}$ time series is given in Figure 7.4. The dashed line represents the trend in the data computed using the Tukey filter described in Appendix A. Times during which missing data was encountered are also indicated. The radar constant used for the day was 76.4 dBm with a peak transmitted power of 137 kw.

The maximum $\bar{\eta}$ value obtained was 4.97×10^{-11} cm^{-1} at 15:39 MDT. The cumulative frequency curve for all hail reports given in Figure 4.5 indicates that approximately 15 percent of all the hail reports occurred with lower values. One may interpret this as suggesting that during the lifetime of storm A the probability of hailfall at the surface was at all times less than approximately 15 percent.

The autocorrelation coefficients of the data for lag one (1.5 min) to

Fig. 7.2: PPI echoes for storm A on 20 July, 1975. Elevation - 1.2^{o} Reflectivity = from 20 dBZ by 10 dBZ. Time = 15:30 - 16:30 MDT.

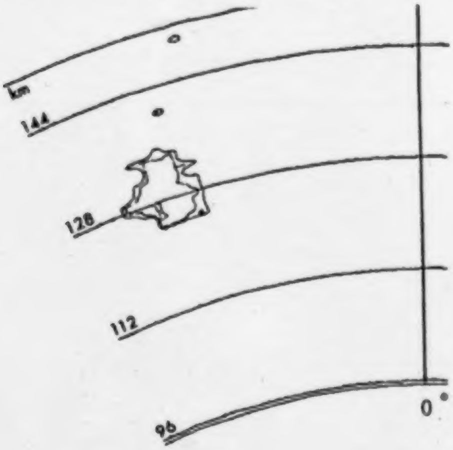

15:30:45 $\overline{\eta} = 3.22\times10^{-11}\mathrm{cm}^{-1}$

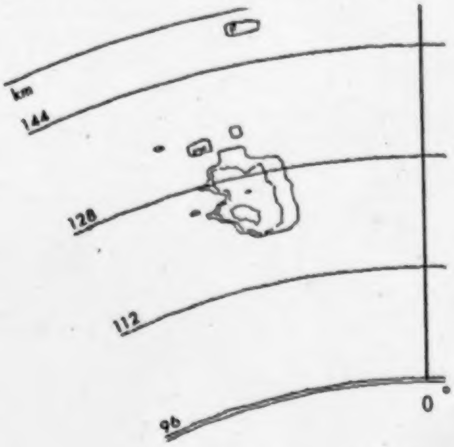

15:45:40 $\overline{\eta} = 3.77\times10^{-11}\mathrm{cm}^{-1}$

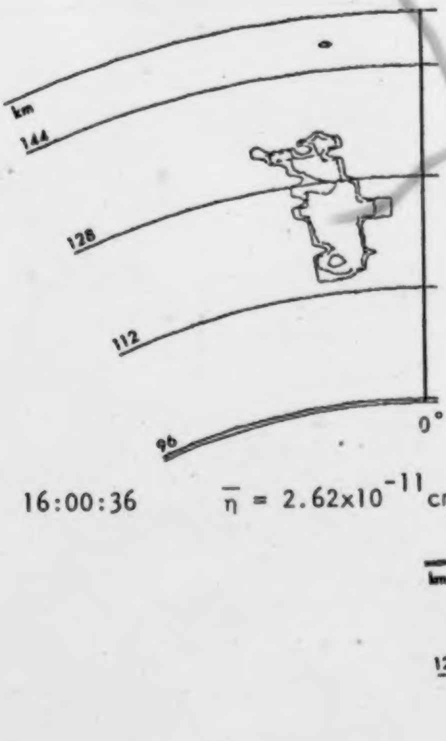

16:00:36 $\overline{\eta} = 2.62\times10^{-11}\mathrm{cm}^{-1}$

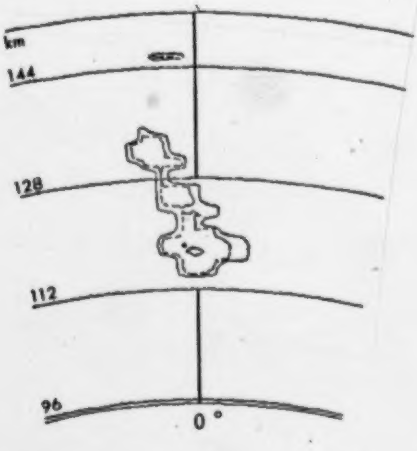

16:15:32 $\overline{\eta} = 2.66\times10^{-11}\mathrm{cm}^{-1}$

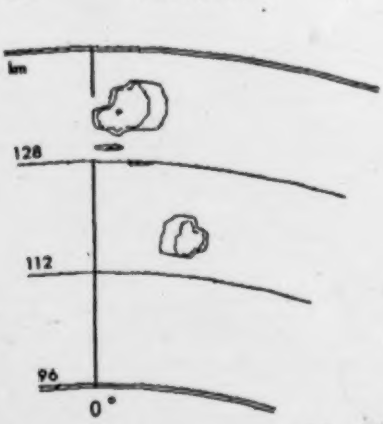

16:30:27 $\overline{\eta} = 4.46\times10^{-11}\mathrm{cm}^{-1}$

Fig. 7.3: PPI echoes for storm A on 20 July, 1975. Elevation ~ 1.2°
Reflectivity = from 20 dBZ by 10 dBZ. Time = 16:45 - 17:15MDT.

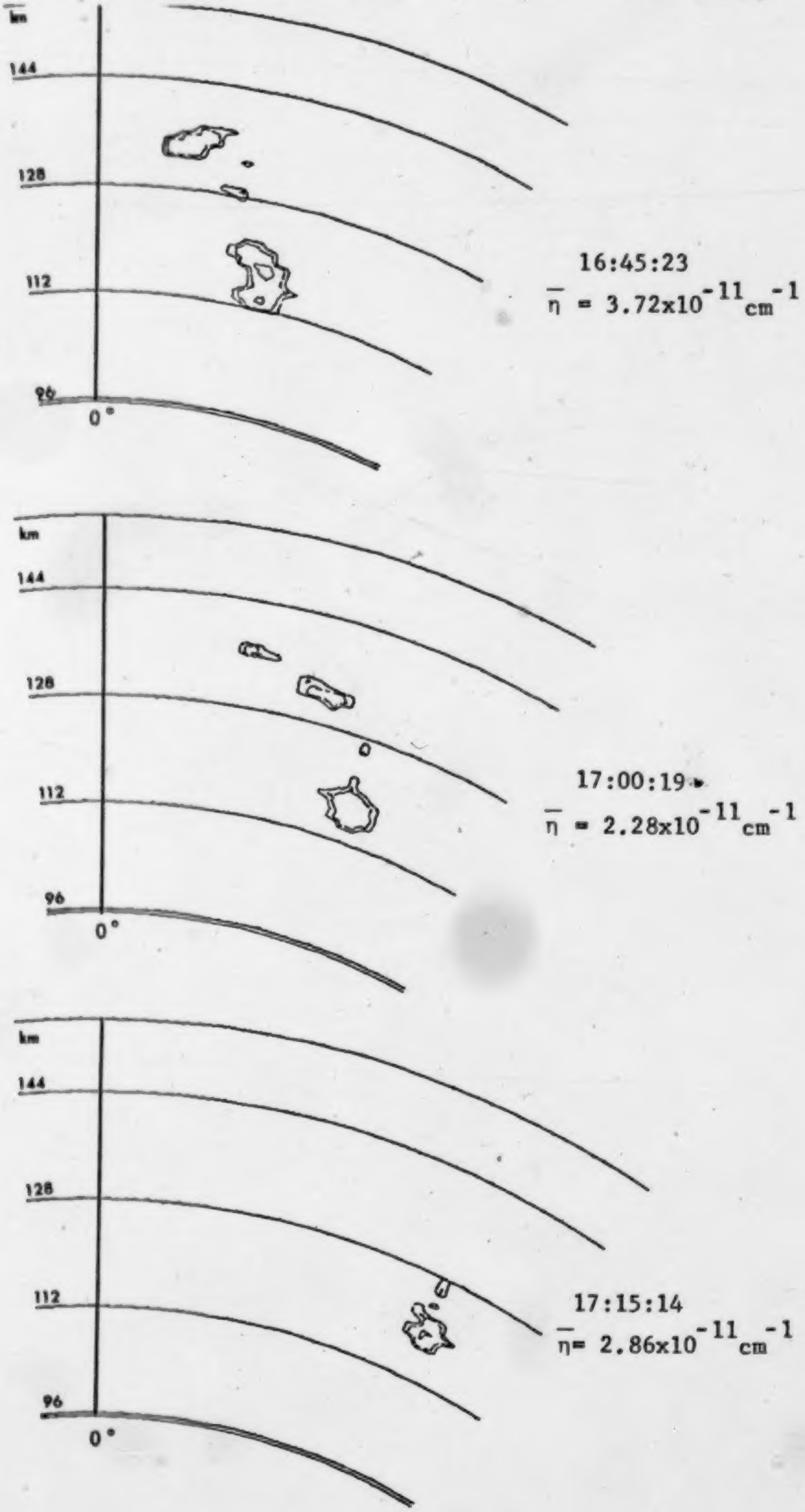

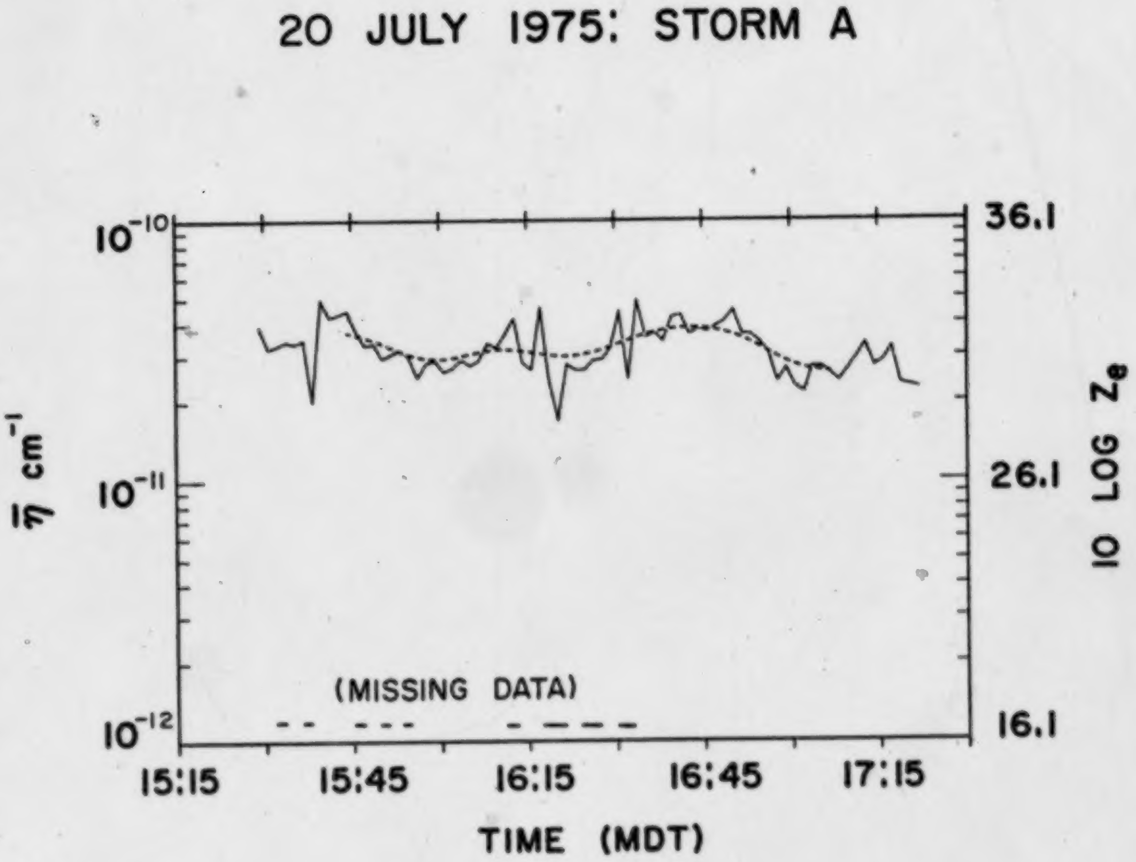

Fig. 7.4: $\bar{n}$ versus time for storm A on 20 July, 1975. Dashed line indicates trend. Times during which missing data was encountered are indicated.

lag ten (15 min) computed using (5.4.2) are given in Table 7.1.

Table 7.1: Lag 1.5 to 15 minute autocorrelation coefficients of $\bar{\eta}$ for Storm A on 20 July, 1975.

LAG NUMBER	TIME LAG (min)	AUTOCORRELATION COEFFICIENT
1	1.5	.404
2	3.0	.406
3	4.5	.400
4	6.0	.255
5	7.5	.107
6	9.0	.076
7	10.5	.021
8	12.0	−.022
9	13.5	.001
10	15.0	−.162

This storm displayed the least autocorrelation at short time lags of any of the storms studied.

The unsmoothed power spectrum of the raw data is given in Figure 7.5 and the smoothed power spectrum using a three-point running average is given in Figure 7.6. The value of the white-noise power is applied to the unsmoothed power spectrum and the values of the red-noise power are applied to the smoothed power spectrum using an autocorrelation value $\rho = .533$. The white-noise spectrum is included since of all storms this one displayed variations closest to random. The

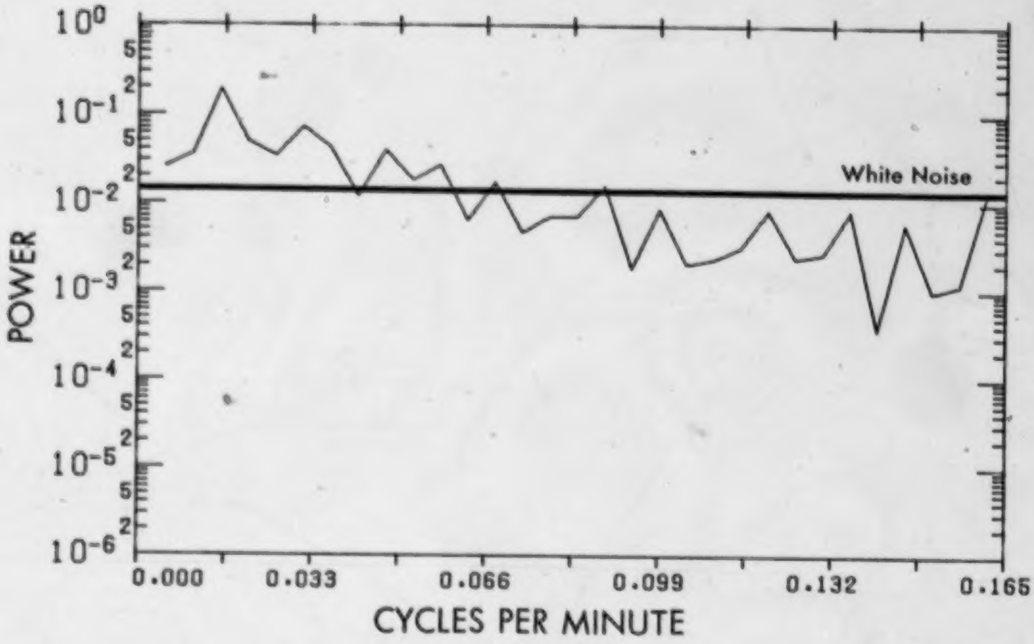

Fig. 7.5: Unsmoothed power spectrum of $\bar{\eta}$ for storm A on 20 July, 1975. The white-noise spectrum is shown.

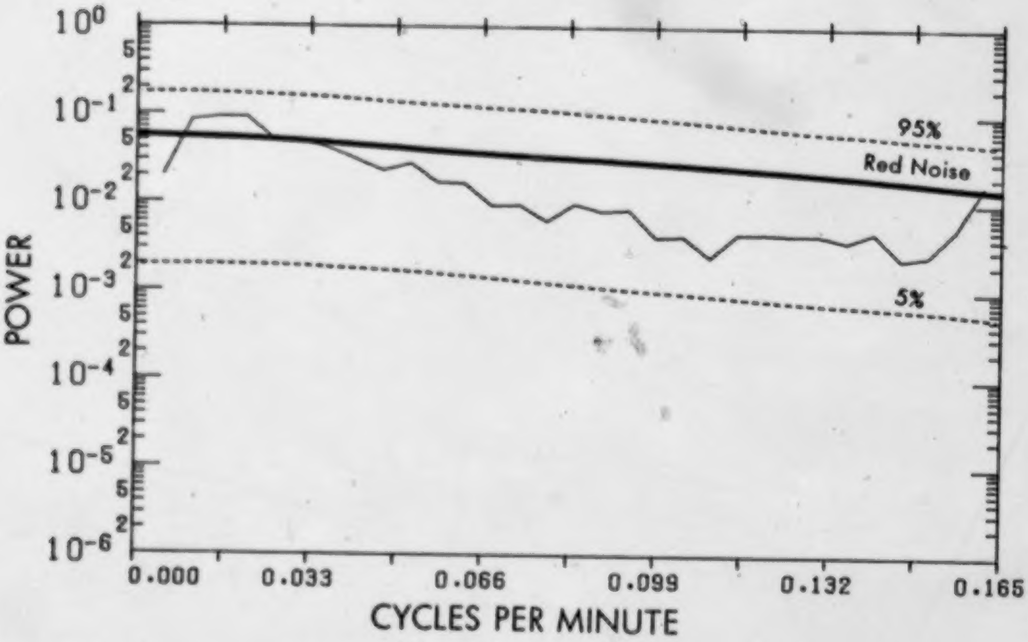

Fig. 7.6: Three-point Daniell-filtered power spectrum of $\bar{\eta}$ for storm A on 20 July, 1975. The red-noise spectrum and 90% confidence interval are shown.

red-noise spectrum which accounts for the persistence, reveals no significant periods in the smoothed power spectrum.

The low energy storm on 20 August, 1976, which was discussed in Section 6.5 and which resulted in 8 reports of pea size hail at the surface, displayed similar values of $\bar{\eta}$. The maximum $\bar{\eta}$ value for 20 August, 1976 was 6.56×10^{-11} cm^{-1}, corresponding to a hailfall probability of slightly greater than 15 percent. However, the majority of the $\bar{\eta}$ values were less than those of storm A. It appears that the parameter $\bar{\eta}$ is not sensitive enough to distinguish small hail from rain with any accuracy.

The spectra from the two storms are significantly different. The storm on 20 August, 1976 displayed high autocorrelation as opposed to the near random nature of $\bar{\eta}$ in storm A on 20 July, 1975. Although some of the randomness may be due to the interpolation of missing rays, it is the lack of a well defined beginning and end to the $\bar{\eta}$ time series which reduces the variance and, therefore, results in small values for short time lag autocorrelation coefficients and low frequency power.

7.3 20 July, 1975: Storm B

The hailswath for storm B 20 July, 1975 is shown in Figure 7.7. The maximum hailsize reported was grape size and the hailswath showed patches of hailfall implying that the storm experienced several cycles in intensity. Also shown in Figure 7.7 is the hailswath from storm C on 20 July, 1975 which will be discussed in the next section.

PPI scans for storm B at approximately 15-minute intervals are given

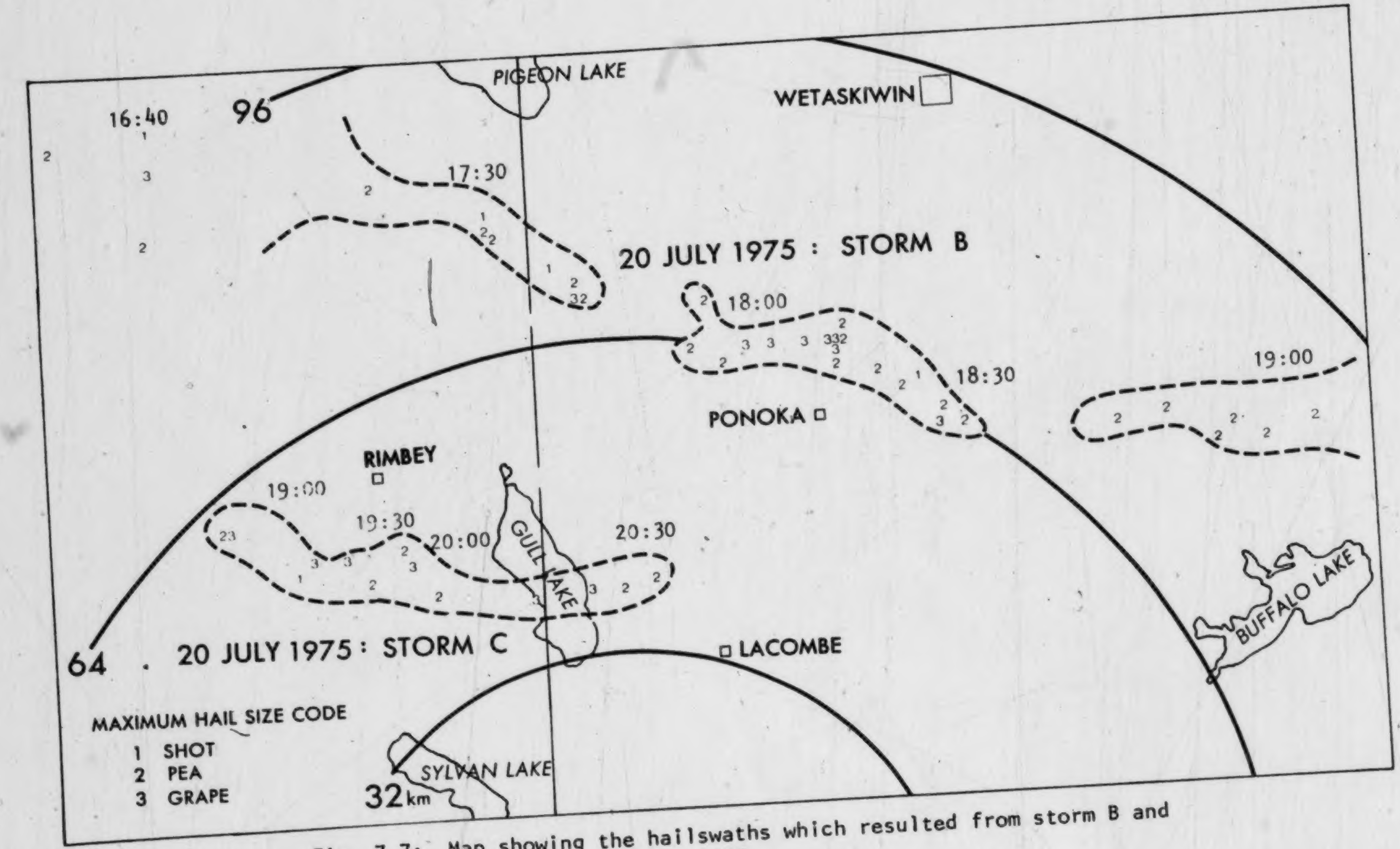
PIGEON LAKE
WETASKIWIN
16:40
96
17:30
20 JULY 1975 : STORM B
18:00
18:30
19:00
PONOKA
RIMBEY
19:00
19:30
20:00
GULL LAKE
20:30
BUFFALO LAKE
64
20 JULY 1975 : STORM C
LACOMBE
MAXIMUM HAIL SIZE CODE
1 SHOT
2 PEA
3 GRAPE
SYLVAN LAKE
32km

Fig. 7.7: Map showing the hailswaths which resulted from storm B and storm C on 20 July, 1975.

in Figures 7.8 through 7.11. The data for storm B suffered extensively from the problem of missing rays in the radar echoes. Figure 7.8 points out several PPI scans which include missing data. The contour program interpolates directly across the gap resulting in the unrealistic straight contour lines.

The $\bar{\eta}$ time series for storm B 20 July, 1975 is given in Figure 7.12 which also indicates the times and amounts of cloud seeding, and the periods of missing data. The dashed line represents the trend in the data computed using the Tukey filter described in Appendix A. The missing data had the most serious effect over the interval from 17:15 MDT to approximately 18:45 MDT as seen by the rather erratic fluctuations in $\bar{\eta}$.

The autocorrelation coefficients of the data for lag one (1.5 min) to lag ten (15 min) computed using (5.4.2) are given in Table 7.2.

The unsmoothed power spectrum of the raw data is given in Figure 7.13 and the smoothed power spectrum using a three-point running average is given in Figure 7.14. The values of the red-noise power are applied to the smoothed power spectrum using an autocorrelation value $\rho = .845$.

The application of the Tukey highpass filter resulted in a data set with an autocorrelation coefficient $\rho = .023$. The smoothed power spectrum for the highpass data with white-noise power applied, assuming a Chi-square distribution, is given in Figure 7.15. There are 3 peaks in the power spectrum that are significant at the 95 percent confidence level with respect to white-noise. The statistically significant frequencies are 0.063, 0.128, and 0.148 cycles per minute. These correspond to cycle periods of 15.9, 7.8, and 6.8 minutes respectively.

Fig. 7.8: PPI echoes for storm B on 20 July, 1975. Elevation ~ 1.1°
Reflectivity = from 20 dBZ to 10 dBZ. Time = 15:30 - 16:45 MDT.

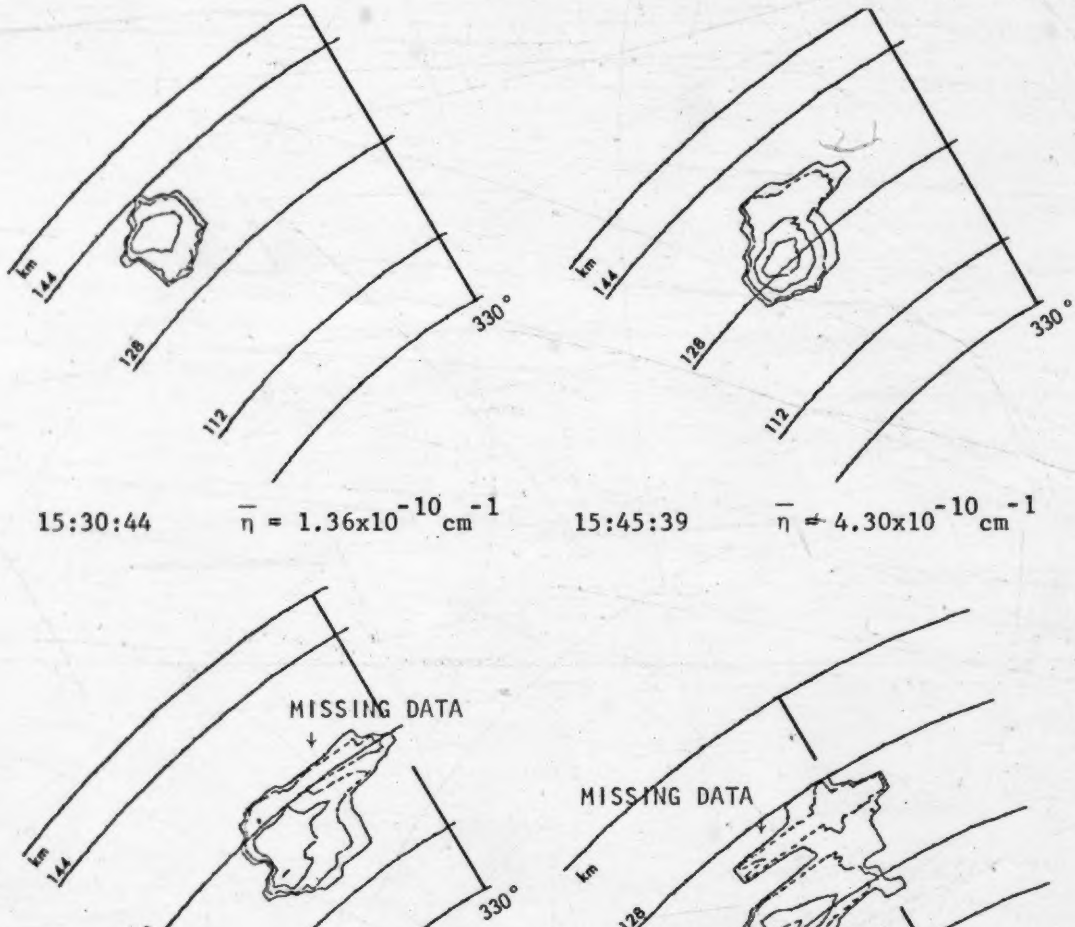

15:30:44 $\bar{\eta} = 1.36\times10^{-10}\,\text{cm}^{-1}$

15:45:39 $\bar{\eta} = 4.30\times10^{-10}\,\text{cm}^{-1}$

16:00:35 $\bar{\eta} = 9.70\times10^{-11}\,\text{cm}^{-1}$

16:15:31 $\bar{\eta} = 1.63\times10^{-10}\,\text{cm}^{-1}$

16:30:27 $\bar{\eta} = 5.90\times10^{-10}\,\text{cm}^{-1}$

16:45:22 $\bar{\eta} = 7.94\times10^{-10}\,\text{cm}^{-1}$

Fig. 7.9: PPI echoes for storm B on 20 July, 1975. Elevation ~1.2°
Reflectivity = from 20 dBZ by 10 dBZ. Time = 17:00 - 18:14 MDT.

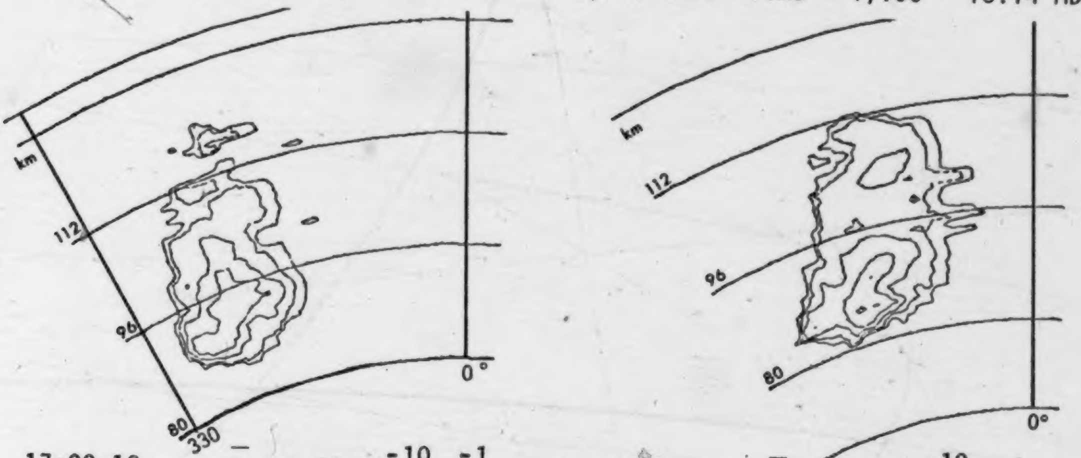
km
112
96
80
330
0°
km
112
96
80
0°

17:00:18 $\overline{\eta} = 4.59\times10^{-10}\,\mathrm{cm}^{-1}$ 17:15:14 $\overline{\eta} = 4.19\times10^{-10}\,\mathrm{cm}^{-1}$

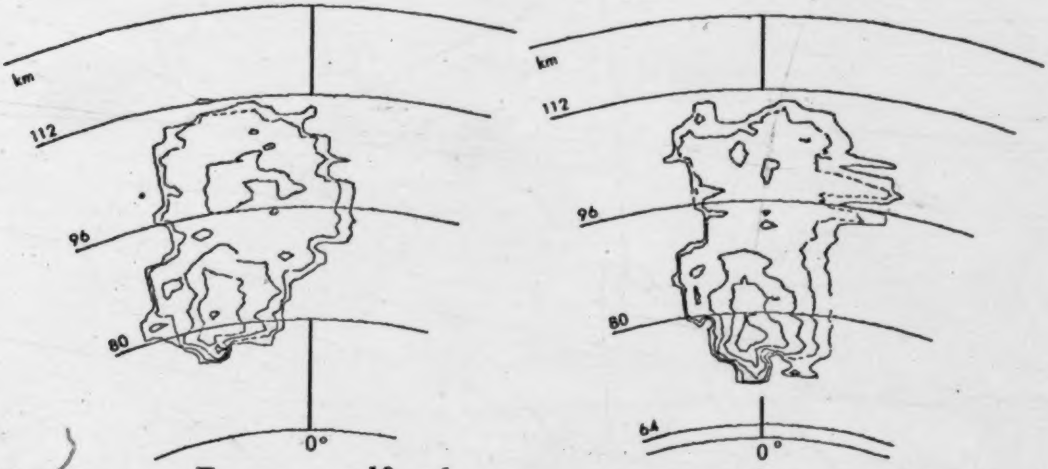
km
112
96
80
0°
km
112
96
80
64
0°

17:30:10 $\overline{\eta} = 3.70\times10^{-10}\,\mathrm{cm}^{-1}$ 17:45:06 $\overline{\eta} = 5.16\times10^{-10}\,\mathrm{cm}^{-1}$

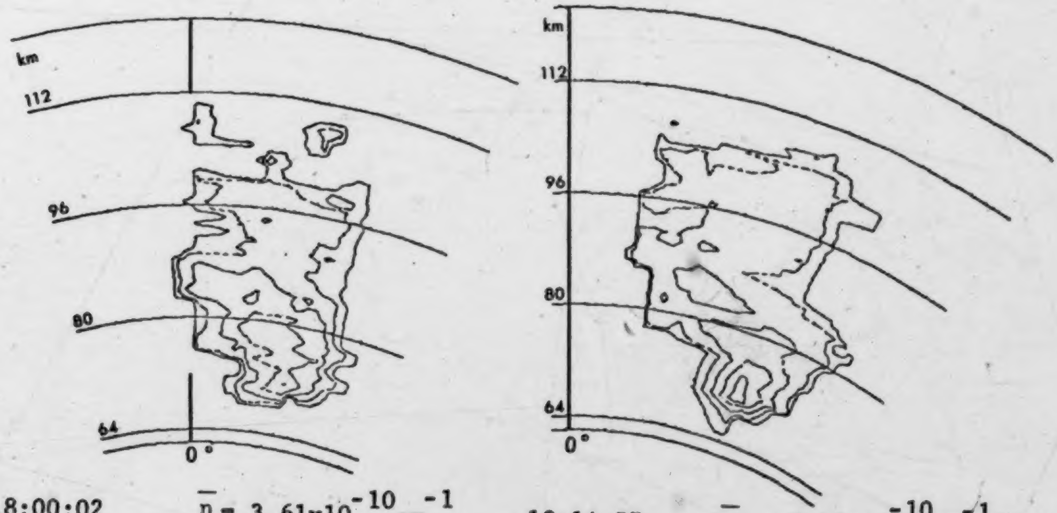
km
112
96
80
64
0°
km
112
96
80
64
0°

18:00:02 $\overline{\eta} = 3.61\times10^{-10}\,\mathrm{cm}^{-1}$ 18:14:57 $\overline{\eta} = 7.38\times10^{-10}\,\mathrm{cm}^{-1}$

Fig 7.10: PPI echoes for storm B on 20 July, 1975. Elevation ~1.3°
Reflectivity = from 20 dBZ by 10 dBZ. Time = 18:29 - 19:01 MDT.

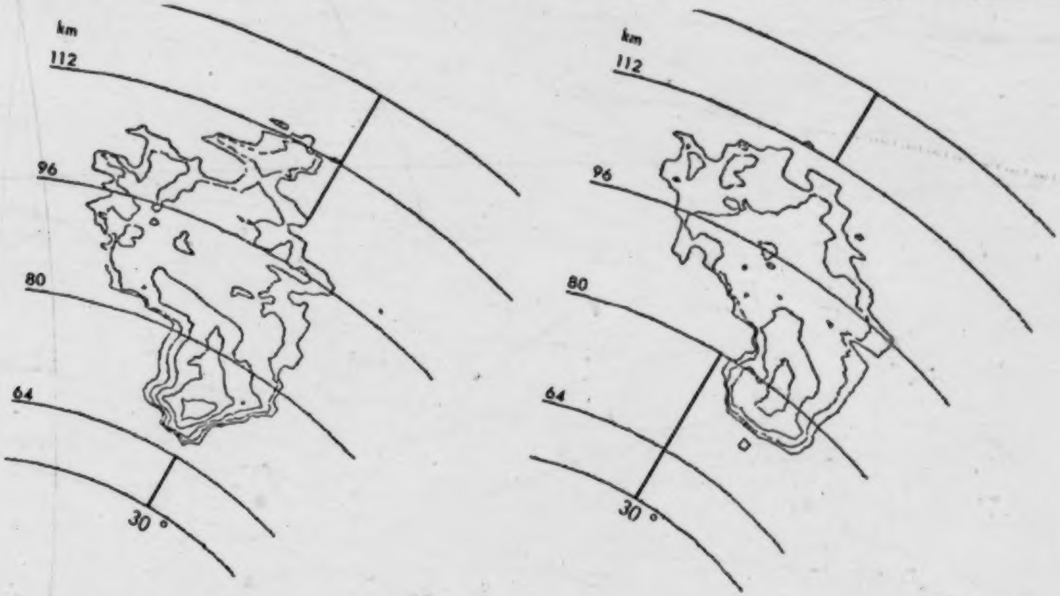

18:29:54 $\overline{\eta} = 4.47\times10^{-10}\,\mathrm{cm}^{-1}$ 18:44:49 $\overline{\eta} = 1.70\times10^{-10}\,\mathrm{cm}^{-1}$

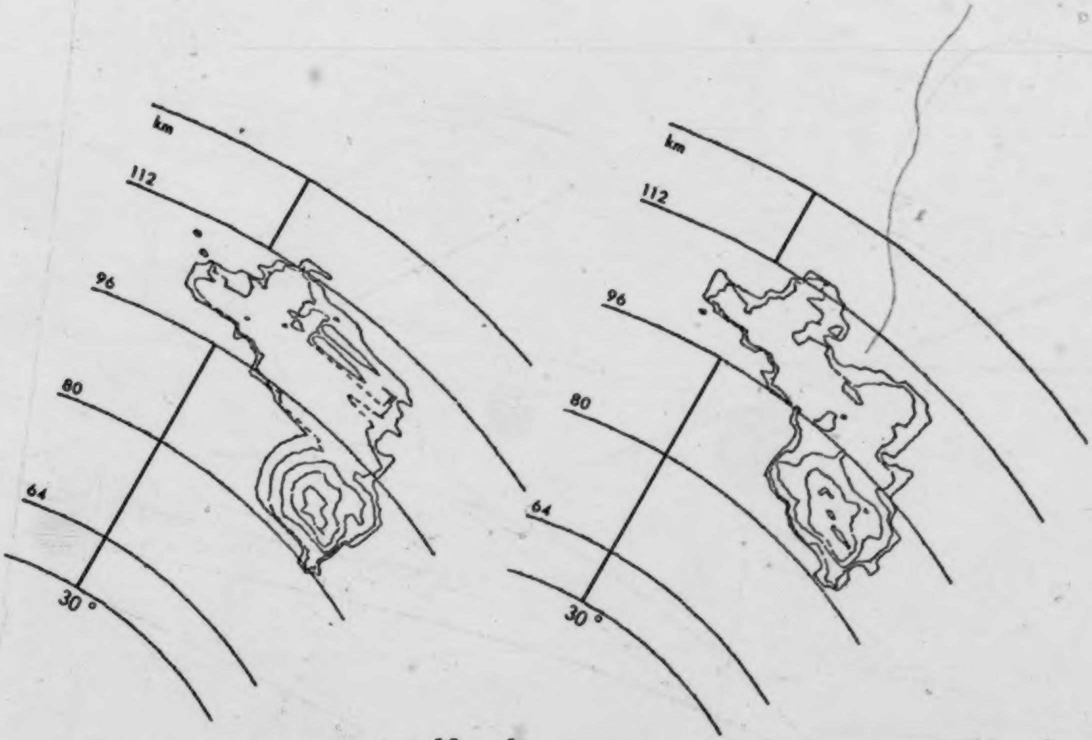

18:59:45 $\overline{\eta} = 9.14\times10^{-10}\,\mathrm{cm}^{-1}$ 19:01:15 $\overline{\eta} = 5.37\times10^{-10}\,\mathrm{cm}^{-1}$

Fig. 7.11: PPI echoes for storm B on 20 July, 1975. Elevation ~ 1.4°
Reflectivity = from 20 dBZ by 10 dBZ. Time = 19:14 - 19:59 MDT.

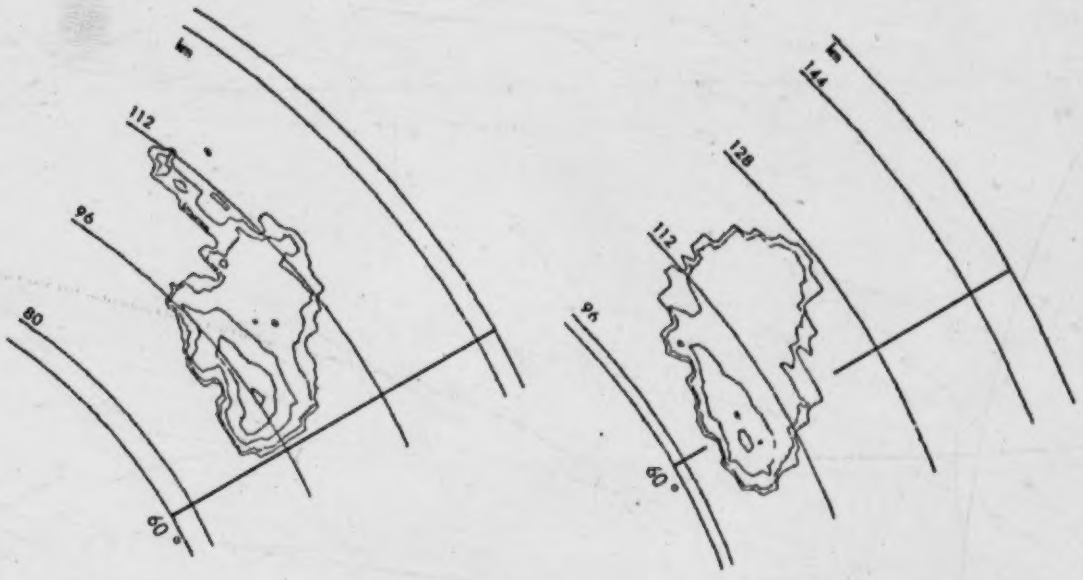

19:14:41 $\overline{\eta} = 4.59\times10^{-10}\,\mathrm{cm}^{-1}$ 19:29:37 $\overline{\eta} = 1.02\times10^{-10}\,\mathrm{cm}^{-1}$

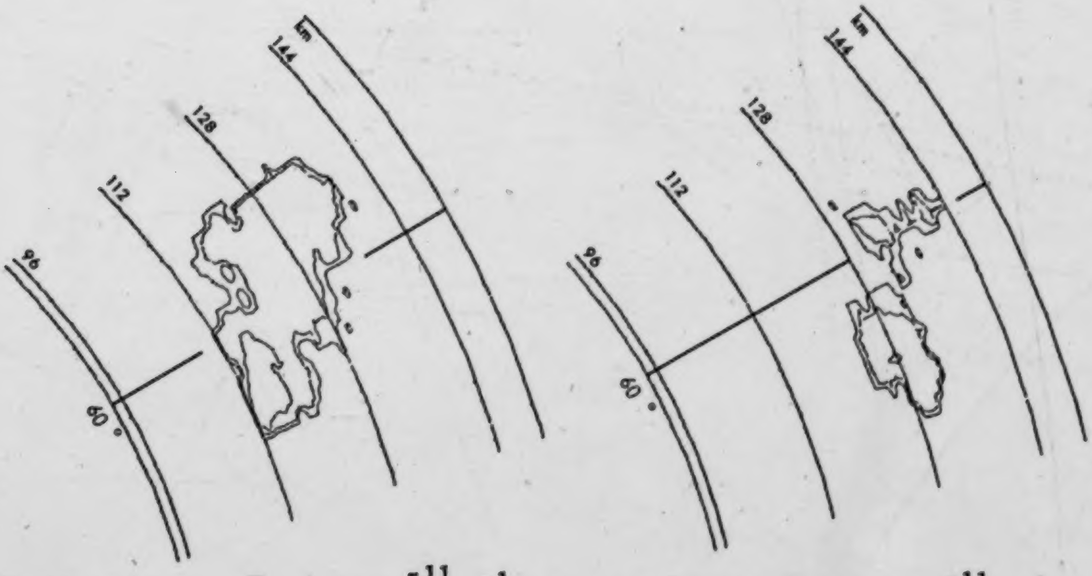

19:44:33 $\overline{\eta} = 4.67\times10^{-11}\,\mathrm{cm}^{-1}$ 19:59:28 $\overline{\eta} = 2.34\times10^{-11}\,\mathrm{cm}^{-1}$

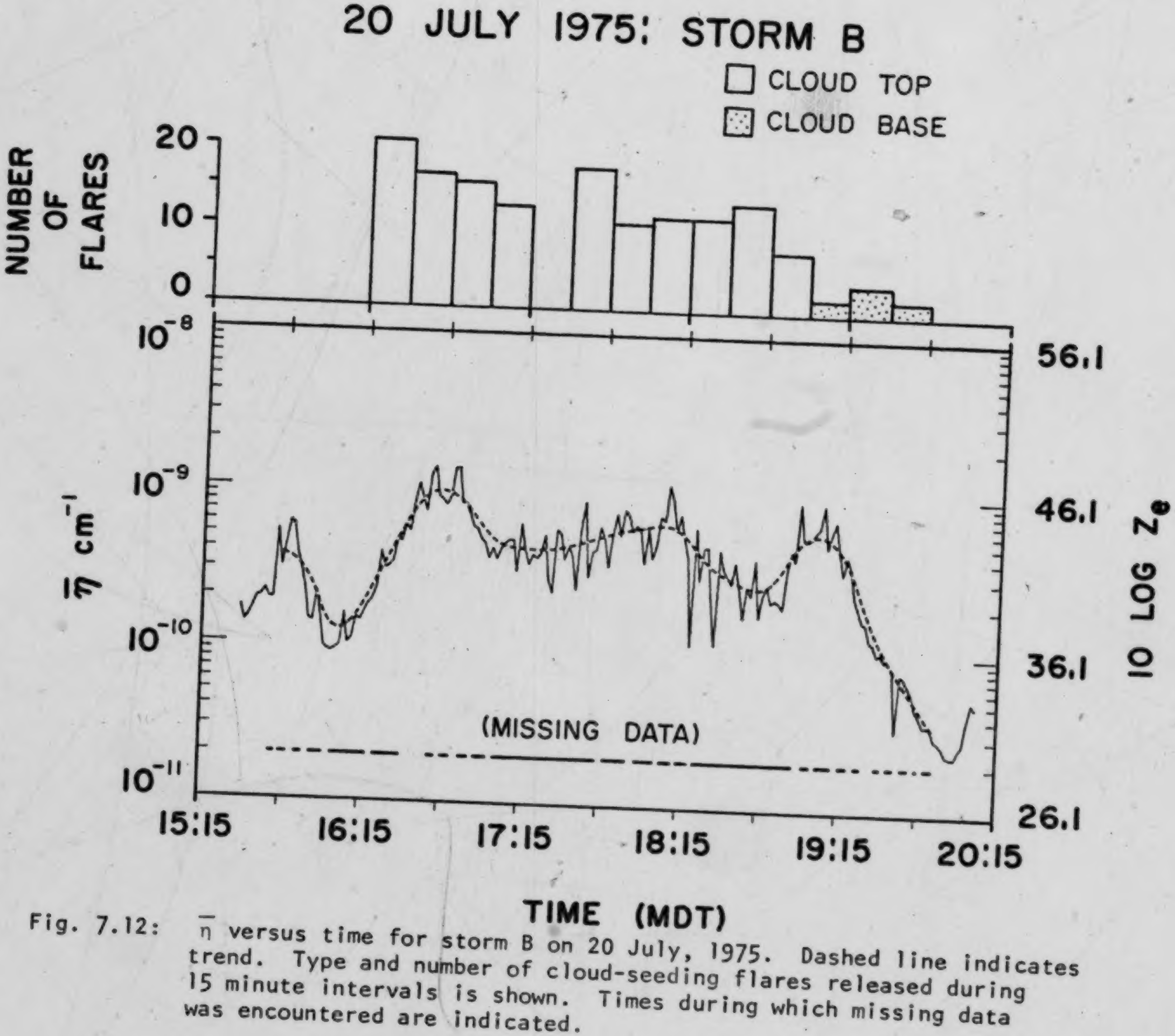

Fig. 7.12: $\bar{\eta}$ versus time for storm B on 20 July, 1975. Dashed line indicates trend. Type and number of cloud-seeding flares released during 15 minute intervals is shown. Times during which missing data was encountered are indicated.

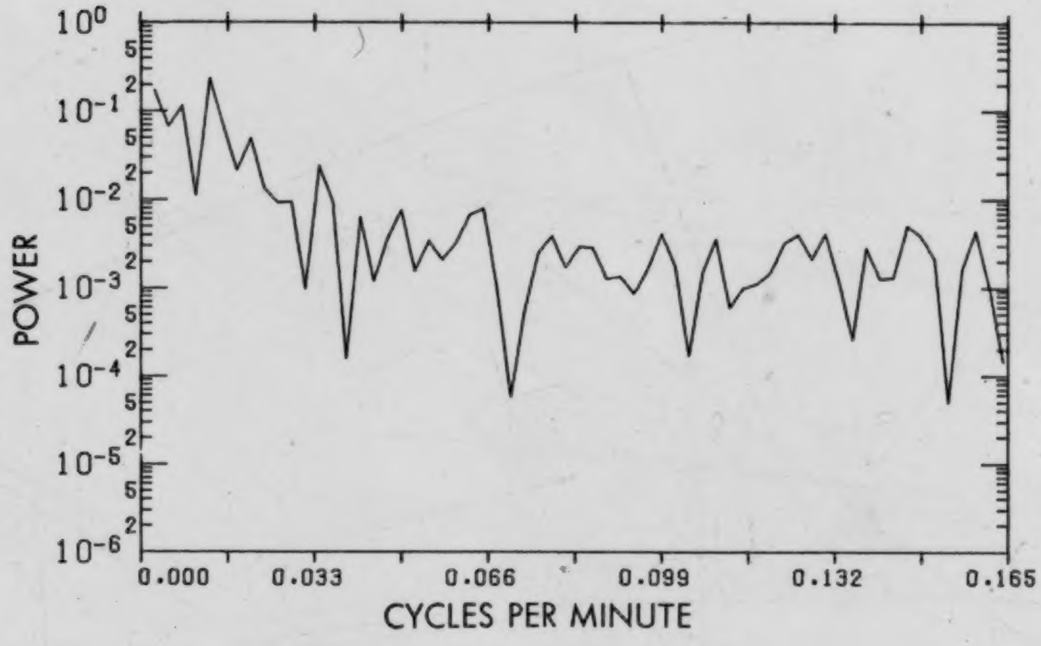

Fig. 7.13: Unsmoothed power spectrum of $\overline{\eta}$ for storm B on 20 July, 1975.

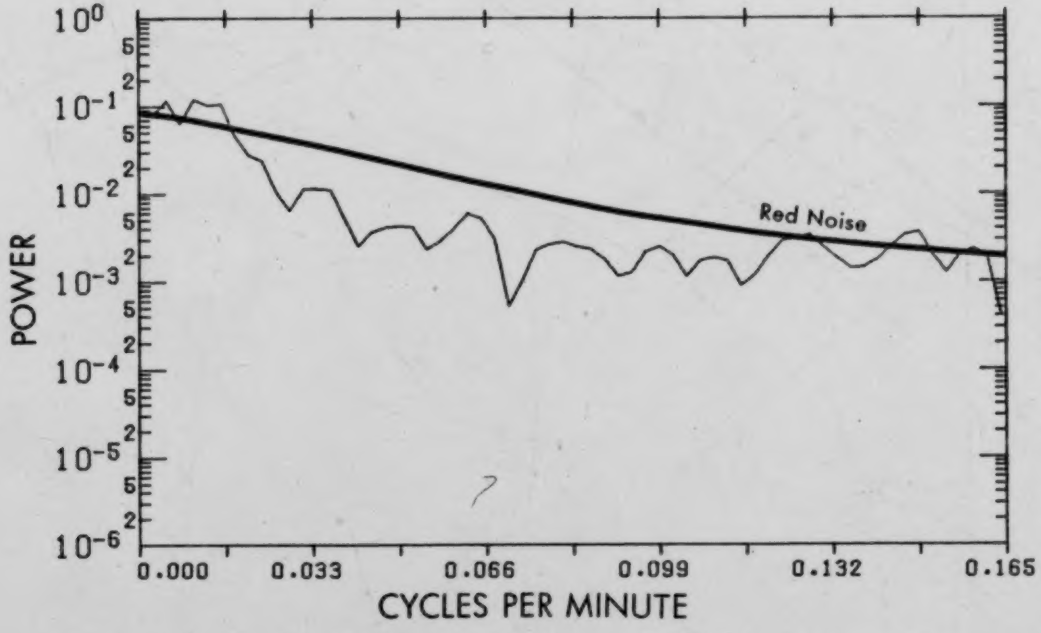

Fig. 7.14: Three-point Daniell-filtered power spectrum of $\overline{\eta}$ for storm B on 20 July, 1975. The red-noise spectrum is shown.

Table 7.2: Lag 1.5 to 15 minute autocorrelation coefficients of $\overline{\eta}$ for Storm B on 20 July, 1975.

LAG NUMBER	TIME LAG (min)	AUTOCORRELATION COEFFICIENT
1	1.5	.828
2	3.0	.743
3	4.5	.734
4	6.0	.668
5	7.5	.608
6	9.0	.580
7	10.5	.485
8	12.0	.431
9	13.5	.408
10	15.0	.341

The effect of the missing data can be seen in the $\overline{\eta}$ series as spikes superimposed on the trend in the data. The missing data does not appear to be serious enough to mask the trend but considerable high frequency noise seems to have been introduced. We may expect approximately 3 spectral lines out of the 64 lines in Figure 7.15 to reach significance by chance at the 95 percent confidence level, therefore, the two peaks in the power spectrum at 0.128 and 0.148 cycles per minute may well have been introduced accidently by the interpolation of the missing data. Any cloud-seeding effects would have to be discussed in terms of the trend in the data.

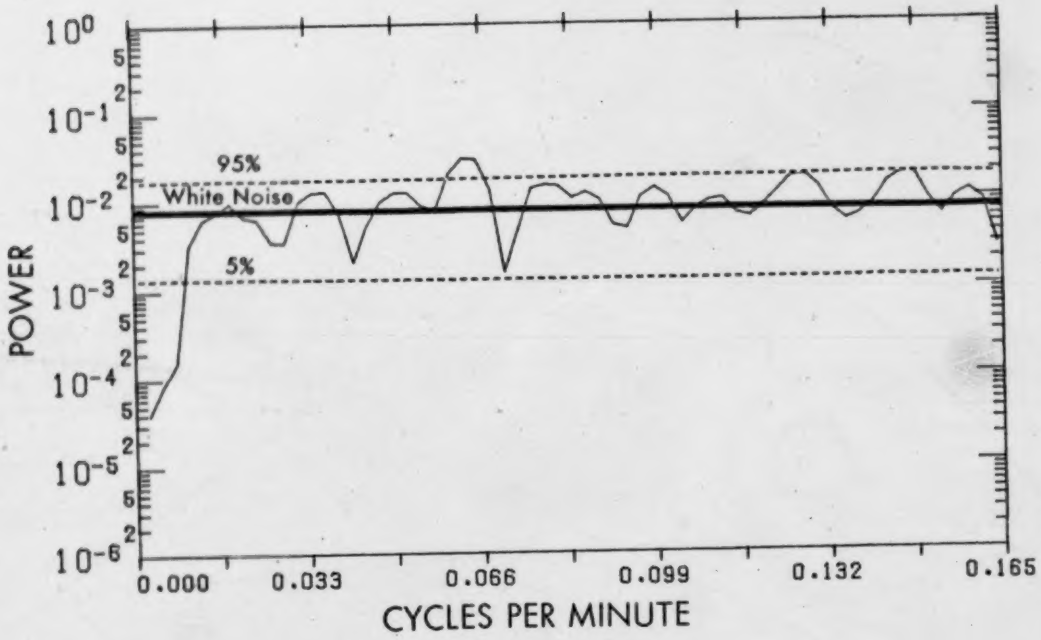

Fig. 7.15: Three-point Daniell-filtered power spectrum of Tukey-filtered $\overline{\eta}$ highpass data for storm B on 20 July, 1975. The white-noise spectrum and 90% confidence interval are shown.

7.4 20 July, 1975: Storm C

The hailswath for storm C 20 July, 1975 is shown in Figure 7.7. As was the case with storm B, grape-size hail was the maximum size reported.

PPI scans for storm C 20 July, 1975 at approximately 15-minute intervals are given in Figures 7.16 through 7.18. The storm was not a single well-defined unit, but consisted of two precipitation cores for a major portion of its lifetime. The storm passed directly over Gull Lake at approximately 19:50 MDT after which it gradually dissipated.

The $\bar{\eta}$ time series for storm C 20 July, 1975, along with the times and amount of cloud seeding, are given in Figure 7.19. Once again there were echoes which contained missing rays and these periods are also indicated in Figure 7.19. The dashed line represents the trend in the data computed using the Tukey filter described in Appendix A. The $\bar{\eta}$ time series appears to go through one major cycle which corresponds with the continuous hailswath at the surface.

The autocorrelation coefficients of the data for lag one (1.5 min) to lag ten (15 min) computed using (5.4.2) are given in Table 7.3.

The autocorrelation coefficients are similar to those found in the 1976 storms. It appears that interpolation due to missing data in the calculation of $\bar{\eta}$ did not result in serious errors.

The unsmoothed power spectrum of the raw data is given in Figure 7.20 and the smoothed power spectrum, using a three-point running average, is given in Figure 7.21. The values of the red-noise power are applied to the smoothed power spectrum using an autocorrelation value ρ = .948. The values of the red-noise

Fig. 7.16: PPI echoes for storm C on 20 July, 1975. Elevation ~ 1.0° Reflectivity = from 20 dBZ by 10 dBZ. Time = 17:45 - 18:59 MDT.

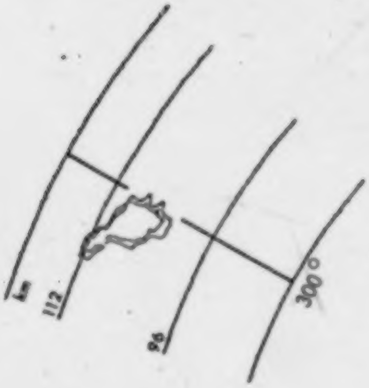

17:45:04 $\bar{\eta} = 2.77\times10^{-11}\,\mathrm{cm}^{-1}$

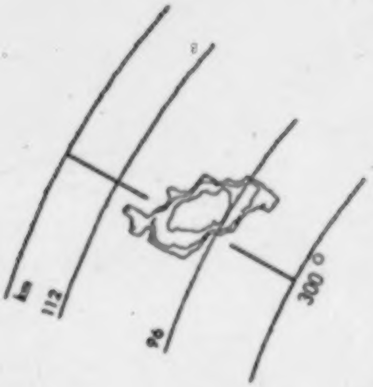

18:00:00 $\bar{\eta} = 9.15\times10^{-11}\,\mathrm{cm}^{-1}$

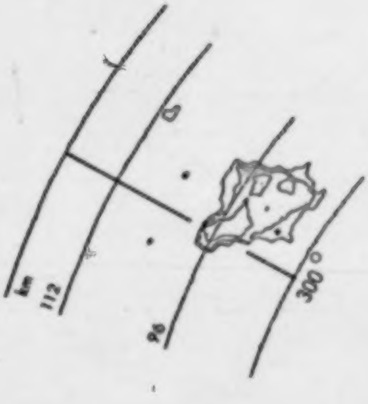

18:14:56 $\bar{\eta} = 8.07\times10^{-11}\,\mathrm{cm}^{-1}$

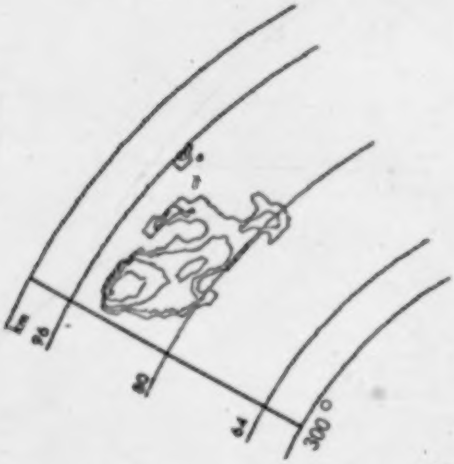

18:29:52 $\bar{\eta} = 3.96\times10^{-10}\,\mathrm{cm}^{-1}$

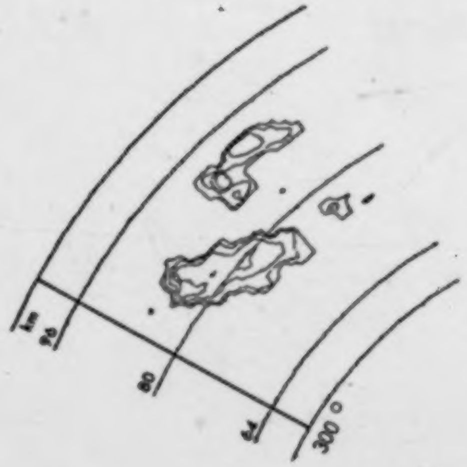

18:44:47 $\bar{\eta} = 3.34\times10^{-10}\,\mathrm{cm}^{-1}$

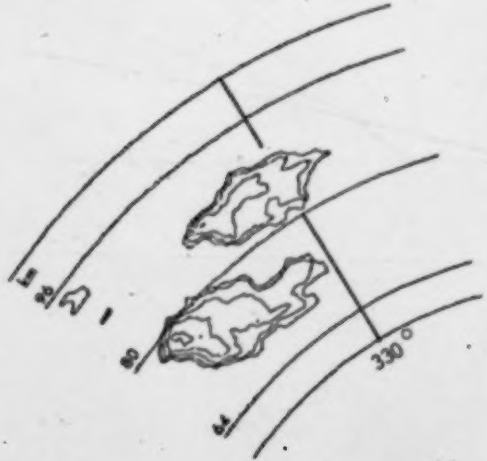

18:59:44 $\bar{\eta} = 5.73\times10^{-10}\,\mathrm{cm}^{-1}$

Fig. 7.17: PPI echoes for storm C on 20 July, 1975. Elevation ~ 1.1°
Reflectivity = from 20 dBZ by 10 dBZ. Time = 19:16 - 20:00 MDT.

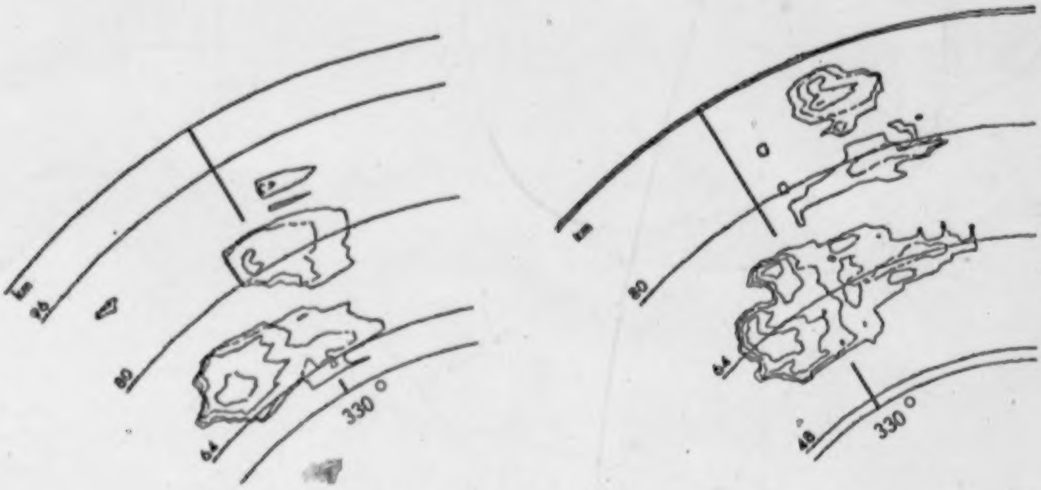
km
25
80
64
330°
km
80
64
48
330°

19:16:09 $\overline{\eta} = 2.36\times10^{-10}\,\mathrm{cm}^{-1}$ 19:31:05 $\overline{\eta} = 2.52\times10^{-10}\,\mathrm{cm}^{-1}$

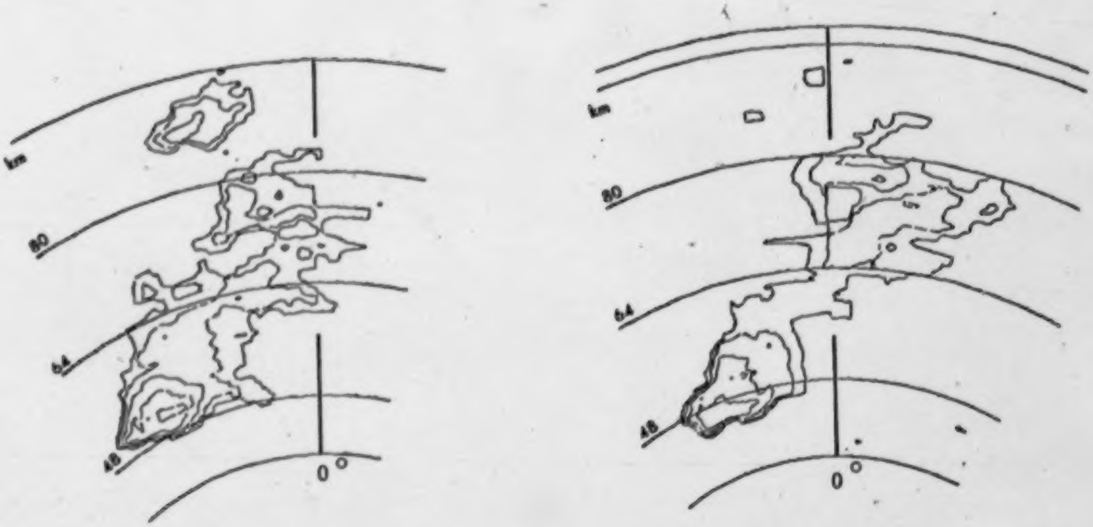
km
80
64
48
0°
km
80
64
48
0°

19:49:00 $\overline{\eta} = 1.50\times10^{-10}\,\mathrm{cm}^{-1}$ 20:00:57 $\overline{\eta} = 1.16\times10^{-10}\,\mathrm{cm}^{-1}$

Fig. 7.18: PPI echoes for storm C on 20 July, 1975. Elevation - 1.3°
Reflectivity = from 20 dBZ by 10 dBZ. Time = 20:15 - 21:00 MDT.

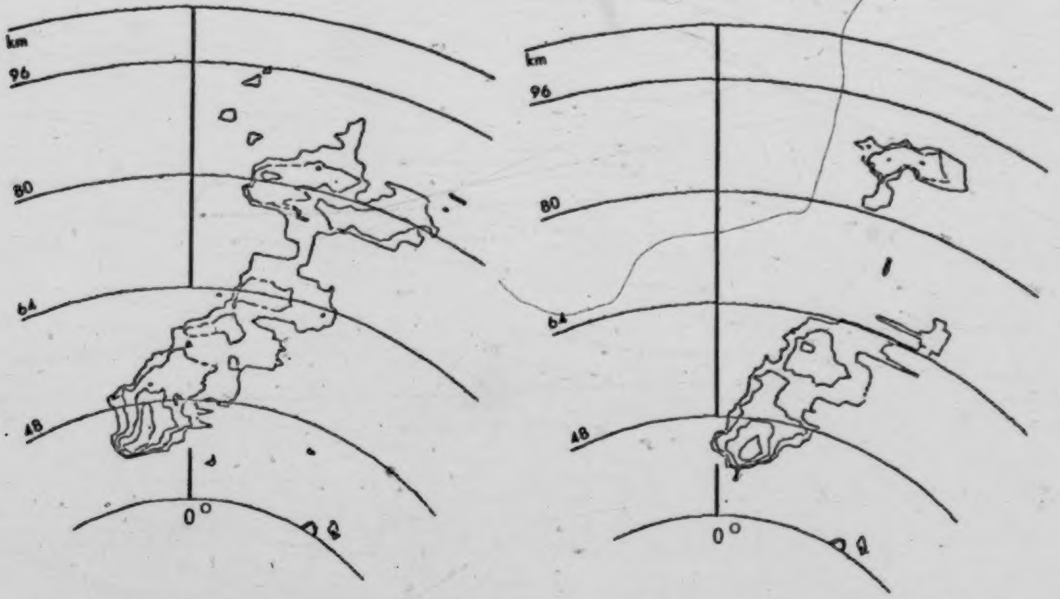

20:15:53 $\overline{\eta} = 5.63\times10^{-11}\,\mathrm{cm}^{-1}$ 20:30:48 $\overline{\eta} = 5.65\times10^{-11}\,\mathrm{cm}^{-1}$

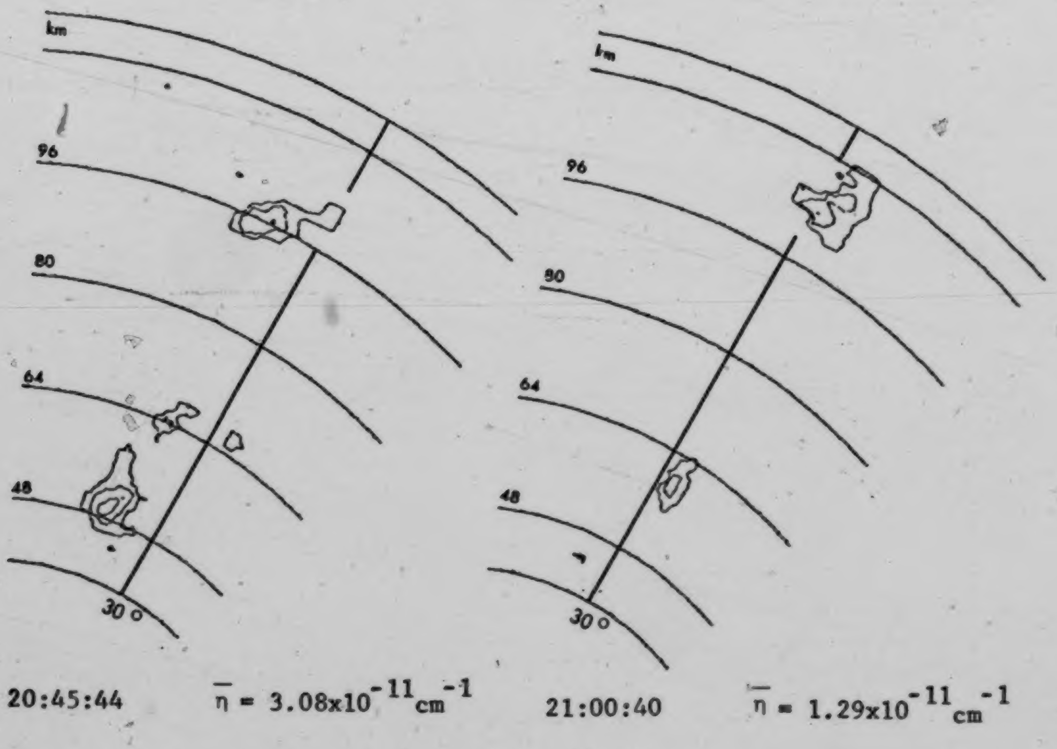

20:45:44 $\overline{\eta} = 3.08\times10^{-11}\,\mathrm{cm}^{-1}$ 21:00:40 $\overline{\eta} = 1.29\times10^{-11}\,\mathrm{cm}^{-1}$

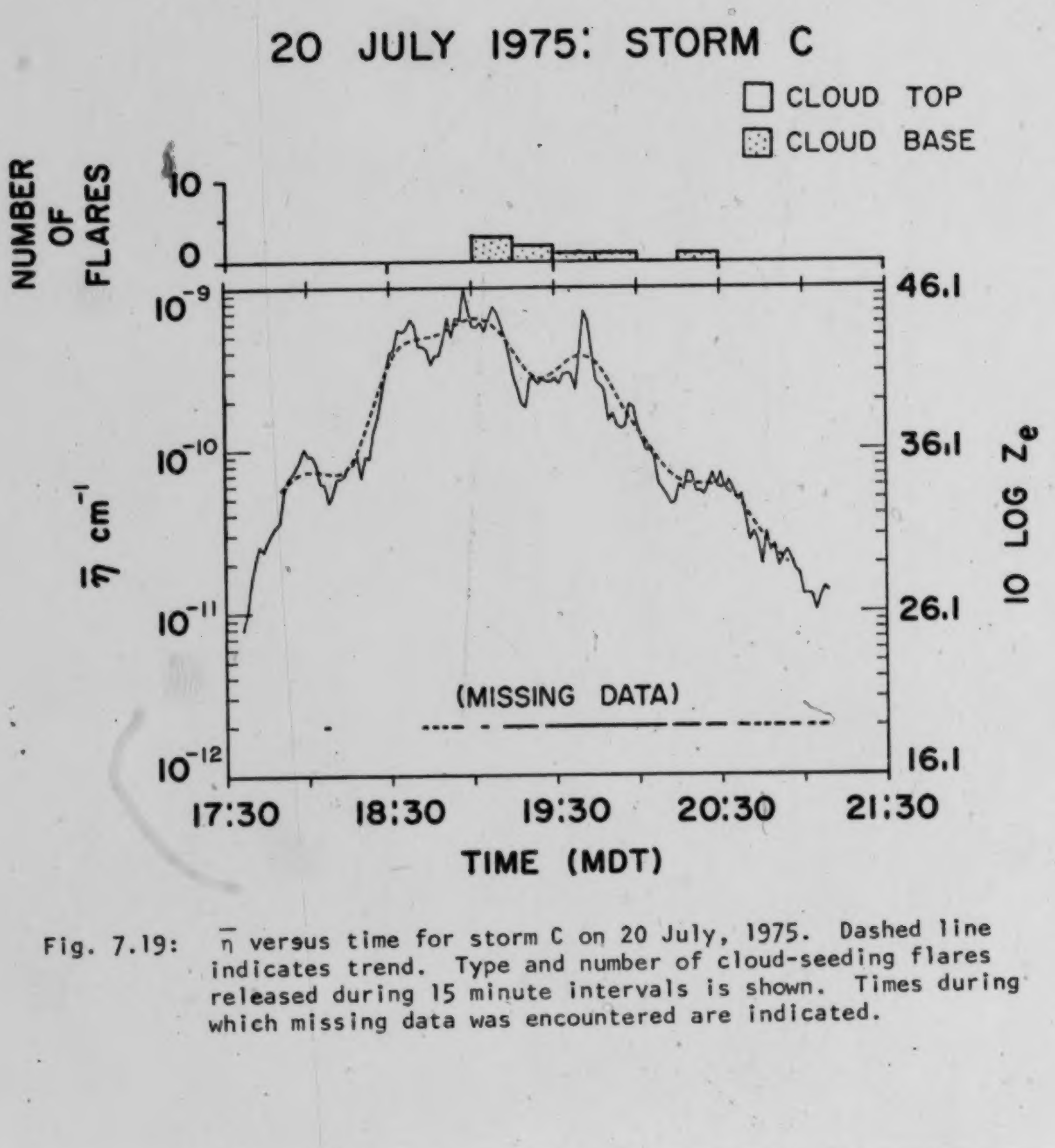

Fig. 7.19: $\bar{\eta}$ versus time for storm C on 20 July, 1975. Dashed line indicates trend. Type and number of cloud-seeding flares released during 15 minute intervals is shown. Times during which missing data was encountered are indicated.

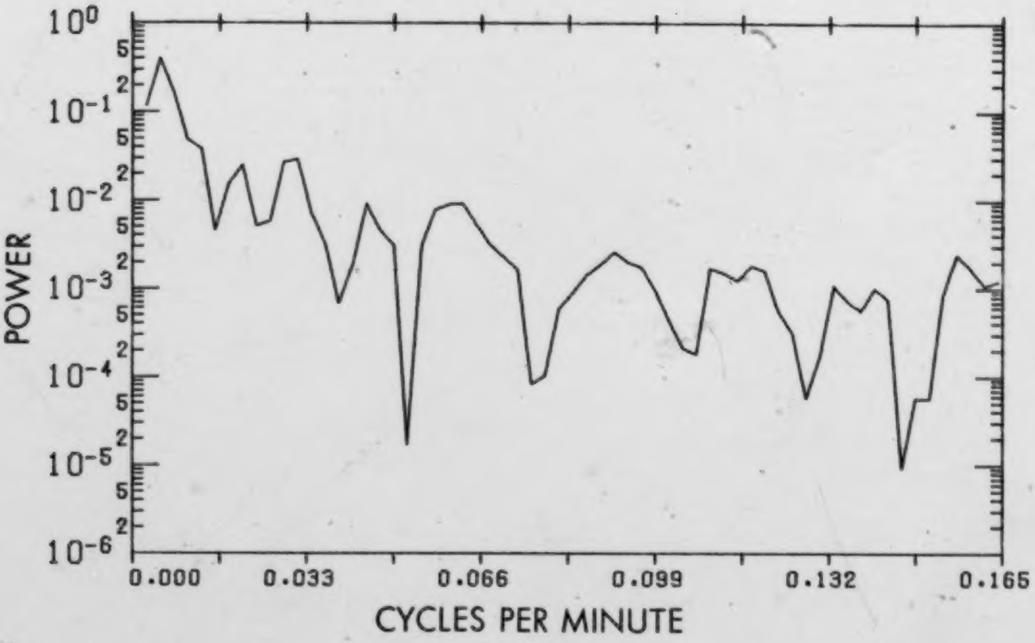

Fig. 7.20: Unsmoothed power spectrum of $\overline{n}$ for storm C on 20 July, 1975.

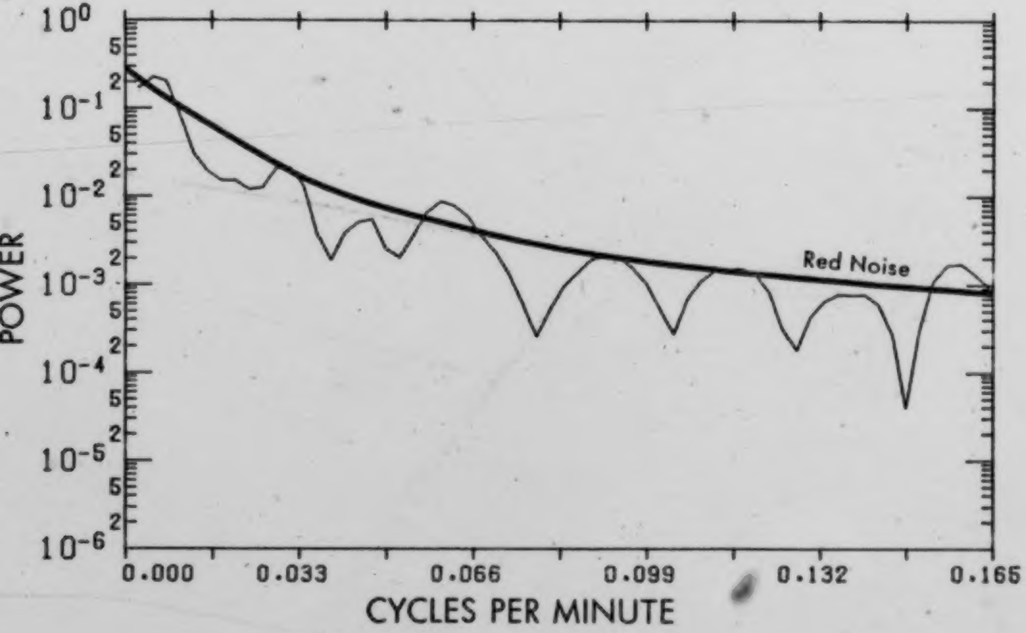

Fig. 7.21: Three-point Daniell-filtered power spectrum of $\overline{n}$ for storm C on 20 July, 1975. The red-noise spectrum is shown.

Table 7.3: Lag 1.5 to 15 minute autocorrelation coefficients of $\overline{\eta}$ for Storm C on 20 July, 1975.

LAG NUMBER	TIME LAG (min)	AUTOCORRELATION COEFFICIENT
1	1.5	.953
2	3.0	.889
3	4.5	.831
4	6.0	.788
5	7.5	.733
6	9.0	.687
7	10.5	.656
8	12.0	.627
9	13.5	.598
10	15.0	.569

power using $\rho =$ .467 are applied to the highpass data smoothed power spectrum in Figure 7.22. A statistically significant peak at the 95 percent confidence level exists at 0.063 cycles per minute, assuming a Chi-square distribution. This corresponds to a cycle period of 15.9 minutes.

7.5 Summary of 1975 Data

The missing data in 1975 definitely hampers an analysis of this type which deals with low-level echoes, and which is responsive to small regions of high reflectivity. From the cases studied, it appears that the interpolation technique used in calculating $\overline{\eta}$ across the gaps in the digitized data seemed to be sufficiently accurate that the trend in the data was not lost. The linear interpolation did

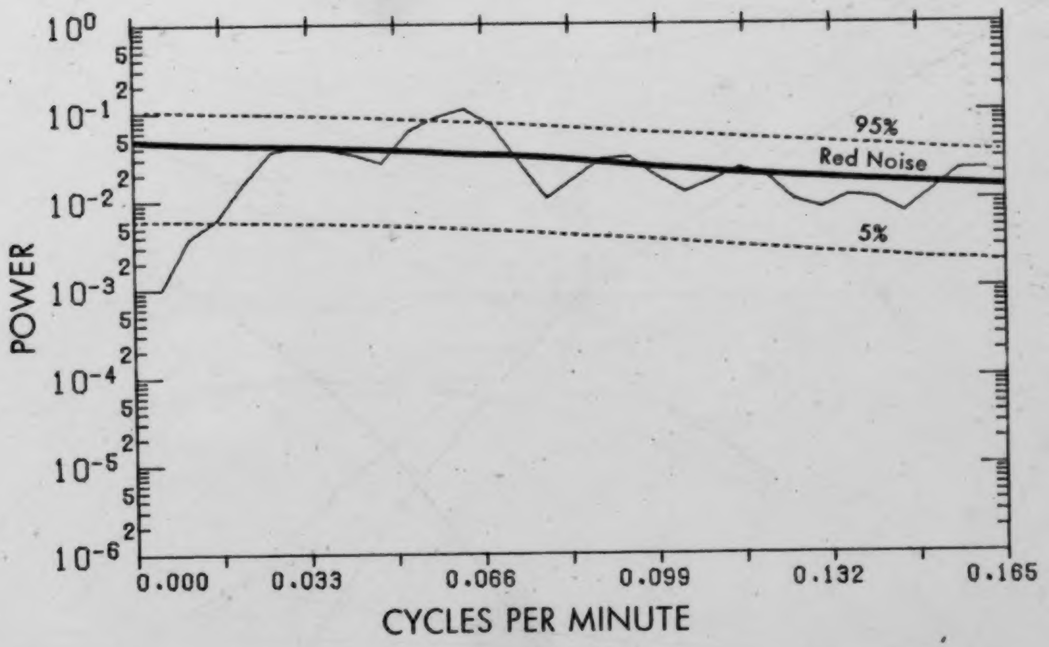

Fig. 7.22: Three-point Daniell-filtered power spectrum of Tukey-filtered $\overline{n}$ highpass data for storm C on 20 July, 1975. The red-noise spectrum and 90% confidence interval are shown.

introduce high frequency noise into the power spectrum, therefore, little confidence should be placed in the small scale variations.

CHAPTER 8

SUMMARY

8.1 Data Summary

The data for each storm has been presented and in each case the resulting hailswath was a reasonable facsimile of what might be reproduced from the $\bar{\eta}$ series using the distributions for maximum hailsize versus $\bar{\eta}$ from Section 4.3. A particularly interesting feature was that the discontinuity of the hailswaths in most cases corresponded well with the trend variation in the $\bar{\eta}$ series. This feature was not always obvious from the individual PPI echoes.

The interpretation of the power spectra, calculated for each storm, must be done with caution since each storm was slightly different in nature. The spectra from the storms which were complex and consisted of two or more precipitation centers should not be compared directly with those of storms which maintained a well-defined identity throughout their lifetime. However, each spectrum does reveal the essential character of the $\bar{\eta}$ variation for that particular storm. Although peaks in a power spectrum may not reach statistical significance at the desired confidence level with respect to the red-noise power spectrum, they still suggest the possibility of preferred cycles in the data. As an attempt to generalize the power spectra data for all storms, a procedure of averaging the highpass data periodograms to obtain one spectral estimate of the data was performed. This method is discussed by Welch (1967). Averaging was applied only to the 1976 storm cases since it was felt that the interpolation of missing data in the 1975 case studies introduced an excessive amount of high frequency noise in the power spectrum. The 7 storm spectral average for the 1976 case studies is given in Figure 8.1.

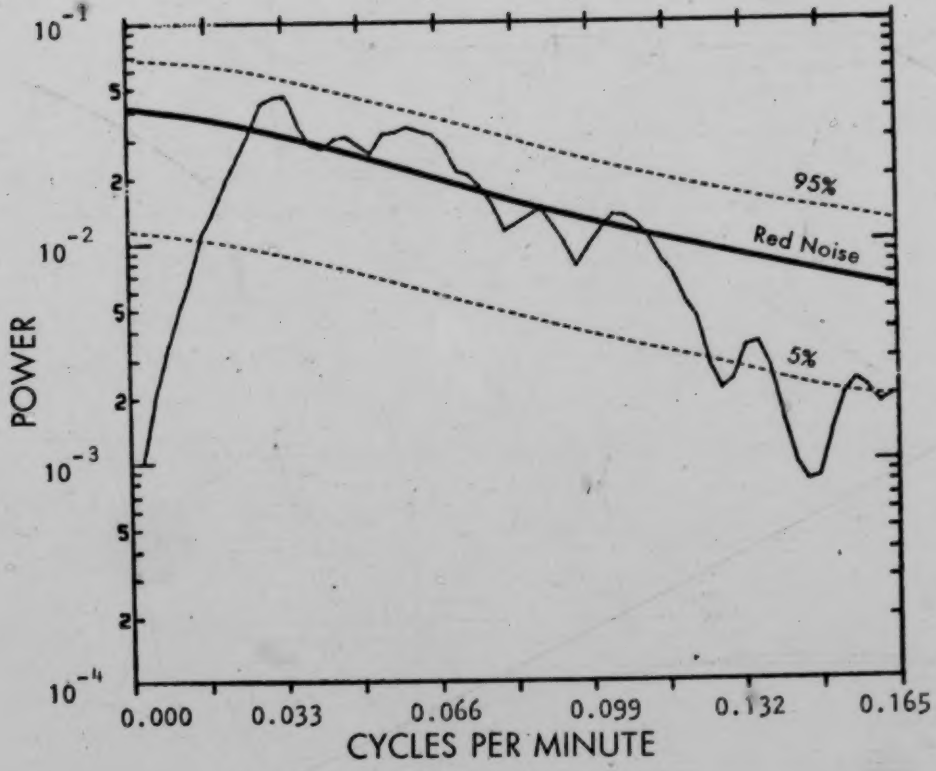

Fig. 8.1: Three-point Daniell-filtered average power spectrum for the seven storms of 1976. The red-noise spectrum and 90% confidence interval are shown.

In general, a large scale cycle in $\bar{\eta}$ was indicated with a frequency of .031 cycles per minute, corresponding to a cycle period of approximately 30 minutes. Secondary preferred frequencies were also found in the data with frequencies of .065, .091, and .104 cycles per minute. The corresponding cycle periods are 15.4, 11.0, and 9.6 minutes, respectively. The presence of these peaks suggests several scales of variability. On one hand, $\bar{\eta}$ seemed to vary with the overall evolution of the storms as they went through their life cycles. On the other hand, small-scale periodicities in $\bar{\eta}$ were superimposed on the trends. Since $\bar{\eta}$ can be related directly to the precipitation falling from cloud base via the meteorological radar equation, this implies that the type, and/or, amount of precipitation displayed this pulsating state which was regular enough that it could be discriminated throughout the lifetimes of all the storms.

The author believes that these small-scale fluctuations in $\bar{\eta}$ are related to the fine-scale features of storms reported by Barge and Bergwall (1976), who proposed a concept of a large circulation cell upon which are superimposed smaller perturbations.

8.2 $\bar{\eta}$, as a Hail Suppression Evaluation Parameter

Since $\bar{\eta}$ has been shown to be related to the precipitation at cloud base, and appears to be correlated with the precipitation at the surface, an attempt was made to use $\bar{\eta}$ as a measure of cloud-seeding effects. However, the results were disappointing.

Five of the hailstorms analyzed were seeded. The amount of cloud seeding is indicated within 15 minute intervals on the $\bar{\eta}$ versus time plots for 17 July, 1976 (storm A), 6 August, 1976, 20 August, 1976, 20 July, 1975 (storm B), and 20 July, 1975 (storm C). In all cases except storm A of 17 July, 1976, the storm was studied for an ample period before cloud seeding commenced and it was possible to study storm behavior before and after seeding. If cloud seeding altered the precipitation mechanism significantly, an effect should be displayed by a change in $\overline{\eta}$. Four hailstorms analyzed were not seeded, therefore, the natural variability of $\overline{\eta}$ could be studied for comparison purposes. Seeding rates and seeding techniques are not emphasized in this study.

According to Warner (1976), a decrease in reflectivity might be found in intense precipitation cores of individual echoes roughly 25 minutes after seeding. This estimate assumes that a sufficiently high concentration of embryos develop in approximately 8 minutes. Another few minutes are required for the embryos to be carried aloft and 10 to 15 minutes are allowed for fallout. Seeding effects are sought first in the trend of the data which is related to the overall storm intensity.

In storm B on 20 July, 1975 (Figure 7.12), $\overline{\eta}$ increased (16:15 - 16:45) when the seeding commenced and, within 30 minutes, $\overline{\eta}$ decreased. No seeding occurred during the interval 17:15 to 17:30 and, 30 minutes later, $\overline{\eta}$ is seen to increase slightly. Seeding commenced once again, and $\overline{\eta}$ decreased and then increased although not reaching the maximum values achieved earlier. Following this, the storm dissipated. The early response of $\overline{\eta}$ suggests a positive seeding effect in this case.

In storm C of 20 July, 1975 (Figure 7.19), seeding commenced after $\overline{\eta}$ had already reached a maximum value. The storm dissipated after 19:30. This cannot be attributed solely to the cloud seeding, since the storm crossed directly over Gull Lake at 19:30, and it has been suggested by Warner (1976), that a lake may have a dissipating effect on storms.

Storm A on 17 July, 1976 (Figure 5.9), was a mature storm by the time it entered the project area. Cloud seeding and radar detection began at approximately the same time. The parameter $\bar{\eta}$ increased when cloud seeding began and, approximately 30 minutes later, $\bar{\eta}$ values decreased. The storm was heavily seeded and $\bar{\eta}$ decreased steadily for approximately 1.5 hours. At 21:45 $\bar{\eta}$ increased, then decreased rapidly. The response of $\bar{\eta}$ approximately 30 minutes after the initial seeding once again suggests a positive seeding effect.

Storm B on 17 July, 1976 (Figure 5.19), was considered to be not seeded although one cloud-top flare was released into the storm early in its lifetime. The $\bar{\eta}$ time series for storm B did not vary as much as that for storm A and this corresponded well with the continuous hailswath. The dissipation rate was not quite as fast for storm B as for storm A. Since the two storms occurred on the same day, developed under similar environmental conditions, and travelled approximately across the same region, these two storms constitute the best examples with which to look for seeding effects. The possible effect storm A had on the environment of storm B would be difficult to assess, and is not considered. The raw data power spectra were shown not to be significantly different using the Chi-square goodness-of-fit test in Section 5.7. The possibility exists that the greater trend variability and sporadic hailswath of storm A were results of the cloud seeding.

The storm on 6 August, 1976 (Figure 6.5) dissipated approximately 30 minutes after the initial cloud seeding, although, the storm was shown to have reached its maximum intensity by the time cloud seeding began. Whether or not the cloud seeding limited the subsequent maximum intensity cannot be assessed. The presence of Buffalo Lake may have contributed to the dissipation of the storm.

The storm on 20 August, 1976 (Figure 6.33), was also seeded, but, as was mentioned in Section 6.5, the storm was not a single entity but consisted of two precipitation cores for a major portion of its lifetime. The storm was not seeded heavily. It is uncertain whether or not $\overline{\eta}$ could show a seeding effect in such a case since the seeding may affect one part of the storm but be masked by the other portion. In any event, the $\overline{\eta}$ series in Figure 6.33 shows that the storm was on a general decline when cloud seeding began. The storm dissipated very slowly.

The non-seeded storms did not display any consistent traits. In general, the non-seeded storms dissipated as rapidly as the seeded storms. The trends in the data for the non-seeded storms were not notably different than those for the seeded storms. For example, the trend in the data for the storm of 24 August, 1976 which was not seeded, was just as variable as the trend in any of the seeded storms.

The technique of averaging the power spectra for the seed and no-seed cases was performed. Figure 8.2 gives the 3-point smoothed average power spectrum of the highpass data for the 4 non-seeded storms in 1976. The values of the red-noise power were applied to the spectrum using the average autocorrelation value for the non-seeded highpass data, $\rho = .622$. A Chi-square distribution was assumed with the number of degrees of freedom equal to the sum of the degrees of freedom for the individual samples. Similarly, the 3-point smoothed average power spectrum

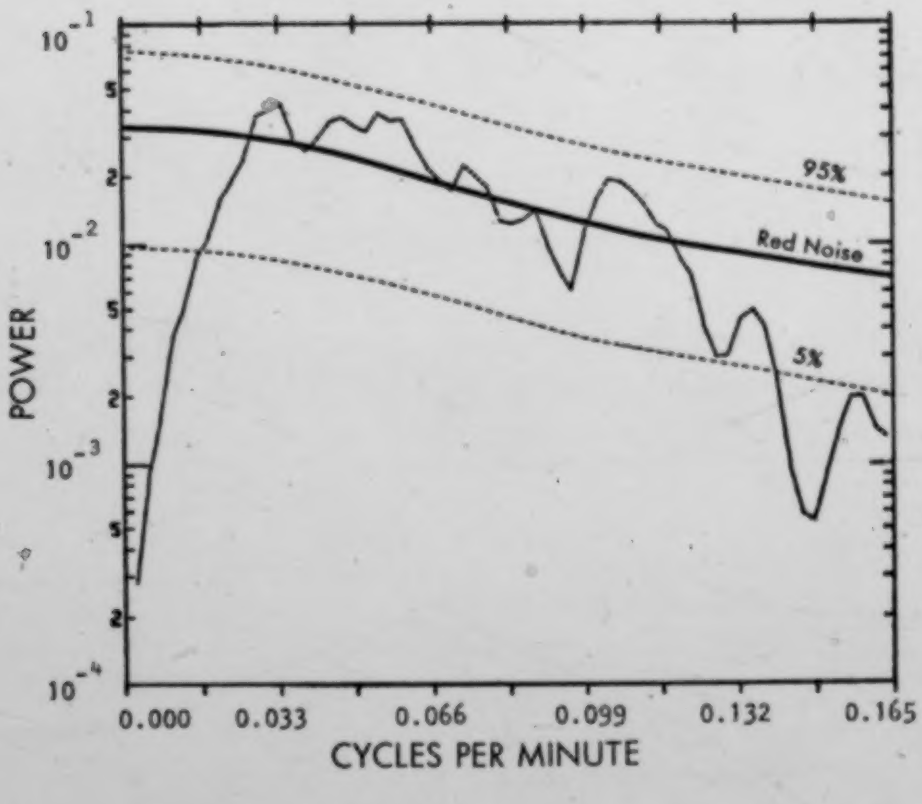

Fig. 8.2: Three-point Daniell-filtered average power spectrum for the four non-seeded storms of 1976. The red-noise spectrum and 90% confidence interval are shown.

for the 3 seeded storms in 1976 is given in Figure 8.3. The values of the red-noise power, assuming a Chi-square distribution, are applied to the spectrum using the average autocorrelation value for the seeded storm highpass data, $\rho = .711$.

There are no significant peaks in either averaged power spectrum. Perhaps the Chi-square distributed red-noise model cannot adequately represent the data. Preferred cycles are suggested in the seed-and no-seed averaged spectra. Their appearance in many storms adds to their significance. Both the seeded and non-seeded average spectra displayed a preferred frequency near .033 cycles per minute. The corresponding cycle period is 30 minutes. This peak may have resulted from the highpass Tukey filter which has effectively removed all cycles with frequencies less than .033 cycles per minute. The average spectrum for the seeded storms displays a well-defined peak at .065 cycles per minute (cycle period: 15.4 minutes), and a minor peak at .091 cycles per minute (cycle period: 11.0 minutes). The average power spectrum for the non-seeded storms indicates a broad, poorly defined peak near .055 cycles per minute (cycle period: 18.2 minutes) and a well defined peak at .105 cycles per minute (cycle period: 9.5 minutes).

A distinction between the two averaged spectra is exhibited by the presence of substantial power near .105 cycles per minute in the non-seeded cases, and the absence thereof in the seeded cases. A hypothetical physical reason for this feature, if it was real, may be that cloud seeding was able to upset the regular production of high reflectivity pulses in the early stages of the developing clouds as they entered the main storm. However, in general, the comment by Panofsky and Brier (1963) that, "Cloud seeders claim they can change the spectrum significantly", was not demonstrated by the parameter $\overline{n}$ in this study.

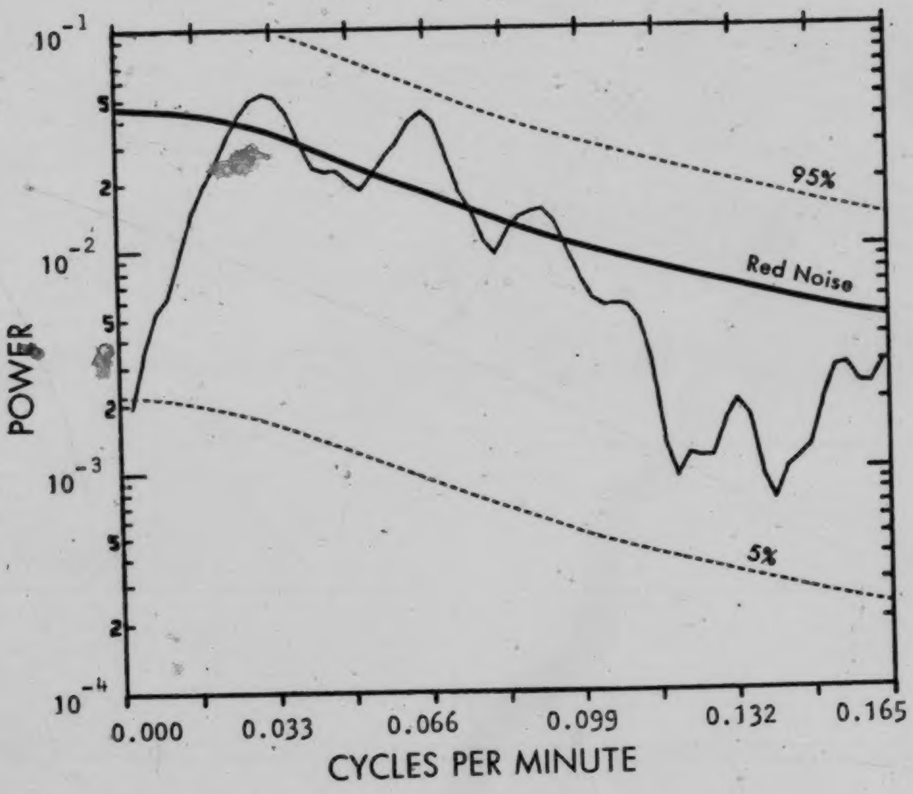

Fig. 8.3: Three-point Daniell-filtered average power spectrum for the three seeded storms of 1976. The red-noise spectrum and 90% confidence interval are shown.

CHAPTER 9

CONCLUSIONS AND RECOMMENDATIONS

9.1 Concluding Remarks

This study has attempted to develop and test a radar parameter which is able to depict storm intensity and precipitation at the surface better than radar reflectivity alone, with hopes that it may be used to detect and measure cloud-seeding effects.

The parameter developed was volume-averaged radar reflectivity $\bar{\eta}$. Its application to low-level PPI scans of 9 hailstorms yielded the relationship between $\bar{\eta}$ and maximum size hail at the surface that was described in Section 4.3. The cumulative distribution curves for $\bar{\eta}$ according to maximum hail size reported at the surface in Figure 4.6, allow one to associate a probability of occurrence of hailfall of a particular maximum size with $\bar{\eta}$ values. This removes the dependence on hail reports and hailpads as the only source with which to define a hailswath. The $\bar{\eta}$-hailsize relation should be tested in real time as an instantaneous indicator of what is happening at the surface.

Since $\bar{\eta}$ and radar reflectivity factor are related, some of the problems associated with their use in hailstorms are comparable. It was possible to distinguish between rain and large hail using $\bar{\eta}$; however, $\bar{\eta}$ values were sometimes similar for rain and rain mixed with small hail. The $\bar{\eta}$ values were measured in this study using a 10.4 cm wavelength radar and were found to increase monotonically with size for hail less than approximately 3 cm in diameter. This monotonic increase was no longer evident for hail larger than 3 cm in diameter. The backscattering from hydrometeors which are no longer small with respect to the wavelength of the radar exhibits oscillations with increasing particle diameter, therefore, the measured $\bar{\eta}$ values for hail were consistent with theoretical calculations.

The question arises as to whether a decrease, due to cloud-seeding, in the volume of all contours corresponding to "mostly hail", may be masked by the concomitant increase in the volumes of all contours corresponding to "mostly rain". If the difference in radar reflectivity between "mostly rain", and "mostly hail" regions is at least 10 dBZ, the overall volume of the "mostly rain" contours would have to increase by at least a factor of two for no net effect on $\bar{\eta}$. The probability of this occurring is not high. Future work for further refinement of this technique should involve the calculation of $\bar{\eta}$ for only those volumes in the storm echo which exceed some assumed threshold radar reflectivity value for "mostly hail"; for example, 40 dBZ.

The 1975 radar data was found to be of sufficient quality for a study of this type if only the trend in the data is required. The small-scale or high frequency fluctuations in $\bar{\eta}$ were greatly affected by the need to interpolate across missing portions of the data.

The volume averaging technique allowed storms of different sizes and at different ranges from the radar to be compared on even terms. Perhaps the greatest consequence of this study is the documentation of the variations in $\bar{\eta}$ with time. A spectral analysis of the $\bar{\eta}$ time series for the storms revealed possibilities of preferred cycles. Fluctuations in $\bar{\eta}$, a parameter related to the instantaneous precipitation from the storm, were shown to imply a storm concept consisting of a large circulation cell with periodicity of approximately 30 minutes, upon which is superimposed small-scale perturbations. The small-scale perturbations have periods of approximately 10 and 15 minutes. Attempts to find statistically significant differences between seeded and non-seeded cases were hindered by the small sample size. Future work should involve the analysis of many more seeded and non-seeded storms.

This study was limited to well-defined storms in order to formulate an accurate $\bar{\eta}$-versus-hailfall relation. However, the technique can be applied to all situations. An $\bar{\eta}$ value can be computed for particular portions of massive storm systems by merely defining the "window" to include only those areas of interest. Changes in $\bar{\eta}$ with time may be more meaningful than the absolute value, allowing one to monitor storm intensification or dissipation with time.

In most cases $\bar{\eta}$ was shown to be more sensitive to overall storm intensity than radar reflectivity alone for revealing trends in the data not obvious from the PPI scans. The analysis of the changes in $\bar{\eta}$ with respect to cloud-seeding events has been discussed. Unequivocal cloud-seeding effects were not detected.

BIBLIOGRAPHY

Atlas, D., 1964: Advances in radar meteorology. Advances in Geophysics, Vol. 10, Academic Press, 318-468.

_____, and F.H. Ludlam, 1961: Multi-wavelength radar reflectivity of hailstorms. Quart. J. Roy. Meteor. Soc. 87: 523-534.

Barge, B.L., 1972: Hail detection with a polarization diversity radar. Sci. Rep. MW-71. Stormy Weather Group, McGill University, Montreal, 80 pp.

_____, 1974: Polarization measurements of precipitation backscatter in Alberta. J.de. Rech. Atmos., VIII Nos. 1-2, 163-173.

_____, R.G. Humphries and M.R. Johnson, 1976: Alberta hail radar-computer considerations; Atmos. Sci. Div. Rep. 76-1, Alberta Research Council, Edmonton, 45-67.

_____, and F. Bergwall, 1976: Fine-scale structure of convective storms associated with hail production. Atmos. Sci. Rep. 76-2, Alberta Research Council, Edmonton, 43 pp.

_____, _____, G.G. Goyer and J.H. Renick, 1976: Fine scale structure of convective storms-implications for cloud seeding in Alberta. Atmos. Sci. Div. Rep. 76-3, Alberta Research Council, Edmonton, 19 pp.

Battan, L.J., 1973: Radar Observation of the Atmosphere. Univ. of Chicago Press, 324 pp.

Blackman, R.B., and J.W. Tukey, 1958: The Measurement of Power Spectra. Dover Publication, New York, 190 pp.

Changnon, S.A., 1972: Illinois radar research for hail suppression applications, 1967 - 1969. Illinois, State Water Survey Report of Investigation 71, Urbana, 23 pp.

_____, and G.M. Morgan, 1976: Design of an experiment to suppress hail in Illinois. Illinois State Water Survey Bulletin 61, Urbana, 194 pp.

Chisholm, A.J., 1968: Observations by 10-cm radar of an Alberta Hailstorm in a sheared environment. Proc. of the Thirteenth Radar Meteor. Conf., Montreal, Amer. Meteor. Soc., 82-87.

_____, and J.H. Renick, 1972: The kinematics of multicell and supercell Alberta hailstorms. Alberta Hail Studies Report 72-2, Alberta Research Council, Edmonton, 24-30.

Deibert, R.J., Ed., 1976: Alberta Hail Project Field Program, 1975. AWMB report 2, Alberta Agriculture, Three Hills, 67 pp.

_____, 1977: Alberta Hail Project Field Program, 1976. AWMB report 4, Alberta Agriculture, Three Hills, Alberta, 83 pp.

Douglas, R.H. and W. Hitschfeld, 1959: Patterns of hailstorms in Alberta. Quart. J. Roy. Meteor. Soc., 85, 105-119.

Eccles, P.J., 1976: Remote measurement of mass and kinetic energy of hail using dual-wavelength radar. Proc., Seventeenth Conf. on Radar Meteor., Seattle, Amer. Meteor. Soc., 192-199.

English, M. 1973: The growth of large hail. Sci. Rep. MW-78, Stormy Weather Group, McGill University, Montreal, 82 pp.

Geotis, S.G., 1963: Some radar measurements of hailstorms. J. Appl. Meteor., 2, 270-275.

Gilman, D.L., F.J. Fuglister and J.M. Mitchell Jr., 1963: On the power spectrum of "red noise", J. Atmos. Sci., 20, 182-184.

Goyer, G.G., 1975: Evaluation measures and procedures. Current research on Alberta hailstorms. Atmos. Sci.Div. Progress Report 1974 - 1975. Alberta Research Council, Edmonton, 95-100.

Gunn, K.L.S., and T.W.R. East, 1954: The microwave properties of precipitation particles. Quart. J. Roy. Meteor. Soc., 80, 522-545.

Hitschfeld, W.F., 1974: Hail suppression: Evaluation and other problems. Preprints, Fourth Conf. on Weather Mod., Ft. Lauderdale, Amer. Meteor. Soc., 97-98.

Humphries, R.G., B.L. Barge, and M. R. Johnson, 1977: Alberta hail radar-computer considerations 11, Atmos. Sci. Div. Rep. 77-3, Alberta Research Council, Edmonton, 35-42.

Jenkins, G.M., 1961: General considerations in the analysis of spectra. Technometrics 3, 133-166.

Kanasewich, E.R., 1975: Time Sequence Analysis in Geophysics, 2nd ed., Univ. of Alberta Press, Edmonton, 364 pp.

Lachapelle, P.A., 1977: Modern Spectral methods with applications to Alberta climatic data. Unpub. MSc. Thesis. University of Alberta, Division of Meteor., Edmonton, 139 pp.

Leung, S.K., 1977: The Alberta Hail Project radar systems. Atmos. Sci. Div. Rep. 77-4, Alberta Research Council, Edmonton, 155 pp.

Marshall, J.S., 1971: Peak-reading and thresholding in processing radar weather data. J. Appl. Meteor., 11, 1213-1223.

Martner, B.E., and J.E. Dye, 1978: The relationship between radar reflectivity factor and hail at the ground for northeast Colorado thunderstorms. 18th conference on radar meteorology, AMS Boston, 322-327.

Marwitz, J.D., 1972: The structure and motion of severe hailstorms. Part 2: Multi-cell storms, J. Appl. Meteor., 11, 180-188.

Neyman, J., 1977: A statisticians' view of weather modification technology. Applied Physical and Mathematical Sciences: Proc. Natl. Acad. Sci. U.S.A., Vol. 74, No. 11, 4714-4721.

Panofsky, H.A. and G.W. Brier, 1963: Some applications of statistics to Meteorology. Pennsylvania State University, 224 pp.

Probert-Jones, J.R., 1962: The radar equation in meteorology. Quart. J. Roy. Meteor. Soc., 88, 485-495.

Ramsden, J., M.R. Johnson, R.G. Humphries and B.L. Barge, 1976: Interactive computer generated displays of radar data. Preprints, Seventeenth Conf. on Radar Meteor., Seattle, Amer. Meteor. Soc., 468-473.

Renick, J.H., 1975: The Alberta Hail Project: Update 1975. J. of Weather Mod., 7, No. 2, 1-6.

Ryde, J.W., 1946: The attenuation and radar echoes produced at centimeter wavelengths by various meteorological phenomena. Meteorological Factors in Radio Wave Propagation. Physical Society, London, 169-188.

Schickendanz, P.T., and S.A. Changnon, 1970: A study of crop hail insurance records for northeastern Colorado with respect to the design of the National Hail Experiment. Illinois State Water Survey Project Report, Urbana, 47 pp.

Simpson, J., W.I. Woodley, H.A. Friedman, T.W. Slusher, R.S. Scheffee and R.L. Steele, 1970: An airborne pyrotechnic cloud seeding system and its use. J. Appl. Meteor., 9, 109-122.

Smith, P.L., 1970: Weather radar. Unpub. manuscript. Inst. of Atmos. Sci., South Dakota School of Mines and Technology, Rapid City.

Sulakvelidze, G.K., N.Sch. Bibilashvili, and V.F. Lapsheva, 1965: Formation of precipitation and modification of hail processes. Israel Program for Scientific Translations 1967, Jerusalem, 208 pp.

Summers, P.W. and L. Wojtiw, 1971: The economic impact of hail damage in Alberta, Canada and its dependence on various hailfall parameters. Preprints, Seventh Conference of Severe Local Storms, Kansas City, Amer. Meteor. Soc., 158-163.

_____, G.K. Mather and D.R. Tredennick, 1972: The development and testing of an airborne droppable pyrotechnic flare system for seeding Alberta hailstorms. J. Appl. Meteor., 11, 695-703.

Warner, C., 1976: Case studies of Alberta Hailstorms. Sci. Rep. MW-86, Stormy Weather Group, McGill University, 72 pp.

Welch, P.D., 1967: The use of fast Fourier transform for the estimation of power spectra: A method based on time averaging over short, modified periodograms. IEEE Transactions on Audio and Electroacoustics, Vol. AU-15, No. 2, 70-73.

Williams, G.N., and R.H. Douglas, 1963: Continuity of hail production in Alberta storms. Sci. Rep. MW-36, Stormy Weather Group, McGill University, Montreal, 16-54.

Wojtiw, L., 1975: Hailfall and crop damage in Central Alberta. J. of Weather Mod., 7, No. 2, 28-42.

_____, 1975: Climatic summaries of hailfall in Central Alberta (1957 - 1973). Atmos. Sci. Div. Rep. 75-1, Alberta Research Council, Edmonton, 102 pp.

Wong, R.K.W., 1975: Evaluation of the current cloud seeding test. Current research on Alberta Hailstorms. Atmos. Sci. Div. Progress Report 1974 - 1975. Alberta Research Council, Edmonton, 101-108.

_____, 1976: Evaluation research: The analysis of thirty-seven years of crop insurance data in a target control historical approach. Current research on hailstorms and their modification. Atmos. Sci. Rep. 76-1, Alberta Research Council, Edmonton, 121-136.

APPENDIX A

THE TUKEY LOW-PASS FILTER

If an original time series contains frequencies or periods which are of no interest, these waves may be reduced or eliminated by statistical filtering. Therefore, if the smooth underlying trend of a time series is desired, the data may be filtered to eliminate the short period variations. A filter of this type is called a low-pass filter since the low-frequency or long-period waves are barely affected.

It is possible to design statistical filters such that only frequencies greater than a specified frequency are eliminated and the amplitudes of all waves in the time series affected by the filtering are known. This information is represented by the frequency response function of the filter.

The smoothing function used in this study is known as the Tukey low-pass filter. The filter consists of a series of weights w(t) which are cumulatively multiplied by consecutive values of the time series to obtain the filtered variable. The weight function is given by (A.1.1) and is illustrated in Figure A.1.

$$W(t) = \begin{cases} 1/2\,(1 + \cos\frac{\pi t}{M}) & |\,t\,| \le M \\ 0 & |\,t\,| > M \end{cases} \qquad (A.1.1)$$

for lag time t up to a maximum time lag M. The frequency response of the weight function is obtained by taking the Fourier transform (A.1.2).

$$W(f) = \int_{-\infty}^{\infty} W(t)\, e^{-i\,2\,\pi f t}\, dt \qquad (A.1.2)$$

The frequency response W(f) is given in (A.1.3).

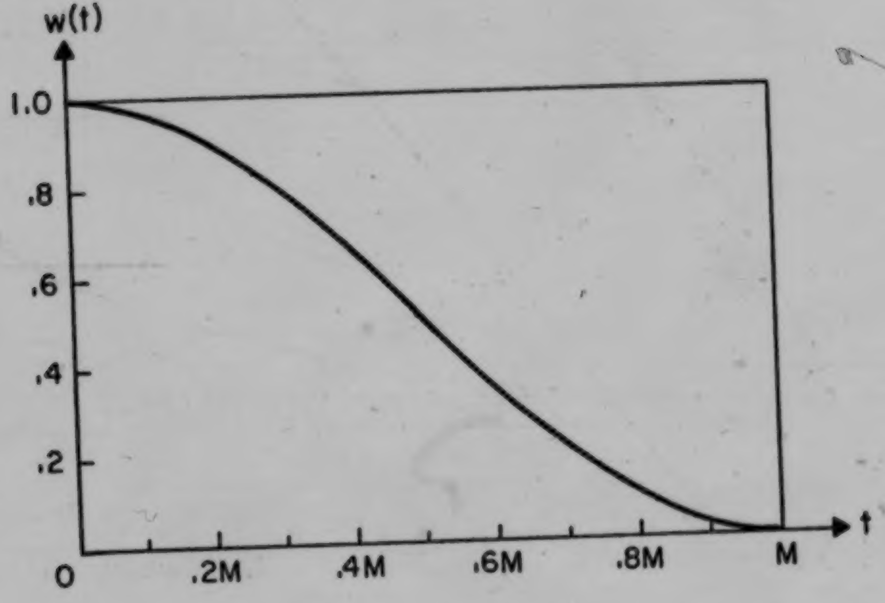

Fig. A.1: The Tukey filter weight function.

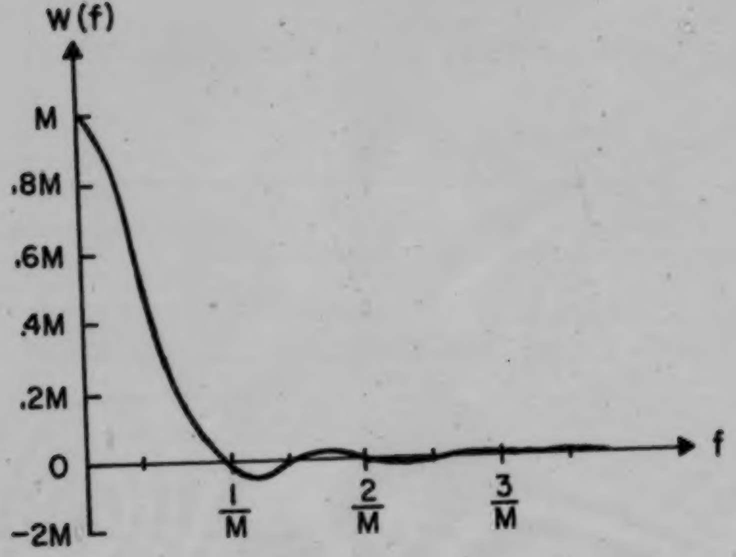

Fig. A.2: The Tukey filter response function.

$$W(f) = M\left\{\frac{\sin 2\pi fM}{2\pi fM} + 1/2\,\frac{\sin 2\pi M(f + 1/2\,M)}{2\pi M(f + 1/2\,M)} + 1/2\,\frac{\sin 2\pi M(f - 1/2M)}{2\pi M(f - 1/2M)}\right\}$$

$$= M\left(\frac{\sin 2\pi fM}{2\pi fM}\right)\left(\frac{1}{1 - (2fM)^2}\right) \qquad \text{(A.1.3)}$$

The frequency response is plotted in Figure A.2.

The trends in this study were computed using M = 15 minutes. The filtered variable was determined using 10 data points on each side therefore 10 data points were lost at the beginning and end of each low-pass filtered series. Thus all frequencies greater than 1/15 = .0667 cycles per minute were eliminated. The trends displayed in the original time series consist of waves with frequencies less than .0667 cycles per minute.

APPENDIX B

THE POWER SPECTRUM OF RED-NOISE AND WHITE-NOISE

A power spectrum which displays an even distribution of relative variance across all frequencies is known as a white-noise spectrum.

According to Kanasewich (1975), a time series is called white-noise if it satisfies the following criteria:

1. The time average of the series is zero.

$$E(x_t) = \lim_{N \to \infty} \frac{1}{2N+1} \sum_{t=-N}^{N} x_t = 0$$

Where $E(x_t)$ is the mean value.

2. The autocorrelation with zero lag is finite.

$$A_x(0) = \lim_{t \to 0} \frac{1}{2N+1} \sum_{t=-N}^{N} x_t^2 = \sigma^2 < \infty$$

The quantity σ^2 is the variance of the time series and also the power of the white-noise.

3. The autocorrelation of the time series is zero for all lags different from zero.

A random time series is an example of white-noise.

The power spectrum of red-noise has been described by Gilman et al. (1963). Specifically it is a first-order linear Markov process. This is a type of random process in which the future development depends upon the most recent state. The variate x(t) is given by:

$$x(t) = \alpha\ x(t-1) + \varepsilon_t$$

where α is the autocorrelation at lag one and ϵ_t is some random input at time t. The red-noise spectrum is given by:

$$\alpha^2(f) = \frac{1 - \alpha^2}{1 + \alpha^2 - 2\alpha\cos(2\pi f)}$$

The striking characteristic of the red-noise power spectrum is the general suppression of relative variance at high frequencies and consequent inflation at low frequencies.

It was found that the spectra of $\overline{\eta}$ for the storms studied fit the red-noise spectral model better than the white-noise spectral model.

APPENDIX C

COMPUTER PROGRAM

The following is a listing of the computer program used in the calculation of $\overline{\eta}$.

```
         INTEGER TIME(2,3),WINDOW(13),WINDOX(13),AZ(3),EL(3),HDR(41)
     *,DIF(147),CTIME(4),TEMP,A,B,C,EOW,EOF
         REAL TABLE(147),TABLE2(147)
         LOGICAL*1 RAY(2,147,3),NAME(10),DATE(9),YR(2)
         EQUIVALENCE (YR,I)

1        FORMAT('$RADAR CONSTANT?  ')
2        FORMAT(F10.0)
3        FORMAT(1X,4A2,F8.1,F12.8)
4        FORMAT('$TAPE DRIVE?  ')
5        FORMAT(Q,10A1)
6        FORMAT('$FILE NUMBER?  ')
7        FORMAT(I10)
8        FORMAT(' DATE DATA LOGGED? DD-MMM-YY'/
     $'S                    ')
9        FORMAT(9A1)
10       FORMAT(///1X,9A1,4X,F10.2)

C-----GET RADAR CONSTANT
         WRITE(5,1)
         READ(5,2)RADCON
         PT=10.**(12.7-RADCON/10.)/(480.*1.75E-6)
         WRITE(5,8)
         READ(5,9)DATE
C-----COMPUTE TABLES
         DO 50 I=1,147
         R=IRCON(I)/200.0
         TABLE2(I)=R*R
         TABLE(I)=TABLE2(I)*0.01832
         R=RADCON+20.0*ALOG10(R)
         DIF(I)=R*2.0-200.0+0.5
D        WRITE(5,11)I,TABLE2(I),TABLE(I),R,DIF(I)
11       FORMAT(1X,I7,3E20.6,I7)
50       CONTINUE
C-----OPEN DISK FILE
         CALL ASSIGN(3,'TERRY.DAT')
C-----GET NAME OF TAPE DRIVE
         WRITE(5,4)
         READ(5,5)LEN,(NAME(I),I=1,LEN)
         CALL SETIDV(NAME,LEN)
C-----GET FILE NUMBER
         WRITE(5,6)
         READ(5,7)I
         CALL FILE(I,HDR,IEND)
C-----PRINT PARAMETERS
         WRITE(5,10)DATE,RADCON

C-----INITIALIZE BUFFER POINTERS
         A=1
         B=2
         C=3
C-----GET FIRST RAY
         CALL XRAY(TIME(1,C),AZ(C),EL(C),RAY(1,1,C),EOW,EOF,WINDOW)
         GOTO500
```

```
C-----ROTATE BUFFER POINTERS AND GET NEXT RAY
100     TEMP=A
        A=B
        B=C
        C=TEMP
        CALL XRAY(TIME(1,C),AZ(C),EL(C),RAY(1,1,C),EOW,EOF,WINDOW)
        IF(EOF.EQ.1 .OR. EOW.EQ.1)GOTO700
C-----STORE WINDOW INFORMATION
        DO 110 I=1,13
110     WINDOX(I)=WINDOW(I)
C-----COMPUTE WIDTH OF RAY
        ANGLE=ICLEAR(AZ(B)-AZ(A))/2+ICLEAR(AZ(C)-AZ(B))/2
C-----PREPARE TO PROCESS CURRENT RAY
200     IBIN1=WINDOX(5)
        IBIN2=WINDOX(6)
D       WRITE(5,12)ANGLE
12      FORMAT(1X,10F10.4)
D       WRITE(5,13)IBIN1,IBIN2,WINDOX
13      FORMAT(1X,16I6)
        IF(WINDOX(7).EQ.0)GOTO220
C-----CONVERT REFLECTIVITY BACK INTO POWER RECEIVED (DBM)
        DO 210 I=1,147
210     IF(RAY(2,I,B).GT.-100)RAY(2,I,B)=RAY(2,I,B)-DIF(I)
C-----INCREMENT SUMS FOR EACH BIN INSIDE THE WINDOW
220     DO 300 IBIN=IBIN1,IBIN2
        N=RAY(2,IBIN,B)
        IF(N.LT.-90)GOTO300
        POWER=10.0**((N-100)/20.0)
        VOLUME=TABLE(IBIN)*ANGLE
        TOTVOL=TOTVOL+VOLUME
        SUM=SUM+VOLUME*TABLE2(IBIN)*POWER
D       WRITE(5,14)IBIN,N,POWER,VOLUME,TOTVOL,SUM
14      FORMAT(1X,2I7,4E20.6)
300     CONTINUE
        IF(EOF.EQ.1)GOTO400
        IF(EOW.EQ.0)GOTO100
C-----COMPUTE AND OUTPUT PARAMETER
400     IF(TOTVOL.EQ.0.0)GOTO450
        PARAM=(7.068E+6/PT)*SUM/TOTVOL
        CALL TIMBIN(CTIME,TIME(1,B),TIME(2,B))
        ELEV=EL(B)/10.
        WRITE(3,30)CTIME,ELEV,PARAM
450     IF(EOF.EQ.1)STOP
C-----INITIALIZE SUMS
500     SUM=0.0
        TOTVOL=0.0
C-----STORE WINDOW INFORMATION
600     DO 620 I=1,13
620     WINDOX(I)=WINDOW(I)
C-----ROTATE BUFFER POINTERS AND GET NEXT RAY
        TEMP=A
        A=B
        B=C
        C=TEMP
        CALL XRAY(TIME(1,C),AZ(C),EL(C),RAY(1,1,C),EOW,EOF,WINDOW)
C-----COMPUTE WIDTH OF RAY (NO PREVIOUS RAY)
        ANGLE=23+ICLEAR(AZ(C)-AZ(B))/2
        GOTO200
C-----COMPUTE WIDTH OF RAY (NO NEXT RAY)
700     ANGLE=ICLEAR(AZ(B)-AZ(A))/2+23
        GOTO200

        END
```